Proteomics Comparison of Extracellular Matrix Remodelling in Porcine Coronary Arteries upon Stent Implantation

Suna, Gonca

Awarding institution:
King's College London

Proteomics Comparison of Extracellular Matrix Remodelling in Porcine Coronary Arteries upon Stent Implantation

Gonca Suna

Supervisors

Professor Manuel Mayr, Professor Wojtek Wojakowski

Submitted for PhD

Cardiovascular Division

King's College London

BHF Centre of Research Excellence

London, 2017

TABLE OF CONTENTS

Acknowledgements **7**

Abstract **8**

Abbreviations **9**

Figures **11**

Tables **12**

1 Introduction **13**

1.1 Vascular biology, stent implantation and consequences 13

1.1.1 Coronary artery disease and atherosclerosis: a clinical perspective 13

1.1.2 Pathophysiology of native atherosclerosis 14

1.1.3 PCI: from plain balloon angioplasty to biodegradable coronary stents 16

1.1.4 DES characteristics 18

1.1.4.1 Molecular basis of mTOR regulation and inhibition 18

1.1.5 Biology of restenosis and stent thrombosis 20

1.1.5.1 In-stent restenosis 20

1.1.5.2 DES thrombogenicity 22

1.1.5.3 In-stent neoatherosclerosis 23

1.1.5.4 miRNAs in restenosis 25

1.1.6 Animal models of coronary stenting 25

1.1.7 Optical Coherence Tomography 26

1.1.7.1 OCT image features 27

1.1.7.2 OCT and restenosis 27

1.2 Vascular ECM 29

1.2.1 Basic ECM features 29

1.2.2 Composition of the vascular ECM 29

1.2.2.1 Elastin 31

1.2.2.2 Collagens 31

1.2.2.3 Proteoglycans 32

1.2.2.4 Integrins 34

1.2.3 ECM degradation 34

1.2.3.1 MMPs 35

1.2.3.2 Adamalysins 35

1.2.3.3 TIMPs 36

1.2.4 ECM remodelling in vascular disease 37

1.2.4.1 ECM remodelling in atherosclerosis 38
1.2.4.2 ECM remodelling in restenosis 39
1.3 Proteomics 41
1.3.1 Introduction into proteomics 41
1.3.1.1 Proteomics as part of systems biology 41
1.3.1.2 Proteomics – Definition and challenges 41
1.3.1.3 Proteomics vs. traditional biological research 42
1.3.2 Proteomics applications 43
1.3.2.1 Proteomics experiments 43
1.3.2.2 Proteomics workflow 43
1.3.3 Two-dimensional gel electrophoresis 46
1.3.3.1 2D DIGE 47
1.3.4 Mass spectrometry based proteomics 48
1.3.4.1 MS principles and instruments 48
1.3.4.2 Overview of MS methods 49
1.3.4.3 Top-down vs. bottom-up proteomics 50
1.3.5 Liquid-chromatography tandem mass spectrometry 51
1.3.5.1 Sample preparation 51
1.3.5.2 MS analysis 51
1.3.5.3 Protein identification algorithms 52
1.3.6 Shotgun proteomics 54
1.3.7 Quantitative proteomics 55
1.3.7.1 Label-free quantification 55
1.3.7.2 Stable isotope-labelling 55
Stable isotope labelling by amino acids in cell culture 56
Isobaric tagging 56
^{18}O labelling 58
1.3.8 Targeted proteomics 59
1.3.8.1 MRM assay generation 60
1.3.8.2 Database search and absolute quantification using MRM 61
1.3.9 Data independent analysis 62
1.3.9.1 DIA in comparison with DDA and MRM 62
1.3.9.2 Data acquisition in the DIA mode 63
1.3.9.3 SWATH-MS and DIA data analysis 63
2 Hypothesis 65
3 Aim 65

4 Materials and Methods 66
4.1 Porcine experiments 66
4.1.1 Porcine model of stent injury 66
4.1.2 OCT image analysis in pigs 67
4.1.3 Porcine sample collection and processing 67
4.2 Mice experiments 68
4.2.1 Mouse model of venous bypass graft 68
4.3 Human tissue collection 68
4.4 Protein extraction 69
4.4.1 ECM protein enrichment 69
4.4.2 Deglycosylation of ECM extracts 70
4.5 Proteomics workflow for pig samples 71
4.5.1 In-solution protein digestion 71
4.5.2 Peptide clean-up using C 18 71
4.5.3 Untargeted LC-MS/MS analysis 72
4.5.4 Database search 72
4.5.5 Generation of custom-made porcine ECM protein database 73
4.5.6 Data analysis: media vs. neointima 73
4.6 Targeted proteomics for mice and human samples 73
4.6.1 PRM in SILAC mice tissue 74
4.6.2 PRM in human tissue 75
4.7 Western blot 75
4.8 Silver staining 77
4.9 Gene expression analysis 77
4.9.1 RNA extraction 77
4.9.2 cDNA synthesis 78
4.9.3 qPCR 78
4.10 miRNA expression analysis 80
4.10.1 RT reaction 81
4.10.2 qPCR 81
4.11 Immunostaining 81
4.11.1 Sample processing 81
4.11.2 Immunohistochemistry (IHC) 82
4.11.3 Immunofluorescence 83
4.12 Cell culture 83
4.12.1 SMC culture 83
4.12.2 EC culture 84

4.12.3 Everolimus treatment 84
4.12.4 Cell counting 85
4.12.5 Viability and cell count 85
4.13 Statistical analysis 85

5 Results 87
5.1 Porcine model of stent injury 87
5.2 OCT findings 88
5.3 miRNA changes in the vascular stent injury model 91
5.4 ECM proteins identified in the media and neointima 92
5.4.1 Impact of custom-made porcine ECM database 92
5.4.2 Comparison between media and neointima 93
5.5 ECM remodelling in the neointima 98
5.5.1 Method reproducibility 98
5.5.2 Neointima comparison between DES and BMS 98
5.6 ECM remodelling in the media 100
5.6.1 Temporal changes in the media post-stenting 100
5.6.2 Media comparison between DES and BMS 100
5.7 Validation of proteomics findings 103
5.7.1 Stent-induced changes in aggrecan and its fragments 103
5.7.2 Aggrecanase changes in stented arteries 105
5.7.3 Aggrecanase expression in cultured ECs and SMCs 106
5.8 Aggrecan in human vasculature 108
5.8.1 Aggrecan in human stented arteries 108
5.8.2 Aggrecan in human aorta and vein 108
5.9 Aggrecan in a mouse model of venous bypass graft 112
5.9.1 Role of mechanical forces in aggrecan expression 112

6 Discussion 114
6.1 Porcine animal model of stent injury 114
6.2 miRNA changes in the stent injury model 115
6.3 Strengths and caveats of the proteomics approach 116
6.4 The role of databases in proteomics data analysis 117
6.5 Identification of ECM proteins using discovery-based proteomics 117
6.5.1 ECM changes in the neointima 117
6.5.2 Early changes upon vascular stent/balloon injury 119
6.5.3 ECM changes in the media 120
6.6 Aggrecan: more than just a cartilage protein 121

6.6.1 Aggrecan structure and function 121
6.6.2 Aggrecan cleavage 122
6.7 Aggrecan in the vasculature 124
6.8 Aggrecanases in the vasculature 125
6.8.1 Shift in vascular aggrecanase activity 127
6.8.2 Regulation of aggrecanase activity 128
6.8.3 Differential aggrecan turnover in DES and BMS 131
6.9 Strengths and limitations 134
7 Future Work 135
8 Conclusion 137
9 Supplemental tables 138
10 Attachment 152
11 References 153
12 Curriculum vitae 174

ACKNOWLEDGEMENTS

I would particularly like to thank my primary supervisor Professor Manuel Mayr, first of all for admitting me to his research group and providing me with such an exciting topic. He introduced me into the fascinating world of mass spectrometry that was largely unknown to me as a clinician and for which I have found great passion over the past three years. Many thanks to Manuel for his continuous support and constructive advice throughout this project. His great enthusiasm and dedication to science were truly inspiring. Thanks also for letting me live out my scientific curiosity and evolve into a researcher with a critical mind.

Many thanks also to Professor Wojtek Wojakowski for the co-supervision of this project. He was readily helpful with suggestions and comments, whenever questions emerged. His advice on both research as well as diving spots were highly appreciated.

Special thanks go to all the members of my lab. It has been a great experience for me to work in the international environment of our highly motivated research group. They were always ready to give me practical advice and comfort, whenever I had a problem. Thanks guys for the pleasant working atmosphere and also for the great time we have spent together outside the lab.

I would also like to thank all the other collaborators for their contributions to this project, whether it was providing samples or methodological help. Their contributions have been essential for the realization of this project.

I am grateful to the British Heart Foundation (BHF) for the financial support of this project. I expressed this appreciation with my personal engagement in BHF charity events during my PhD. I hope, I was able to give something back.

I am entirely grateful to my family for their eternal support and for unshakably believing in me. My parents have always worked so hard to offer me the education, that was not granted to them. Finally, thank you Patrick for your love, support and cheering me up with your enthusiasm for life and your endless optimism. You have always been there for me, whenever I needed you, despite the thousand kilometres between us for most of the time.

Even though the past three years have been exciting and varied, it was not always easy. In moments of despair, I have been guided by the following simple but true maxim:

ABSTRACT

BACKGROUND Extracellular matrix (ECM) remodelling related to arterial injury and healing after stenting contributes to both, in-stent restenosis and thrombosis. Despite its important clinical implications little is known about ECM changes post-stent implantation.

METHODS Bare-metal (BMS) and drug-eluting stents (DES) were implanted in pig coronary arteries with an overstretch under optical coherence tomography guidance. Stented segments were harvested 1, 3, 7, 14 and 28 days post-stenting for proteomics analysis of the media and neointima.

RESULTS A total of 151 ECM and ECM-associated proteins were identified by mass spectrometry. The composition of the neointimal ECM was more diverse than of the media, and proteins involved in regulating calcification were upregulated in the neointima of DES. After stent implantation the earliest changes in the media were proteins involved in inflammation and thrombosis, followed by changes in regulatory ECM proteins. By day 28, basement membrane proteins were reduced in DES compared with BMS. In contrast, the large aggregating proteoglycan aggrecan was increased. Aggrecanases of the ADAMTS (a disintegrin and metalloproteinase with thrombospondin motifs) family contribute to the catabolism of vascular proteoglycans. An increase in ADAMTS-specific aggrecan fragments was accompanied by a notable shift from ADAMTS1 to ADAMTS4 expression after stent implantation. Immunostaining in human stented coronary arteries confirmed the presence of aggrecan and aggrecan fragments, in particular at the contacts of the stent struts with the artery. Further investigation of aggrecan presence in the human vasculature revealed that aggrecan and aggrecan fragments were more abundant in human arteries compared to veins. Also, aggrecan synthesis was induced upon grafting a vein into the arterial circulation, indicating an important role for aggrecan in vascular plasticity.

CONCLUSIONS Significant differences were identified by proteomics in the ECM of coronary arteries after BMS and DES implantation, most notably an upregulation of aggrecan, a major ECM component of cartilaginous tissues that confers resistance to compression. The accumulation of aggrecan coincided with a shift in ADAMTS expression. This study provides the first evidence implicating aggrecan and aggrecanases in the vascular injury response after stenting.

ABBREVIATIONS

2D DIGE	two-dimensional difference gel electrophoresis
A.U.	arbitrary units
ACS	acute coronary syndrome
ADAM	a disintegrin and metalloproteinase
ADAMTS	a disintegrin and metalloproteinase with thrombospondin motifs
BM	basement membrane
BMP1	bone morphogenetic protein 1
BMS	bare-metal stent
CAD	coronary artery disease
cat. no.	catalogue number
CD	cluster of differentiation
CID	collision-induced dissociation
CSPG	chondroitin sulfate proteoglycan
DDA	data-dependent acquisition
DES	drug-eluting stent
DIA	data-independent acquisition
EC	endothelial cell
ECM	extracellular matrix
ESI	electrospray ionization
GAG	glycosaminoglycan
HCAEC	human coronary artery endothelial cells
HPLC	high-performance liquid chromatography
HPLN1	hyaluronan and proteoglycan link protein 1
IGD	interglobular domain
IAA	iodoacetamide
IL	interleukin
iTRAQ	isobaric tagging for relative and absolute quantification
IVUS	intravascular ultrasound
ISR	in-stent restenosis
LAD	left anterior descending artery
LC	liquid chromatography
LC-MS/MS	liquid chromatography tandem-mass spectrometry
LCX	left circumflex artery
LRP1	low density lipoprotein receptor-related protein 1
LST	late stent thrombosis

MGP	matrix Gla protein
MMP	matrix metalloproteinase
MRM	multiple reaction monitoring
MS	mass spectrometry/spectrometer
NO	nitric oxide
mTOR	mammalian target of rapamycin
mTORC1	mTOR complex 1
OCT	optical coherence tomography
PBS	phosphate-buffered saline
PBST	phosphate-buffered saline with Tween
PDGF	platelet-derived growth factor
PC	proprotein convertase
PCI	percutaneous coronary intervention
PGCA	aggrecan
PLLA	poly-L-lactic acid
POBA	plain old balloon angioplasty
PRM	parallel reaction monitoring
PTM	post-translational modification
qPCR	quantitative polymerase chain reaction
RCA	right coronary artery
RT	reverse transcription or retention time
SDS	sodium dodecyl sulphate
SDS-PAGE	SDS polyacrylamide-gel electrophoresis
SILAC	stable isotope labelling by amino acids in cell culture
SLRP	small leucine-rich proteoglycan
SMC	smooth muscle cell
SPARC	secreted protein acidic and rich in cysteine
SPP24	secreted phosphoprotein 24
SWATH	sequential windowed acquisition of all theoretical mass spectra
TCFA	thin-cap fibroatheroma
TGF-β	transforming growth factor-beta
TIC	total ion current
TIMP	tissue inhibitors of metalloproteases
TNF-α	tumor necrosis factor-alpha
TMT	tandem mass tag
VEGF	vascular endothelial growth factor

FIGURES

Figure 1. Vascular wall in health and disease 16
Figure 2. Coronary artery stenting. 17
Figure 3. Simplified schematic representation of mTORC1 signalling 19
Figure 4. Mechanisms of thrombosis and restenosis upon stent implantation 22
Figure 5. OCT principles 28
Figure 6. Fibrillar collagen structure 32
Figure 7. Domain structure of the ADAMTS family 36
Figure 8. Proteomics workflow 46
Figure 9. Overview of proteomics approaches 50
Figure 10. Protein identification by LC-MS/MS 54
Figure 11. Stable isotope-labelling. 58
Figure 12. SRM/MRM analysis on a triple quadrupole (QQQ) MS 61
Figure 13. Comparison of data acquisition using the MRM, DDA or DIA method 63
Figure 14. Determination of the Ct-value 79
Figure 15. Porcine model of stent injury 88
Figure 16. OCT findings 89
Figure 17. miRNA changes upon stenting 91
Figure 18. Impact of custom-made database on protein identification and quantification. 92
Figure 19. ECM proteins identified in the media and neointima 93
Figure 20. Reproducibility of LC-MS/MS 98
Figure 21. Comparison of neointimal BMS and DES 99
Figure 22. ECM remodelling in the media over time 101
Figure 23. Comparison of BMS vs. DES in the media 102
Figure 24. Aggrecan fragments in DES and BMS 105
Figure 25. Aggrecanase changes in stented porcine coronary arteries 106
Figure 26. Validation of findings in cultured cells 107
Figure 27. Immunostaining on human coronary arteries 109
Figure 28. Aggrecan in human stented coronary artery 110
Figure 29. Aggrecan in human vessels 111
Figure 30. Aggrecan induction upon mechanical forces 113
Figure 31. Schematic structure of aggrecan and its cleavage sites 124
Figure 32. Regulation of aggrecanase activity 130
Figure 33. Induction of large aggregating proteoglycans upon stenting. 133

TABLES

Main tables

Table 1. Classification of glycosylated ECM proteins. 30
Table 2. List of precursor ions for PRM in mouse tissue 74
Table 3. PRM fragment list used for human protein quantification 75
Table 4. Primers used for qPCR analysis 80
Table 5. TaqMan miRNA assays used for qPCR analysis 81
Table 6. Antibodies and dilutions used for IHC in human and mice tissue samples 83
Table 7. Sample characteristics 90
Table 8. Extracellular proteins identified by proteomics analysis in the media of stented/balloon dilated porcine coronary arteries. 94

Supplemental tables

Supplemental table 1. Porcine ECM database entries 138
Supplemental table 2. Extracellular proteins identified by proteomics analysis in the neointima of stented porcine coronary arteries. 147
Supplemental table 3. Significant extracellular protein changes between BMS/DES day 28 vs. POBA late 150
Supplemental table 4. Differentially expressed proteins between DES and BMS over time 151

1 INTRODUCTION

1.1 Vascular biology, stent implantation and consequences

1.1.1 Coronary artery disease and atherosclerosis: a clinical perspective

Coronary artery disease (CAD) also known as ischemic heart disease is the most common cardiovascular disease and the leading cause of death worldwide.[1, 2] It is characterized by an imbalance between myocardial oxygen supply and demand due to restricted blood flow to the myocardium. The chronic and common manifestation of CAD is stable angina pectoris resulting from coronary stenosis, which usually manifests with a characteristic chest pain upon exercise. The acute forms of the disease are the acute coronary syndromes (ACS), including unstable angina, ST-elevation myocardial infarction (STEMI) and non-STEMI (NSTEMI).

Atherosclerosis is the underlying cause of CAD. While it was previously considered as a mere cholesterol storage disease[3], atherosclerosis is now understood as a chronic progressive inflammatory disease. Atherosclerotic lesions start with early intimal thickening, progress to 'fatty streaks' as the correlate for infiltrating lipid-laden macrophage foam cells and gradually evolve into fibroatheromas, the characteristic plaques. Acute rupture or erosion of such a 'vulnerable plaque' is by far the most common cause of an ACS. Subsequent platelet activation and aggregation results in thrombus formation with the partial or complete occlusion of the coronary arterial lumen.

Numerous landmark studies, with the Framingham Heart Study leading the way, have identified several risk factors for developing CAD, with dyslipidaemia and current smoking being the most influential ones.[4] Thus, the prevention of modifiable risk factors remains the first-line measure against CAD. However, primary prevention with drugs is indicated in patients with higher risk for developing cardiovascular events to prevent progression of atherosclerosis.[5] These include lipid-lowering drugs such as statins or the recently approved proprotein convertase subtilisin/kexin type 9 (PCSK9) inhibitors in case of insufficient statin therapy[6, 7], as well as angiotensin converting enzyme (ACE) inhibitors. Antiplatelet therapy with low-dose aspirin is effective for the secondary prevention of cardiovascular events. The cornerstone therapy for symptomatic disease are antianginal drugs, i.e. cardioselective β-blockers reducing myocardial oxygen demand, nitrates and calcium channel blockers and additional dual antiplatelet therapy in ACS. Nevertheless, coronary revascularization is indicated for severe disease. Though surgical revascularization is primarily chosen for patients with multivessel disease, the less

invasive coronary angioplasty/percutaneous coronary intervention (PCI) has emerged as the standard of care for coronary revascularization in recent years.

1.1.2 Pathophysiology of native atherosclerosis

The substrate for coronary angioplasty is generally an atherosclerotic plaque in the vessel wall. For comparison, the wall structure of a physiologic coronary artery is shown in Figure 1A. It consists of three layers: intima, media and adventitia. The intima comprises an inconspicuous monolayer of endothelial cells (ECs) with an underlying basal lamina, which lines the arterial lumen and is therefore crucial for an integral vessel. The intima is separated from the underlying media, which consists of multiple layers of smooth muscle cells (SMCs) and elastin, by the internal elastic lamina. The media is separated from the adventitia by the external elastic lamina. Finally, the adventitia is mainly composed of fibroblasts and loose extracellular matrix (ECM). The vascular ECM content is explained in chapter 1.2.2 in detail.

Atherosclerosis is a progressive inflammatory disease in the vessel wall[8], predominantly affecting the intimal layer. Though a systemic vascular disease, atherosclerotic plaques are not uniformly distributed.[9] This is likely due to the local biomechanical forces acting within the artery. Arterial regions that are exposed to disturbed blood flow e.g. curvatures and bifurcations result in low shear stress, which induces plaque development and progression. Regions of disturbed flow are associated with both increased EC proliferation and apoptosis, higher permeability, increased expression of inflammatory mediators and production of reactive oxygen species (ROS).[10] Atherogenesis comprises the four stages of adaptive intimal thickening, intimal xanthoma (fatty streak), pathological intimal thickening and fibroatheroma (modified AHA classification) (*Figure 1B*).[11] The first stage is often observed in atherosclerosis-prone arteries and is considered as rather physiological. It describes the natural accumulation of SMCs in the absence of lipid or macrophage foam cells. The actual atherosclerotic lesion formation is commonly triggered by endothelial dysfunction and subendothelial lipoprotein retention usually at vascular regions with disturbed blood flow.[12] The highly negatively charged glycosaminoglycan (GAG) side chains of proteoglycans are postulated to interact with lipoproteins and contribute to their retention, initiating and maintaining atherosclerosis.[13, 14] Recruited blood monocytes differentiate into macrophages and eventually into foam cells upon internalization of the retained lipoproteins, resulting in so called ‘fatty streaks’ (stage two). Lesion progression involves SMC proliferation and phenotypic switching with the accumulation of ECM and lipid material (stage three or pathological intimal thickening). The ECM is mainly composed of hyaluronan, collagen type III and proteoglycans (biglycan, versican, decorin) with a lipid pool and free

cholesterol. Eventually these lesions develop into fibroatheromas and characteristic plaques (stage four). Fibroatheromas are characterized by an acellular necrotic core with a fibrous cap. The necrotic core is generated by macrophage infiltration into lipid pools and their apoptosis and necrosis, hence it coined the term 'grave yard of macrophages'. Based on the composition of the core it can be divided in an early and late stage, as the necrotic core develops and expands. The necrotic core of late fibroatheromas is large and poor in ECM, probably due to degradation by metalloproteinases (MMPs) and ADAMTS proteases (a disintegrin and metalloproteinase with thrombospondin motifs). Furthermore, the late core exhibits extensive cellular debris and sometimes also calcification and intraplaque haemorrhage.

The fibrous cap above the necrotic core is the critical component of a fibroatheroma, which determines its stability. Thick fibrous caps are usually ECM-rich interspersed with SMCs, which at this stage are regarded to have plaque-stabilizing properties. On the other hand, thin-cap fibroatheromas (TCFA) or 'vulnerable plaques' are more prone to rupture and predominantly infiltrated by macrophages with potential protease release but have hardly any SMCs. However, recent studies suggest that this concept may be too simplistic as it postulates a homogenous population of SMCs within the plaque.[15] On the contrary, recent genetic lineage tracing studies have demonstrated that SMC phenotypic switching may also result in macrophage-like-cells.[16] These SMC-derived cells lack the classical set of SMC markers, but express macrophage markers, which is why traditional methods such as immunostaining have failed to identify their origin. The protective role of SMC in the cap is attributed to their ability to repair subclinical plaque rupture by proliferating and synthesising ECM. Indeed, episodes of plaque disruption and subsequent healing have been observed on plaques.[17] Thus, plaque progression has also been suggested as a result of such episodes of silent rupture and healing. Similarly, plaque evolution is not always a linear process as depicted above. A serial intravascular ultrasound study showed that while some plaques transformed into advanced lesions with thin fibrous caps, others regressed and healed over time.[18] Thus, prediction of a plaque rupture from imaging alone remains challenging. A recent tissue-based proteomics study from our group identified a 4-biomarker signature, including matrix metalloproteinase 9 (MMP9), S100A8/S100A9, lysosomal cathepsins and galectin-3-bining protein), with differential expression between symptomatic compared to asymptomatic plaques.[19] This 4-biomarker signature was subsequently measured in plasma and improved risk prediction for cardiovascular events in two community-based studies.

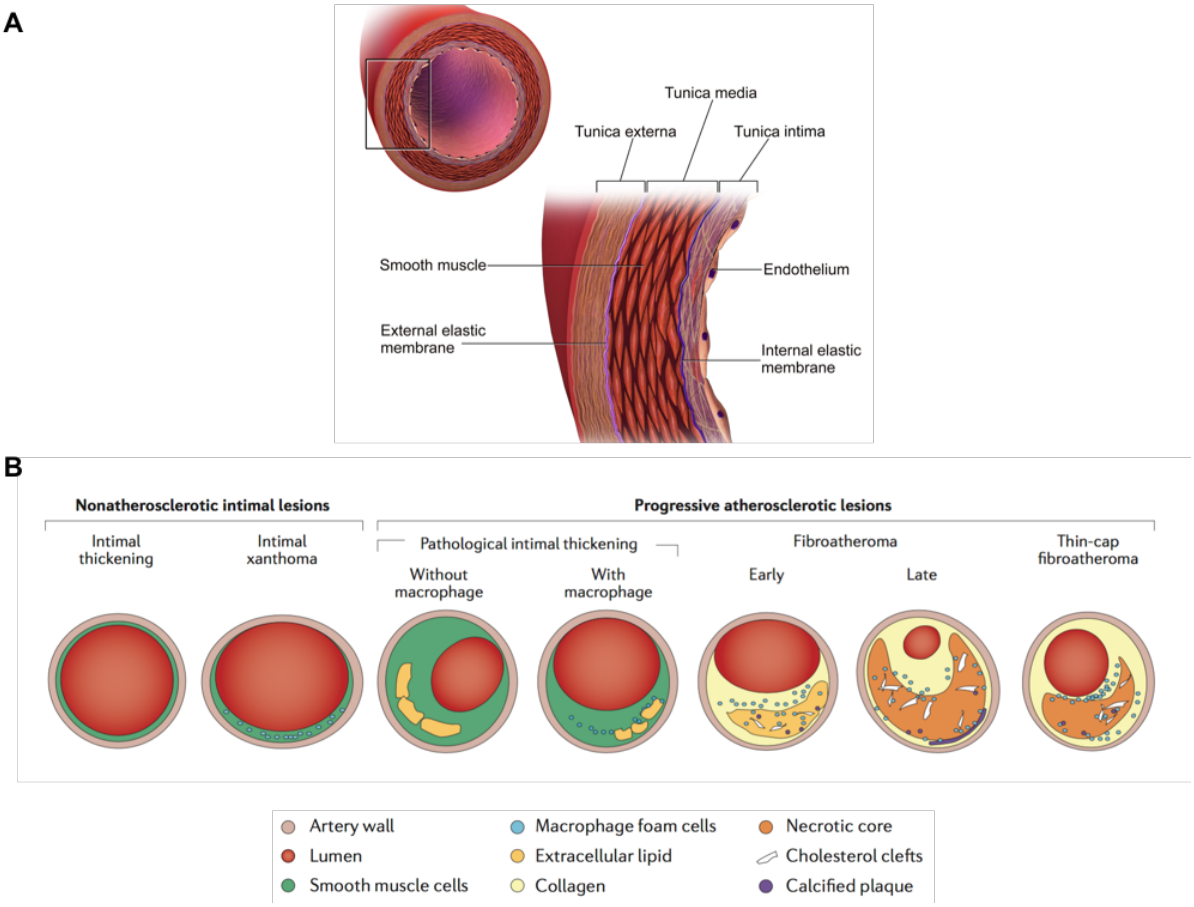

Figure 1. Vascular wall in health and disease (A) Coronary artery wall structure. The physiologic arterial wall structure is depicted. Adapted from Blausen.com staff in *Medical gallery of Blausen Medical 2014*. **(B) Atherosclerotic lesion morphologies.** Atherosclerosis is a progressive inflammatory disease of the vessel wall comprising the four stages of adaptive intimal thickening, intimal xanthoma (fatty streak), pathological intimal thickening and fibroatheroma. Adapted from Yahagi et. al in *Nature Reviews Cardiology,* 2016.[11]

1.1.3 PCI: from plain balloon angioplasty to biodegradable coronary stents

PCI has become the reperfusion treatment of choice for CAD, representing one of the greatest therapeutic advances in medicine. Since the introduction of coronary angioplasty by Andreas Grüntzig *et al.* in 1977 the techniques and equipment used for PCI have been widely refined.[20] The general principle, however, remains the same: an inflatable balloon catheter is inserted through a peripheral artery under local anaesthesia and is gradually expanded to dilate an obstructed coronary artery, thus restoring blood flow and ensuring myocardial blood supply. In the early days of PCI, restenosis of dilated vessels occurred in 30-60% of cases and has limited the use of plain balloon angioplasty.[21] Restenosis in these days was a result of contractive recoiling, as well as neointima and constrictive remodelling[22, 23], which required a further revascularization procedure. In order to prevent acute recoil, stents have been introduced. Stents are usually metallic scaffolds placed into the stenosed artery segment to hold it open (*Figure 2*).[24] The earliest form of stents were

bare-metal stents (BMS). Stent implantation has significantly reduced the incidence of restenosis as demonstrated by randomized clinical trials by the mid 1990s and largely obviated the need for emergency bypass surgery.[25, 26] With the widespread use of stent implantation, the restenosis frequency decreased to 15-30%.[27] By the late 1990s, stents were applied to 84% of all PCIs.[28]

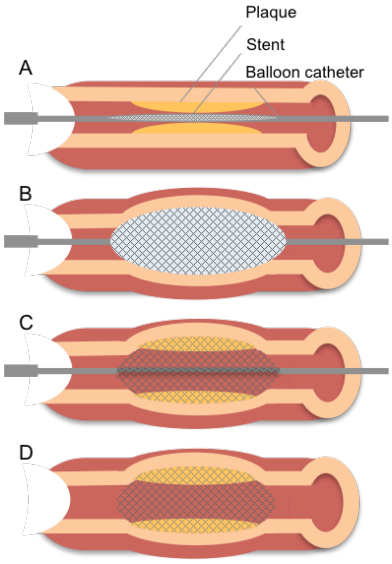

Figure 2. Coronary artery stenting. (A) In PCI, an inflatable balloon catheter surrounded by a compressed stent is inserted into the stenosed coronary artery through a peripheral artery. (B) The balloon is gradually inflated, which compresses the plaque against the vessel wall and expands the stent. (C) The balloon is then deflated and the catheter can be removed. (D) The stent remains at the vessel wall to hold the now dilated artery open restoring blood flow.

Although stent implantation has become a standard of care for coronary revascularization, in-stent restenosis (ISR) due to neointimal hyperplasia as well as subacute thrombosis emerged as complications associated with stents.[29] Neointimal hyperplasia involves luminal narrowing due to SMC proliferation and ECM deposition.[30] To overcome stent-mediated neointimal proliferation, drug-eluting stents (DES) have been developed and resulted in a further reduction of restenosis and repeat-revascularization compared with BMS.[31-33] However, long-term safety and efficacy studies on these so called first-generation DES (sirolimus- and paclitaxel-eluting stents) have revealed that DES are linked to an increased late stent thrombosis (LST) rate and demonstrated failure to improve mortality.[34, 35] LST has been associated with impaired re-endothelialisation, as well as induction of inflammation due to durable polymer coatings on stents, resulting in a need for prolonged dual antiplatelet therapy. Continuous development in stent design with regards to eluted drugs, stent platforms as well as polymer coatings lead to the introduction of second-generation DES (zotarolimus- and everolimus-eluting stents). These stents are characterized by thinner struts, more deliverable novel anti-proliferative agents and biocompatible polymers aiming at minimizing the vascular inflammation and accelerating vessel re-endothelialisation. Indeed, restenosis and thrombosis rate with these newer generation DES were lower in the first two years of use.[36, 37] Another development in stent technology introduced biodegradable polymers as well as fully

biodegradable scaffolds on the basis of poly-L-lactic acid (PLLA) or magnesium alloys.[38-40] The rationale behind biodegradable stents is to provide initial mechanical support as the vessel heals but to dissolve over time to restore native vessel integrity. Thus, biodegradable stents may address some of the caveats associated with metallic DES, such as LST, restenosis and impaired vasomotion of the stented segment.[41] Their safety and efficacy profile is still being evaluated in large randomised clinical trials. However, the result of the first meta-analyses of current generation biodegradable scaffolds compared with metallic everolimus-eluting stents was not in favour of biodegradable scaffolds.[42] As these are only the first generation biodegradable stents further research is required for this technology.[43]

1.1.4 DES characteristics

Since SMC proliferation with subsequent ECM accumulation is critical to neointimal hyperplasia, the design of DES focused on inhibiting SMC proliferation. Moreover, the drugs have immunosuppressive effects as they also inhibit the proliferation of immune cells. This concept has been a key advance in restenosis reduction, as previous attempts of systemic anti-inflammatory treatment have failed in humans.[27, 44] Compared with BMS, which are simply a metallic stent platform, DES consist of three components: usually a metal stent platform, a polymer coating and an antiproliferative agent. Most stents are made of stainless steel or cobalt chromium alloys releasing the drug over a period of weeks or month.[45] In Xience V®, the everolimus-eluting coronary stent system of Abbott, 80% of the drug is delivered within the first month.[46] The maximum time to everolimus disappearance from blood is seven days[47], ensuring a predominant local rather than a systemic effect.

The potent antiproliferative DES agent sirolimus and its analogues zotarolimus and everolimus act by inhibiting the activation of the mammalian target of rapamycin (mTOR), eventually causing cell cycle arrest. On the other hand, paclitaxel acts by inhibiting the disassembly of microtubules, which form the mitotic spindle during cell division, thereby inducing mitotic arrest.[48]

1.1.4.1 Molecular basis of mTOR regulation and inhibition

Cell growth and proliferation depends on the availability of sufficient amino acids and energy metabolites for protein synthesis.[49] The mTOR signalling pathway is crucial for this regulation (*Figure 2*). mTOR in complex controls protein synthesis and cell division in response to resources availability and mitogenic stimuli. The mTOR complex 1 (mTORC1) contains the highly conserved protein kinase mTOR, raptor (regulatory associated protein of mTOR) and LST8. mTORC1 targets components of the translation machinery, such as eukaryotic translation initiation factor 4E-binding protein (4E-BP). Its phosphorylation and

release by mTORC1 allows the initiation of translation. Besides nutrients such as amino acids, growth factors activate mTORC1, mainly via the phosphatidylinositol 3-kinase (PI3K) / AKT pathway. AKT activates mTOR in complex 1 indirectly by phosphorylating other upstream proteins in the cascade. The Ras/ERK signalling pathway has also been shown to activate mTORC1 signalling. Everolimus and its analogues are inhibitors of mTOR signalling pathway. The drug forms a complex with the cytoplasmic protein FKBP-12 (FK 506 binding protein).[47] The generated complex is a highly potent and specific inhibitor of mTOR, through direct binding to mTORs FRB (FKB12-rapamycin-binding) domain. Eventually the inhibition of the mTORC1 results in cell growth and proliferation inhibition.

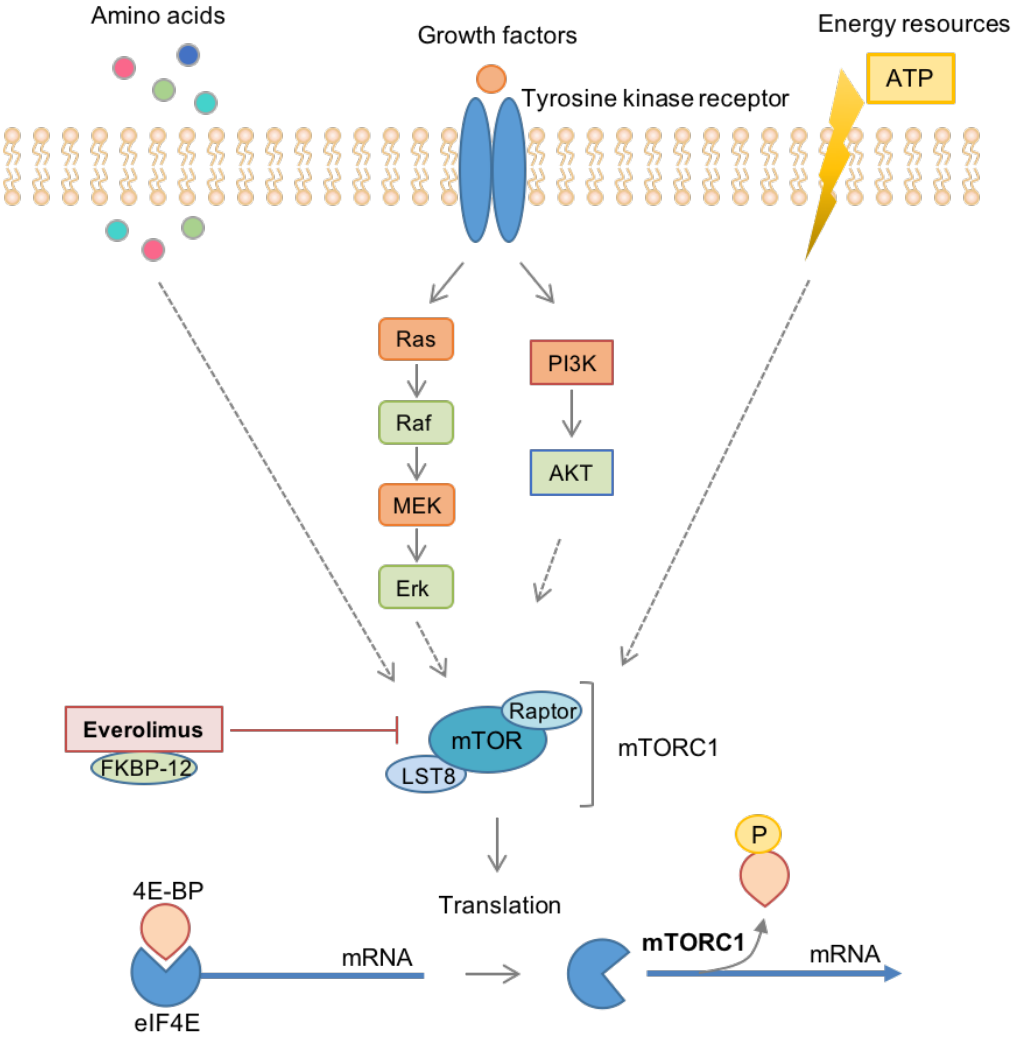

Figure 3. Simplified schematic representation of mTORC1 signalling. Mammalian target of rapamycin complex 1 (mTORC1) is stimulated in response to nutrient and energetic resources availability, as well as by growth factor signalling. Upon phosphorylation and release of eukaryotic translation initiation factor 4E-binding protein (4E-BP) by mTORC1 translation is initiated, allowing cell growth and proliferation. Everolimus and its analogues are inhibitors of mTOR signalling pathway.

1.1.5 Biology of restenosis and stent thrombosis

Stent implantation causes mechanical vascular injury, disrupting the endothelial layer in the arterial wall, which is generally previously impaired by the presence of a coronary atherosclerotic plaque. This may heal adequately over time or in case of inadequate re-endothelialisation result in restenosis or occasionally in thrombotic occlusion (LST).

Despite continuous development and improvement in stent technology, LST and especially ISR remain a considerable cause of treatment failure after PCI.[50] Large-scale angiographic surveillance studies with over 10, 000 patients estimated the restenosis rate at approximately 12% with newer generation DES.[51, 52] On the other hand, very recent randomized trials without angiographic surveillance showed rates of clinically relevant restenosis of <5% at 1 year post-stenting.[53] However, despite low ISR rates in relative terms, the absolute number of patients presenting with stent failure is still significant since stenting has become a very common procedure and their management is challenging. Overall rates of early and late stent thrombosis are even lower with 1.5%, owing to adequate antithrombotic therapy.[54]

1.1.5.1 In-stent restenosis

Angiographic restenosis is defined as luminal area narrowing of more than 50% by neointimal tissue.[50] Using intravascular ultrasound (IVUS) or optical coherence tomography (OCT), restenosis is defined as re-narrowing of more than 75% of the vessel area in cross-section, as these modalities acquire data in three-dimensions. Restenosis upon PCI is well characterized as a distinct pathophysiological process of its own entity rather than an accelerated form of atherosclerosis.[50] The contributing factors are divided in five categories: 1. prolapse of the disrupted plaque, 2. elastic recoil of the vessel wall, 3. constrictive vascular remodelling, 4. neointimal hyperplasia and 5. neoatherosclerosis. While the first three factors were mainly prevented by the introduction of stents, the latter two largely evolved due to stent-induced vascular injury with or without drugs, playing the major role in ISR development. Thus, according to the current understanding the substrate of ISR ranges from neointimal hyperplasia to neoatherosclerosis. However, stent underexpansion is also a common cause for restenosis. Finally, restenosis between BMS and DES is considerably different, not only in composition of the neointimal tissue[55], but also in the time-course of the appearance of ISR.[56]

Mechanisms of neointimal hyperplasia

Vascular stent injury with inadequate re-endothelialisation and healing results in neointimal hyperplasia. Neointima formation involves the interaction between platelets, inflammatory cells, ECs and SMCs. It can be divided into an early (days to weeks) and a

late phase (weeks to months): the early phase is characterised by platelet activation and inflammation; the late phase by SMC migration and proliferation resulting in ECM remodelling.[57] Under physiologic circumstances, the intact endothelial monolayer maintains an antithrombotic and anticoagulant surface, which is crucial for vessel patency. This monolayer is established by intercellular junctions regulating endothelial permeability. Besides the linkage of ECs with each other by transmembrane proteins such as occludin and claudin, integrins are responsible for the adhesion of the ECs to the subendothelial ECM proteins such as fibronectin and vitronectin. Both interactions are equally important for vascular integrity. Further, the endothelial surface is maintained by the production of molecules with antithrombotic properties, including but not limited to nitric oxide (NO), prostacyclin, tissue plasminogen activator, thrombomodulin, heparin-like molecules and tissue-factor pathway inhibitor.[58] As explained above, the underlying pathology for stenting, atherosclerosis *per se* is accompanied by EC dysfunction, not only in disease initiation but also in lesion progression.[59] However, upon balloon dilatation and vascular stenting the endothelial integrity is severely disrupted (complete to partial denudation of the EC layer) and the antithrombotic surface is impaired. This results in crushing and lifting of the plaque from the underlying arterial wall with subsequent exposure of the subendothelial matrix, but also in tearing and stretching of the medial wall.[60]

Thus, the initial response to mechanical damage with endothelial denudation and matrix exposure is fibrin and platelet deposition. Platelets adhere due to exposure of collagens. Histologic studies have identified fibrin-rich thrombi around stent struts one day post BMS implantation.[60] Platelet activation is accompanied by recruitment of circulating leukocytes reacting to stent struts. Their interaction is crucial for the initiation and progression of neointimal formation. Endothelial adhesion molecules such as VCAM-1, ICAM-1 and E-selectin are expressed on regenerating ECs upon pro-inflammatory cytokine release such as interleukin-1 (IL-1) or tumor necrosis factor-α (TNF-α) via the nuclear factor-κB (NF-κB) pathway.[59] These adhesion molecules induce their attachment and transmigration across surface-adherent platelets eventually aggravating vascular inflammation.[30] Notably, in stented human vessels vascular inflammation is already present due to the underlying atherosclerotic lesion. Besides platelets, leukocytes contribute to the secretion of growth factors and cytokines and induce SMC proliferation. These factors include fibroblast growth factor (FGF), insulin-like growth factor (IGF), transforming growth factor beta (TGF-β) platelet-derived growth factor (PDGF) and vascular endothelial growth factor (VEGF). Activated by growth factors/cytokines, SMC migrate from the media towards the intima and their subsequent proliferation initiates the remodelling phase. These changes require a phenotypic switch of SMCs from a

contractile to a synthetic phenotype producing excessive ECM, eventually resulting in neointimal hyperplasia.[60] A schematic illustration of the mechanisms of thrombosis and restenosis upon stent implantation is provided in *Figure 4*. The precise role of ECM in restenosis will be elucidated in section 1.2.4.2.

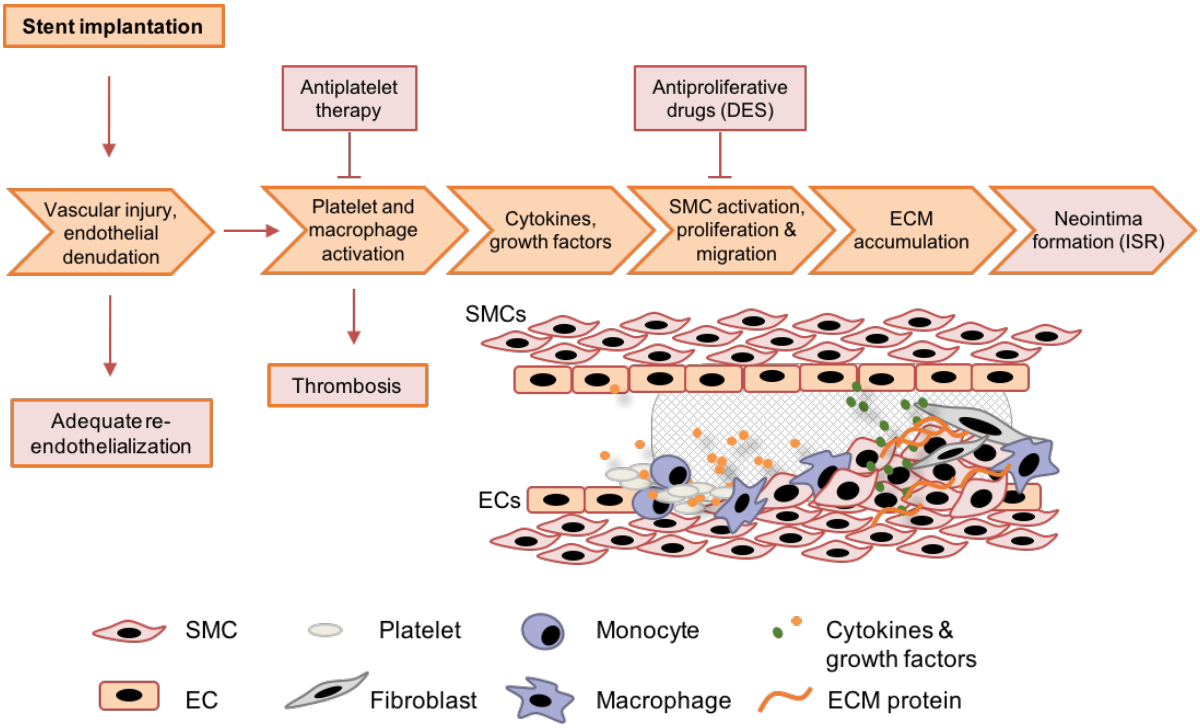

Figure 4. Mechanisms of thrombosis and restenosis upon stent implantation. Stent implantation inevitably causes mechanical vascular injury and endothelial denudation. Consequent exposure to subendothelial matrix induces platelet activation, which may result in thrombotic occlusion. At the same time excessive local inflammation is triggered, which stimulates SMC proliferation and ECM deposition leading to neointimal proliferation, thus restenosis. Antiplatelet therapy and antiproliferative agents on DES are used as preventive measures.

1.1.5.2 DES thrombogenicity

The substantial reduction of restenosis rates with DES came at the expense of increased risk for late (30 days up to 1 year) and very late (after 1 year) stent thrombosis.[35, 61] Stent thrombosis is defined as an abrupt thrombotic occlusion of a previously patent stent. It is a rare but a serious complication that can cause sudden death or acute coronary syndromes. Thus, the application of prolonged dual antiplatelet therapy following DES deployment is indicated and improves long term safety of DES as demonstrated in large clinical trials.[62] Overall rates of early and late stent thrombosis are currently low with 1.5%, owing to adequate antithrombotic therapy.[54] Premature discontinuation of antiplatelet therapy is the most important predictor for early stent thrombosis.[63]

Mechanisms of thrombogenicity of DES

The thrombogenicity of DES has been explained with delayed/impaired re-endothelialisation.[64, 65] The antiproliferative agents inhibit the proliferation of both SMCs as well as ECs, thus delaying re-endothelialisation and arterial healing. Vessels with incompetent endothelial cells, which are characterized by poor cell-to-cell junctions and reduced secretion of antithrombotic molecules, are more prone to thrombosis and neoatherosclerosis development.[58] Besides EC dysfunction and impaired re-endothelialisation, stent-induced shear stress increases thrombogenicity and inflammation.[66] Uncovered stent struts protruding into the vessel lumen alter blood flow and result in spatiotemporal changes in local shear stress distribution. High shear can activate platelets through the release of thromboxane A_2 and ADP. Additionally, durable DES polymer coatings can induce excessive inflammation and hypersensitivity reactions, which have been suggested as another cause for thrombogenicity.[65] Furthermore, recently rupture of neoatherosclerotic plaques have been associated with very LST.[56]

To overcome the limitations of ISR and LST, new DES technologies focus on development of drugs that can selectively inhibit SMC proliferation while allowing re-endothelialisation.[67, 68] Common and unique environmental cues that regulate EC versus SMC proliferation need to be explored. ECM proteins are likely to impact these processes.

1.1.5.3 In-stent neoatherosclerosis

In recent years in-stent neoatherosclerosis has been increasingly recognized as an important substrate for late stent failure for both BMS and DES, especially in the extended phase.[69, 70] Initial evidence for neoatherosclerosis came from intravascular imaging[71, 72] and histopathologic studies.[56] Neoatherosclerosis is the development of atherosclerosis in stented vessels. It is defined as the accumulation of lipid-laden macrophage foam cells within the neointima of stented arteries, with or without necrotic core formation or calcification or thrombosis.[73] Notably, the development of in-stent neoatherosclerosis has been considered independent from the underlying native atherosclerosis, as there is no communication between the neointima and the underlying lesion.[69] Furthermore, it was shown that neoatherosclerotic plaques originate and remain within the stented area and are less likely to be an extension of native disease from proximal or distal non-stented segments.[69] In a recent study, however, neoatherosclerosis was found to be more common in patients with concurrent progression of native atherosclerosis, as demonstrated with angiographic evidence during a 5 year follow-up period.[74] This finding suggests that similar pathophysiological mechanisms are at work for native and de novo atherosclerosis. The main difference between native coronary atherosclerosis and in-stent neoatherosclerosis is the time-course for lesion development. While native atherosclerosis

takes decades to develop, neoatherosclerosis is seen over a period of months to only a few years.

There are major differences in neoatherosclerosis formation between BMS and DES with regard to its incidence and temporal onset. Neoatherosclerosis seem to occur more rapidly and frequently in DES than BMS.[69] The first indication for neoatherosclerosis is considered as the accumulation of lipid-laden foam cells frequently around the stent struts. In an autopsy study the earliest time-point for their detection was four months after implantation of first generation DES (sirolimus-eluting-stent, SES), but occurred only after two years in BMS and remained a rare phenomenon up until 4 years.[56] The order for the appearance of a fibroatheroma with necrotic core was similar in both types (1 year SES vs. 2.5 years for BMS). Beside the accelerated onset in DES, the incidence of neoatherosclerosis was also significantly greater in DES (31%) than in BMS (16%).[56] Surprisingly, however, there was no difference in the incidence of neoatherosclerosis between first and the second-generation everolimus eluting stent, though the latter demonstrated a later onset with 9 months after implantation.[75]

These findings suggest a triphasic luminal response after BMS implantation, with an early restenosis due to neointimal hyperplasia, an intermediate regression upon complete healing and a late luminal re-narrowing likely due to neoatherosclerosis beyond four years.[70] On the other hand, DES show a continuous neointimal growth during long-term follow-up, after an initial suppression of intimal growth, coined the “late catch-up” phenomenon.[70]

Mechanisms of neoatherosclerosis

The precise mechanisms of neoatherosclerosis formation, and especially their accelerated onset in DES remains unknown to date and is likely to be multifactorial. However, the delayed and incomplete re-endothelialisation with impaired EC function is thought to be crucial in this process. It is suggested that the impaired barrier function is responsible for an excessive entrance of lipoproteins and subsequent macrophage infiltration into the subendothelial layer.[69, 73] Furthermore, the greater accumulation of ECM proteoglycans in DES[55] is likely to contribute to lipoprotein retention due to interactions with their GAG side chains.[14] Moreover, shear induced EC phenotype changes (mechanotransduction) with expression of adhesion molecules might further allow inflammatory cell attachment.[56] Polymer associated chronic inflammation is likely to be another contributing factor. Furthermore, the established link between platelet activation and inflammation might contribute to accelerated neoatherosclerosis in DES, since thrombogenicity is increased in DES for the reasons highlighted above. Finally, clinical risk factors have been identified for

increased neoatherosclerosis risk, such as younger age, longer implant duration and stenting for acute myocardial infarction.[56]

1.1.5.4 miRNAs in restenosis

Recent studies have shown that miRNAs are also critically involved in neointimal hyperplasia upon vascular injury.[76, 77] miRNAs are small, highly conserved noncoding RNAs, which are around 22 nucleotides long.[78] They are involved in the posttranscriptional regulation of protein expression. miRNAs act by binding to the untranslated region of mRNAs (3'UTR) with their seed region, which either induces degradation of the target mRNA or silences its translation dependent on the base complementarity. They originate from primary transcripts (pri-miRNAs) of either introns of protein coding genes, or noncoding genes, which are then processed by the endonucleases Drosha and Dicer.[79] The primary transcript is folded to a double-stranded hairpin structure, called pre-miRNA, in the nucleus and is then cleaved and unwinded to two single strands (the guide and passenger strand) upon transport in the cytoplasm. The mature miRNA strand is loaded into the RNA-induced silencing complex (RISC), which is directed to its target mRNA preventing its translation. The fact that a single miRNA can supress multiple target genes, and again the same gene can be supressed by different miRNAs, presents a challenge in untangling miRNA functions.

The importance of miRNAs in neointimal hyperplasia is mainly supported by their association with the phenotypic modulation of SMCs.[80] miR-21 induces neointimal growth through proliferative and antiapoptotic effects on SMCs.[77] miR-221 and miR-222 were also found to regulate SMC phenotype.[81] miR-143/-145 promote differentiation and repress proliferation of SMCs, thus inhibit the switch from contractile to the synthetic phenotype.[82] Similarly, endothelial miRNAs were shown to be modulated after vascular injury. miR-126, which is highly enriched in ECs, is involved in VEGF signalling and EC dysfunction.[83] A recent clinical study found that transcoronary gradients of miR-126 and miR-145 correlated with the extent of TCFAs, suggesting that instable plaques might affect the local uptake or degradation of these miRNAs.[84]

1.1.6 Animal models of coronary stenting

For coronary stenting different animal models are available including rabbit, sheep, dog and pig. While in large animals the coronary artery itself is used for stenting, in smaller animals, such as mouse and rabbit, generally the aorta is stented. The pig coronary stenting model is a gold-standard for evaluating safety, but is also useful to gain insight into biology of stenting, as it most closely simulates human disease.[60] It is the most useful and practical model.[85] However, its major limitation is the absence of atherosclerosis, which can be addressed by using genetically modified pigs with lipid alterations. The

porcine PCI model is performed in a similar way to the clinical procedure. All three arteries (the anterior descending artery, the circumflex branch and right coronary artery) can be used for stent deployment. Generally, disease-free juvenile animals weighing between 20-30kg are used for reasons of practicality, availability and cost. The nature and severity of the injury determines the vessel response.[85] For example, with balloon denudation, a superficial endothelial injury can be created or a focal deep tear with asymmetric healing and formation of a neointima. On the other hand, stent implantation imposes a long-lasting stretch upon the artery, with a more symmetrical neointima. By using deep injury with metal wire coils with an oversized high-pressure balloon a model of proliferative human restenosis is mimicked.[86] Generally, the neointima formation in the porcine model is complete by 28 days.

1.1.7 Optical Coherence Tomography

Optical coherence tomography (OCT) is a real-time intravascular imaging modality based on near-infrared light.[87] It has an excellent resolution allowing an accurate characterization of coronary artery morphology revealing vascular pathology, such as plaques and response to coronary stents. OCT image resolution (axial 10 μm, lateral 20 μm) is an order of magnitude greater than the commonly used intravascular ultrasound (IVUS) (100-200 μm), as it uses light as energy source instead of sound. However, its tissue penetration (1-2.5 mm) is lower compared to IVUS (10 mm). Currently OCT is rather utilized for research than for routine clinical practice.

Images are generated by directing a low-coherence, near-infrared light of 1.3 μm wavelength at the target tissue. Light is emitted from a distal tip of an optical fibre located within the imaging catheter and images are acquired, as the catheter is sequentially pulled back. The interferometer splits the light beam into a sample and a reference arm.[88] While the reference arm is directed to a mirror, which reflects the light directly back to the interferometer, the light of the sample arm is absorbed, refracted or reflected from the sample tissue because of its varying optical impedances. The scattered/reflected light travels back to the interferometer and interacts with the reference light. The interaction between these two light waves are then measured by the detector and determine the OCT image (*Figure 5A*). OCT requires a blood-free zone for imaging, because erythrocytes strongly scatter light, thus attenuate the image. Current instruments utilize a non-occlusive contrast flushing method to create a blood-free zone, inducing a transient ischemia. Overall, it is a safe technique with 0.2% incidence of vessel dissection due to the imaging system.[87] Also coronary spasms appear to be less than 1% when intracoronary nitroglycerin is administered prior to image acquisition.

1.1.7.1 OCT image features

The normal coronary artery is visualized with its three layers on OCT: The intima and adventitia appear as a signal-rich band with the media as an area of low signal intensity in-between. The internal and external elastic lamina can be distinctly defined as signal-rich thin bands within the dark band of the media (*Figure 5B*). OCT assessment of intimal thickness is highly accurate, allowing to detect intimal thickening due to lipid deposition as an early indication for atherosclerosis. Coronary plaques are detected by focal thickening and loss of the normal vessel architecture. While fibrous plaques produce a relatively homogenous and highly backscattering signal, calcified plaques appear signal poor with sharply delineated borders.[88] The fibrous cap is typically a homogenous signal-rich band overlying the signal-poor lipid core. The minimal thickness of the fibrous cap is relevant to determine TCFA. OCT plaque characterization of atherosclerotic arteries in autopsy samples and additional histology characterization as the gold standard revealed a high correlation in terms of sensitivity and specificity (overall agreement kappa=0.83).[89] However, false-negative diagnosis of lipid pools was frequent, which was attributed to the limited penetration of OCT. Thus, lipid pools were misinterpreted as fibrous plaques. Also OCT is prone to artefacts.[88]

1.1.7.2 OCT and restenosis

Due to its high-resolution OCT is a powerful tool for the long-term follow-up of stenting, to assess stent strut apposition, tissue coverage and neointimal growth and composition. Metal stent struts are highly reflective and generate a strong signal with shadowing behind the stent strut ('blooming'), while this is not seen in bioabsorbable stents.[87] Beyond assessing the extent of tissue coverage (neointima measure from the inner stent strut surface to the luminal surface), OCT can be utilized for the diagnosis of ISR and therapy guidance. It is well-suited to primarily distinguish precisely between the two principal causes of restenosis: stent underexpansion (for example due to undersizing or low deployment pressure) and neointimal hyperplasia.[50] This distinction is helpful to guide the therapy, as the latter is treated by repeat stenting or drug coated balloon angioplasty, while aggressive non-compliant balloon angioplasty is required for stent underexpansion.[51] Due to lower tissue penetration of OCT compared to IVUS external elastic lamina is not always well imaged hampering accurate vessel sizing. On the other hand, its better resolution allows accurate characterization of neointimal tissue, including neoatherosclerosis, which is limited with IVUS. Restenotic tissue is categorized into three main groups by OCT: homogenous, heterogeneous or layered.[90, 91] Homogenous describes the uniform high signal intensity with low back scatter, typical of areas of high SMC composition. This pattern was found to be typical for BMS restenosis.

Heterogeneous displays a mixed signal intensity, which may represent proteoglycan-rich neointimal, granulation tissue or early neoatherosclerotic plaques. Layered is seen as superficial high signal intensity and deep low signal intensity often in peristrut areas. A fourth category, 'attenuated' is likely indicative of lipid-core plaques. The last three patterns are more commonly seen in DES restenosis and may represent delayed vessel healing or neoatherosclerosis. Although systematic OCT deployment sounds attractive for ISR intervention, there is no clinical trial evidence supporting its clear advantage.[50] However, early detection of restenosis would be beneficial to optimize secondary prevention.

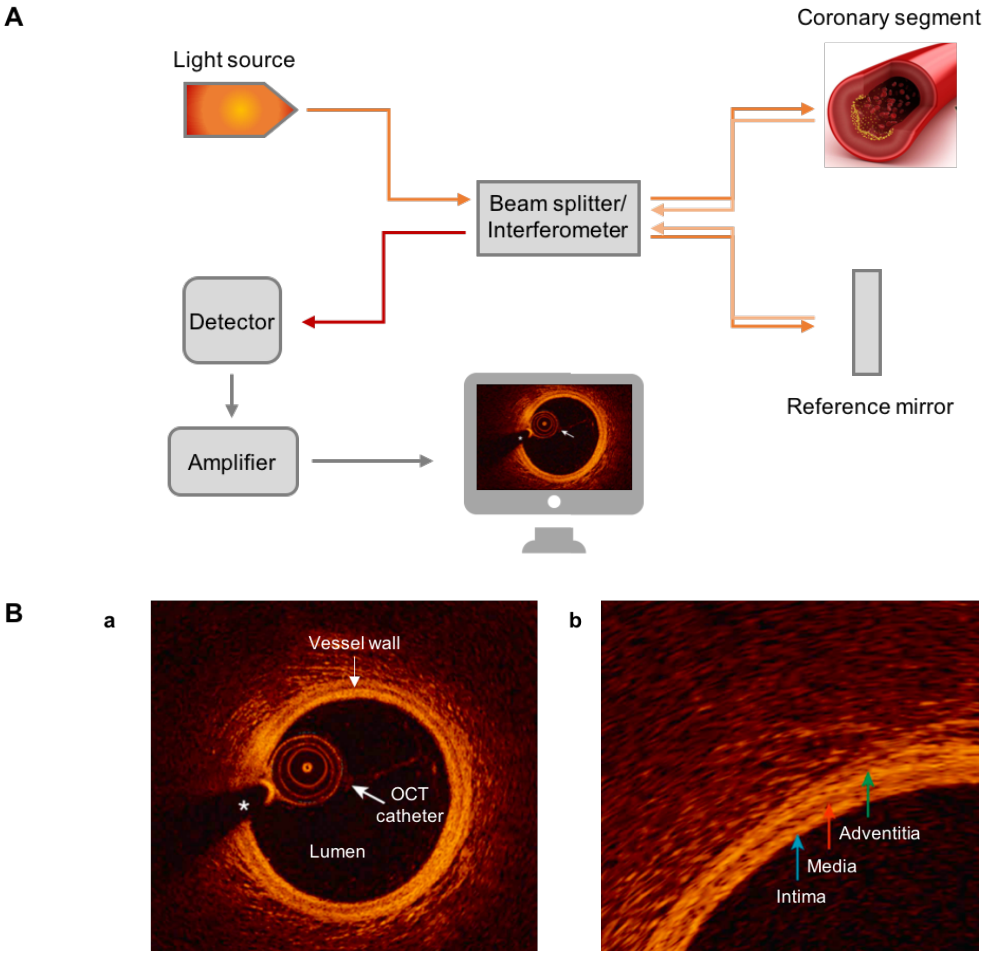

Figure 5. OCT principles. (A) The principles of OCT image acquisition are illustrated. (B) OCT image of normal coronary artery. (a) OCT catheter in overview image is marked with arrow. * indicates shadow artefact of guide wire. (b) The three arterial layers are revealed in the magnified image. Adapted from Abtahian et al. in *Cardiovascular Intervention,* 2016.[87]

1.2 Vascular ECM

1.2.1 Basic ECM features

The ECM is the highly interactive and dynamic network of non-cellular components present within all tissues. It consists of structural and regulatory proteins and is constantly remodelled to control tissue homeostasis.[92] Its composition is unique to every tissue and contributes significantly to the tissue properties. For example, the vascular ECM mainly defines the mechanical and physical properties of the vasculature. It is designed to provide elastic recoil.[93] The ECM is well known for its ability to provide structural support to tissue and organs. However, beyond their physical functions for tissue integrity, the ECM proteins play important non-structural roles in cell differentiation, proliferation, survival and migration, as well as cell-to-cell communication.[94] Importantly, the ECM is involved in binding and retention of soluble bioactive molecules including lipoproteins, growth factors, cytokines, proteases and protease inhibitors. Thus, matrix signalling regulates the microenvironment, in which the cells are embedded in.

The importance of the ECM is illustrated by the numerous pathologies related to ECM dysfunction. For the vasculature, the loss of ECM integrity is associated with weakening of the vessel wall and can even lead to its rupture in the case of aneurysms. The ECM is constantly remodelled through synthesis, degradation and chemical modification.[92] Maintaining the appropriate balance of ECM synthesis and degradation is a continuous process and needs to be tightly regulated in the vasculature. Increased ECM deposition is associated with neointimal hyperplasia and restenosis. On the other hand, excessive matrix degradation is linked to plaque rupture and aneurysm formation.

1.2.2 Composition of the vascular ECM

The vascular ECM is predominantly produced by SMCs in the vessel media, though the cells of the remaining vascular layers, namely ECs and fibroblasts also produce ECM.[95] The vascular ECM is composed of elastin, collagens, proteoglycans and glycoproteins. ECM proteins are characterized by their multidomain structure. Domains are defined as homolog sequence units and are highly conserved.[96] Individual domains may have distinct functions, and exert their function even after fragmentation. Thus, the combination of different domains provides multiple functions to ECM proteins. Moreover, due to the domain interactions the formation of fibres and other large ECM protein assemblies are favoured. Enzymatic processing of ECM proteins for example by MMPs, can release proteolytic ECM fragments with biological activity, so called 'matrikines'.[97, 98] The functional properties of ECM proteins are further altered by glycosylation (*Table 1*), the most complex post-translational modification. Beside the role of glycosylation in correct

protein folding and degradation protection, glycosylation significantly contributes to the biological functions of proteins. Glycoproteins are proteins with short glycans attached, mainly N- (asparagine) or O-linked (serine, threonine, hydroxyproline or hydroxylysine) branched oligosaccharides. On the other hand, proteoglycans consist of a core protein with large polysaccharides attached, namely GAGs.

The vascular ECM is divided into the basement membrane (BM) and the interstitial matrix. The **BM** is deposited underneath the ECs forming a sheet-like barrier between the endothelium and the underlying vascular layers. It is involved in cell adhesion, regulation of permeability as a selective barrier, control of cell growth, differentiation and migration as well as angiogenesis.[99] The BM components are mainly produced by ECs and are self-assembled on competent cell surfaces through binding interactions among its proteins.[99, 100] Collagen type IV is the most abundant BM protein, representing about 50% of its total protein content.[101] Type IV collagens assemble to a flexible, felt-like network, giving the BM its tensile strength.[102] Further BM components include collagens XV and XVIII, as well as laminins, perlecan, agrin and nidogen, which are linked in the network via their interactive domains. Remarkably, perlecan has the largest core protein of all proteoglycans (600 kDa). Notably, endorepellin, a C-terminal proteolytic perlecan fragment[103], and endostatin, a C-terminal fragment of collagen XVIII[98] inhibit angiogenesis.

The **interstitial matrix** mainly determines the mechanical properties of the vessel and consists largely of the fibrillar collagens type I and III, together with elastic fibres and proteoglycans - all of which will be discussed in the following section.

Table 1. Classification of glycosylated ECM proteins.

GLYCOPROTEINS			PROTEOGLYCANS			
Prototypical matricellular proteins	Fibers	Others	Lecticans	Basement membrane proteoglycans	Cell surface proteoglycans	Small leucine rich proteoglycans
Thrombospondin	Collagens	Fibronectin	Aggrecan	Perlecan	Syndecan	Class I: Decorin, Biglycan, Asporin
SPARC	Elastin	Laminin	Versican	Collagen XVIII	Glypican	Class II: Lumican, Fibromodulin, PRELP, Keratocan, Osteoadherin
Tenascin			Brevican	Agrin		Class III: Osteoglycin, Epiphycan, Optican
Osteopontin			Neurocan			Class IV: Chondroadherin, Nyctalopin, Tsukushi
Periostin						Class V: Podocan, Podocan-like protein 1

The cardiovascular ECM consists of structural proteins, including fibrillar collagens and elastin (grey), and ECM proteins with non-structural functions (orange). The majority of ECM proteins are capable of both functions (green). SPARC denotes “secreted protein acidic and rich in cysteine”. Adapted from Rienks et al. in *Circ Res*, 2014.[104]

1.2.2.1 Elastin

Elastic fibres in the vascular media enable vessels to recoil upon transient stretch. They consist mainly of elastin and are surrounded by a sheath of microfibrils, including the large glycoprotein fibrillin and fibulin.[105] Mutations in the fibrillin gene result in *Marfan's syndrome*, a condition linked to aortic aneurysms. Elastic fibres are deposited and organized early in development and have long half-lives (50-70 years in human arteries).[105] Since they cannot be re-organized in adulthood, their mechanical damage or proteolytic degradation results in irreversible changes. This is best demonstrated in the ageing-induced arterial stiffening, which involves the loss of the elastic fibres by normal degradation. Tropoelastin is the biosynthetic precursor of elastin and is soluble compared to elastin itself. Upon secretion, the lysine residues of the tropoelastin molecules are highly cross-linked to each other, resulting in the elastin insolubility.[106] It is this cross-linking process which confers elastin its elasticity. The ability of the large arteries to respond to the pulsatile cardiac output with an even and smooth flow is attributed to their elastic ECM composition.[93] This phenomenon, of storing a portion of the stroke volume in systole and releasing it with diastole is known as the 'Windkessel effect'. Besides providing an even flow it also helps to decrease the cardiac afterload.

1.2.2.2 Collagens

Collagens are the most abundant proteins in mammals.[102] To date there have been 28 different collagen types described.[107] Among those, type I (60%) and III (30%) collagen are the major fibrillar collagens of the vessel, constituting 90% of the vascular collagens.[106] The remaining 10% include the collagens type V (fibrillar), XII, XIV (non-fibrillar) IV and VIII (BM). Collagen fibres provide the vessel its tensile strength, which is attributed to their structure. Collagen fibre formation is a hierarchical process: in essence, individual polypeptide *chains* are assembled to *collagen* molecules, then to *fibrils* and eventually to *fibres* (*Figure 6*).

Fibrillar collagens are characterized by their triple helix structure, consisting of three polypeptide chains, known as α-chains. The chains are either identical forming homotrimers (e.g. collagen type III) or different resulting in heterotrimers (e.g. collagen type I). Each chain consists of the repeating amino acid motive Glycine-X-Y, where X and Y can be any amino acid but are often proline and hydroxyproline.[107] Collagens are produced as procollagens – a precursor form with additional C- and N-terminal propeptide extensions to prevent a premature assembly into large collagen fibrils within the cell.[102] In addition, the procollagen chains undergo extensive post-translational modifications, i.e. enzymatic hydroxylation of proline and lysine residues. Proline hydroxylation helps to form hydrogen bonds between the α-chains that stabilizes the triple-helix. The consequences

of instable triple helix formation, due to lack of proline hydroxylation is demonstrated in scurvy, a disease caused by vitamin C deficiency. Vitamin C is required for adequate hydroxylation as it is a co-factor for enzymatic hydroxylation. Upon secretion, the propeptides are enzymatically cleaved, and the collagen triple-helices aggregate into larger collagen fibrils. In addition, the collagen molecules are cross-linked (inter- and intramolecular) by the enzyme lysyl oxidase (LOX), increasing their tensile strength. Through the cross-linking, the collagen fibres also become increasingly insoluble. Finally, these fibrils are packed together in even thicker mature collagen fibres. The fibres are additionally stabilized via interactions with fibril-associated collagens with interrupted triple helices (FACIT), such as collagen type XII and XIV.[107] FACITs have a different structure to standard fibrillar collagens as they contain non-triple helical regions.

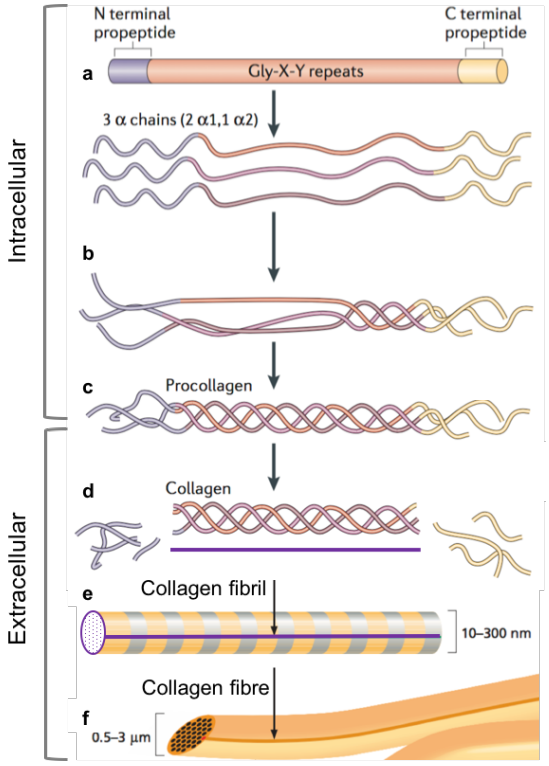

Figure 6. Fibrillar collagen structure. Collagen fibre assembly is a hierarchical process, taking place intra- and extracellularly. (a) Each α-chain consists of the repeats Glycine-X-Y and has additional propeptides. (b) 3 α-chains form a triple helix in the endoplasmatic reticulum initiated by their C-terminal propeptide. (c) The resulting procollagen is secreted into the extracellular space. (d) Propeptides are cleaved enzymatically to form mature collagen. (e) Collagens then self-assemble into collagen fibrils and finally these are organized into (f) collagen fibres. Adapted from Mouw et al. in Nature Reviews *Molecular Cell Biology*, 2014[107] and Alberts et al. in *Molecular Biology of the Cell*, 2008.[102]

1.2.2.3 Proteoglycans

Proteoglycans are distributed within the vascular interstitial matrix as well as the BM and have multiple regulatory functions within the vessel wall ranging from involvement in collagen fibril assembly[108] to growth factor binding[94]. Proteoglycans are characterized by a core protein with variable GAGs attached, which can be a single one as in case of decorin or many dozens as found in the lectican family members. They are usually attached at serine residues within the core protein through O-linked glycosylation.[102] GAGs are large unbranched polysaccharides consisting of repeating disaccharide units. Depending on the

disaccharide structure, four main types of GAGs are distinguished: (1) hyaluronan, (2) chondroitin sulfate / dermatan sulfate, (3) heparin sulfate and (4) keratan sulfate. GAGs are highly negatively charged molecules, due to their sulfate or carboxyl groups on their sugars. Thus, they attract counter-ions and draw water into the tissue, which enables the matrix to resist compressive forces. For example, this mechanism provides the basis for the viscoelastic properties of cartilage, which is enriched with the proteoglycan aggrecan.[109] Also, the negatively charged GAGs allow numerous interactions with other ECM components. Hyaluronan is the largest GAG and the only one not attached to a core protein as a side chain.[104] It is known to form non-covalently linked aggregates with proteoglycans such as aggrecan and versican. The proteoglycans within the vessel wall are the large aggregating proteoglycans (i.e. versican with hyaluronan), the small leucine-rich proteoglycans (SLRPs) and the cell surface proteoglycans (i.e. syndecan, fibroglycan and glypican).[106] The latter are relevant for anchoring and signalling between cells and the ECM mediating cell-matrix interactions.[110]

Versican is one of the principal vascular ECM components and present in all three wall layers, though prominently found in the intima and adventitia.[111] It is a large chondroitin sulfate proteoglycan (CSPG) and as such a member of the lectican (also known as hyalectin) family together with aggrecan, neurocan and brevican. Aggrecan is predominantly found in cartilage, while neurocan and brevican are mainly distributed in the central nervous system. Versican consists of two globular domains at either end of the protein and an interglobular region carrying the chondroitin sulfate attachments.[112] Due to alternative RNA splicing versican exists in at least four different isoforms (V0-V3), which differ in size and the amount of chondroitin sulfate chains. The V3 isoform lacks the interglobular domain, thus has no GAGs at all. Elucidating functional differences of the various isoforms are subject to ongoing research. Via its N-terminal G1 domain versican binds to hyaluronan stabilized by the link protein to form large aggregates. These aggregates build a reversibly compressive compartment and provide a swelling pressure within the vascular ECM.[111] Though versican plays important roles in the healthy vasculature, i.e. for cell adhesion and ECM assembly including elastic fibre assembly[112], it is substantially increased in vascular disease.[111] Accumulation of versican has been associated with restenosis and in atherosclerosis it has been implicated in lipoprotein retention.[13, 113] In contrast, a proteomics study analysing the ECM content of abdominal aortic aneurysms revealed a reduction in versican, possibly due to degradation.[114] A decrease in versican, especially its V0 isoform had been reported previously in abdominal aortic aneurysms.[115] It remains subject to debate, whether versican is the culprit in pathogenesis of vascular disease or its increased expression represents a counter-

regulatory, thus protective mechanism. Nevertheless, there is sufficient evidence for its key role in vascular pathology.[111]

SLRPs are small molecules with a core protein size of around 40 kDa. They feature leucine-rich repeats flanked by cysteine-rich domains, hence their name.[116] Based on parameters such as gene organization and sequence homologies, SLRPs are divided in five classes (*Table 1*). Prominent vascular SLRPs include decorin, biglycan and lumican. Decorin and biglycan are crucially involved in collagen fibril formation. However, they have also important matricellular functions influencing cellular proliferation, differentiation, survival and adhesion, as they interact with numerous proteins.[117] Decorin is an important anti-fibrotic agent, as it inhibits TGF-β and interacts with connective tissue growth factor (CTGF).[118]

1.2.2.4 Integrins

Integrins, although not regarded as ECM proteins *per se*, are important ECM-associated glycoproteins, as they connect the matrix to the cell cytoskeleton.[119] Integrins are a diverse family of heterodimeric transmembrane cell adhesion receptors with at least 24 members, composed of an α- and β-subunit.[120] The extracellular domains of integrins are connected to the ECM glycoproteins laminin, fibronectin and vitronectin as well as collagens. However, integrins are not simply adhesion molecules, but act as true signalling receptors. Upon binding their ligands, they can transmit signals in both directions, and impact many aspects of cell behaviour from survival to migration and proliferation. Further, integrin-mediated adhesion is involved in transmitting physical forces into intracellular biochemical signals, a process known as mechanotransduction.[121] Besides ECM proteins, other ligands for integrins include members of the immunoglobulin superfamily such as ICAM-1 on ECs, which are expressed upon pro-inflammatory cytokine release. Thus, through this earliest induction of inflammation, integrin signalling is also involved in the pathogenesis of atherosclerosis.[122] Notably, integrin αIIbβ3, which binds to fibrinogen, is involved in platelet aggregation and as such acts as a prominent anti-thrombotic drug target, inhibited by the antibody fragment abciximab.[123]

1.2.3 ECM degradation

Vascular cells constantly remodel their surrounding ECM for migration, proliferation or just adaptation to external stimuli. Moreover, ECM degradation is required for the release of biologically active molecules such as growth factors.[94] The turnover of the vascular ECM is usually a slow, continuous process, as mature collagen and elastic fibres are degraded only in small amounts.[106] However, in processes such as tissue repair or in vascular diseases the ECM is rapidly degraded. Degradation is achieved by extracellular

proteolytic enzymes (proteases), most notably the family of matrix metalloproteinases (MMPs) or adamalysins, a family of proteases comprising the a disintegrin and metalloproteinases (ADAM) and a disintegrin and metalloproteinases with thrombospondin motifs (ADAMTS). But also other proteases such as the cathepsins contribute to ECM degradation.

Naturally, ECM degradation needs to be tightly regulated to prevent increased and uncontrolled ECM loss consequently compromising tissue integrity. Besides transcriptional control of proteases, one control mechanism includes the secretion of inactive precursor proteases – so called zymogens, which are locally activated when needed. Another mechanism is to specifically inactivate the proteases with inhibitors, such as tissue inhibitors of metalloproteases (TIMPs).

1.2.3.1 MMPs

MMPs are supposed to be the major protease family involved in ECM degradation.[92] Collagenases and elastases mainly belong to the MMP family. To date 23 MMPs have been described, each generally specific for multiple target substrates. For example, MMP9 not only cleaves the collagens type IV, V, VII and X, but also elastin and fibronectin. MMPs are multidomain enzymes containing a pro-peptide, a catalytic domain and a C-terminal haemopexin-like domain, involved in substrate specificity. For their activity MMPs depend on zinc as a cofactor, hence belonging to the superfamily of zinc-based proteases, the metzincins. Commonly MMPs are secreted as zymogens and are activated upon proteolytic cleavage of the propeptide, which reveals their zinc bound catalytic domain. MMPs are either soluble or attached to the cell membrane such as MMP14. Upon secretion the inactive MMPs can bind to their substrates, forming a reservoir that can be activated upon demand by their catalytic activation.[110] The relevance of MMPs for ECM remodelling is underpinned by the finding that circulating MMPs may identify patients at greater risk of developing ISR following DES deployment.[124] Significant elevations in MMP-9 levels at baseline and MMP-2 and MMP-9 levels 24h post-PCI were associated with ISR development.

1.2.3.2 Adamalysins

Adamalysins are another family within the zinc-based proteinases and include the ADAMs and ADAMTS, which have additional thrombospondin motifs. ADAMs are largely cell membrane-associated metalloproteinases and about half of the known 21 human ADAMs possess proteolytic activity. They play a relevant role in cell signalling, as they cleave transmembrane protein ectodomains releasing cytokines and growth factors.[125] Moreover, ADAMs are involved in cell-adhesion, as their disintegrin domains can interact with integrins and syndecans on neighbouring cells.[126] They also contribute to cell-matrix

interactions, by binding fibronectin or laminin (e.g. ADAM13). However, certain ADAMs (e.g. ADAM10, ADAM15) also exhibit collagenase activity, thus degrade the ECM.

In contrast, the ADAMTS are secreted metalloproteinases and the ADAMTS family comprises 19 members to date.[127] Their common domain organisation includes a signal peptide, a propeptide, a zinc bound catalytic domain, a disintegrin-like domain, a central thrombospondin repeat, a cysteine-rich domain and a spacer domain (*Figure 7*). Moreover, all ADAMTS, except ADAMTS-4 have additional thrombospondin motifs. Like MMPs, the cleavage of the ADAMTS propeptide is required to gain enzymatic activity. Convertases such as furin or furin-like enzymes are involved in this activation process. ADAMTS-13, however, cleaves von Willebrand factor and has been shown to be enzymatically active even without the cleavage of its relatively short pro-domain.[128] ADAMTS-1, -4, -5, -8, -9, -15 and -20 are the proteoglycan degrading enzymes. Degradation of proteoglycans, including the large aggregating proteoglycans, appears to be their major ECM-related function. Due to their cleavage of aggrecan, ADAMTS-1, ADAMTS-4 and ADAMTS-5 are also referred to as aggrecanases, with the latter two showing the highest activity. Furthermore, ADAMTS-2, -3 and -14 are involved in processing of procollagen to collagen by cleaving the N-terminal propeptide of procollagen.[129]

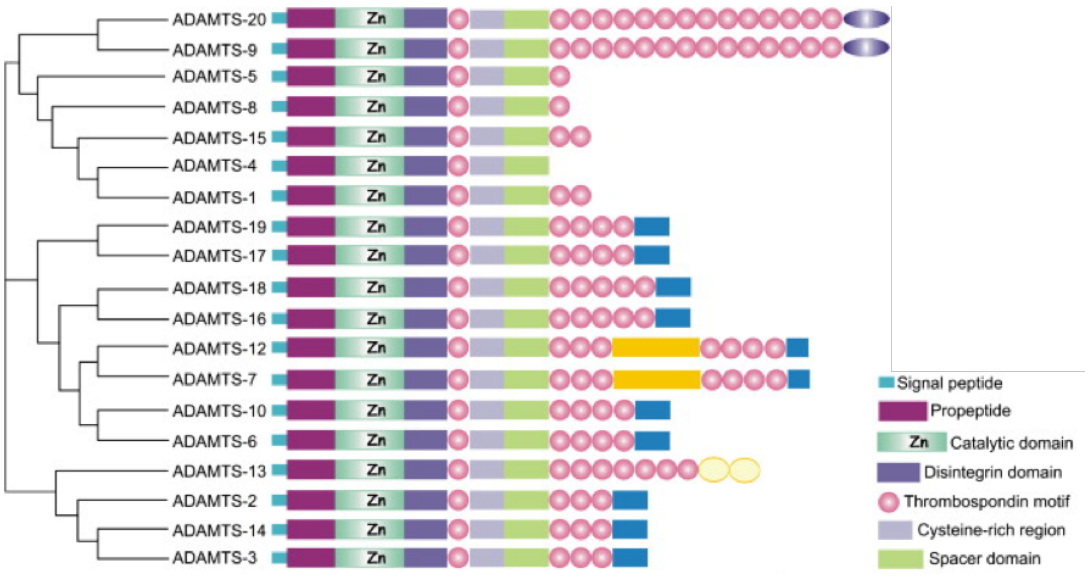

Figure 7. Domain structure of the ADAMTS family. Also phylogenetic analysis of the family members is shown. Adapted from Stanton et. al in *Biochimica et Biophysica Acta*, 2011.[127]

1.2.3.3 TIMPs

TIMPs are specific metalloproteinase inhibitors allowing control of protease activity. Four TIMPs (TIMP-1 to 4) have been identified in human to date.[130] They are relatively small molecules that bind to the activated enzymes blocking their activity. TIMPs inhibit all

MMPs with various specificity. It has been shown that SMCs of normal arteries constitutively produce MMP-2 (specific for collagens, elastin and fibronectin), but also TIMP-1 and TIMP-2. However, no enzymatic activation is detectable, suggesting its tight control by the inhibitors.[131] Notably, TIMP-3 is a better inhibitor of ADAMTS than for MMPs.

1.2.4 ECM remodelling in vascular disease

As stated in the introduction, in physiological conditions ECM degradation and re-synthesis is in a steady-state to maintain vessel wall integrity. It is obvious, that metalloproteinases are important in vascular repair processes, but excess activity is harmful for vascular integrity.[132] On the other hand, increased ECM deposition is the vessel wall is associated with neointimal hyperplasia. Thus, ECM dysregulation is implicated in almost every vascular disease including atherosclerosis, aneurysms[133], varicose veins[134], diabetic vasculopathy[135] and restenosis, which is of particular interest for this study.

Inflammatory cells, including lymphocytes, monocytes/macrophages but also neutrophils, infiltrate the vessel wall upon vascular injury. They are an important source of proteases degrading the vascular ECM.[136] Also, cytokines and growth factors released by inflammatory cells, such as TNF-α, IL-1 or PDGF have been shown to stimulate MMP synthesis in SMCs[137, 138], which is likely associated with the secretory switch in SMCs. In general, in vascular pathology and healing there is an interplay of ECM proteins and inflammation, as ECM components modulate immune reactions. For example, upon injury low molecular weight fragments of hyaluronan are generated, which are known to induce proinflammatory signalling in macrophages via Toll-like receptor (TLR) 4 and TLR2.[139] Thus, their clearance through a CD44-dependent signalling contributes to resolution of inflammation. On the other hand, proteases released by inflammatory cells or activated SMCs generate active ECM fragments, with impact on chronic inflammation.[140]

Regulation of SMC differentiation and ECM synthesis

As mentioned above (section 0), vascular SMCs de-differentiate upon injury, thus undergoing a phenotypic switch.[141, 142] Usually SMCs in the blood vessel are quiescent cells with low proliferation rate and low ECM synthetic activity. Their main function is to contract and regulate the blood vessel tone, also in response to EC-derived NO. They are characterized by the expression of contractile SMC makers, such as smooth muscle α-actin (SMA), myosin heavy chain (MYH11), calponin (CNN1) and transgelin (TAGLN). However, unlike skeletal or cardiac myocytes, SMCs are not terminally differentiated and are highly plastic cells. In response to environmental cues they can de-differentiate to

become migratory, hyper-proliferative and synthetic. This change plays a relevant role in the pathophysiology of atherosclerosis[15, 143] or restenosis[60] and is associated with ECM accumulation. However, SMC differentiation is not only limited to two states. The SMC phenotypic switch includes also an osteoblast-like phenotype, as seen in vascular calcification[144], but also a macrophage-like phenotype, as described in recent lineage tracing studies and mentioned above (section **Error! Reference source not found.**).[145, 146] The mechanisms, which control SMC plasticity are not entirely understood. However, there is evidence that factors such as PDGF, TGF-β as well as MMPs are actively involved in this process.[142] In addition, MMP2 can release and activate TGF-β itself from its inactive complexed form with the latency associated peptide (LAP) and latent TGF-β binding protein (LTBP).[147] Downstream involved factors include myocardin and Kruppel-like factor 4 (KLF4). Recent studies, have also implicated a role for microRNAs in the control of SMC de-differentiation as described above.

1.2.4.1 ECM remodelling in atherosclerosis

ECM remodelling in early atherosclerosis contributes to lipid retention, as described above for proteoglycans, especially versican.[13] This is further supported by a study which showed that SMCs expressing the versican V3 isoform, hence lacking GAGs, are forming a matrix, which is resistant to lipid deposition and macrophage accumulation despite hyperlipidemia.[148] However, plaque stability in advanced atherosclerosis is also strongly influenced by ECM remodelling.[149] Fibrillar collagens, particularly type I, are the major components of the fibrous cap.[150] As they provide tensile strength, they seem to be crucial in stabilising the plaque. Thus, local MMP overexpression in the vulnerable shoulder regions derived from macrophages and SMCs provides a potential explanation for plaque destabilization through weakening of the ECM.[131, 136] Notably, MMP 9 in particular, has been linked to acute coronary syndromes.[151] Moreover, ADAMTS-1 has been implicated in atherosclerosis.[152] ADAMTS-1 expression was reported to be upregulated in plaques of a mouse model of atherosclerosis. The authors concluded that ADAMTS-1 may be involved in atherogenesis by promoting SMC migration through the cleavage of ECM proteins, such as versican. Further evidence for an involvement of ADAMTS-1 in plaque destabilization, came from a histopathological study investigating coronary atherectomy specimens obtained from patients with acute myocardial infarction (AMI) or stable angina.[153] ADAMTS-1 was more strongly expressed in AMI plaques than in stable plaques and co-localized with macrophages, suggesting its role in plaque instability. No differences were detected for ADAMTS-4 and 5 between the two groups. Finally, ADAMTS-4 and ADMATS-8 were shown to be expressed in macrophage-rich areas of human atherosclerotic plaques.[154] This suggests, that macrophages are a major source of

these two proteases in plaques. Their expression was found to be inflammatory regulated and induced upon monocyte to macrophage differentiation. In addition, ADAMTS-4 expression was strongly upregulated during atherosclerosis development in mice. However, the exact role of the ADAMTS enzymes in atherosclerosis, especially their impact on the development of atherosclerosis is still unclear and needs to be further elucidated.

1.2.4.2 ECM remodelling in restenosis

The ECM accounts for >50% of the neointimal volume in restenotic lesions as shown in stented human coronary arteries in histopathological studies.[155] Despite this large portion, the ECM composition and organization is not well characterized, especially not using a holistic approach at the protein level. Within the developing stent-induced neointima, ECM proteins modulate crucial processes including cell adhesion, proliferation and migration, as well as growth factor expression resulting in vascular remodelling. Farb et al. found that in the early neointima, a thin provisional ECM is formed consisting of fibrin, fibronectin and water entrapping matrix proteins such as versican and hyaluronan as an initial response to stent injury. This initial ECM environment allows inflammatory cells to adhere and begin the repair process. Further secretion of proteoglycans by SMCs stabilize the fibrin-enriched ECM, providing viscoelasticity to the healing tissue and allowing more SMCs to bind and proliferate. Therefore, the initial neointima remains hypercellular and rich in type III collagen, versican and hyaluronan. Increased versican accumulation during the initial period of one – three months upon coronary angioplasty has also been reported in previous studies[156], thus supporting the findings of Farb et al. Further, Farb et al. revealed that over time, MMPs released by inflammatory cells progressively degrade hyaluronan. In addition, partial reabsorption of type III collagen and synthesis of type I collagen, decorin and biglycan allow wound healing with cross-linking of type I collagen. Cross-linked collagen inhibits SMC proliferation, resulting in a cell-depleted, but collagen- as well as proteoglycan-rich ECM.[60, 155] Similarly Chung et al. found, again using histopathological methods, that neointimal lesions beyond two months upon stent implantation, consist primarily of large amounts of proteoglycan-rich ECM and are rather cell poor.[157] However, a more recent study comparing the neointimal characteristics in restenotic DES vs. BMS beyond one year implant duration revealed greater proteoglycan content and less SMCs over time in DES, while BMS showed a greater cell density and collagen deposition.[55]

Moreover, the study of Chung et al. found 80% TGF-β1 positive staining in the in-stent restenotic tissue[157], which is likely to influence the ECM accumulation in restenotic lesions[158] – TGF-β1 is known to regulate the synthesis and turnover of various ECM components such as proteoglycans, hyaluronan, fibronectin and collagen. Thus in a

pharmacological animal study, Backes et al. intended to target TGF-β induced matrix deposition to prevent restenosis using pirfenidone.[159] The exact mechanism of action for pirfenidone is not fully understood yet, however it has been demonstrated to inhibit primarily TGF-β induced collagen synthesis. Indeed, neointima formation in rats treated with pirfenidone upon balloon injury of the carotid artery was strongly reduced compared to controls. Cell proliferation was unaffected by the drug (as indicated by PCNA staining), however collagen deposition (picrosirius red) was markedly reduced, suggesting a primary effect on ECM synthesis. Indeed, the FDA has only recently (October 2014) approved pirfenidone (Esbriet) for the treatment of idiopathic pulmonary fibrosis[160], upon positive effects in randomized, placebo-controlled phase III trials.[161] However, despite promising results in this preclinical study of Backes et al., a current PubMed search (September 2016) did not reveal any follow-up studies using pirfenidone on coronary stents. The same is true for dichloroacetate, that has also been shown to reduce neointima formation by preventing hyperpolarization of the mitochondrial membrane potential.[67]

1.3 Proteomics

1.3.1 Introduction into proteomics

1.3.1.1 Proteomics as part of systems biology

Biological processes are by no means linear systems, but rather represent dynamic networks with crosstalks of their components at multiple levels. This concept is best expressed in the research field of systems biology or the omics technologies. Systems biology uses a systematic, holistic, rather than the traditional reductionist approach studying one gene or protein at a time, to reveal the mechanisms and interactions in biological systems in an unbiased way. Omics experiments has only become feasible with the advent of high-throughput technologies to analyse vast amounts of data. Particularly genomics with the *Human Genome Project* paved the way to systematic high-throughput sciences.[162] Proteomics, aiming to deliver a "protein complement of the genome" evolved as an essential part of systems biology.[163] Since its introduction proteomics research has grown rapidly, also reflected in the increasing number of publications (currently >6000 publications each year[164]) and establishment of journals serving this research field such as *Proteomics*, *Journal of Proteomics, Journal of Proteome Research* or *Molecular and Cellular Proteomics*.

1.3.1.2 Proteomics – Definition and challenges

The term "proteome" was first introduced in the mid 1990s in analogy to the term "genome" and refers to the entire set of proteins produced by an organism, tissue or cell at any given time.[165, 166] Proteomics is the large-scale study of the entire proteome including protein isoforms and modifications, their abundance and structure as well as the interactions between them.[167] Thus, the overall aim of proteomics is to contribute to a comprehensive description of cellular function. Proteomics is particularly suited for this, since proteins are the major effector molecules in every biological process ultimately determining the phenotype of a cell. Therefore, by systematically analysing proteins, proteomics bears great potential for the identification of novel prognostic and diagnostic targets (biomarker discovery). Also, it holds promise towards better patient stratification.[19, 168]

Previous achievements of genomics were essential for progress in proteomics, providing the 'blueprint' of potential gene products. Unlike genomics studies however, proteomics is characterized by a higher degree of complexity and dynamics.[163] The relationship between the genome and proteome is not linear, i.e. the concept that one gene encodes one protein does not apply. Post-transcriptional control such as RNA

editing and alternative splicing results in a greater protein diversity. Moreover, only a certain set of genes are transcribed in a cell at a given time point in response to environmental cues. Further complexity is added by post-translational modifications (PTM), such as glycosylation or phosphorylation, as well as protein degradation. In addition, what renders proteomics most challenging are the detection of very low abundant proteins which have to be quantified in the excess of other proteins. The dynamic range of protein concentrations in a sample often exceeds the resolution capacities of proteomics technologies (currently 4-6 orders of magnitude). Especially the plasma proteome represents a major challenge, spanning ten orders of magnitude.[169] Unlike PCR, proteomics techniques lack the ability to amplify their targets upon detection. Thus, proteomics strongly relies on enrichment and subfractination of complex samples. For example, extracellular matrix (ECM) proteins, which are less abundant than cytosolic or mitochondrial proteins in the heart are less likely to be identified when whole tissue lysates are analysed. Thus, methods enriching for ECM proteins can overcome this issue.[114, 170] Therefore, appropriate sample preparations are essential for reproducible proteomics experiments. Another example is the depletion of the highly abundant plasma proteins albumin or the immunoglobulins.[171] (Another approach to tackle the great dynamic range of the plasma proteome is to shift biomarker discovery approaches from plasma to tissue-based proteomics. In the affected tissues, the potential biomarkers are less dilute and their cellular origin is less uncertain.[172] Finally, technological advances in proteomics instrumentation, mainly mass spectrometers (MS) and analysis techniques are contributing to overcome these difficulties, such as targeted proteomics or data-independent analysis (DIA) methods which will be discussed in the subsequent sections.

1.3.1.3 Proteomics vs. traditional biological research

Traditional biochemistry approaches using the workhorse techniques such as Western blotting or microscopy focus on single known proteins at a time highlighting only a limited part of interconnected protein networks.[173] Notably, these techniques are based on *a priori* assumptions on the proteins of interest and rely on the availability of antibodies. Though antibodies usually exhibit great specificity, their use is associated with notorious limitations such as epitope masking, non-specific binding or cross-reactivity between species. In contrast, untargeted proteomics research is not constrained by *a priori* assumptions but provides an unbiased comprehensive analysis of the protein composition in a sample. Thus, untargeted proteomics is less a hypothesis-driven but rather a discovery-based approach. On the contrary, the unbiased findings of proteomics studies often trigger the formulation of new hypotheses, consequently being also referred as “hypothesis-generating” strategies.[174] Taken together, proteomics does not replace, but is highly

complementary to traditional biological research, providing an opportunity for genuine progress in biological research.

1.3.2 Proteomics applications

1.3.2.1 Proteomics experiments

Three major types of proteomics analysis exist.

Firstly, proteomics is used for compositional analysis, which simply aims to identify all proteins present in a sample.

Secondly, proteomics enables characterization of protein-protein interactions. This is mainly accomplished by affinity purification coupled to mass spectrometric (AP-MS) identification. For this purpose, the protein of interest ("bait protein") together with its interaction partners is captured with a ligand coupled to a solid-phase support and subsequently analysed by proteomics techniques.[175] As targeting ligands often antibodies (immunopurification) or epitope tags are used, after the tag of choice, such as a His-Tag or FLAG is fused to the protein of interest on the DNA level. Main limitation of this application is the co-purification of non-specific interactors, so called "background contaminants", due to their unspecific binding to the solid phase, antibody or epitope tag. Thus, appropriate controls are necessary: such as utilizing the same isotype antibody, an antibody recognizing a different epitope or AP in the absence of the bait. A contaminant repository, the "CRAPome", a freely accessible database containing common background contaminants for the scoring of true protein-protein interactions has been established.[176]

Lastly, the main area of application for proteomics is differential protein expression profiling in response to biological perturbations. In this approach, quantitative protein changes between two or more different, well-defined conditions, such as control and diseased samples, are compared. However, differential regulation is not only reflected in protein abundance, but might also be expressed in differential post-translational modification. This type of proteomics experiments are the typical settings for discovery projects such as biomarker discovery. For example, a protein found increased in diseased samples may serve as a useful diagnostic marker or a drug target. In a second step, after identifying the significantly differential expressed proteins, these putative candidates are mostly validated in larger sample cohorts to assess their reproducibility in larger populations.

1.3.2.2 Proteomics workflow

A typical proteomics study involves the following steps (*Figure 8*):

1. As any other study also proteomics starts with a well-conceived **experimental design** (sample size, group balance, degree of biological variation, etc.). It would be

wrong to assume that proteomics experiments can be implemented with a premature plan, since untargeted proteomics is a hypothesis-generating approach. On the contrary, proteomic analysis are very laborious and expensive and most notably they generate vast amounts of data. Thus, without a precisely formulated question, the data interpretation can be very cumbersome and conclusions may not be drawn reliably.

2. **Sample preparation** is paramount for accurate and reproducible proteomics analysis. This already starts with appropriate sample collection, handling and storage conditions. For example, immediate sample freezing upon collection or treatment with protease inhibitors upon thawing is crucial to prevent protein degradation. Protein extraction from a biological sample can be managed in a single step or subfractination methods can be applied. This is performed for better protein solubility as well as reducing sample complexity or to study a specific subproteome as described above.[177-180] Further sample preparation requirements such as protein labelling, denaturing, reduction or enzymatic digestion are dependent on the method chosen for protein analysis and will be discussed throughout the respective sections.

3. Due to sample complexity further **sample separation** steps are required prior to analysis. This is necessary to overcome undersampling of low-abundant peptides/proteins, because failing that, the analysers are dominated by high-abundant peptides/proteins. This can be achieved by methods such as one- or two-dimensional gel electrophoresis (1-DE, 2-DE) or high-performance liquid chromatography (HPLC). Due to rapid advances in MS technology, laborious gel electrophoresis methods are more and more receding, even though 2D gels have a very high resolution capacity. On the other hand, HPLC separation is standard procedure in proteomics, mainly because of the switch from protein to peptide-based proteomics. The most commonly applied chromatography for proteomics is reversed-phase LC using C18 columns. The separation is based on physico-chemical interactions of the proteins/peptides with the C18 residues on the stationary phase, the column. Depending on their hydrophobicity level and the gradient of the mobile phase with increasing organic content the peptides/proteins elute at different time points from the column, resulting in different retention times for each peptide/protein.

4. Separation is followed by **mass spectrometric analysis**, the actual measurement of the sample. MS is the workhorse of modern proteomics and brought the most significant breakthrough in proteomics research. Current MS have exceptional mass accuracy, resolution and detection sensitivity (dynamic range), reaching to attomole amounts.[181] However, as explained above the true sensitivity of MS is determined by the nature of the sample.[182] Moreover, MS analyse multiple proteins at the same time and offer automation, thus high throughput.[183] The mass spectrometer determines the mass-

to-charge ratio (*m/z*) of an ionized molecule generating large amounts of MS spectra. A detailed description on MS principles and instrumentation will be given in section 1.3.4.1

5. Next step in the workflow is **data analysis** for **protein identification and quantification**. After all, MS simply measures the *m/z* of a protein/peptide. So how is the protein sequence retrieved ultimately? The unambiguous identification of the actual protein occurs after correlation of the MS spectra to a database with the assistance of software tools and scoring algorithms.[184] Considering the amount of generated data, this is only possible with automated software solutions. Even though the single spectra are not manually matched anymore, this is still a very time-consuming part of proteomics analysis together with the subsequent data interpretation. The exact sequence determination process as well as quantification will be discussed in section 1.3.5.3

6. **Validation** is the final workflow step, which especially applies to differential expression proteomics studies. It is important to realize that a proteomics experiment does not finish with the identification of differentially expressed proteins, but requires extensive validation. First of all, a major challenge in data interpretation is to discern those proteins with functional relevance from the many other differentially expressed proteins. Thus, a solid biomedical knowledge is beneficial to select the target proteins for follow-up studies. Usually independent techniques, such as Western blotting or immunohistochemistry, are applied to validate the proteins of interest. Targeted proteomics is also gaining importance as a robust system to validate findings from discovery based approaches, as will be explained in section 1.3.8. Moreover, results of discovery projects can be validated by analysing larger sample cohorts. Finally, detailed physiological analysis is needed to decipher the role of a putative candidate in biological processes. These analyses can range from *in vitro* studies to the generation of knock out animals. However, this may not be easily manageable for a single laboratory but might require collaborations with specialized laboratories all around the world to provide appropriate equipment or knowledge.

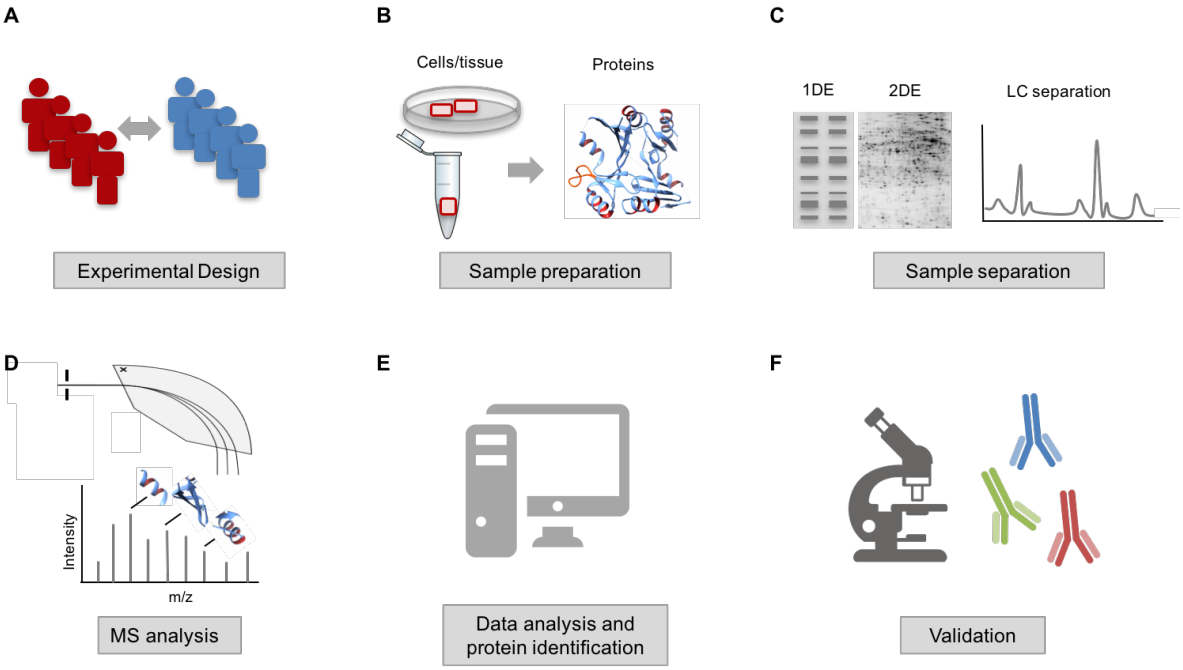

Figure 8. Proteomics workflow. Proteomics analysis involves multiple progressive steps. (**A**) A well-conceived experimental design is crucial for proteomics experiments, especially for reliable data interpretation later. (**B**) Protein extraction is critical as subfractination is required to detect low abundant proteins. (**C**) Sample complexity and undersampling is further reduced by sample separation (gel separation, LC), prior to MS analysis (**D**). (**E**) Detected proteins are identified upon computational spectrum matching. (**F**) Finally proteins of interest are validated by independent techniques, such as immunoblotting or immunohistochemistry.

1.3.3 Two-dimensional gel electrophoresis

Even though advances in mass spectrometry are widely replacing gel-based proteomics techniques, 2-DE is still in use, owing to its unique separation power. It allows the resolution of more than 10 000 proteins on a single gel.[185] Since its introduction in 1975,[186, 187] the technique has been widely refined, the general principle however is the same: proteins are separated in two dimensions, first based on their isoelectric point and second by their molecular mass using SDS-PAGE. Due to the use of 2 separation dimensions, 2-DE gels have a higher resolving capacity than 1-DE (SDS-PAGE). In the first dimension proteins are separated by the concentrating technique of isoelectric focusing (IEF). The sample is loaded onto a strip with an immobilized pH gradient (IPG). These strips consist of acidic and basic buffering groups covalently linked to the gel matrix generating a pH gradient. Wide pH gradients of 3-10 are used for an overview of protein composition, while narrow-range IPF strips of 3 pH steps provide a better resolution for unambiguous protein identification.[188] Upon application of an electric field, proteins migrate according to their intrinsic charge until they reach the pH at which their overall charge is neutral – their isoelectric point. This migration results in focused, discrete protein

bands on the strip. This strip is then placed on a large SDS polyacrylamide gel for separation in the second dimension. Proteins now migrate orthogonally to their previous movement according to their molecular mass. Thus, 2-DE gels produce a complete map of intact proteins in form of multiple “spots”. The spots are visualized by Coomassie, zinc, silver or fluorescent staining, with silver being the most commonly applied. Immunodetection or radiolabelling are also used. Following staining, gel images are digitalized and the spots are detected and directly quantified using densitometry. Spot patterns between multiple gels are compared for differential expression with the help of image analysis software, providing automated spot-detection.[189] However, visual inspection is still essential. Spots of interest are excised and the proteins are identified by mass spectrometry. Same proteins can be detected in different spots, since post-translational modifications, isoforms or degradation products cause a shift in isoelectric point and molecular weight. Unlike other proteomics techniques, quantitation with 2-DE is performed directly on the gel at the protein level and not after identification by mass spectrometry.

1.3.3.1 2D DIGE

Technical irreproducibility due to gel-to-gel variation remains the main limitation of 2-DE gels. A significant improvement was achieved with the introduction of the more sophisticated two-dimensional difference gel electrophoresis (2D DIGE) technique.[190] This technique allows the comparison of two or three protein samples simultaneously on the same gel, thus limiting experimental gel-to-gel variation. This is achieved by labelling the proteins of each sample with a different fluorescent Cy-dye (Cy2, 3 and 5), which are designed not to interfere with the migration properties of the labelled proteins. The differently labelled samples are then mixed together in equal amounts and run on the same gel in two dimensions. Often a differently labelled pool of all experimental samples is included serving as an internal standard for normalization. Proteins common to both samples appear as spots with a common fluorescent signal due to overlay, while the differentially expressed proteins emit the signal of their own labelled fluorescent dye. The gel is analysed using a fluorescent gel imager (scanner- or camera-based system) detecting the emission wavelength of each Cy-dye, which can have an integrated spot-picking robot. Again, software packages such as DeCyder are deployed to determine the differential spots to be picked. DIGE is capable of reliably quantifying protein differences as low as 15% over a protein concentration range of over 4 orders of magnitude.[191] However, despite its high sensitivity and improved reproducibility the limited resolution of hydrophobic proteins such as transmembrane proteins (causing precipitation during IEF) and very large or small proteins remain a caveat of this technique. Interference from high-

abundant proteins is a further limitation. Last but not least, image analysis and spot picking can be a very tedious process representing a bottleneck in the entire process.

1.3.4 Mass spectrometry based proteomics

1.3.4.1 MS principles and instruments

MS is the main driver of proteomics research. It determines the *m/z* of an ionized molecule. The measurement is carried out using electromagnetic fields in a vacuum. Thus, peptides/proteins first need to be transferred from the liquid into the gas phase (volatized) and electrically charged (ionized). This is accomplished using matrix-assisted laser desorption ionization (MALDI) or especially electrospray ionization (ESI).[192, 193] It was the advent of these techniques that MS became applicable for proteomics analysis, and for which (ESI) John B. Fenn and Koichi Tanaka were awarded the Nobel Prize in Chemistry in 2002. MALDI sublimates and ionizes the samples out of a dry, crystalline matrix via laser pulses.[194] Surface-enhanced laser desorption ionization (SELDI) is a variation of MALDI, where proteins are bound to a surface with a substrate, which allows contaminants being washed away.[195] In contrast, ESI ionizes proteins/peptides directly out of a solution by application of high voltage to the liquid and is therefore readily interfaced with LC. Thus, ESI-MS coupled to LC is the method of choice for the analysis of complex samples. Peptides are typically doubly protonated by ESI.

In simple terms, mass spectrometers consist of 3 parts: (1) an ion source as explained above, (2) the mass analyser(s) and (3) a detector. The mass analyser is the central part of an MS in determining the *m/z*. While the ions are accelerated through an electric or magnetic field in vacuum they undergo a deflection according to their mass and charge state, which is reflected in the *m/z* ratio. The stream of sorted ions reaches the detector, such as an electron multiplier. The detector registers the intensity of ions of the same *m/z*, thus their relative abundance, which is displayed as spectra. There are different type of mass analysers using either static or dynamic and magnetic or electric fields, each with its own strength and weakness. In many mass spectrometers, especially in newer types, several analysers are put together to take advantage of the strengths of each. In proteomics four basic types of mass analysers are used: In brief, these are time-of-flight (TOF), ion trap (including the orbitrap), quadrupole mass filters and Fourier transform ion cyclotron resonance (FTMS) analysers. For a detailed technical review on MS instrumentation see review by Aebersold and Mann.[194] The mass analysers are characterized by the key parameters such as sensitivity (dynamic range), resolution and mass accuracy. A high resolution allows the MS to distinguish many different proteins/peptides of slightly different *m/z* from each other and display them as single

peaks. This is required for their accurate identification. The mass accuracy is the ratio of the *m/z* measurement error to the true *m/z* and is measured in ppm.

1.3.4.2 Overview of MS methods

Advances in proteomics are tightly linked to the development of mass spectrometry technology, which is in a constant state of flux. Due to the rapid development of MS technology at all levels there is no straightforward classification of MS based proteomics. MS approaches can be categorized from various viewpoints: Firstly, it can be divided in gel-based (2-DE or Gel-LC-MS/MS) or gel-free (shotgun proteomics) methods. In terms of quantification it can be distinguished between label-free and isotopic labelling (SILAC, iTRAQ, TMT) techniques. These quantification techniques are relative, while absolute quantification can be achieved with stable-isotope labelled standards in targeted proteomics. Finally, depending on the method of protein analysis, proteomics is subdivided into a "top-down" and "bottom-up" approach. The bottom-up strategy means the identification of a protein via its peptides after its proteolytic digestion (relies on tandem MS) and is by far the most commonly applied strategy. Within the field of bottom-up proteomics, there is still a great variety of MS strategies and acquisition modes (MS operating modes for data acquirement), which can be overwhelming when first introduced to proteomics. Currently there are three main strategies used in this field.[196] The first and most widely used strategy is known as shotgun or untargeted discovery proteomics with the MS operated in data-dependent acquisition (DDA) mode. The second strategy is targeted proteomics, carried out by multiple reaction monitoring (MRM) (also called selected reaction monitoring, SRM). The final approach is the newly emerging data-independent acquisition (DIA) mode. Both, DDA (biased) and DIA (unbiased) are discovery based methods, which globally profile the proteome of a given sample, while MRM is a targeted method only identifying preselected proteins of interest. Further, these three approaches differ with regards to their analytical performance in terms of sensitivity, reproducibility, limit of detection and resolving power.[197] Limit of detection refers to the minimal quantity of an analyte that can be confidently detected. In the following sections all these introduced methods and MS acquisition modes will be discussed in detail. A schematic overview of proteomics approaches is given in *Figure 9*.

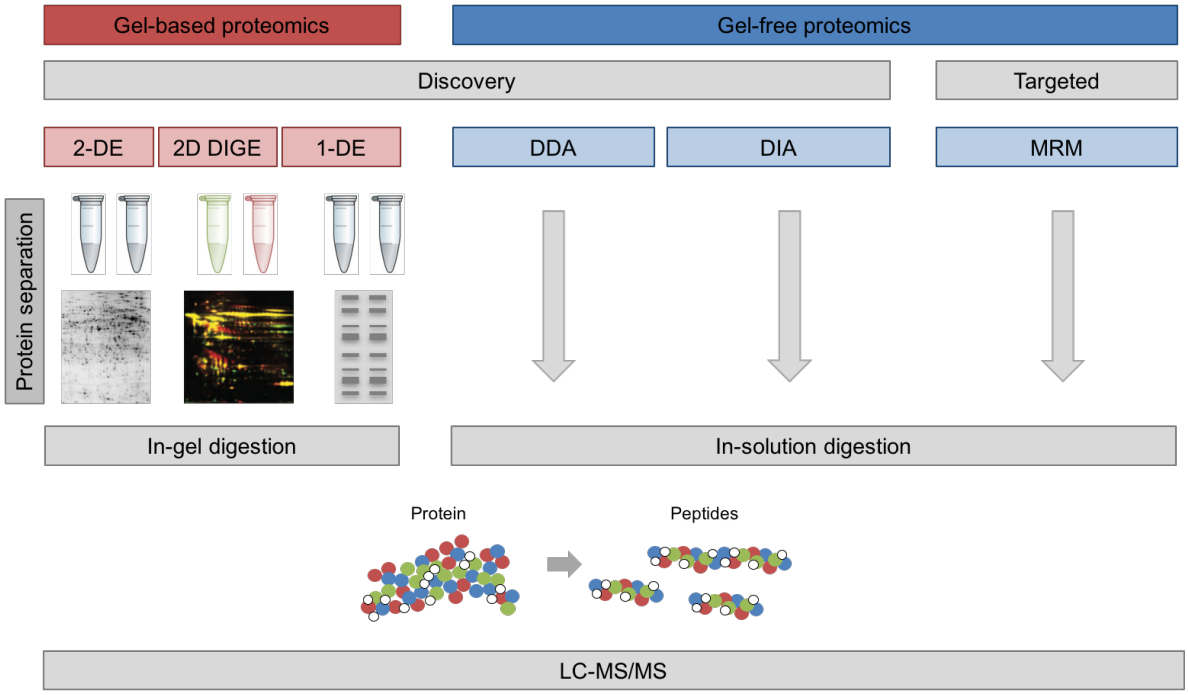

Figure 9. Overview of proteomics approaches. Using gel-based methods fractionation of protein extracts is accomplished on protein level. Separated proteins are excised and subjected to in-gel digestion. Upon alternative fractionation gel-free proteomics approaches directly proceed to in-solution digestion and LC-MS/MS analysis. There are three data acquisition modes in bottom-up proteomics: DDA, DIA and MRM, whereas MRM is a targeted approach, while DDA and DIA are discovery-based.

1.3.4.3 Top-down vs. bottom-up proteomics

Two different methodologies are used for protein analysis by MS.

In the less-used **top-down** approach intact proteins without prior digestion are analysed by MS. It starts with the ionization and measurement of the whole protein, which is then fragmented in the MS, mostly using a Fourier transform MS.[198] This approach has the advantage that it provides a high protein sequence coverage and accurate PTM localization. Furthermore, unlike in the bottom-up approach, protein isoforms and degradation products can be unambiguously determined. Yet, top-down proteomics remains technically challenging, because of separation and quantification difficulties of whole proteins.

In contrast, in the **bottom-up** approach a peptide-to-protein sequence is followed for protein identification, which is based on the mass spectrometric measurement of peptides. The mass range and fragmentation characteristics of peptides, rather than that of intact proteins are better suited to MS capabilities, which is why the bottom-up approach has become the method of choice for protein analysis. However, at the same time protein identification became more challenging, since the identified peptides had to be reassigned back to the original protein using a method called protein inference.[199] The

problem was tackled with the development of efficient computational methods and software tools.[200] Nevertheless, the problem is aggravated by the fact that the same peptide sequence can be found in multiple different proteins, making an unambiguous protein identification difficult. Especially the identification of protein isoforms or protein degradation products is not trivial as they generate a large set of identical peptides. Thus, generally a protein is considered to be confidently identified with at least two unique peptides.

1.3.5 Liquid-chromatography tandem mass spectrometry

1.3.5.1 Sample preparation

Protein analysis with the bottom-up approach relies on liquid chromatography tandem mass spectrometry (LC-MS/MS), which is the current gold standard technique for proteomics analysis. It provides a robust method for large-scale, high-throughput protein analysis. Upon denaturation (mostly urea), reduction (mostly DTT) and alkylation (mostly iodoacetamide), proteins in a sample are digested into peptides **in-solution**, usually with the protease trypsin. In case of gel-separated proteins digestion is performed directly in gel (often robotic **in-gel digestion**), followed by elution of the resulting peptide mixture (Gel-LC-MS/MS). Trypsin usually generates peptides between 0.5 to 3 kDa, which is an optimal mass range for chromatographic separation and ionization.[196] Enzymatic cleavage with trypsin occurs at the carboxyl side of the amino acids lysine or arginine, except when either is directly followed by proline. Thus, peptides found without a lysine or arginine residue – so called “non-tryptic” peptides - often indicate their endogenous cleavage as degradation products. Trypsin is most commonly used, since it has a high cleavage specificity and is robust and cheap. However, missed cleavages with trypsin are common and need to be considered for the subsequent database search.[201]

1.3.5.2 MS analysis

Following enzymatic digestion, peptides are purified mainly using C18 reversed-phase resins and separated by reversed-phase LC according to their hydrophobicity. LC is directly coupled to the MS, so that eluted peptides are immediately ionized by ESI and enter the MS. Despite high resolving capabilities of LC, simultaneous co-elution and co-ionization of peptides cannot be fully prevented, which has an impact on the subsequent analysis performance. The peptides are identified in two steps, hence the term tandem MS or MS/MS: in the first step, MS^1 or survey scan, the *m/z* and intensity of the intact ionized peptide (precursor ion) is determined. To identify its sequence, in addition to its exact mass, the peptide is isolated and fragmented along its backbone, usually by energetic collision with an inert gas such as helium, nitrogen or argon, in a process called

collision induced dissociation (CID).[202] In a second mass analyser the *m/z* ratios of the generated fragment ions are measured, resulting in the MS^2 or MS/MS spectrum. *Figure 10A* illustrates the LC-MS/MS approach from digestion to protein identification. The following example gives an idea of the amount of the collected data in the above described analysis platform: an MS^1 spectrum is obtained roughly every two seconds. From this, in a typical shotgun approach up to 15 peptides are selected for fragmentation and their MS/MS spectrum is recorded simultaneously with the MS^1 spectrum. Thus, in a usual two – four hours chromatography run this adds up to an enormous amount of collected data.[173]

1.3.5.3 Protein identification algorithms

Upon obtaining the MS^2 spectra there are two ways of identifying the protein sequence: database search or de novo sequencing.[184, 203]

In **de novo sequencing** the sequence is directly retrieved from the spectra, independently of pre-existing protein databases.[204] Fragmentation at the peptide bond generates peptides of increasing size: b-ions containing the N-terminus or y-ions with the C-terminus. Fragments are numbered depending on the amino acids they contain. For example, a fragment containing the N-terminus with 3 amino acids is called a b3 ion, while a fragment with the C-terminus and 2 amino acids is termed a y2 ion. Thus, the sequence information can be deduced from the mass difference between two consecutive fragment ion spectra, each corresponding to an amino acid, for each of which the mass is known (*Figure 10B*). This approach is particularly useful for peptide precursors which are not present in a sequence database. For example, a sequence carrying unexpected modifications with an altered mass profile or for the identification of proteins from species with incompletely sequenced genomes. However, de novo sequencing is quite an intricate process, since a complete fragmentation ladder is very rarely provided and because of the presence of noise peaks. Also high-throughput experiments generating an enormous amount of peak data are ill-suited for this approach.

Thus, the much simpler **database search** is more commonly applied for protein identification.[205, 206] In this approach, the measured fragment spectra are matched against a protein database with a search engine, such as Mascot[200], SEQUEST[207] or X!Tandem.[208] The databases contain theoretical fragment spectra of *in silico* digested peptides according to the known cleavage patterns of the used proteases, most commonly trypsin. The match between an actual measured fragment spectrum and a theoretical database spectrum is given a score. Thus, the peptides with the highest matching scores are selected and lead to highly confident protein identification. Since mass shifts can result from PTMs or artificial modifications while sample preparation such

us a cysteine modification due to alkylation with iodoacetamide, these alterations need to be considered and set for search algorithms. Thus, matching occurs within a pre-set mass tolerance. Ultimately, accurate identification relies on the availability of complete and accurately annotated sequence databases.[199] This approach fails to recognize peptides not present in the database. While for human and mice mainly complete sequence databases exist this is more challenging for other species. However, complete software packages such as PEAKS, which contains features of both approaches, de novo sequencing as well as database search options are available to alleviate disadvantages of both methods.[209] Pig and human proteins share high sequence homologies due to their phylogenetical similarity[210] (e.g. >90% similarity for decorin as scored in BLAST). Thus, for example, pig insulin was historically used to treat human patients with diabetes.[211] Though this similarity allows protein identification using human databases for porcine proteins, the protein quantification and identification can be further improved with a porcine database. Thus, for our study we have generated a custom-made porcine database for ECM proteins. Finally, to quantify confidence in correct peptide identification or false positive identification respectively, false discovery rate (FDR) estimation can be used.[212] The most common method of estimating FDR is by searching the data against a decoy database. A decoy database contains randomized non-natural peptide sequences for example by reversing the genuine amino acid sequences of all database entries. Thus, a match against a decoy database is random and per definition false. FDR can be estimated by comparing distributions of randomized and non-randomized matches.

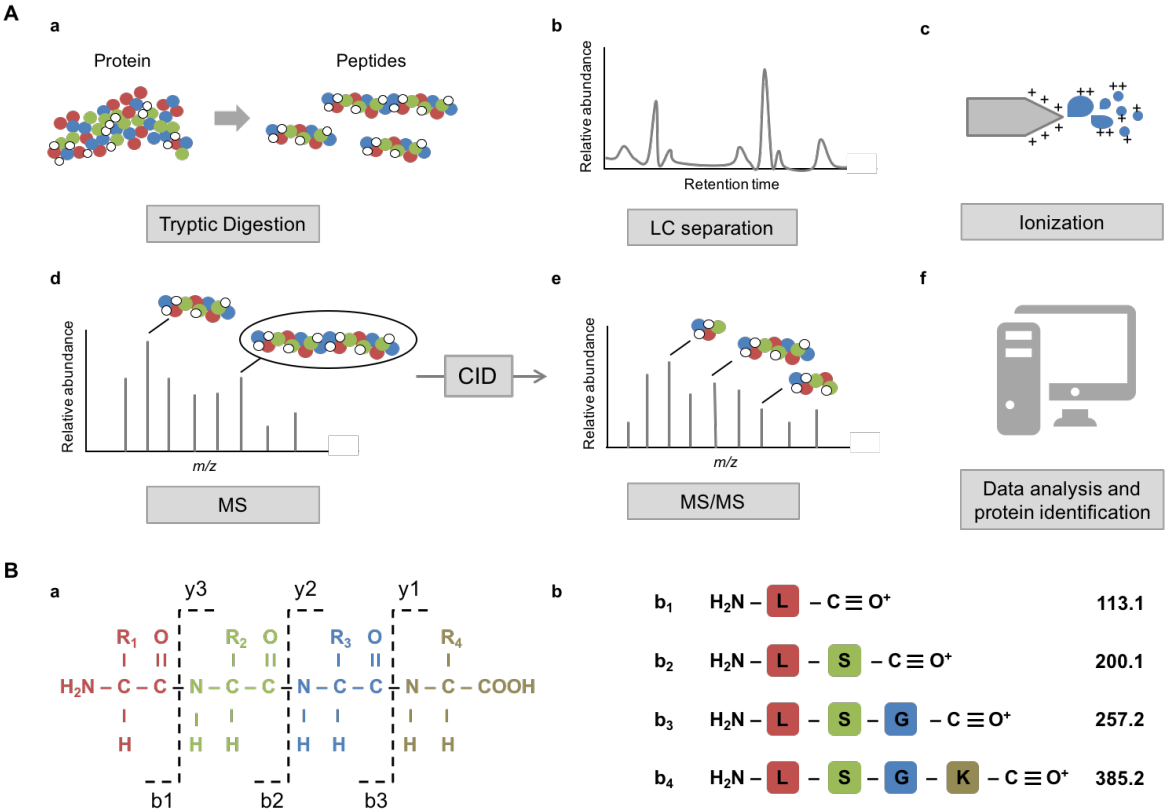

Figure 10. Protein identification by LC-MS/MS. (**A**) (a) Tryptic digestion of protein mixtures is followed by LC separation of the resulting peptides to reduce sample complexity (b). Separated peptides are ionized and directly injected into the MS (c). (d) In a survey scan the *m/z* and relative abundance of ionized peptides are determined by the first mass analyser. (e) Peptides are selected for fragmentation by CID on the basis of their abundance. The *m/z* of the resulting fragment ions is measured by tandem MS (MS/MS). (f) Protein identification is commonly accomplished by database searching, which contains all theoretical MS/MS spectrum patterns resulting from *in silico* fragmentation of all known protein sequences. (**B**) **De novo sequencing**. Using this method protein sequence is directly retrieved from the spectra, independent of protein databases. (a) Fragmentation at the peptide bond generates b-ions containing the proteins N-terminal end and y-ions with the C-terminus. (b) The sequence information is deduced from the mass difference of two consecutive fragment ion spectra, as the mass for each amino acid is known. By analysing both, b and y ions the sequence is determined. Here, generically only b-ions are shown.

1.3.6 Shotgun proteomics

The term shotgun proteomics simply refers to the application of LC-MS/MS to globally profile proteins in a complex sample in a high-throughput manner. In this method peptide identification is usually accomplished by database matching as described above. Shotgun proteomics relies on the DDA method. “Data dependent” in this context refers to the selection criteria of peptides for fragmentation in MS^2. That means in complex samples, where multiple peptides are simultaneously ionized, it is not possible to select all peptides in the survey scan for fragmentation, as this would overwhelm the sequencing capabilities of most instruments. Instead, a deliberate peptide selection for fragmentation is required, which is based on predefined criteria, hence data dependent. These are: protein abundance, signal intensity and charge state. Selection is made real time by the MS software during the survey scan and newer MS are able to select the 15 most abundant – “top 15” – proteins. Thus, a fixed number of precursor ions is selected in every MS^1 survey scan and analysed by MS^2. Charge state preselection is used to exclude singly charged ions, which are mostly contaminants.[196] In addition, the acquisition parameter “dynamic exclusion” is enabled to prevent repeated selection of the same peptide, thus overcoming interference from high abundant proteins and also allowing low abundant proteins to be identified. Nevertheless, under sampling of low abundant peptides is not completely eliminated and remains a bias, not even in newer instruments with increased sequencing speed. Precursor selection is a stochastic and irreproducible process, which will never be exactly the same between two runs of an identical sample due to variability of chromatographic separation. Thus, reproducible quantification, especially of low-abundant peptides remains a challenge. However, the run-to-run variability remains within an accepted range for most discovery based proteomics studies, especially with extensive prefractionation, making shotgun proteomics a robust platform for global protein analysis.

1.3.7 Quantitative proteomics

In biological studies, especially in differential expression studies, it is not only of interest to identify a protein in a sample but also to obtain its quantity. Yet, mass spectrometry itself is not truly quantitative due to sequence-specific differences in ionization efficiency of peptides (and ion suppression). However, MS-based quantification strategies are well suited for relative quantification between samples run under the same MS conditions. Absolute quantification can be achieved by using internal standard peptides with targeted proteomics as will be discussed in section 1.3.8.2. Generally, quantification with MS can be divided in label-free and stable isotope-labelling methods.[213]

1.3.7.1 Label-free quantification

Label-free quantification became possible with advances in computing power. There are two different approaches for label-free quantification using either mass spectrometric signal intensity or spectral counting.[214] The latter is based on the obvious rationale that more abundant peptides generate more MS^2 spectra. Therefore, relative quantification is achieved by counting the number of MS^2 spectra assigned to a protein across the samples. However, this approach is still controversial, since it does not take the direct physical peptide properties into account assuming a linear response for every peptide.[215] The second approach uses spectral ion currents for relative quantification. Advanced pattern comparison software is applied to align ion intensities of the same peptide on MS^1 and MS^2 level in different samples. The main advantages of label-free quantification are that it is cost-effective, achieves higher proteome coverage and it does not require laborious labelling workflows. Thus, making it the preferable method for large sample analysis.

1.3.7.2 Stable isotope-labelling

This approach is based on the incorporation of stable isotope tags into peptides or proteins either by a chemical reaction, a metabolic or enzymatic process. Stable heavy isotopes have the same physico-chemical properties as their light counterparts, meaning they behave identically on chromatography. However, due to their slight mass difference, they generate distinguishable signals in the MS, making them ideal for quantification purposes. Compared to label-free methods, the labelling approach provides a higher quantitative accuracy and consistency. This is due to near equal ionization efficiencies of the isotope tags. The most commonly used labelling methods are stable isotope labelling by amino acids in cell culture (SILAC), tandem mass tags (TMT) and isobaric tagging for relative and absolute quantification (iTRAQ) (*Figure 11*).

Stable isotope labelling by amino acids in cell culture

SILAC is an *in vivo* metabolic labelling approach on the protein level (*Figure 11A*).[216] This means proteins are already labelled during their synthesis in cells. This is achieved by growing cells in a medium containing isotopically labelled amino acids, which are incorporated in the proteins. Mostly arginine and/or lysine are heavy labelled with ^{13}C isotope (instead of ^{12}C) or ^{15}N isotope (instead of ^{14}N) to ensure that all tryptic peptides contain a labelled isotope. Lysine has the additional advantage of being an essential amino acid, which cannot be produced *de novo*. At the same time cells of the other experimental condition are grown in normal medium, containing the normal or "light" amino acids. Eventually both samples are multiplexed and analysed in the same MS run, which reduces experimental variability. The heavy and light labelled protein pairs co-elute on chromatography. Due to the characteristic mass shift in their MS^1 spectra (for example 6 Da for ^{13}C lysine) the relative quantity for each protein can be calculated. An equal ratio between both samples indicates no difference in abundance. If the heavy labelled peptide exhibits a higher peak intensity, than the protein was more abundant in the labelled sample and vice versa.

Application of SILAC goes beyond cells in culture, but is also used for mice without affecting their development, growth or behaviour[217] – as the proteins are chemically identical except for their mass difference. However, SILAC diet is expensive, thus limiting its use to small animal models. SILAC is also a very useful tool to assess protein turnover.[218, 219] Upon feeding a SILAC diet to animals the amino acids are gradually incorporated into the newly synthesized proteins and are clearly distinguishable from pre-existing proteins. Thus, the ratio between heavy and light peptides indicates the protein's synthesis rate and can be compared across different proteins.

Isobaric tagging

In the mass tagging approach proteins or peptides are chemically tagged with a stable isotope-containing molecule *in vitro*. Thus, unlike SILAC this approach is also applicable to human samples. The most commonly used tags are TMT[220] and iTRAQ[221], both belonging to the category of isobaric mass tags. The tags are available with different isotopic substitutions (reporter regions) creating distinct mass differences to allow multiplexing of currently up to ten samples with TMT (10-plex) and eight with iTRAQ (8-plex). Again multiplexing offers the advantage of reducing experimental error. Each tag consists of three functional regions (*Figure 11B*). The amine-reactive region is equal in all tags and allows the binding to the N-terminus and side chain amines of peptides. In addition, they have a mass reporter and a balance region, which are different and unique to each tag, due to isotopes substituted at various regions. As the name indicates the function of the balance region is to compensate the variable mass of the reporter region,

so that the intact tag has the same mass in all samples, hence the term “isobaric”. Thus, after mixing of all differently labelled samples the peptides remain undistinguishable during chromatographic separation and MS^1. Only upon fragmentation in MS^2, the different reporter regions are released enabling the distinction and quantification of the peptide in different samples.

Cysteine-reactive mass tags are also available (iodoTMT), to specifically label cysteine-containing peptides, commonly applied in the field of redox-proteomics. In comparison to the isotope coded affinity tags (ICAT), multiplexed quantification (up to 6-plex) is possible. ICAT, also with specificity towards sulfhydryl groups, contains an additional biotin affinity tag.[222] This tag enables purification by avidin affinity chromatography. Thus, it allows further reduction of sample complexity by targeted labelling and enrichment, but only to identify proteins with cysteinyl residues.

The downside of isobaric mass tagging is that labelling occurs at the peptide level, thus late in the experimental workflow. Therefore, potential experimental variations before labelling cannot be prevented. In comparison SILAC provides a very accurate quantification with minimal experimental error, since the introduction of isotopes occurs as early as possible during synthesis. A further caveat associated with this method is that a complex background can lead to inaccurate quantification. Mixed MS/MS spectra resulting from the simultaneous fragmentation of more than one peptide from different proteins, can lead to erroneous combination of their reporter ions.[223]

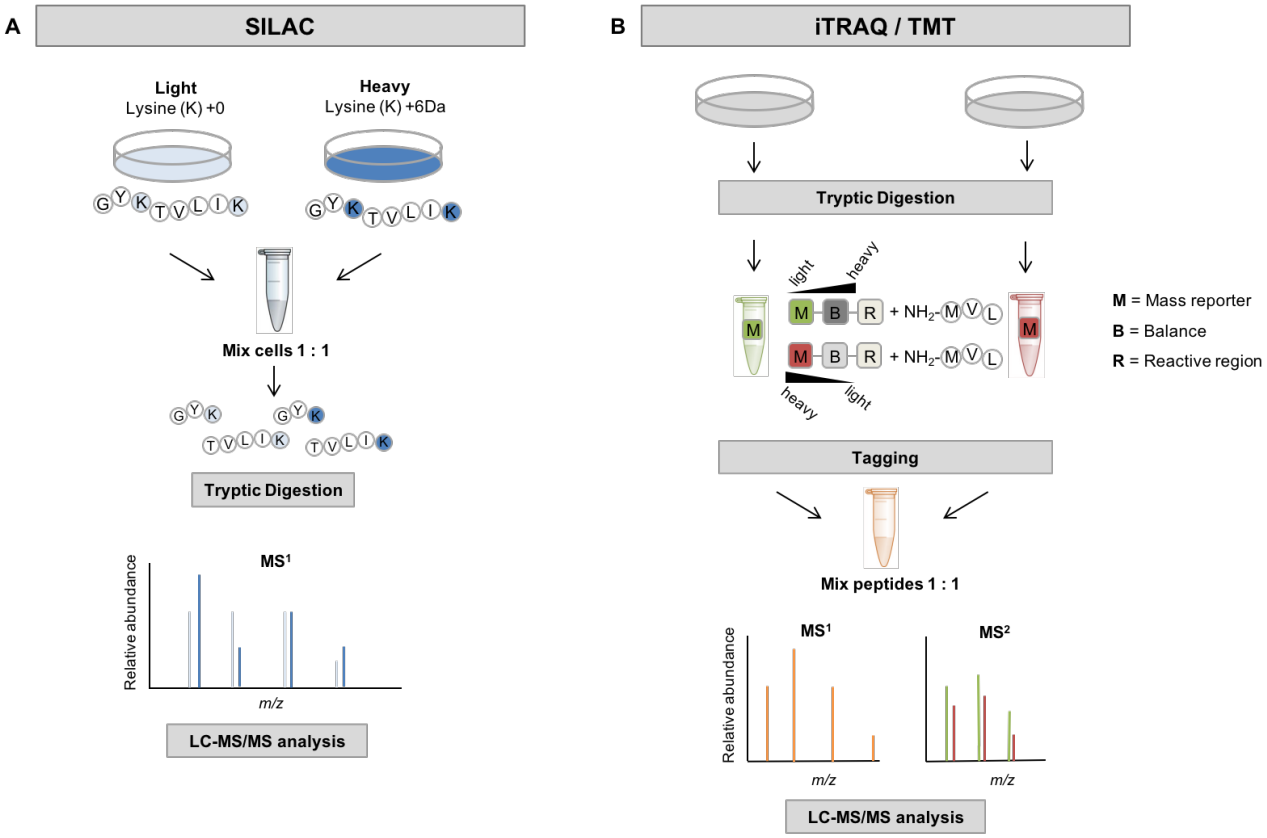

Figure 11. Stable isotope-labelling. (A) The SILAC approach allows an early metabolic labelling already at the protein level during protein synthesis by incorporation of heavy or light amino acids. Proteins are mixed, digested and analysed by LC-MS/MS. Due to their characteristic mass shift in MS^1 their relative quantity can be determined. (B) In contrast, using iTRAQ or TMT labelling is performed only at the peptide level. Different tags allow multiplexing and reduce experimental error. Upon individual labelling of each sample, peptides are mixed. Both iTRAQ and TMT are 'isobaric' tags, meaning that the peptides co-elute in chromatography and cannot be distinguished in MS^1 due to their balance region. Only in MS^2 peptides can be relatively quantified due to the mass shift in the reporter regions.

^{18}O labelling

Another labelling method is the enzymatic incorporation of stable isotopes, such as ^{18}O instead of ^{16}O.[224] In this approach isotopic labelling occurs during the proteolytic digestion of proteins. The cleavage of peptide bonds requires the addition of H_2O. If the reaction is performed in the presence of ^{18}O labelled water ($H_2{}^{18}O$), the generated peptides have either a 2 or 4 Da mass shift compared to their natural counterparts, depending on cleavage occurring at either one or both ends. Though it is highly specific and universally applicable a major limitation of this method is the enzyme-mediated back-exchange of ^{18}O with ^{16}O, resulting in complicating data analysis.[225] However, by using immobilized trypsin which is removed upon digestion/labelling, the back-exchange can be widely prevented.[213, 226] Also software tools for efficient quantitative analysis of complex samples have been developed.[227]

Further, this principle is also applied for PTM studies, namely for the identification of N-linked glycosylation sites on proteins.[228] During enzymatic deglycosylation of N-linked glycans under incorporation of H_2O, the enzyme PNGase-F converts asparagine to aspartic acid via a deamidation reaction causing a mass shift of 0.984 Da. Thus, if $H_2{}^{18}O$ is used, it leads to a mass shift of 2.99 Da, which leads to increased search specificity and indicates the former presence of glycosylation at that position.

1.3.8 Targeted proteomics

In contrast to discovery or shotgun proteomics as extensively discussed in section 1.3.6, targeted proteomics allows the precise identification of specific proteins of interest. Thus, it provides a hypothesis-driven proteomics strategy,[229] which is often deployed to validate and complement the findings obtained from discovery approaches. The focus on predetermined target proteins offers a significantly higher sensitivity, quantitative accuracy and reproducibility than the DDA approach. Indeed, due to these highlighted characteristics together with its advantages over conventional antibody detection, targeted proteomics has been appreciated as the method of the year 2012 by the journal *Nature Methods*.[230]

The typical MS method for targeted proteomics is selected reaction monitoring (SRM) mainly carried out on triple quadrupole instruments (QQQ). Due to the multiplexed analysis capability the method is also called multiple reaction monitoring (MRM), which is used synonymously with SRM.[231] In SRM, the first mass analyser (Q1) selects precursor ions within a mass range around the mass of the predetermined targeted peptides, which are then fragmented by CID in the collision cell (Q2). The specific fragment ions of the targeted peptide are then selected and measured by the second mass analyser (Q3) (*Figure 12 A*). A specific precursor – fragment ion pair is termed a transition. The high selectivity and specificity of this method is given by the two levels of mass selection in Q1 and Q3 acting as a two-stage mass filter. In principle, the instrument is preprogramed to consistently monitor the same set of predefined transitions (Q1/Q3 pairs) and record their intensities over the entire chromatography run. This is considered as the basis for its high reproducibility in repeated samples. Thus, analysis time is optimally used on the peptides of interest, largely eliminating interference from high abundant/ contaminant peptides. On the other hand, its use is only limited to preselected peptides, as no full mass-spectra are recorded. Currently the number of peptides that can be monitored in a single run without compromising performance is limited to around 100 peptides. Multiplexing up to 1000 proteins is possible, however at the cost of reduced quantification accuracy.[232]

1.3.8.1 MRM assay generation

A selective transition/inclusion list needs to be generated to set the instrument and start the experiment. This strongly depends on the knowledge of the MS characteristics of a peptide and its fragmentation products. The required MRM transition data for a given protein is called an MRM assay. This information is mostly derived from previous untargeted MS experiments or alternatively the MRM assays can be retrieved from an online compendium (see below).

Firstly, a number of rules need to be considered when selecting the optimal peptides.[233] In essence, the selected peptides need to be unique for the protein of interest, or proteotypic as it is also called. Preferably, the peptide should be of medium length, fully tryptic and should not contain abundant PTMs or amino acids prone to variable chemical modifications such as asparagine (N) deamidation or methionine (M) oxidation. In terms of their MS parameters peptides with the most intense transition peaks are selected. In addition to their *m/z* values, the optimal collision energy and the chromatographic retention times are retrieved. The latter is used to monitor the expected transitions close to their corresponding elution time.[234] Due to these timed ion selection windows in the so called "scheduled MRM" approach more transitions can be monitored/multiplexed in one run. All these considerations together contribute to the unprecedented sensitivity of this method. Although initially laborious, once the assays are established, they can be used in a highly multiplexed manner with great reproducibility across different sample sets. Indeed, the extensive effort required to develop MRM assays has been considered as the main reason for MRM becoming only lately popular in the field of proteomics,[232] even though it has been widely applied to the measurement of small molecules such as drugs or metabolites in the past decades. Thus, great effort is put to improve the situation for example by the introduction of freely-accessible validated online transition lists, such as the SRMAtlas (http://www.srmatlas.org/) to retrieve the MRM assays needed. This is a compendium of highly specific MRM assays that has enabled the quantification of 99.7% of the > 20 000 annotated human proteins.[235] The assays are developed and validated by the wider proteomics community.[236]

Parallel reaction monitoring (PRM) is a newer targeted proteomics development, where Q3 of a triple quadrupole is substituted with a high-resolution accurate mass analyser such as TOF or orbitrap.[237] This allows the accurate detection of all fragment ions due to higher resolution, while in MRM the transitions are usually restricted to a maximum of 5. Thus, PRM requires less time for assay development, since it monitors all transitions and obviates the need for preselecting target transitions.

1.3.8.2 Database search and absolute quantification using MRM

For analysis of targeted proteomics data, mainly the open-source software *Skyline* is deployed. Even though the software offers an automatic selection of the best transition matches for each peptide, the correct attribution/identification needs to be visually matched and the peak areas manually integrated, making the data analysis a cumbersome process.

Most importantly, SRM is the prototypical MS quantification method, as it is highly consistent and accurate. It allows absolute quantification, by spiking-in heavy labelled reference peptides of known concentrations. Additionally, iRT standards are used for retention time calibration. Briefly, the fragment ion intensities of peptides of interest are related to corresponding signals of isotopically labelled peptides with the same sequence (*Figure 12B*). Finally, due to the above highlighted characteristics of targeted proteomics without the constraints of antibody based protein detection and quantification, MRM is emerging as a promising alternative to traditional protein quantification methods such as ELISA. By applying this method, commercially available kits such as PlasmaDive™, allow the absolute quantification of up to 100 proteins in human serum or plasma.[238] The increasing importance of targeted MS technologies for clinical application is reviewed by Carr et al.[239]

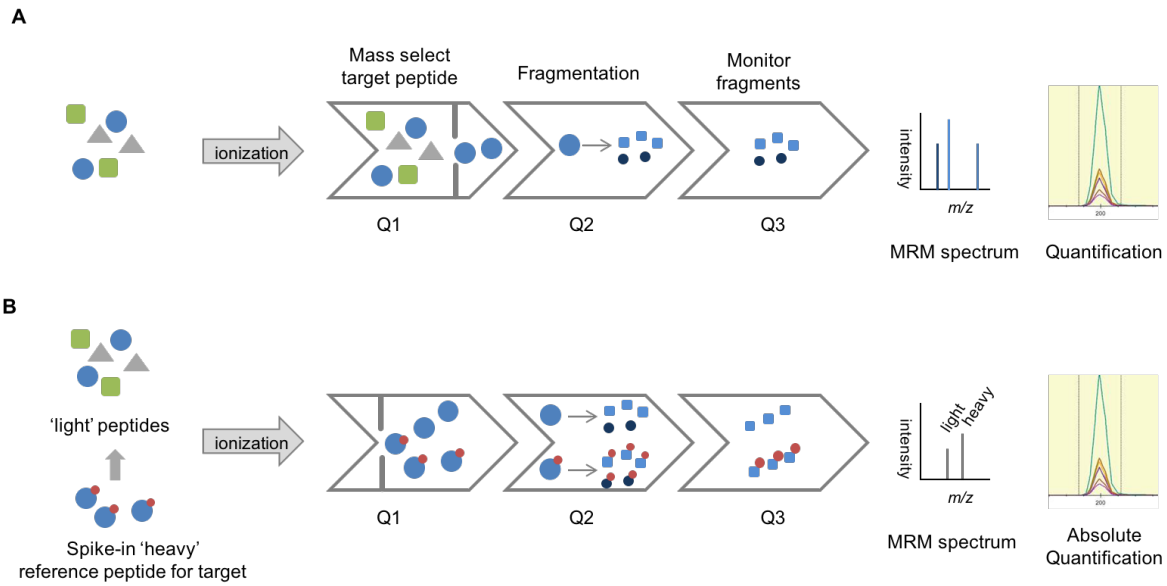

Figure 12. SRM/MRM analysis on a triple quadrupole (QQQ) MS. (A) Most co-eluting peptides are filtered by the first quadrupole (Q1) based on a predetermined list of targeted precursor – fragment ion pairs (transitions). The selected peptides are subjected to fragmentation by CID in Q2 and their fragment ions are selected and measured by Q3. (B) Heavy labelled reference peptides of known concentration can be spiked-in as standards, which allows absolute quantification of the targeted peptides.

1.3.9 Data independent analysis

1.3.9.1 DIA in comparison with DDA and MRM

Neither the untargeted discovery nor the targeted proteomics approach on its own is able to quantify every single component of a proteome. Each method is a compromise that improves analytical performance at some level, while reducing it at another. DDA is biased due to its random selection of peptides for fragmentation. Thus, reproducible quantification, especially of low-abundant peptides remains its major limitation. On the other hand, MRM is limited to the detection of preselected peptides requiring *a priori* knowledge. Therefore, it is not suitable for a discovery-based approach. Additionally, it has a limited multiplexing capacity. To overcome the limitations of both methods and combine their advantages the unbiased data-independent acquisition (DIA) mode was adopted for proteome analysis. This method aims to obtain the MS^2 spectra of every single precursor ion regardless of its abundance or its prior knowledge, hence the term "data independent". Therefore, DIA provides an unbiased discovery approach for reproducible and accurate quantification of the entire proteome in a sample without being restricted to predefined peptides. A comparative summary on the data acquisition mode in all three bottom-up proteomics approaches is given in *Figure 13*.

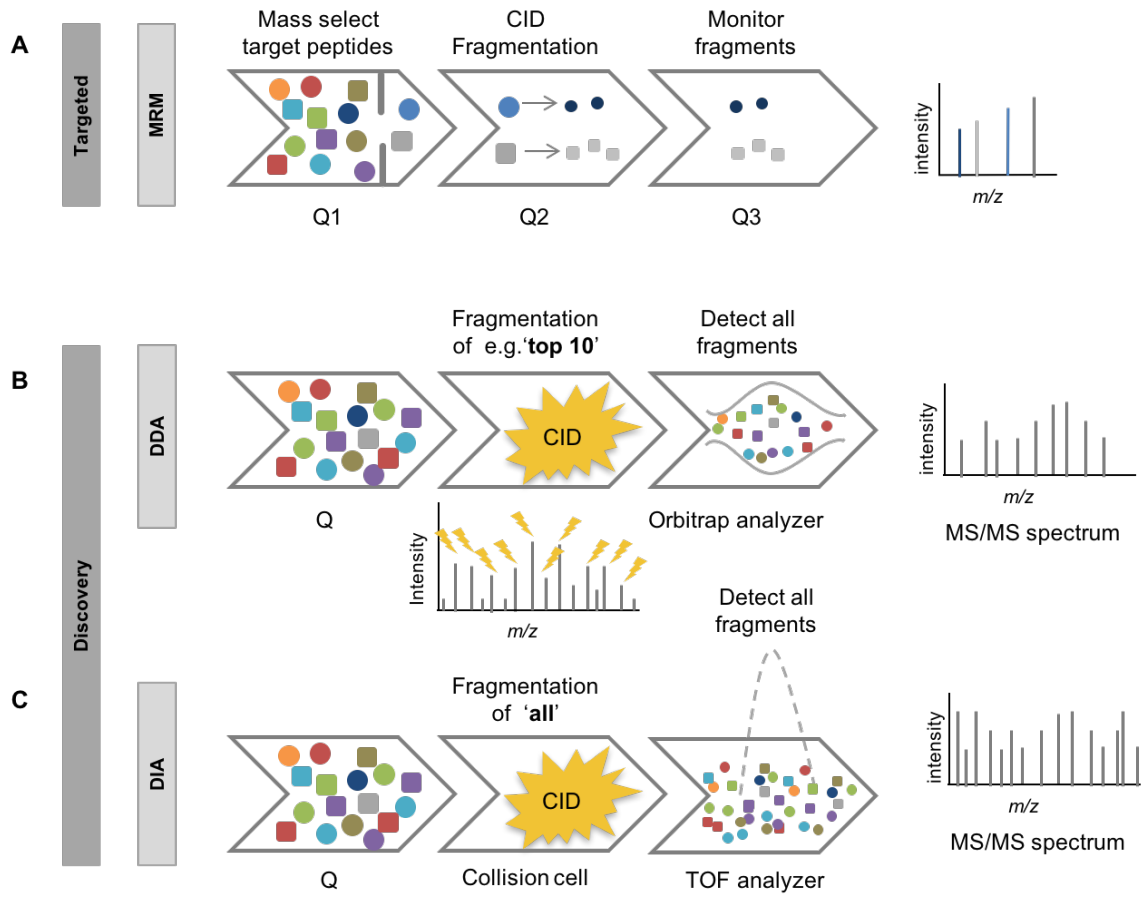

Figure 13. **Comparison of data acquisition using the MRM, DDA or DIA method**. Both DDA and DIA are discovery based approaches, while MRM allows targeted identification of only preselected peptides (A, Figure 12). (B) In the DDA mode, peptides for fragmentation are selected on the basis of their abundance upon a survey scan in Q1. Top 6-20 ions (a fixed number depending on the instruments' capacities) are fragmented in Q2 and their complete fragment ion array is measured in Q3 resulting in the full-scan MS/MS spectrum. Due to the biased selection, reproducibility is a limitation of the DDA mode, especially of low abundant peptides. (C) In contrast, in the unbiased DIA approach all peptides within a defined isolation window are subjected to fragmentation (Q2) and detected by a high-resolution TOF analyser. This results in highly multiplexed fragmentation maps which are analysed by targeted data extraction based on established spectral libraries.

1.3.9.2 Data acquisition in the DIA mode

The key to achieve a complete MS^2 spectrum is the sequential isolation window acquisition principle.[240] More precisely, the MS triggers fragmentation of *all* precursor ions within a predefined *m/z* isolation window. Due to seamlessly adjacent isolation windows the entire precursor *m/z* range expected for tryptic peptides can be covered in a single duty cycle. What is more, the width of a cycle is adjusted to be shorter than the chromatographic elution time of a peptide. Eventually, while the instrument repetitively cycles through the consecutive isolation windows fragmenting each peptide, MS^2 spectra of all possible precursors are recorded in real time. This results in the generation of complete, but complex fragment ion maps. However, due to this multiplexed recording of MS^2 spectra originating from multiple precursors, the relationship between the fragment ion and its precursor is lost. For comparison, in the DDA method the MS^2 spectrum is generally well associated with the MS^1 spectrum. Thus, the uncoordinated record of precursors and their fragment ions immensely complicates the data analysis. Therefore, the main challenges of the DIA mode are data processing and interpretation of multiplexed MS^2 spectra.

1.3.9.3 SWATH-MS and DIA data analysis

The DIA strategy of unbiased MS^2 data acquisition is not new, several DIA methods with various isolation window widths have been proposed previously.[241-245] However, recent improvements in MS instruments regarding their resolution power, mass accuracy and scan speed have greatly contributed to the maturation of the DIA strategy. Currently the most advanced DIA strategy in applied proteomics is SWATH-MS (sequential windowed acquisition of all theoretical mass spectra).[246] SWATH-MS experiments are typically performed on high resolution quadrupole TOF instruments. In this setup 32 fixed precursor isolation windows (swaths) with a width of 25 *m/z* each are used to cover a mass range of 400 – 1200 *m/z* (allowing an overlap of 1 Da between two adjacent windows). With a dwell time of 100 msec for each window, the total cycle time adds up to 3.2 sec. The data from all windows is compiled together in a single map, termed the

SWATH map. The reason for SWATH-MS's success lies in the novel data analysis strategy, which is fundamentally different from the standard database searching tools applied in previous DIA methods. Though a discovery based approach, the data analysis is accomplished using a targeted data extraction strategy for confident scoring. The data in generated fragment ion maps are mined using fragment ion spectral libraries supported by software such as OpenSWATH or Skyline. The spectral or assay libraries contain the exact MS coordinates for each targeted peptide including the precursor *m/z*, the fragment ion *m/z*, their intensities and their chromatographic retention time. Thus, peptides in the map can be uniquely identified with MRM-like reproducibility and quantification accuracy. However, currently as a developing MS technique, DIA cannot compete with MRM in terms of sensitivity, especially for low abundant peptides.[240, 247] Moreover, for successful data analysis, availability of high-quality assay libraries as complete as possible is crucial.[248] Any possible peptide of interest (including isoforms, degradation products or PTM carrying forms) can be queried in DIA maps. Since the SWATH map is a permanent digital record of fragment ion spectra for all peptides in a sample, it is possible to reanalyse the data as new targets of interest arise. The permanent nature of SWATH maps has also compelled researchers to convert tissue biopsy samples into permanent digital maps that can be perpetually queried *in silico*.[249]

Notably, the query of DIA data is quite a recent strategy compared to DDA, which has been optimized over the past two decades. Thus, facilitation of DIA data analysis by optimized protocols for spectral library generation, automated data extraction or scoring tools is currently work in progress expected to provide better solutions in the coming years.[196]

2 HYPOTHESIS

Despite continuous improvements in stent technology, stent failure still occurs. In-stent restenosis and neoatherosclerosis are the major causes. Coronary artery stent implantation induces vascular injury resulting in ECM remodelling. Modulating ECM deposition might be a promising approach for preventing restenosis after stent implantation without interfering with re-endothelialisation.

3 AIM

The aim of the study is to obtain temporal profiles of ECM changes following implantation of BMS and DES, thus characterising ECM proteins contributing to vascular healing in response to stent injury. Our current understanding of ECM remodelling upon stent implantation is based on histopathological studies, investigating the role of only few selected ECM proteins. In comparison, proteomics provides a more holistic approach to profile ECM changes post-stenting, rather than just individual ECM proteins by antibody staining. By applying proteomics to a large animal model of vascular stent injury, this study aims to identify changes in key regulatory ECM proteins after stent-induced vascular injury.

4 MATERIALS AND METHODS

4.1 Porcine experiments

4.1.1 Porcine model of stent injury

All procedures in pigs were approved by the local ethical committee for animal experiments, Institute of Pharmacology Polish Academy of Sciences, Cracow, Poland. For this study PCI was performed in 12 healthy male and female Polish domestic swine (Polska Biala Zwisloucha), which are a crossbreed of the European and the German domestic swine. All animals were obtained from the same supplier Institute of Zootechnology, National Research Institute, Experimental Centre in Grodziec Slaski. By the time of intervention all animals were between 3-4 months old and weighed between 28-48 kg. Pigs were premedicated with intramuscular atropine sulfate (0.05mg/kg) and anaesthetized by intravenous (i.v.) injection of ketamine hydrochloride (20 mg/kg), xylazine (2 mg/kg) and propofol (20-40 mg/kg) followed by intubation. Anaesthesia was maintained with continuous i.v. propofol infusion (2-4 mg/kg/h). Anticoagulant therapy with heparin (5000 IU) was administered prior to the procedure and additional i.v. bolus injections of heparin (2000 IU) were administered every 30 min during interventions lasting longer than 60 min. To prevent the risk of in-stent thrombosis pigs received a loading dose of 150 mg aspirin and 150 mg clopidogrel bisulphate orally 1 day prior to coronary intervention and remained on dual anti-platelet therapy with 75 mg each orally once daily until termination.

PCI was performed through femoral access by an experienced interventional cardiologist in accordance with equal guidelines applied to humans: sterile conditions, activated clotting time > 250 sec, use of sterile disposable equipment and ECG-, O_2 saturation- and blood pressure monitoring. The coronary arteries of each animal, i.e. the left anterior descending artery (LAD), the left circumflex artery (LCX) and the right coronary artery (RCA) were either stented with a BMS (MULTI-LINK cobalt chromium stent, Abbott Vascular, US) or everolimus-eluting DES based on the same cobalt-chromium platform (XIENCE PRO Everolimus Eluting Coronary Stent System, Abbott Vascular, US) or had balloon angioplasty alone without stent implantation (plain old balloon angioplasty - POBA). Stents were supplied free of charge by Abbott Vascular. Full strut expansion was achieved for each deployed stent. Intracoronary nitroglycerin (1 mg-wise) was given when intracoronary spasms occurred. Further medication included the application of prophylactic post-interventional single dose i.v. wide spectrum antibiotics lincomycin hydrochloride (5 mg/kg) and spectinomycin sulfate (10 mg/kg) (Linco-Spectin,

Pfizer, US), as well as the antiparasitic agent ivermectin (10mg) (IVOMEC, Merial, France). Quantitative coronary angiography and OCT were performed on follow-up procedure 1, 3, 7, 14 or 28 days post-stent implantation, followed by harvesting of the coronary arteries. These procedures were performed by a team around Prof. Wojtek Wojakowski from the 3rd Division of Cardiology, Medical University of Silesia, Katowice, Poland.

4.1.2 OCT image analysis in pigs

OCT imaging was performed at stent implantation and at follow-up using the ILUMIEN OPTIS imaging system (St. Jude Medical, US). The OCT probe (mid marker of the OCT Dragonfly catheter) was positioned 5 mm distally to the analysed stent. All OCT imaging was performed using automated pullback triggered by hand injection of contrast. Every 1 mm of the stent was scrutinized by OCT to assess minimal lumen area, stent strut apposition, stent strut coverage and neointimal volume. Also, qualitative analysis of the neointima was performed classifying the neointima into heterogeneous, layered or homogenous with peristrut attenuation or ring. If peristrut attenuation was visible in the whole circumference of the stent at the single OCT cross-sectional frame, the peristrut ring was recognized. The data was analysed using the OCT image analysing system CAAS IntraVascular (version 1.1, Pie Medical Imaging). This procedure was performed by a team around Prof. Wojtek Wojakowski from the 3rd Division of Cardiology, Medical University of Silesia, Katowice, Poland.

4.1.3 Porcine sample collection and processing

Upon harvest, the arteries including the stents were immediately snap frozen with liquid nitrogen and subsequently kept therein until shipment in dry ice. Perivascular tissue and stent struts were carefully removed from the arteries under a dissecting microscope. Non-stented artery segments were removed and a piece of the dissected stented/POBA treated artery sections were used for proteomics analysis. Another piece of the same artery was used for RNA extraction for validation studies. In the tissue used for proteomics analysis the neointimal tissue, that had developed in stented arteries at day 28 were dissected from the media and analysed separately. In total, 31 samples were analysed for the media by LC-MS/MS (n=3 BMS and n=3 DES at each time-point 1, 3, 7 and 28 days; n=4 POBA early [day1-day3] and n=3 POBA late [day 14 - day28]). For the neointima a total of 14 samples were analysed (n=7 BMS, n=7 DES at 28 days) including the neointima of arteries of a second cohort with 4 samples each for BMS and DES day 28. In addition, six coronary arteries of 4.5 months old healthy, untreated pigs were harvested as unstented controls and used for validation studies.

4.2 Mice experiments

4.2.1 Mouse model of venous bypass graft

Mice experiments were performed by authorized researchers (Dr. Ursula Mayr) in the Cardiovascular Division at King's College London. Housing and animal care were in accordance with the UK Animals (Scientific Procedures) Act 1986. An established mouse model of venous bypass graft was used by grafting isogeneic *venae cavae* to common carotid arteries of C57BL/6J mice, as described previously.[250] Mice were anaesthetised by intraperitoneal injection of ketamine (75 mg/kg) and medetomidine HCL (1 mg/kg). A segment of vena cava of approximately 1 cm from a donor animal was grafted end-to-end to carotid arteries using a cuff technique. Briefly, this technique involves, that the ligated ends of the dissected artery are passed through a cuff over which a segment of the artery is everted and fixed with a suture. The harvested vena cava segment is then grafted between the two ends of the carotid artery by pulling the ends of the vein over the artery cuff and suturing them together. Upon detection of vigorous pulsations in the grafted vessel, the skin incision was closed.

Vessels of SILAC fed mice for targeted proteomics analysis

Post-surgery 9 mice were fed a SILAC diet containing heavy lysine (Lys+6) *ad libitum* to label the newly synthetized proteins upon surgery. SILAC feed was obtained from Silantes, Germany. Mice were euthanized by anaesthetic overdose 28 days postoperatively. The vein grafts were harvested by cutting the implanted segment from the native vessel at the cuff end, together with the native vena cava and the aorta. The vessels were processed for targeted proteomics analysis using the three-step extraction method as described below.

Grafts for histology

Additional mice (i.e. 2 per group) were fed a normal diet upon surgery and the grafts together with vena cava were harvested at time point 3, 7 and 28 days post-surgery for histological characterization.

4.3 Human tissue collection

All procedures involving use of human tissues were approved by a local Research Ethics Committee of St. George's Hospital London, United Kingdom. Formal written consent was obtained from all patients prior to surgery. Normal saphenous vein specimens were taken by surgical resection in patients undergoing coronary artery bypass surgeries; the segment of the saphenous vein near the knee level was collected for analysis from each patient. Control aortic samples from patients without connective tissue disorder were obtained upon aortotomy performed during routine aortic valve replacement from positions

of the ascending aorta that were free of macroscopically evident vascular pathology. All samples were snap frozen following surgical removal. There were no known potential confounders during sampling of clinical specimens and tissues. The tissues were collected by a team around Prof. Marjan Jahangiri of St. George's Healthcare NHS Trust, London, United Kingdom. ECM extracts of these tissues were used for targeted proteomics and immunoblot analysis. The aorta was also used for immunofluorescence analysis.

4.4 Protein extraction

4.4.1 ECM protein enrichment

To enrich ECM proteins in samples, the proteins of the porcine media as well as human and SILAC mice tissues were extracted in a three-step manner, using a method previously developed in our laboratory.[114] For this purpose, the samples were partially thawed, diced into smaller pieces to enforce protein extraction and weighed. On average approximately 50 mg tissue per porcine media sample, 30-40 mg per human and around 10 mg per mouse sample were placed in ice-cold phosphate-buffered saline (PBS) to remove plasma contaminants. A mixture of commercially available protease inhibitors (Sigma-Aldrich) was added according to the manufacturer's guidelines to inhibit broad range proteinase activity and consequently prevent ECM protein degradation. In addition, 25 mM EDTA, a chelator binding metal ions, was included to ensure metalloproteinase inhibition. In total the tissue was washed 3 times with PBS supplemented with protease inhibitor to ensure effective removal of plasma contaminants.

After the wash-steps the proteins were stepwise extracted: first in salt (NaCl)-, followed by sodium dodecyl sulphate (SDS)- and finally in guanidine hydrochloride (GuHCl)- buffer. For the first extraction step, the diced samples were incubated with 0.5 M NaCl buffer, pH 7.5, further containing 10 mM Tris, 25 mM EDTA and proteinase inhibitors (Sigma-Aldrich). Buffer volume to tissue weight ratio was adjusted to 10:1 (µl/mg) and the samples were mildly vortexed for 1.5 h at room temperature. Subsequently the NaCl solution was removed and stored frozen at -80 °C for later use. The rationale behind the NaCl treatment is to induce displacement of polyionic interactions between proteins through the salt ions, thus facilitating the extraction of loosely bound extracellular proteins. These include newly synthesized ECM proteins and degradation products providing an overview of tissue turnover. Next, after a brief wash with distilled water, the samples were incubated with 0.08% SDS (buffer volume to tissue weight 10:1) supplemented again with protease inhibitors and 25 mM EDTA. The sample buffer mixture was mildly vortexed for 1.5 h at room temperature and subsequently the SDS solution was stored frozen for later

use. The SDS is used to solubilize cell membrane lipid bilayers, therefore removing the cellular material while preserving the ECM and its associated proteins. Finally, 4M GuHCl buffer, pH 5.8, including 50 mM sodium acetate, protease inhibitors and 25 mM EDTA was added to the washed tissue samples in a 5:1 ratio of buffer volume to tissue weight. Incubation was performed for 48 h at room temperature with vigorous vortexing to enhance solubilisation of the ECM components. GuHCl is an effective buffer to solubilize most of the strongly bound ECM components, as it induced disaggregation of ECM components by destabilizing the ionic, disulphide-dependent protein conformation. Proteins of the more fragile porcine neointima samples (average tissue weight 25 mg) were extracted only in a single step in GuHCl buffer for 48h.

Protein concentration of GuHCl and NaCl extracts were determined using a spectrophotometer at 280 nm (NanoDrop, Thermo Scientific). Protein concentration in SDS extracts were measured using the Pierce™ BCA protein assay kit (Thermo Fisher, cat. no. 23227) according to the manufacturer's protocol for more accurate results, as the SDS buffer interferes with the NanoDrop measurement. For proteomics analysis an aliquot of 15 µg protein of each GuHCl sample was mixed with 100% ethanol (10:1 volume ratio) and stored at -20 °C overnight to remove guanidine, which otherwise would interfere with further processing steps. Precipitated proteins were pelleted by centrifugation (12 000 rpm for 50 min at 0 °C) and upon removal of ethanol the pellets were dried using a concentrator (SpeedVac Plus SC110 A, Savant) and kept at -20 °C until further use.

4.4.2 Deglycosylation of ECM extracts

After extraction and precipitation, proteins were deglycosylated for two reasons: first to facilitate the amino acid sequence determination of proteins by MS and second to improve epitope recognition by antibodies. Removal of the oligo- and polysaccharides was achieved using specific deglycosylation enzymes. Protein pellets of GuHCl extracts after ethanol precipitation were resuspended in 1x deglycosylation buffer (25 mM EDTA, 50 mM sodium acetate, 50 mM Tris, pH 6.8) supplemented with deglycosylation enzymes and incubated at 37 °C in agitation (200 rpm) for 24 h in the first step. The deglycosylation enzymes included: chondroitinase ABC (1:100), keratinase (1:500) and heparinase II (1:500) (all from Sigma-Aldrich) for the removal of GAG side chains; 2 different debranching enzymes including α2-3,6,8,9-neuraminidase (1:200) and ß-N-acetylglucosaminidase (1:200) as well as O-glycosidase (1:200) for the removal of the remaining O-linked sugars (all from Merck-Millipore). After the initial incubation samples were speed-vac dried. To identify N-linked glycosylation sites by isotopic mass-differences later in the mass spectrometer, PNGase F (1:200, from Merck-Millipore) was added

together with ^{18}O water (Sigma-Aldrich). Removal of N-linked sugars requires the incorporation of an –OH group from H_2O molecule, which converts the asparagine into aspartic acid and alters the mass of the remaining peptide. When isotopically labelled water is used, the mass difference is +2.99 Da instead of +0.98 Da with normal water. The higher mass shift is easier identified by the MS and also reduces false positive identifications of N-linked glycosylation sites due to a spontaneous deamidation. Further 48 h of incubation followed after adding of PNGase F. When samples were deglycosylated for immunoblot analysis, no ^{18}O water was used, and deglycosylation was accomplished in a single step including all enzymes or only the GAG removing enzymes in 48 h.

4.5 Proteomics workflow for pig samples

4.5.1 In-solution protein digestion

Deglycosylated proteins were subjected to in-solution digestion to be analysed by a bottom-up proteomics approach with LC-MS/MS. 15 µg of deglycosylated protein was denatured with 6M urea and 2M thiourea in each sample. Next, samples were reduced with dithiothreitol (DTT) (final concentration 10mM) and incubated at 37 °C for 1 h in agitation (200 rpm). For alkylation iodoacetamide (IAA) was added (final concentration 50 mM) followed by incubation at room temperature for 1h in the dark. Proteins were then precipitated with ice-cold acetone (6x the reaction volume) overnight at -20 °C, followed by centrifugation at 13000 rpm for 30 min at 4 °C. The protein pellets were speed-vac dried and resuspended in 30 µl of 0.1 M tetraethylammonium bromide (TEAB) buffer, pH 8.2, containing trypsin at a trypsin:protein ratio of 1:50. The samples were left for digestion at 37 °C in agitation at 200 rpm overnight and 10% trifluoroacetic acid (TFA) was added to stop the reaction (final concentration 1% TFA).

4.5.2 Peptide clean-up using C 18

For purification of the peptide samples C18 clean-up was performed using a 96-well C18 spin plate (Harvard Apparatus). The resin was initially wetted and activated in 200 µl methanol (100%) and centrifuged at 1000 x g for 1 min. Next, the resin was equilibrated in 200 µl cleaning solution (80% acetonitrile and 0.1% TFA) and washed 3 x with 200 µl of washing solution (1% acetonitrile and 0.1% TFA) with centrifugation after each step. Only then samples were loaded onto the resin and centrifuged at 1500 x g for 1 min; the flow through was reloaded onto the resin to maximise peptide binding and centrifugation was repeated. The resin was then washed with 200 µl of washing solution for 3 times and centrifuged after each step. Eventually, the samples were eluted in 170 µl of elution solution (50% acetonitrile and 0.1% TFA) twice and collected in the same plate. The

eluted samples were frozen in -80 °C for 4 h and immediately lyophilised in a freeze dryer (Christ Alpha 1-2 LD Freeze Dryer) at -55 °C overnight. The lyophilised peptides were resuspended in 30 µl of 2% acetonitrile, 0.05% TFA in HPLC-grade H_2O resulting in a final peptide-concentration of 0.5 µg/µl. Samples were kept frozen at -20 °C until LC-MS/MS analysis.

4.5.3 Untargeted LC-MS/MS analysis

The tryptic peptides of the porcine media and neointima were separated using a nanoflow HPLC system (UltiMate 3000 RSLCnano, Thermo Scientific) with subsequent MS/MS analysis on an orbitrap MS (Q Exactive Plus mass spectrometer, Thermo Scientific). Peptides were separated on a reversed-phase HPLC column (Acclaim®, PepMap 100 C18 peptide column, 3 µm, 100 Å, 50 cm x 75 µm, Thermo Scientific) at a flow rate of 300 nl/min and eluted with a 240 min gradient using a mobile phase solvent composition with increasing acetonitrile content. The following gradient was set: 2-10% B from 0-10 min; 10-30% B from 10-200 min; 30-40% B from 200-210 min; 99% B from 210-220 min and eventually 2% B from 220-240 min; the mobile phase solvent compositions were as follows: A = 0.1% formic acid (FA) in HPLC grade H_2O; B = 80% acetonitrile, 0.1% FA in HPLC grade H_2O). The sequentially eluted peptides were directly analysed by an orbitrap mass analyser using a full ion scan mode over the *m/z* range of 350 – 1600 and a resolution of 70,000 at 200 *m/z*. Data-dependent MS/MS analysis was performed using higher-energy collisional dissociation (HCD) on the 15 most abundant ions in each full MS scan with dynamic exclusion enabled for 30 sec.

4.5.4 Database search

Spectral raw files were searched using Proteome Discoverer™ software (version 1.4, Thermo Scientific) against a custom-made hybrid database using Mascot (version 2.3.01, Matrix Science). The custom-made database contained a comprehensive porcine ECM protein list with a human proteome background (UniProtKB/Swiss-Prot, release 2014_06, 20220 protein entries) (see section 4.5.5 for its generation). The mass tolerance was set at 10ppm for the precursor ions and at 20 mmu (0.02 Da) for fragment ions. Carbamidomethylation of cysteines due to alkylation with IAA was chosen as a fixed modification. Oxidation of methionine, lysine and proline, since hydroxylysine and hydroxyproline are common modifications on collagens as well as deamidation of asparagine with ^{18}O water (+2.99 Da) were defined as variable modifications. Only tryptic peptides were included in the analysis. Two missed cleavages were allowed. Scaffold (version 4.3.2, Proteome Software Inc., US) was used to validate MS/MS-based peptide and protein identifications and quantification.[251, 252] Peptide identifications were accepted if they were established with greater than 95% probability as specified by the Peptide

Prophet algorithm.[251] Protein identifications were accepted if they were established at greater than 99% probability with at least 2 unique peptides.[252] The normalised total ion current (TIC) of MS/MS spectra of the peptides from the same protein was used for quantification. All data were exported to mzIdentML format using Scaffold and deposited to the ProteomeXchange Consortium via the PRIDE partner repository with the dataset identifier PXD005726 and 10.6019/PXD005726.

4.5.5 Generation of custom-made porcine ECM protein database

To achieve the best peptide sequence coverage on database search, and identify as many proteins as possible, a search database containing a comprehensive list of porcine ECM proteins was generated. Previously reported cardiovascular ECM proteins identified in human, porcine and murine cardiovascular tissues[170, 253, 254] were searched for their porcine sequences in the UniProt protein database (www.uniprot.org/). Porcine sequences of many of these proteins were found and retrieved from UniProt either as annotated proteins or after blasting the human sequence against non-annotated, uncharacterized porcine proteins. The remaining ECM proteins with no matching sequences in UniProt were deduced from public nucleotide databases (including mRNA annotated sequences and expressed sequence tags [EST]) using tBLASTtn. Exclusively the best matches (≥ 90% identity) were assigned to a protein sequence and retrieved for the database. The final database contained a total of 246 manually included porcine ECM protein sequences. All canonical human sequences were used as background in order to obtain a database suitable for search algorithms (i.e. Mascot). To avoid redundancies all human ECM proteins were manually removed and replaced by their porcine counterparts. The included porcine proteins are listed in *Supplemental table 1* and the porcine sequence database is attached to the thesis in an electronic form.

4.5.6 Data analysis: media vs. neointima

The total spectral counts of all ECM proteins in all samples (BMS + DES) at day 28 provide the total ECM count. This was calculated separately in both groups, neointima (n=14) and media (n=6). Then, the total spectral counts of each ECM protein across all samples were divided by the total ECM count within each group to calculate its percentage of the total ECM count in the media or neointima.

4.6 Targeted proteomics for mice and human samples

Targeted proteomics was applied to validate selected proteins of interest. Principles of this method were explained in section 1.3.8. Sample preparation prior to LC-MS analysis, namely in-solution protein digest upon protein extraction and C18 peptide clean-up were accomplished using the same methodology as described for pig samples above in

sections 4.5.1 and 4.5.2. Also the HPLC configurations and the eluting gradients were the same in the targeted method.

4.6.1 PRM in SILAC mice tissue

Samples were run in PRM mode (MS/MS resolution of 30,000 at 200 *m/z*) using the Q Exactive Plus mass spectrometer (Thermo Scientific), allowing to detect all generated fragment ions. Selection of proteotypic peptides and generation of scheduled PRM assays were based on previous untargeted experiments in our lab. All proteotypic peptides were lysine (K)-terminated to allow quantification of SILAC incorporation. Selected peptides are shown in (*Table 2*).

Table 2. List of precursor ions for PRM in mouse tissue

Protein	Proteotypic peptide	Amino acid position	Collision energy	Retention time (min)	m/z light	m/z heavy	charge state
Aggrecan	GDPETSVSGVGDDFSGLPSGK	G1172 – K1192	37.1	n/a	1004.4607	1007.4708	2
	TVYLYPN[+3]QTGLPDPLSK	T661 – K677	35.3	163.22	954.9956	958.0057	2
Versican	VSVPTHPDDVGDASLTMVK	V101 – K119	36.4	92.82	984.4908	987.5008	2
	VSVPTHPDDVGDASLTMVK	V101 – K119	27.8	92.82	656.6629	658.6697	3
Decorin	DLHTLILVNNK	D101 – K111	24	84.52	640.3721	643.3821	2
	DLHTLILVNNK	D101 – K111	19.3	84.52	427.2505	429.2572	3
	NSGIENGAFQGLK	N183 – K195	25	n/a	667.8386	670.8487	2
	VVQC[+57]SDLGLDK	V59 – K69	23.2	37.16	617.3108	620.3209	2

Skyline software (version 2.6, MacCoss Lab, University of Washington, Seattle) was used beforehand to generate the transition list with predicted collision energies and optimized retention times, and later after PRM to quantify peak areas for MS/MS fragment ions. The identity of a specific peptide was confirmed by the presence of multiple transitions within the same retention time. Retention time windows were set +/- 4 min. A mass tolerance of 5 ppm was used as a minimum requirement for fragment ions. All peaks were manually reviewed and integrated. SILAC incorporation rates were derived from the proportion between ions derived from peptides containing either heavy (Lys+6) or light lysine using the following formula: Incorporation rate = [Heavy] / [Heavy + Light]. The intensities of heavy and light peptides were calculated using the peak areas of selected fragment ions after MS/MS. Because unique, proteotypic peptides were previously selected for each protein, the final protein incorporation rate was equivalent to that obtained for the proteotypic peptides. For proteins with more than one peptide the average value was considered.

4.6.2 PRM in human tissue

For targeted proteomics analysis of the human aorta and saphenous vein GuHCl extracts same PRM methodology was applied as explained above except the SILAC specific data analysis and the following differences. Fragmentation was performed with a normalised collision energy (NCE) of 35 V for all precursor ions. As the retention time (RT) during the entire run has shifted slightly, RT given in the list below is the average RT of all samples. Total peak areas from selected fragment ions with high intensities were used for quantification. Then the values were normalized to the average of all values in each group to allow relative quantification between the different proteins (adjusted peak area). Monitored peptides and fragment ions in human tissue are shown in *Table 3*.

Table 3. PRM fragment list used for human protein quantification

Protein	Proteotypic peptide + position	Average RT (min)	Precursor *m/z*	Precursor z	Fragment ion	Fragment ion *m/z*
Aggrecan	C[+57]GGNLLGVR	45.0	473.2504	2	y3	331.21
	C318 - R326				y4	444.29
					y5	557.38
					y6	671.42
					y7	728.44
					y8	785.46
Versican	LATVGELQAAWR	124.6	657.8619	2	y4	503.27
	L277 - R288				y5	631.33
					y6	744.42
					y7	873.46
					y8	930.48
					y9	1029.55
					y10	1130.60
					y11	1201.63
Decorin	NLHALILVNNK	67.6	416.9189	3	y3	375.20
	N106 - K116				y4	474.27
					y5	587.35
					y6	700.44

4.7 Western blot

SDS-polyacrylamide gel electrophoresis (SDS-PAGE) allows the separation of charged proteins in an electric field. Proteins are first solubilized with the negatively charged SDS molecules, which denature proteins and mask their intrinsic charge. This causes the proteins to migrate towards the positive electrode within the mesh of a polyacrylamide gel according to their molecular weight, but independent of their native charge state. In the subsequent western blot method, proteins of interest can be detected using specific antibodies, after transferring (‘blotting’) the separated proteins from the gel onto a sheet of

nitrocellulose paper. In this study, western blotting was applied for the detection of proteins of interest in the GuHCl extracts from porcine and human tissue.

Porcine samples

10 µg of deglycosylated (for aggrecan neo blots: GAG removal, for versican neo blots: pan-deglycosylation) GuHCl, NaCl or SDS extracts of stented porcine coronary artery media samples or 7 µg of non-deglycosylated neointima extracts were denatured and reduced in sample buffer (100 mM Tris, pH 6.8, 40% glycerol, 0.2% SDS, 2% β-mercaptoethanol and 0.02% bromophenol blue) at 95 °C for 5 min. Protein samples were separated on precast 4-12% bis-tris gradient gels (NuPage®, Thermo Fisher Scientific, cat. no. EC60385BOX) in SDS running buffer (NuPage® Mops, Thermo Fisher Scientific, cat. no. NP0001) at 130 V until the tracking dye reached the bottom of the gel. 7 µl of pre-stained protein standards (Novex®, Thermo Fisher Scientific, cat. no. LC5800) were used as a molecular weight marker. Subsequently proteins were blotted to a nitrocellulose membrane (GE healthcare, cat. no. RPN2020D) in ice-cold transfer buffer (25 mM Tris base, 200 mM glycine dissolved in 20% methanol) for 2 h at 350 mA constant current. Efficient transfer and equal loading was determined with reversible Ponceau S (Sigma-Aldrich, Cat. no. P7170) staining. Next, membranes were incubated in 5% milk in PBS with 0.1% Tween (PBST) for 1 h on a horizontal shaker at room temperature. The rationale behind the incubation with milk proteins is to prevent unspecific antibody binding to the membrane later. After a brief wash in PBST, the membranes were incubated overnight in primary antibody solution at 1 µg/ml dilution (unless otherwise stated) in 5% bovine serum albumin (Sigma-Aldrich, cat. no. A2153) and 0.01% sodium azide (Sigma-Aldrich, cat. no. S2002) in PBST at 4 °C. Primary antibodies were used to detect the aggrecan NITEGE neoepitope (Thermo Fisher, AF-PA1-1746), the versican DPEAAE neoepitope (Abcam, ab19345) and LRP1 (Abcam, ab92544; 0.046µg/ml). The following day, membranes were washed 3 x for 15 min each with PBST and treated with the appropriate horseradish peroxidase (HRP)-conjugated light chain-specific antibody (1:5000, Jackson ImmunoResearch, cat. no. 211-032-171) diluted in 5% milk in PBST for one hour. The membranes were washed again 3 times for 15 min each with PBST and developed using enhanced chemiluminescence detection reagent (ECL, GE Healthcare, cat. no. RPN2106) and X-ray films (FujiFilm) on a Xograph processor in 10-30 sec increments. Bands were quantified by densitometry using ImageJ software (v. 1.49, NIH, USA). Intensity is given in arbitrary units (A.U.) to compare abundance levels.

Human samples

Same protocol was applied for human sample western blots. 7 µg of GuHCl extracts of human aorta and saphenous vein were loaded per lane. Antibodies against the aggrecan

NITEGE neoepitope (Thermo, AF-PA1-1746), versican (Santa Cruz, sc-25831) and decorin (Thermo Fisher PA5-19151) were used. This western blot was run by Marc Lynch, MSc, of King's College London.

4.8 Silver staining

Silver staining was performed based on a silver nitrate staining protocol for visualization of separated proteins in gel in order to investigate equal loading. 5 µg of porcine GuHCl extracts were loaded on each lane. Following electrophoresis proteins in gel were fixed in fixing solution (50% methanol, 5% acetic acid) for 30 min and subsequently incubated in distilled H_2O overnight to re-expand the gel following methanol-induced shrinkage. Next, proteins were sensitized for 1 min with 0.8 M sodium thiosulphate pentahydrate, followed by 3 brief washes of 1 min each and silver staining in 6 mM silver nitrate for 30 min at 4 °C. Again after 3 brief washes, gels were soaked in developing solution (180 mM sodium carbonate, 0.04% formaldehyde) and stop solution (5% acetic acid) was added, once the protein bands on gel became visible. After 5 min gels were immersed in distilled H_2O and scanned with a calibrate scanner (GS-800, Bio-Rad).

4.9 Gene expression analysis

4.9.1 RNA extraction

Total RNA from porcine tissue and cultured human cells was isolated using the miRNAeasy Mini kit (Qiagen, cat. no. 217004) according to the manufacturer's instructions. First, porcine tissue was homogenized in 700 µl lysis buffer (QIAzol Lysis Reagent, Qiagen, cat. no. 79306) using ceramic spheres (Lysing Matrix D, MP Biomedicals) with a tissue homogenizer (Precellys®24, Bertin Corp., US). Homogenates were then incubated in lysis buffer for 5 min at room temperature. The lysis buffer contains the strong denaturant guanidinium thiocyanate, which immediately inactivates RNases preserving RNA. Next, homogenates were vigorously shaken with 140 µl of chloroform, which causes protein denaturation and leaves them soluble in the organic phase, while nucleic acids remain in the upper aqueous phase. After further 5 min incubation at room temperature, samples were centrifuged at 12000 rpm for 15 min at 4 °C. Subsequently 280 µl of the upper aqueous phase were combined with 420 µl of 100% ethanol in a fresh tube. After thorough mixing samples were transferred to an RNeasy mini column to bind the RNA to a silica-based membrane. The remaining wash and centrifugation steps were carried out at room temperature according to the manufacturer's protocol to wash away the contaminants. RNA was then eluted with 25 µl of RNase-free water by centrifugation at 12000 rpm for 1 min.

Determination of RNA concentration

RNA concentration was determined using spectrophotometry at a wavelength of 260 nm with a NanoDrop device, relying on light absorption of RNA at this wavelength. Absorbance measurements at 280 nm allows determination of the protein concentration in the sample. Thus, protein contaminations of the sample can be estimated by calculating the OD_{260}/OD_{280} ratio. For 'pure' RNA the ratio is around 2. Therefore, lower values indicate a contamination of the sample with proteins, or phenol or other contaminants absorbing light at 280 nm. After determining the RNA concentration samples were stored at -80 °C until further use.

4.9.2 cDNA synthesis

Complementary DNA (cDNA) was synthesized from extracted total RNA by the enzyme reverse transcriptase, an RNA-dependent DNA polymerase, using SuperScript® VILO MasterMix (Invitrogen, cat. no. 11755050). This kit contains all necessary components for the reverse transcription reaction including the reverse transcriptase, RNAse inhibitors, dNTPs, $MgCl_2$ and random primers to ensure priming of total RNA. 2 µl of mastermix were combined with a fixed amount of total RNA for each sample (130 ng for porcine samples) and water to a total reaction volume of 10 µl. The reverse transcription (RT) reaction was performed in a Veriti Thermal Cycler (Applied Biosystems) using the following settings: initial incubation at 25 °C for 10 min, followed by incubation at 42 °C for 120 min. The reaction was terminated by heating the sample to 85 °C for 5 min and samples were stored at -20 °C for later use in quantitative polymerase chain reaction (qPCR).

4.9.3 qPCR

Relative expression levels of the genes of interest derived from proteomics studies were determined using qPCR.

Principles of qPCR

The gene amplification part of this method is not different from conventional PCR and relies on repetitive cycles of denaturation, annealing and elongation, exponentially amplifying the gene of interest, which is determined by the used primers. The quantitative part is retrieved from measured fluorescence signals, which are generated only when the dye is bound to double-stranded DNA products of the PCR reaction and are accumulated during amplification. The quantification is based on a direct relationship between the original cDNA concentration in the sample and the rate at which the PCR product is generated.[255] This means, the more of a specific gene was present at the start of the reaction, the more fluorescence signal will be generated upon its exponential amplification. For better comparability across the samples and to overcome background signal interference a threshold for the fluorescence signal is set (just above background

fluorescence, in the linear phase of the amplification plot), at which the cycle number of the reaction is determined (*Figure 14*). This is known as the threshold cycle (Ct-value) and defines the number of cycles it takes in each reaction to detect the set threshold signal. The Ct-value is inversely proportional to the amount of the target gene in the sample. Thus, higher Ct values indicate low amounts of the target gene, while lower Ct values mean a higher expression of the target gene. Eventually, comparison of Ct-values for a target gene across all samples allows its relative quantification.

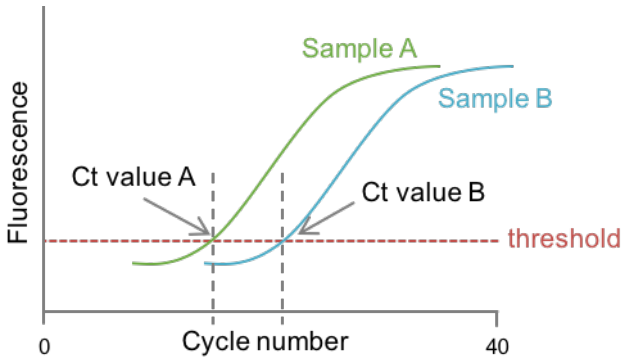

Figure 14. Determination of the Ct-value. Schematic illustration of the qPCR amplification curves for a gene of interest in two samples are shown. The spot where the reaction curve intersects the threshold line is defined as the Ct-value. The expression of the gene of interest in sample A is higher than in B, as it takes fewer cycles to reach the set threshold.

Experimental workflow

The RT product was diluted with nuclease-free water to obtain a cDNA concentration of 3 ng/µl in each sample. Either TaqMan® or SYBRgreen assays were used to detect the genes of interest (*Table 4*). For TaqMan® assays the assay mix contained 2.5 µl of 2x TaqMan® Universal PCR Master Mix, no AmpErase® UNG (Applied Biosystems, cat. no. 4324018) and 0.25 µl of the appropriate TaqMan® expression assay (20x). For SYBRgreen assays, primer pair sequences were obtained from PrimerBank and reconstituted in nuclease-free H_2O at a concentration of 10 µM. Each SYBRgreen assay mix consisted of 2.5 µl of SYBR Select Master Mix (Life Technology, cat. no 4472908), 0.1 µl of both the forward and reverse primer and 0.3 µl nuclease-free H_2O. Assay mix (2.75 µl or 3 µl for TaqMan reaction or SYBRgreen reaction, respectively) and diluted sample (2.25 µl or 2 µl for TaqMan reaction or SYBRgreen reaction, respectively) were combined in a MicroAmp Optical 384-well reaction plate (Applied Biosystems) to a final volume of 5 µl using a Bravo Automated Liquid Handling Platform (Agilent Technologies Inc.). The plate was sealed, briefly centrifuged at 1000 rpm for 1 min and placed in a ViiA™ 7 Real-Time PCR system (Applied Biosystems) and set to run under following conditions for the TaqMan reaction: incubation at 95 °C for 10 min for polymerase activation, followed by 40 cycles of 95 °C for 15 sec (denaturation yielding single-stranded DNA) and 60 °C for 1 min (annealing and elongation). The programme for SYBR green was set as follows: 50 °C for 2 min, then 95 °C for 2 min, followed by 40 reaction cycles

(same settings as for TaqMan). Data was analysed using ViiA 7 Software (Applied Biosystems) and Microsoft Excel. If the qPCR software reported undetermined values for individual replicates, a Ct-value of 40 was assumed. Expression levels were standardized to the expression of β-actin (ACTB). Relative amounts of the targets were quantified using the $2^{-\Delta\Delta CT}$ method.[256]

Pre-amplification of cDNA

As cadherin 5 gene expression levels were found to be relatively low, a pre-amplification reaction was performed for this cDNA prior to qPCR analysis. 2.5 µl of diluted cDNA sample (conc. 3 ng/µl) were mixed with 2.5 µl of 1:100 diluted cadherin 5 TaqMan® expression assay (0.2x) and 5 µl of TaqMan® PreAmp Master Mix (Applied Biosystems, cat. no. 4391128). The pre-amplification reaction was performed in a Veriti Thermal Cycler (Applied Biosystems) using the following settings: initial incubation at 95 °C for 10 min, followed by 12 cycles of 95 °C for 15 sec and 60 °C for 4 min, and terminated at 99 °C for 10 min. The reaction product was diluted 1:10 for use in the qPCR reaction.

Table 4. Primers used for qPCR analysis

	Gene	TaqMan	SYBRgreen	
		Assay ID	forward (5' to 3')	reverse (5' to 3')
Porcine	Aggrecan	Ss03373377_m1		
	Versican	Ss04323140_m1		
	HAPLN1	Ss03391707_m1		
	Cadherin 5	Ss03378336_u1		
	β-actin	Ss03376160_u1		
	ADAMTS1		CGTGAACAAGACCGACAAGA	AACTCCTCCACCACACGTTC
	ADAMTS4		CCCCATGTGCAACGTCAAG	AGTCTCCACAAATCTGCTCAGTGA
	β-actin		TCTGGCACCACACCTTCT	GATCTGGGTCATCTTCTCAC
Human	Aggrecan	Hs00153936_m1		
	Versican	Hs00171642_m1		
	HAPLN1	Hs01091999_m1		
	ADAMTS1	Hs00199608_m1		
	ADAMTS4	Hs00192708_m1		
	β-actin	Hs01060665_g1		

4.10 miRNA expression analysis

miRNA expression was determined in porcine samples using the extracted RNA as described above in section 4.9.1.

4.10.1 RT reaction

RT reaction was performed using the TaqMan MicroRNA Reverse Transcription Kit (Applied Biosystems, cat. no. 4366596) and was used at a final reaction volume of 10 µl as follows: 100 ng RNA in 4.3 µl H_2O, 1 µl 10x RT buffer, 0.3 µl 100 mM dNTPs with dTTP, 1.2 µl 25 mM $MgCl_2$, 0.2 µl RNase Inhibitor, 1 µl of 10x Megaplex RT Primers (Human Pool A version 2.1, Applied Biosystems, cat. no. 4399966) and 2 µl Multiscribe Reverse Transcriptase. The RT-PCR reaction was performed in a Veriti Thermal Cycler (Applied Biosystems) with the following settings: 40 cycles of 16 °C for 2 min, 42 °C for 1 min and 50 °C for 1 sec, followed by incubation at 85 °C for 5 min to terminate the reaction.

4.10.2 qPCR

qPCR was conducted using TaqMan® assays according to the same protocol applied for gene expression analysis using the RT product in a concentration of 1 ng/µl. Used TaqMan® miRNA assays (life technologies) are listed in *Table 5.* U6 expression was used for normalisation.

Table 5. TaqMan miRNA assays used for qPCR analysis

Target miRNA	Assay ID	miRBase accession
U6 snRNA	001973	
hsa-miR-21-5p	000397	MIMAT0000076
hsa-miR-29b-3p	000413	MIMAT0000100
hsa-miR-133a-3p	002246	MIMAT0000427
hsa-miR-143-3p	002249	MIMAT0000435
hsa-miR-145-5p	002278	MIMAT0000437
hsa-miR-195-5p	000494	MIMAT0000461
hsa-miR-221-3p	000524	MIMAT0000278

4.11 Immunostaining

4.11.1 Sample processing

Human coronary arteries were collected under the Bristol Coronary Biobank ethical approval 08/H0107/48, which included both stented and unstented sections of coronary arteries and were provided for this study by Dr. Stephen J. White of the School of Clinical Sciences, University of Bristol. Human aorta and mice vessels (vein graft and inferior vena cava) were collected as described in section 4.3 and section 4.2, respectively. Tissues were immediately fixed in 10% formalin for 24 h at 4 °C to cross-link proteins and

prevent their degradation preserving the tissue architecture. Stented arteries were cut longitudinally and the stent was removed as careful as possible. Using an automated tissue processor tissues were dehydrated in graded ethanol baths and cleared in xylene, as both water and ethanol are largely immiscible with paraffin and were subsequently manually embedded in paraffin. Paraffin embedded samples were sectioned at 3 µm thickness (5 µm for human aorta) using a microtome and placed on adhesion glass slides. For the graft samples histological sectioning began at the centre of the graft to avoid cuff effects. Sections were baked at 37 °C in an oven overnight and subsequently stored at room temperature until staining.

4.11.2 Immunohistochemistry (IHC)

Sections were deparaffinised and rehydrated in graded ethanol baths with descending ethanol concentration. Next, sections were incubated in 0.3% H_2O_2 for 10 min to block endogenous peroxidases. Upon 3 wash steps with PBST for 5 min each, antigen retrieval was performed by incubating the slides in a boiling water bath in preheated 10 mM sodium citrate buffer (pH 6.0) for 30 min. The slides were allowed to cool down for further 30 min, followed by further 3 wash steps with PBST for 5min each.

Sections were blocked with either 20% goat (for rabbit primary antibody) or rabbit serum (for goat primary antibody) in PBS for 1 h at room temperature. The used blocking serum is derived from the same species as the secondary antibody to prevent its unspecific binding. The blocking solution was tipped-off and replaced with primary antibody or matched IgG control (5 µg/ml) in 1% goat/rabbit serum and incubated at 4 °C overnight. Applied primary antibodies and dilutions are listed below in *Table 6*.

The following day, after 3 washes in PBST for 5 min each, the slides were incubated with biotinylated goat anti-rabbit (human tissue: 1:250; Sigma-Aldrich, B7389; mice tissue: 1:400; Vector labs, BA-1000) or rabbit anti-goat (1:250; Dako, E0466) secondary antibodies for 1 h at room temperature. After further 3 wash steps sections were incubated with Extravidin-HRP (1:250, Sigma-Aldrich, E2886; mice tissue: Avidin D, 1:400, Vector labs, A-2004) in PBS for 1 h. Upon 3 washes, detection was carried out using the diaminobenzidine (DAB) solution (Vector labs, SK-4100) for 10 min. Sections were washed in dH_2O, counterstained for 15 sec in modified Harris Haematoxylin, dehydrated in graded ethanol baths and mounted in DPX. Histological slides with human sections were scanned using a digital scanning system (LEICA SCN400F) to provide a high resolution digital image. Images from mice sections were taken using a Leica DM2000 microscope interfaced to LAS software (version 4.3.0; Leica microsystems). IHC for the graft samples were performed by Marc Lynch, MSc, of King's College London.

Table 6. Antibodies and dilutions used for IHC in human and mice tissue samples

Target protein	Antibody ID	Species	Dilution	
			human	mouse
aggrecan	Abcam, ab36861	rabbit polyclonal	1:400	1:100
aggrecan neo (NITEGE)	Thermo, AF-PA11746	rabbit polyclonal	1:400	n/a
HPLN1	Abcam, ab103455	rabbit polyclonal	1:200	n/a
versican neo (DPEAAE)	Abcam, ab19345	rabbit polyclonal	1:400	1:100
MGP	Abcam, ab86233	rabbit polyclonal	1:100	n/a
SPP24	Santa Cruz, sc-169408	goat polyclonal	1:50	n/a
Decorin	Sigma-Aldrich, SAB2100539	rabbit polyclonal	n/a	1:00

4.11.3 Immunofluorescence

Human coronary arteries and aorta samples were processed as described for immunohistochemistry. After deparaffinising, sections were incubated with 0.5 unit/ml chondroitinase ABC (Sigma-Aldrich, C3667) for 1 h at 37 °C to improve antibody recognition. After blocking with 10% donkey serum in PBS for 1 h, sections were co-incubated with primary antibodies to aggrecan (1:10; Abcam, ab3778) and the aggrecan NITEGE neoepitope (1:200; Thermo, AF-PA11746) as well as matched isotope IgGs for negative controls. Following day, upon washing secondary antibodies (Alexa Fluor 647, cat. no. A31571 and Alexa Fluor 568, cat. no. A21069, Life technologies) were applied according to the primary antibody species for 1 hour at room temperature. After 3 washes cell nuclei were stained with DAPI (1:1000, Life Technology) for 10 minutes. Sections were visualized with a 20x CFI S Plan Fluor ELWD ADM objective or 60x Plan Apo VC NA 1.40 Nikon using an inverted Nikon NI-E microscope equipped with a Yokogawa CSU-X1 Spinning disk confocal unit and an Andor iXon 3 EM-CCD camera. Images were acquired using NIS-elements 4.0 software, and represent a maximum projection image of a Z-stack of 0.5 µm steps compassing 9 µm. Images were acquired at the Nikon Imaging Centre at King's College London with the help of Dr. Chris Molenaar and Dr. Ruifang Lu, King's College London.

4.12 Cell culture

4.12.1 SMC culture

Human coronary artery SMCs (HCASMC) were obtained from PromoCell (C-12511) and grown in M199 medium (Gibco™, cat. no 22340020) supplemented with 20% heat-inactivated FBS (Gibco™, cat no. 10500064) and antibiotics (100 U/ml penicillin and 100 µg/ml streptomycin) ('complete medium') on 0.04% gelatine at 37 °C in a humidified

atmosphere of 95% air/5% CO_2. The medium was changed every 2 days. For cell passaging upon 60-80% confluence the growth medium was removed and cells were washed 2 x with pre-warmed DMEM (Gibco™, cat. no. 10938025). Cells were detached with trypsin-EDTA 0.05% (Gibco™, cat. no.25300096) for few minutes at room temperature and trypsin activity was stopped by adding equal amounts of complete medium. The cell suspension was centrifuged at 1000 rpm for 5 min at room temperature and the supernatant was removed. Cells were resuspended in complete medium, counted and seeded at a density of $1x10^5$ in 6-well plates coated with 0.04% gelatine. Cells were washed with cold PBS twice and scraped off the surface with 700 µl lysis buffer (QIAzol Lysis Reagent, Qiagen, cat. no. 79306) for RNA extraction. The experiments were carried out with cells at passage 7-11.

4.12.2 EC culture

Human endothelial cells from different vascular territories were obtained from PromoCell (Human aortic EC (HAoEC): C-12272; Human umbilical vein EC (HUVEC): C-12250; Human coronary artery EC (HCAEC): C-12222; Human saphenous vein EC (HSaVEC): C-12232). Cells were cultured to confluence in T25 flasks cells on 0.04% gelatine in appropriate Endothelial Cell Growth Medium (PromoCell C-22011, C-22010, C-22020, C-22022, with the company provided SupplementMix) supplemented with antibiotics (100 U/ml penicillin and 100 µg/ml streptomycin) at 37 °C in a humidified atmosphere of 95% air/5% CO_2. For comparison analysis with SMCs, HCAECs were seeded at a density of $1x10^5$ in 6-well plates (Greiner bio-one) coated with 0.04% gelatine. Cells were washed with cold PBS twice and scraped off the surface with 700 µl lysis buffer (QIAzol Lysis Reagent, Qiagen, cat. no. 79306). The experiments were carried out with cells at passage 4-9.

4.12.3 Everolimus treatment

Everolimus was a kind gift from Novartis, Switzerland and was shipped under a material transfer agreement with King's College London. It was dissolved in dimethyl sulfoxide (DMSO) and aliquots with a stock concentration of 20 µM were prepared and kept at -20 °C. 24 h after cells were seeded in complete medium (density of $1x10^5$ in 6-well plates), cells were washed twice with DMEM and were cultured in either serum-free M199 medium for HCASMCs or HCAEC culture medium with growth factors (PromoCell, C-22020) supplemented with 20 nM everolimus or equivalent concentration of DMSO control for 48 h. Each experiment was performed in triplicates. RNA was harvested as described above.

4.12.4 Cell counting

To determine the cell number, 10 µl of a cell suspension were pipetted into a glass slip covered Neubauer counting chamber (AC1000). All cells within the 4 squares placed at the corners (each 1 mm^2) were counted under a microscope. The average count was then multiplied by 10^4 to determine the number of cells in 1 ml.

4.12.5 Viability and cell count

Viability and cell count of HCAECs were determined using the Nucleo Counter® NC-3000™. This system enables automated cell counting. Cells were seeded in 6-well plates at a density of $1x10^5$ and treated with everolimus or DMSO as described above for 24 h. To retrieve the total cells, cell medium was collected including the floating dead cells, and combined with the detached cells of each well. After centrifugation cells were resuspended in growth medium and 'solution 18' was added in a 1:20 ratio. 'Solution 18' contains acridine orange, staining all living and dead cells, thus providing a total count. It further contains DAPI, which stains all dead cells. The cell suspension is then loaded on slides and analysed by the Nucleo Counter® NC-3000™ with the 'Viability and Cell Count - Method 2 Assay'. The viability is calculated by the NucleoView NC-3000™ software as follows: $\%viability = \frac{Ct-Cnv}{Ct} \text{ x } 100\%$.

(C_t: concentration of total cells, C_{nv}: concentration of non-viable cells)

4.13 Statistical analysis

Data are shown as average (Av) ± standard error of the mean (SEM). If standard deviation (SD) is used, it is indicated. MS data of untargeted proteomics were quantified using normalized ion intensities (total ion current = TIC). IBM® SPSS® statistics software (version 22-24) and Microsoft® Excel® (version 15.20) were used for statistical calculations, GraphPad Prism® (version 6.0e) and Microsoft® Excel® (version 15.20) were used for data illustration. For OCT analysis, 2-way analysis of variance (ANOVA) was applied to assess neointimal volume, minimal lumen area and strut coverage between BMS and DES over time. 1-way ANOVA was applied for time-dependent changes in protein expression in BMS and DES. Unpaired Student's *t*-test with unequal variance was applied for proteomics differences between neointimal BMS and DES, POBA early and late, for differences between BMS and DES at each time point as well as the comparison between BMS/DES day 28 and POBA late. *T*-test was not performed if a protein was undetectable in the majority of samples from 1 of the 2 groups compared, which is denoted as n/a (not applicable). Unpaired Student's *t*-test with unequal variance was also used for targeted proteomics analysis between aorta and vein samples. MultiExperiment Viewer software (MeV, version 4.9) was applied using a Pearson

Correlation for protein clustering. For gene expression analysis of porcine tissue *t*-tests were applied for differences between BMS and DES and regression analysis for changes over time (*P*-value for trend). Differences in gene expression between different EC territories were assessed by 1-way ANOVA. Differences in gene expression between ECs and SMCs or treated and untreated cells respectively were determined using the Student's *t*-test. Student's *t*-test with unequal variance was also used for densitometry quantification of immunoblots. P-values ≤ 0.05 were considered significant.

5 RESULTS

5.1 Porcine model of stent injury

BMS or DES were implanted in porcine coronary arteries during coronary angioplasty under OCT guidance. Coronary arteries subjected to POBA alone without stent deployment served as controls. To prevent the risk of in-stent thrombosis pigs were treated with dual anti-platelet therapy daily. At five consecutive time points 1, 3, 7, 14 and 28 days post-stent implantation, follow-up OCT was performed before harvesting the arteries for protein extraction. Macroscopically all stented arteries at day 28, regardless of the deployed stent type showed a neointima formation covering the stent struts. The evolved neointima was separated from the media and analysed in a separate proteomics analysis. The study design is summarized in *Figure 15A* and characteristics of all analysed samples are shown in *Table 7*. ECM proteins of the vascular media were sequentially extracted using a three-step extraction method as previously described[114], while the more fragile neointima was extracted in a single step (*Figure 15B)*. In total 45 samples were analysed by proteomics (*Figure 15C*). A close-up of the separated neointima is shown in *Figure 15D*.

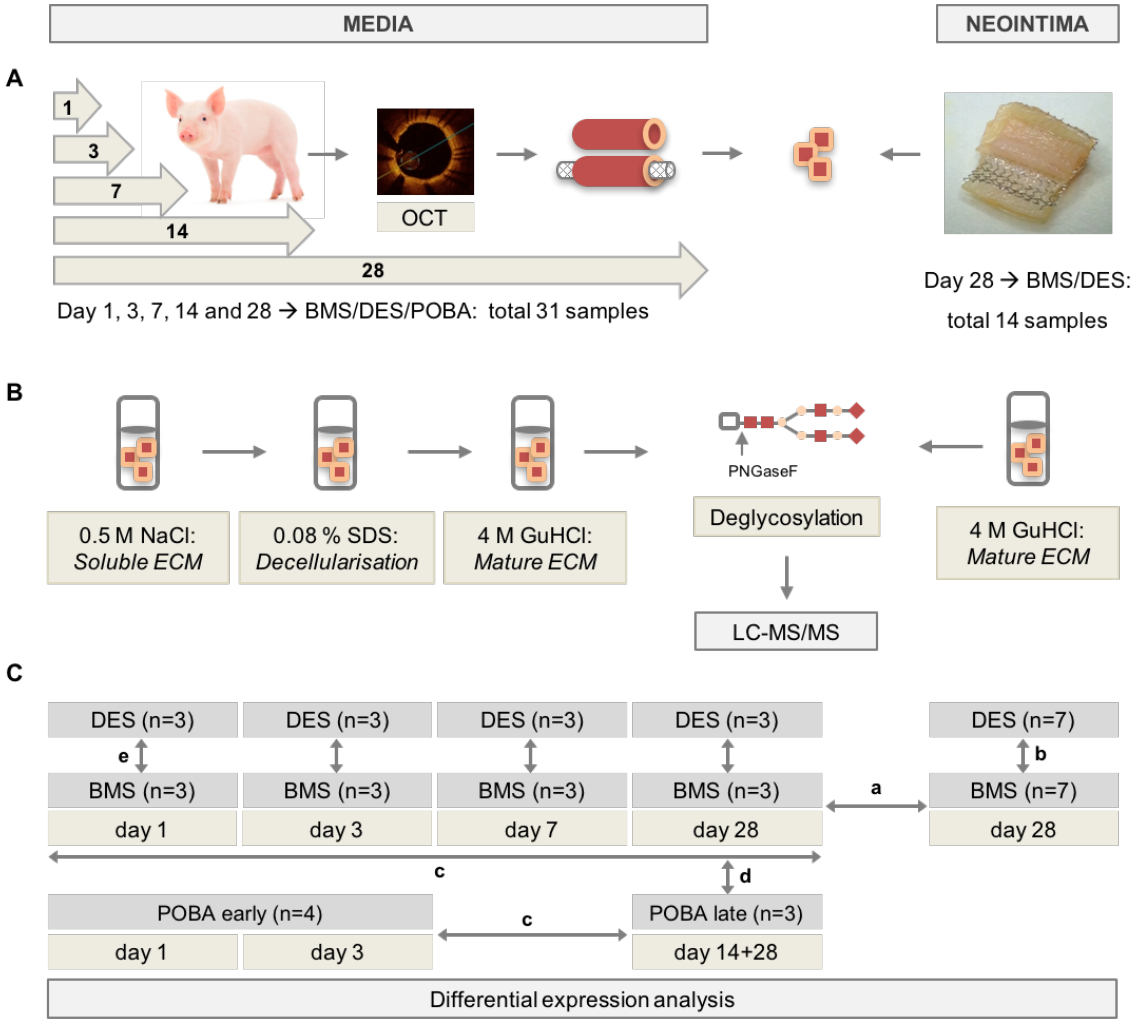

D

Figure 15. Porcine model of stent injury. (A) Pigs underwent PCI with BMS/DES/POBA treatment. Following OCT analysis coronary arteries were harvested for proteomics analysis at 1, 3, 7, 14 and 28 days after stent deployment. The evolved neointimal lesions at day 28 were analysed separately. (**B**) ECM proteins were obtained using our previously published extraction procedure in three steps for the media and in a single step for the neointima, followed by LC-MS/MS analysis of the deglycosylated tryptic peptides. (**C**) In total, 45 samples were analysed by proteomics. An overview of the conducted proteomics comparisons is shown: a) Media vs. neointima. b) Stent dependent changes in the neointima. c) Time dependent changes in BMS/DES/POBA. d) Stent vs. POBA at late stage. e) Stent dependent changes in the media at each day. (**D**) Close-up of the neointimal tissue (right) upon separation from the media (tissue including stent struts). Stent strut impressions are visible on the neointimal tissue.

5.2 OCT findings

OCT on follow-up was deployed for qualitative characterization of the neointima, classifying the neointimal patterns into homogenous with peristrut attenuation or with ring, heterogeneous or layered according to its backscatter and optical intensity (*Figure 16A*). At day 14 almost 80% of the neointima in both groups (BMS=78.3%, DES 78.5%) showed a homogenous pattern, for DES this increased to 98.5% at day 28. In contrast, no heterogeneous pattern was present at day 28 in both groups, while 39.8% for BMS had a layered pattern. In addition, OCT was used to assess differences in neointimal volume, minimal lumen area, stent strut coverage and apposition between BMS and DES stented arteries. OCT analysis revealed that up to 14 days post-stent implantation neointimal volume was higher in BMS compared to DES (P=0.025), but no difference was evident at day 28 (P=0.890) (*Figure 16B*). The minimal lumen area (P=0.894), malapposed struts (P=0.238) and stent strut coverage (P=0.778) were not different for BMS and DES during the 28 day follow-up. Thus, molecular differences for the clinically observed different BMS/DES healing responses were investigated using proteomics.

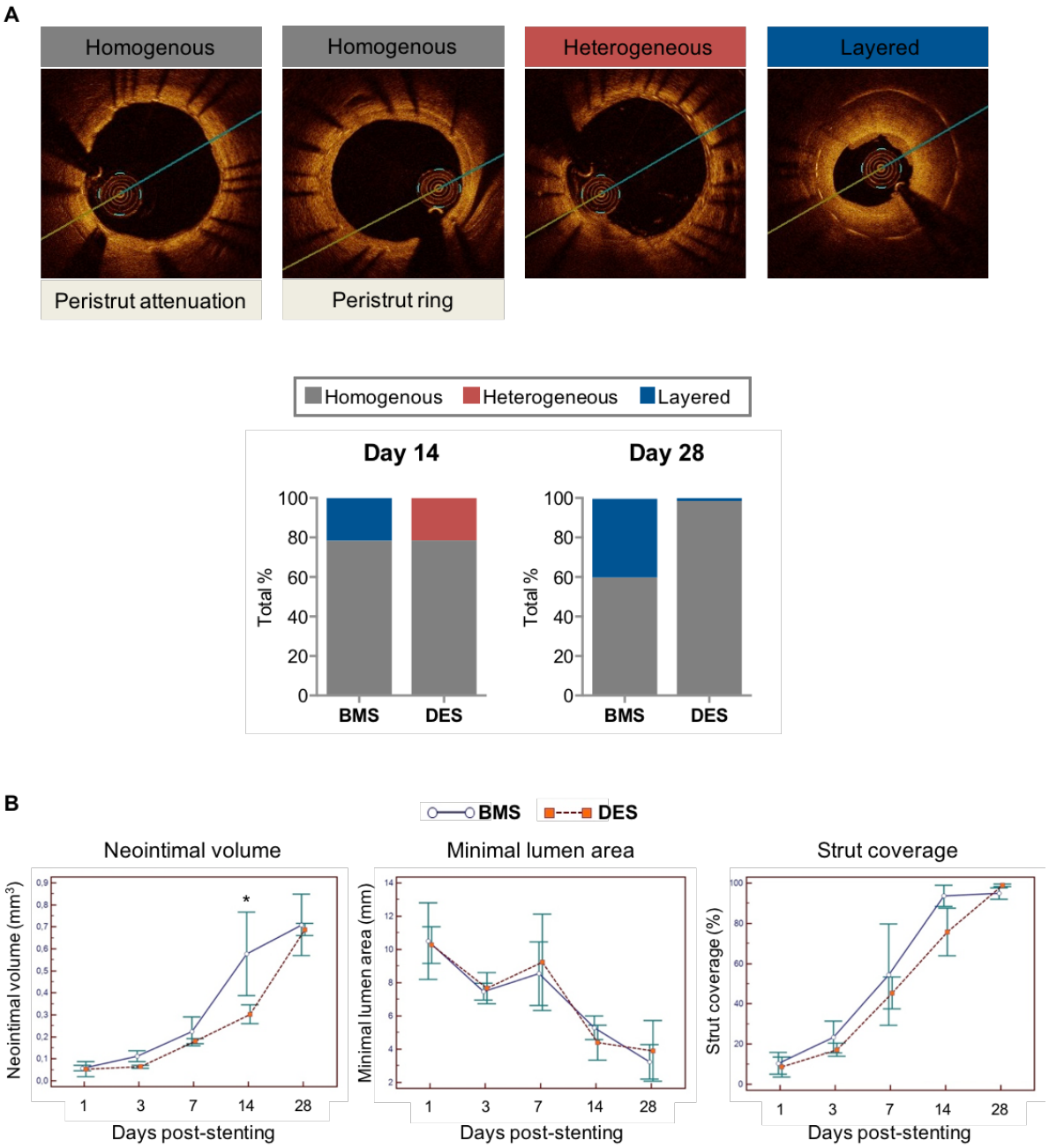

Figure 16. OCT findings. (A) Neointimal patterns as characterized by OCT: representative images of homogenous with peristrut attenuation/ring, heterogeneous and layered. Percentage distribution of the three main patterns in BMS and DES at day 14 and day 28. (n=3 for each group, except BMS day 14 n=2). **(B)** At 14 days post-stent implantation neointimal volume was higher in BMS compared to DES (**P*=0.025) but showed no significant difference at day 28. *P*=0.89 (2-way ANOVA). The OCT data were generated by Dr. Wojtek Wojakowski and colleagues.

Table 7. Sample characteristics

MEDIA									
Lifetime [days]	Stent/ POBA	Coronary artery	Sex	Weight [kg]	Age [months]	Size [mm]	AVD [mm]	Target overstretch [mm]	Inflation [atm]
1	BMS	LAD	M	35	3	3,5x15	3.4	4.1	22
		LCX dis	M	35	3	3,5x15	3.0	3.5	12
		RCA prox	F	38	3	3,5x15	3.0	3.6	12
	DES	LAD	F	38	3	3,0x15	3.0	3.5	23
		LCX prox	F	38	3	3,5x15	3.1	3.7	12
		RCA	M	35	3	3,0x15	3.0	3.6	24
	POBA early	LCX prox	M	35	3	3,5x15	3.0	3.5	28
		RCA dis	F	38	3	3,5x15	2.9	3.5	12
3	BMS	LAD	M	45	4	3,0x15	2.7	3.2	15
		LCX	F	45	4	3,0x15	2.8	3.3	16
		RCA dis	M	45	4	3,0x15	2.7	3.2	14
	DES	LAD	F	45	4	3,0x15	2.8	3.3	14
		LCX	M	45	4	3,0x15	2.6	3.1	11
		RCA prox	F	45	4	3,0x15	2.7	3.0	14
	POBA early	RCA prox	M	45	4	3,0x15	2.8	3.4	16
		RCA dis	F	45	4	3,0x15	2.5	3.0	14
7	BMS	LAD prox	M	32	3	3,5x15	3.1	3.7	14
		LCX prox	F	33.5	3	3,5x15	2.9	3.4	10
		RCA prox	F	33.5	3	3,0x15	2.8	3.4	18
	DES	LAD prox	F	33.5	3	3,5x15	3.0	3.5	9
		LCX prox	M	32	3	3,5x15	3.0	3.6	9
		RCA prox	M	32	3	3,0x15	2.4	2.9	10
14	POBA late	LCX prox	M	33	3	3,0x15	2.5	2.9	14
28	BMS	LAD prox	F	29	3	3,5x15	2.9	3.5	10
		LCX prox	F	28	3	3,0x15	2.5	3.0	10
		RCA prox	F	28	3	3,0x15	2.0	2.4	10
	DES	LCX prox	F	29	3	3,5x15	3.0	3.5	9
		RCA medial	F	29	3	3,5x15	3.1	3.5	9
		RCA dis	F	28	3	3,0x15	2.0	2.4	9
	POBA late	LAD	F	28	3	3,5x15	2.9	3.5	10
		RCA prox	F	29	3	3,5x15	2.9	3.5	12

NEOINTIMA									
Lifetime [days]	Stent	Coronary artery	Sex	Weight [kg]	Age [months]	Size [mm]	AVD [mm]	Target overstretch [mm]	Inflation [atm]
28	BMS	LAD prox	F	29	3	3,5x15	2.9	3.5	10
		LCX prox	F	28	3	3,0x15	2.5	3.0	10
		RCA prox	F	28	3	3,0x15	2.0	2.4	10
		RCA prox	M	47	3.5	3,5x8	3.0	3.6	12
		RCA dis	M	47	3.5	3,0x12	2.8	3.4	20
		RCA prox	M	48	3.5	4,0x14	3.4	4.1	12
		LCX	M	48	3.5	3,0x15	2.8	3.4	16
	DES	LCX prox	F	29	3	3,5x15	3.0	3.5	9
		RCA medial	F	29	3	3,5x15	3.1	3.5	9
		RCA dis	F	28	3	3,0x15	2.0	2.4	9
		LAD dis	M	47	3.5	3,0x15	2.6	3.1	12
		LCX med	M	47	3.5	3,5x18	3.2	3.9	18
		RCA dis	M	48	3.5	3,5x15	2.9	3.8	12
		LAD med	M	48	3.5	3,0x18	2.4	2.9	9 →12

Clinical characteristics of pigs (lifetime, sex, weight, age at intervention) and PCI specific parameters are shown, including used stent type, balloon/stent size at implantation, average vessel diameter (AVD) as measured by angiography before dilatation, final size of stent/balloon after expansion (target overstretch) as well as the applied inflation pressure. Macroscopically neointima formation was detected in all arteries at 28 days, independent of stent type. Prox = proximal, dis = distal.

5.3 miRNA changes in the vascular stent injury model

Since previous studies had shown that miRNAs are critically involved in neointimal hyperplasia in proliferative vascular diseases[76, 77], we aimed to investigate the changes of representative miRNAs associated with SMC proliferation (miR-21, miR-133, miR-143, -145 and -221) and fibrosis (miR-21, miR-29b, miR-195) in our stent injury model (*Figure 17*). Except for miR-133a and miR-145, other evaluated miRNAs were differentially expressed compared to controls at day 28, either for BMS/DES or for both. Especially the pro-fibrotic miRNA, miR-21, showed a remarkable increase in stented arteries similar to previous reports in stented arteries[257] and vein grafts[258]. Also, miR-221, which is implicated in SMC phenotypic switch, showed a notable increase.

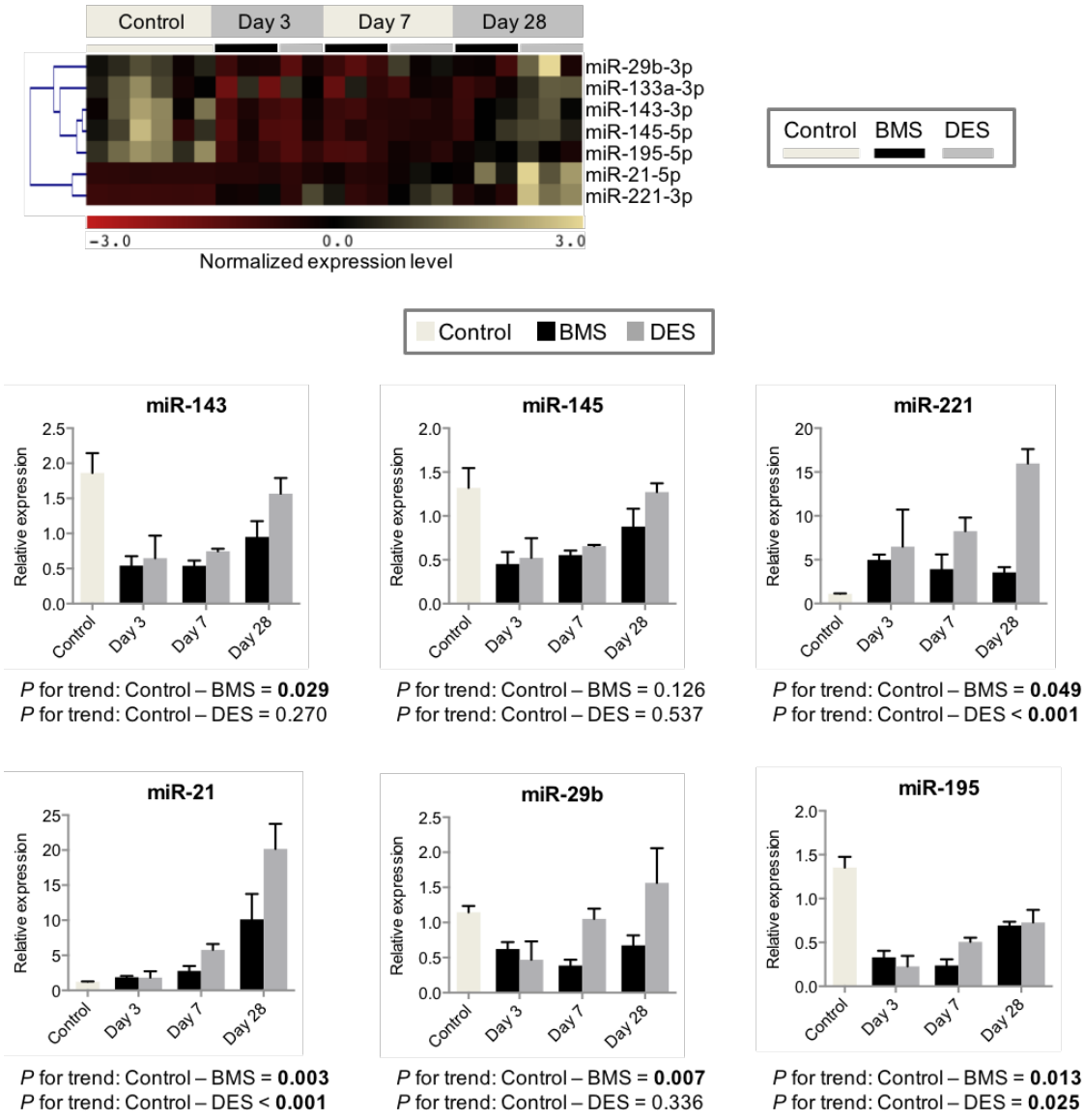

Figure 17. miRNA changes upon stenting. Heat map for evaluated miRNA changes. Pearson correlation. Changes displayed in bar graphs, except for miR-133a, which was not significant (*P* for trend Control-BMS = 0.062, Control-DES = 0.859). n=3 per time point for stented arteries, except DES day 3: n=2. n=6 unstented control coronary arteries. miRNA expression values were normalized to unstented control arteries. Linear regression analysis for *P*-value for trend.

5.4 ECM proteins identified in the media and neointima

5.4.1 Impact of custom-made porcine ECM database

To improve the identification of ECM proteins upon LC-MS/MS analysis, a custom-made porcine ECM database was generated for database search. This database contained a comprehensive porcine sequence list of previously published ECM proteins on the background of a conventional human database. The commonly available porcine databases are incomplete, thus do not contain the whole sequence of all proteins. In addition, not every protein is well annotated in porcine databases. Despite highly conserved protein sequences in humans and pigs for many proteins, e.g. 90.3% similarity between porcine and human decorin, the remaining differences in the sequence prevent an optimal peptide match, thus lowering the proteomics quantification yields for affected proteins. *Figure 18* shows the improvement in protein identification and quantification using the custom-made porcine database compared to the standard human, the standard pig and to the combination of both in a hybrid database.

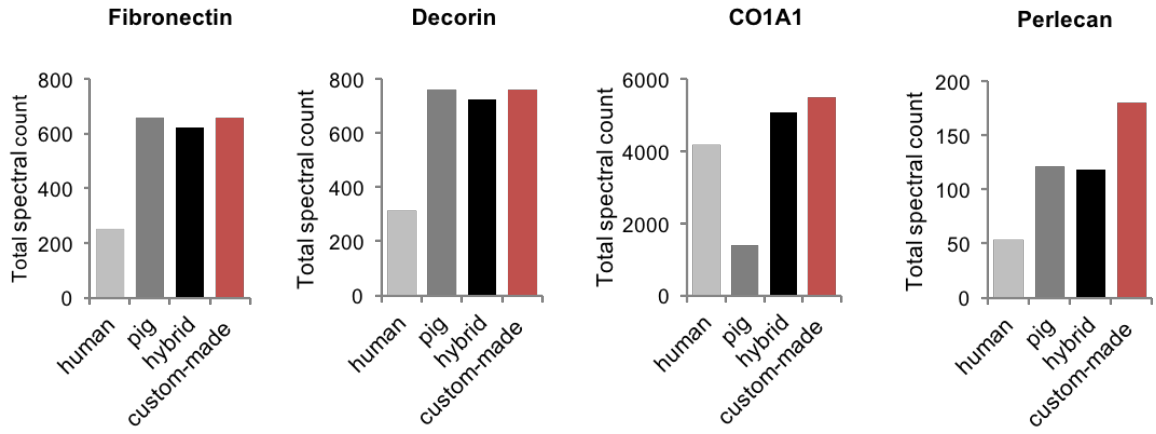

Figure 18. Impact of custom-made database on protein identification and quantification. The sum of total spectral counts in 5 samples are shown for selected proteins. Search with a hybrid database, which is the combination of a pig and human database is superior to a human database for protein identification and quantification due to a higher sequence coverage. For many ECM proteins, such as fibronectin and decorin, which are well annotated and fully sequenced, the custom-made database does not offer a major improvement. However, for other proteins, such as collagen alpha-1 (I) (CO1A1) and perlecan for example, which are not well annotated and fully sequenced, the custom-made database has a remarkable impact on the sequence coverage.

5.4.2 Comparison between media and neointima

A total of 151 unique ECM proteins were identified overall in the media (*Table 8*) and neointima (*Supplemental table 2*) with a minimum of 2 high-confidence peptides (*Figure 19A*). Proteins only identified in the media (n=11) or neointima (n=26) are marked with an asterisk in the table. Despite being plasma-derived, lipoproteins were included to the list due to their intimate relationship with proteoglycans and their obvious importance in cardiovascular pathology. While the 10 most abundant ECM proteins of the media made up more than half of the ECM content of the media, the same ECM proteins constituted less than a third of the neointima, indicating a more diverse ECM composition of the neointima compared to the media (*Figure 19B*). Fibrillar collagens and small leucine-rich proteoglycans (SLRPs) were increased in the vessel media, while basement membrane proteins were more abundant in the neointima. The difference in ECM composition is highlighted by the collagen alpha-1 (I) to fibronectin ratio in the media and neointima of stented vessels (*P*=0.003) (*Figure 19C*).

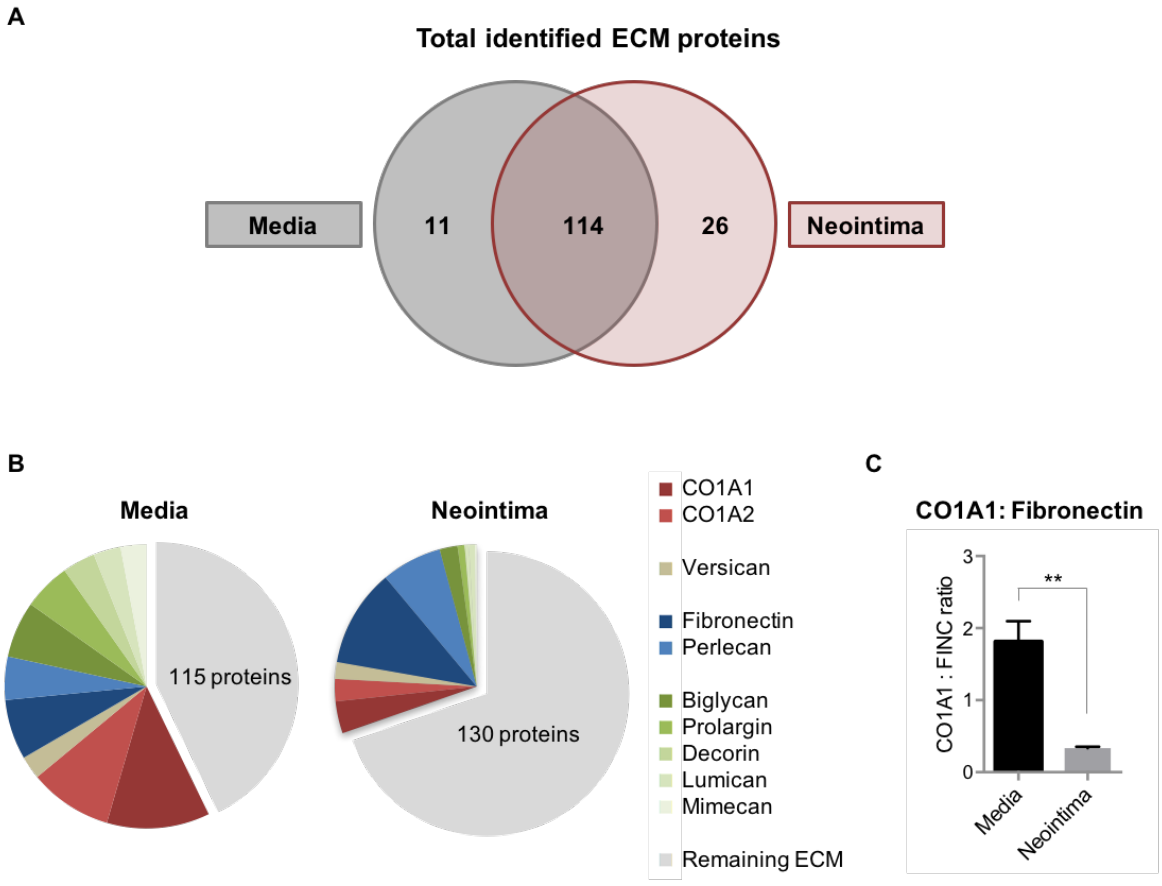

Figure 19. ECM proteins identified in the media and neointima. (**A**) Overall in the media and neointima a total of 151 unique ECM proteins were identified. The Venn diagram depicts the distribution of the proteins in the media and neointima. (**B**) Pie charts illustrate the relative contribution of the top 10 abundant ECM proteins in the media and neointima of stented vessels. (**C**) Collagen alpha-1 (I) (CO1A1) to fibronectin ratio in the media and neointima of stented vessels is shown. n=6 (media), n=14 (neointima). ***P*<0.01 (*t*-test with unequal variance).

Table 8. Extracellular proteins identified by proteomics analysis in the media of stented/balloon dilated porcine coronary arteries.

		Bare-metal stent Total ion current x 10^6 Av±SD					Drug-eluting stent Total ion current x 10^6 Av±SD					Plain old balloon angioplasty Total ion current x 10^6 Av±SD		
Identified Proteins	**Accession Number**	**BMS 1**	**BMS 3**	**BMS 7**	**BMS 28**	***P* BMS**	**DES 1**	**DES 3**	**DES 7**	**DES 28**	***P* DES**	**POBA early**	**POBA late**	***P* POBA**
Adipocyte enhancer-binding protein 1	F1SSF7_PIG	0.3±0.5	0.2±0.3	1.6±1.3	1.1±0.5	0.136	0.1±0.2	0.0±0.0	1.0±0.9	6.2±4.8	**0.046**	0.9±0.6	2.0±1.2	0.258
Aggrecan	F1SKR0_PIG	6.5±2.3	2.7±0.9	18.0±11.4	28.2±9.0	**0.010**	5.2±2.1	10.9±9.3	18.3±7.6	52.5±11.1	**0.000**	5.3±3.0	17.3±10.7	0.187
Agrin	I3LGD9_PIG	5.7±2.5	5.4±2.8	8.7±1.1	9.4±1.7	0.112	5.7±3.3	5.2±3.5	8.8±1.3	6.2±1.6	0.400	5.6±4.0	9.9±1.1	0.118
Alpha-2-HS-glycoprotein	FETUA_PIG	1.4±1.4	1.6±1.5	2.6±1.9	5.2±8.5	0.717	4.0±2.1	3.7±2.4	3.7±3.7	7.8±7.5	0.623	3.7±2.2	1.9±1.4	0.232
Annexin A1	ANXA1_PIG	1.8±0.8	2.3±1.0	1.7±0.6	2.0±2.2	0.943	2.4±1.1	3.7±1.6	3.7±2.9	3.7±0.9	0.765	3.1±0.8	0.5±0.2	**0.005**
Annexin A2	ANXA2_PIG	10.8±1.8	14.2±4.7	24.3±4.3	37.2±31.9	0.265	9.5±1.5	12.7±7.0	20.8±4.3	28.1±7.7	**0.016**	14.2±10.5	14.9±2.9	0.898
Antithrombin-III	Q7M364_PIG	2.5±1.3	0.8±0.5	0.0±0.0	0.7±0.8	**0.028**	1.4±0.7	14.2±17.7	2.1±1.1	1.7±0.7	0.289	2.5±1.8	0.3±0.5	n/a
Apolipoprotein A-I	APOA1_PIG	18.7±4.3	11.0±8.0	21.2±12.5	25.6±16.3	0.484	17.5±2.2	26.8±13.5	19.1±13.2	24.8±10.0	0.686	19.5±7.7	12.7±5.6	0.231
Apolipoprotein A-IV	APOA4_PIG	0.1±0.1	0.0±0.0	0.1±0.1	0.4±0.6	0.394	0.0±0.1	1.7±1.1	0.4±0.5	0.5±0.3	0.053	0.0±0.0	0.1±0.1	n/a
Apolipoprotein C-III	APOC3_PIG	4.4±2.5	2.3±1.4	0.6±0.6	0.7±0.7	**0.049**	4.3±1.7	5.6±2.9	0.5±0.6	0.8±0.4	**0.016**	6.5±3.9	0.2±0.4	**0.048**
Apolipoprotein E	APOE_PIG	15.7±4.0	11.3±7.0	1.8±1.7	1.6±0.7	**0.006**	8.9±4.2	82.2±70.2	8.9±6.2	1.9±2.4	0.071	26.2±20.3	1.2±0.3	n/a
Apolipoprotein H	I3LGN5_PIG	21.7±6.2	20.3±5.4	18.7±2.7	29.4±18.3	0.603	26.7±5.1	36.6±27.2	29.3±14.7	59.5±10.6	0.139	23.1±4.4	19.5±8.5	0.551
Apolipoprotein R	APOR_PIG	1.6±1.1	1.0±0.3	0.8±0.8	0.3±0.3	0.213	2.6±1.6	6.8±2.7	0.9±0.8	0.5±0.5	**0.006**	1.9±2.3	0.0±0.0	n/a
Asporin	F1SUE4_PIG	78.2±16.2	62.0±11.9	86.2±17.1	150.3±37.5	**0.007**	77.5±16.5	81.7±37.1	90.1±30.2	157.3±43.8	0.059	61.0±14.8	87.4±40.2	0.375
Biglycan	K7GP55_PIG	796.0±130.8	648.1±186.6	952.7±42.3	1503.4±443.4	**0.014**	748.6±200.3	750.0±367.0	1002.9±236.7	1972.6±202.2	**0.001**	659.9±210.4	971.4±110.9	0.056
Carboxypeptidase-like protein X2	F1SEC6_PIG	0.0±0.0	0.0±0.0	0.0±0.0	0.0±0.0	n/a	0.0±0.0	0.0±0.0	0.0±0.0	0.4±0.2	n/a	0.0±0.0	0.0±0.0	n/a
Cathepsin D	Q4U1U3_PIG	1.6±0.5	1.9±0.3	7.2±4.8	8.8±13.1	0.523	1.1±1.5	2.3±1.6	4.1±3.6	3.7±1.8	0.412	3.6±3.7	3.2±1.8	0.852
Cathepsin G	F1SGS1_PIG	0.5±0.3	0.0±0.0	0.0±0.0	0.0±0.0	n/a	0.8±0.8	0.8±0.7	0.1±0.1	0.0±0.0	0.201	0.7±0.9	0.0±0.0	n/a
Chitinase-3-like protein 1	CH3L1_PIG	0.0±0.0	0.0±0.0	0.0±0.0	0.3±0.5	n/a	0.0±0.0	0.0±0.0	0.0±0.0	0.0±0.0	n/a	0.0±0.0	0.0±0.0	n/a
Chondroitin sulfate proteoglycan 4*	CSPG4_ HUMAN	0.1±0.1	0.0±0.0	0.3±0.5	0.0±0.0	0.415	0.0±0.0	0.0±0.0	0.0±0.0	0.0±0.0	n/a	0.1±0.2	0.0±0.0	n/a
Clusterin	CLUS_PIG	98.2±51.7	59.8±17.0	45.6±16.8	16.4±10.7	**0.048**	59.0±19.6	273.4±202.6	61.0±24.0	21.2±10.8	0.060	95.9±46.7	19.7±8.5	**0.044**
Collagen alpha-1 (I)	CO1A1_PIG	2915.1±375.6	2913.2±993.1	4118.5±199.0	2622.2±1399.4	0.244	2749.1±797.9	1973.1±1213.2	3353.0±487.7	3996.0±273.1	0.062	2055.2±391.6	2088.2±468.7	0.926
Collagen alpha-1 (II)*	I3LSV6_PIG	108.4±22.4	127.9±54.4	149.6±3.8	68.4±34.1	0.090	100.9±39.9	77.0±38.5	122.7±62.7	116.6±15.0	0.584	82.5±12.5	67.2±16.1	0.248
Collagen alpha-1 (III)	F1RYI8_PIG	332.8±111.3	571.8±520.0	454.4±127.6	472.3±201.4	0.797	302.2±59.7	185.0±119.2	318.7±83.5	480.3±67.1	**0.019**	252.0±85.1	431.9±112.0	0.087
Collagen alpha-1 (IV)	M3V819_PIG	3.1±2.1	5.7±1.9	7.5±2.2	8.8±3.3	0.091	2.5±0.4	4.2±2.5	6.6±0.9	4.3±1.2	0.055	4.3±2.7	5.2±1.7	0.628
Collagen alpha-1 (V)	F1S021_PIG	81.8±19.0	108.4±42.0	181.5±36.4	174.3±88.5	0.128	82.2±11.7	109.9±66.9	126.0±20.7	251.3±25.0	**0.003**	75.2±29.8	96.9±37.1	0.453
Collagen alpha-1 (VI)	CO6A1_PIG	4.5±1.2	3.6±3.9	2.0±0.4	10.3±8.4	0.221	4.8±2.2	6.2±5.1	2.6±2.9	1.8±0.3	0.371	6.2±4.7	7.9±6.9	0.746
Collagen alpha-1 (VIII)	F1SKX7_PIG	0.2±0.3	0.2±0.4	1.5±0.6	0.5±0.4	**0.013**	0.1±0.2	0.4±0.4	1.8±0.9	3.2±1.0	**0.002**	0.2±0.4	0.2±0.3	n/a
Collagen alpha-1 (XI)	F1S571_PIG	48.9±9.7	50.3±22.3	111.5±27.7	103.7±54.7	0.088	45.9±2.4	62.4±36.9	60.7±17.8	190.8±17.9	**0.000**	42.1±14.8	56.5±23.0	0.408
Collagen alpha-1 (XII)	COCA1_PIG	7.1±0.5	3.4±2.9	17.2±16.6	46.9±52.0	0.273	5.7±0.7	3.8±1.8	14.2±10.6	53.7±15.8	**0.001**	6.1±2.5	3.4±3.6	0.338
Collagen alpha-1 (XV)	COFA1_PIG	3.2±1.0	2.5±0.9	9.0±2.7	9.5±4.8	**0.028**	2.3±1.8	2.1±1.2	10.0±2.2	14.1±3.8	**0.001**	4.4±3.8	6.8±4.6	0.491
Collagen alpha-1 (XVIII)	COIA1_PIG	10.5±3.5	12.3±7.3	11.4±1.1	6.7±1.3	0.420	8.5±3.5	12.9±5.7	12.2±4.8	1.6±0.3	**0.035**	10.6±4.7	10.5±1.4	0.990

Collagen alpha-1 (XX)	COKA1_PIG	14.6±12.5	5.7±4.3	22.3±9.2	60.8±43.8	0.081	8.2±2.6	4.0±2.6	24.8±9.2	22.2±2.9	**0.003**	12.5±4.4	21.3±4.4	0.053
Collagen alpha-2 (I)	F1SFA7_PIG	2540.2±281.6	2097.8±569.3	3114.0±344.6	2616.7±1337.8	0.482	2441.6±563.3	1949.6±1173.6	2966.9±215.8	4329.5±613.6	**0.019**	1819.5±446.0	2184.2±434.5	0.332
Collagen alpha-2 (IV)	F1RLL9_PIG	3.1±1.8	6.9±2.4	7.2±4.2	7.8±0.2	0.184	1.9±0.6	4.1±3.7	8.4±3.2	2.1±0.4	**0.038**	5.4±6.5	5.6±2.6	0.961
Collagen alpha-2 (V)	Q59IP2_PIG	84.2±45.2	108.2±40.4	172.3±73.6	173.7±84.4	0.281	87.0±14.8	91.2±57.0	156.5±6.4	200.7±119.1	0.188	75.8±40.3	84.1±59.3	0.846
Collagen alpha-2 (VI)	I3LQ84_PIG	13.4±3.9	15.3±15.9	7.1±1.6	41.7±41.5	0.309	14.8±5.6	23.3±24.5	10.3±4.8	8.5±3.2	0.534	24.5±16.6	31.7±22.6	0.669
Collagen alpha-2 (XI)*	A5D9K7_PIG	23.6±4.3	36.2±12.2	49.2±10.5	37.8±22.7	0.250	22.2±5.9	32.8±16.0	30.3±10.1	52.3±10.3	0.055	24.6±9.4	25.0±7.5	0.951
Collagen alpha-3 (V)	Q59IP1_PIG	1.1±0.7	1.6±1.2	1.9±0.8	5.8±5.3	0.220	1.2±0.7	1.9±2.1	2.1±1.0	3.2±1.3	0.402	0.6±0.4	1.2±0.9	0.338
Collagen alpha-3 (VI)	I3LUR7_PIG	42.7±11.3	38.2±40.2	16.2±6.8	92.4±98.5	0.411	32.6±15.3	41.5±39.4	21.3±16.8	18.4±11.3	0.624	58.0±38.7	63.2±66.2	0.911
Collagen alpha-6 (VI)	CO6A6_PIG	0.0±0.0	0.0±0.0	0.0±0.0	14.1±24.5	n/a	0.0±0.0	0.0±0.0	0.0±0.0	0.0±0.0	n/a	0.2±0.3	0.0±0.0	n/a
Complement C3	CO3_PIG	4.3±1.1	0.1±0.2	0.6±0.3	1.8±3.1	0.063	3.3±1.4	14.2±20.9	1.4±1.6	0.4±0.6	0.405	12.3±8.9	1.8±2.1	0.097
Complement component C9	A0SEG9_PIG	0.0±0.0	0.0±0.0	0.0±0.0	0.0±0.0	n/a	0.0±0.0	1.0±1.7	0.0±0.0	0.0±0.0	n/a	0.0±0.0	0.0±0.0	n/a
Connective tissue growth factor	CTGF_PIG	0.4±0.3	0.3±0.5	0.7±0.6	0.0±0.0	0.308	0.8±0.4	0.4±0.3	0.7±0.4	0.1±0.2	0.212	0.2±0.2	0.0±0.0	n/a
Decorin	PGS2_PIG	581.1±67.5	418.8±208.1	411.1±91.6	1166.4±602.8	0.064	610.5±85.3	554.8±357.0	441.8±67.1	1145.6±50.6	**0.008**	369.9±68.6	569.0±248.3	0.298
Dermatopontin	DERM_PIG	52.5±13.7	43.6±33.0	45.1±3.3	126.2±69.7	0.090	64.5±12.2	59.9±38.4	80.7±23.7	150.5±20.2	**0.008**	36.2±8.6	74.7±13.9	**0.022**
Dystroglycan	I3LD20_PIG	1.2±1.1	0.6±0.5	0.7±0.2	0.7±0.6	0.729	0.9±0.6	0.8±1.1	0.6±0.2	0.8±0.5	0.945	0.5±0.3	2.2±0.6	**0.026**
EMILIN-1	F1SDQ5_PIG	6.1±3.2	8.3±2.1	7.9±2.5	10.7±2.4	0.261	5.6±1.8	6.4±2.8	9.1±1.0	8.8±3.8	0.316	9.4±4.2	14.5±3.6	0.148
Fibrillin-1	FBN1_PIG	0.2±0.4	0.8±1.4	0.0±0.0	0.0±0.0	0.519	0.2±0.3	0.0±0.0	0.0±0.0	0.0±0.0	n/a	0.0±0.0	0.0±0.0	n/a
Fibrinogen beta chain	F1RX37_PIG	1240.6±374.6	268.9±219.0	49.0±38.0	3.3±0.7	**0.000**	1240.6±892.3	2814.7±3732.6	77.6±53.1	53.8±46.6	0.317	1514.5±1633.6	17.6±25.7	0.164
Fibrinogen gamma chain	F1RX35_PIG	1124.9±400.8	267.0±197.3	43.8±31.0	8.0±0.7	**0.001**	994.9±674.2	2014.6±2519.2	69.7±42.6	39.7±31.3	0.277	1214.6±1333.0	16.2±19.1	0.170
Fibromodulin	F1S6B5_PIG	144.8±77.4	73.5±29.1	200.7±36.9	299.2±28.4	**0.002**	135.1±50.9	62.4±47.7	185.0±36.5	598.9±175.3	**0.001**	76.2±40.4	273.4±67.2	**0.019**
Fibronectin	F1SS24_PIG	557.8±157.1	983.5±206.3	1109.9±420.0	503.9±198.9	0.055	527.0±248.9	1237.2±357.0	870.3±360.6	925.0±188.5	0.104	996.9±285.9	314.4±116.2	**0.011**
Fibronectin type III domain-containing protein 1	F1SB59_PIG	0.0±0.0	0.0±0.0	0.0±0.0	0.2±0.2	n/a	0.0±0.0	0.0±0.0	0.0±0.0	1.0±1.5	n/a	0.0±0.0	0.0±0.1	n/a
Fibulin-1	F1SM61_PIG	0.3±0.1	0.0±0.1	0.4±0.3	0.4±0.5	0.438	0.1±0.2	0.3±0.6	0.4±0.2	2.0±1.5	0.077	0.6±0.4	0.3±0.3	0.269
Fibulin-2	FBLN2_PIG	0.0±0.0	0.2±0.3	0.3±0.3	0.3±0.4	0.634	0.0±0.0	0.0±0.0	1.5±1.4	4.0±2.0	**0.011**	0.2±0.3	0.2±0.4	n/a
Fibulin-3	F8SIP2_PIG	0.0±0.0	0.0±0.0	0.0±0.0	0.2±0.3	n/a	0.0±0.0	0.0±0.0	0.0±0.0	0.0±0.0	n/a	0.0±0.0	0.0±0.0	n/a
Fibulin-5	F1SD87_PIG	11.3±1.8	4.4±1.7	7.6±1.1	17.7±13.6	0.185	9.5±2.7	7.4±3.1	7.3±3.9	7.8±1.5	0.772	10.0±5.2	14.0±8.2	0.511
Galectin-1	LEG1_PIG	16.2±4.0	23.5±12.5	40.8±10.8	30.3±8.2	0.062	23.7±5.0	14.6±10.3	34.3±3.1	25.7±8.6	0.062	22.8±13.4	44.5±6.0	**0.041**
Galectin-3	A3EX84_PIG	0.1±0.1	0.2±0.3	1.0±0.2	3.9±6.0	0.421	0.2±0.2	0.1±0.1	0.5±0.4	1.1±0.2	**0.002**	0.1±0.2	0.2±0.1	n/a
Galectin-3-binding protein	M3V7X9_PIG	0.4±0.8	2.4±3.2	4.1±1.5	0.7±0.6	0.127	0.0±0.0	1.3±2.0	1.8±1.5	1.3±0.9	0.475	4.7±7.0	0.0±0.0	n/a
Gelsolin	GELS_PIG	217.8±17.2	129.6±51.0	160.6±18.1	179.7±80.3	0.246	227.7±68.3	150.1±78.2	194.7±35.8	155.4±18.4	0.345	164.9±7.5	250.3±39.5	0.061
Hyaluronan and proteoglycan link protein 1	HPLN1_PIG	2.6±2.2	3.5±2.7	7.1±2.5	3.4±0.7	0.128	4.4±2.5	9.6±2.5	10.9±6.5	0.9±0.8	**0.036**	6.1±3.8	9.8±4.3	0.302
Hyaluronan and proteoglycan link protein 3*	HPLN3_ HUMAN	0.2±0.3	0.4±0.8	0.6±0.7	0.0±0.0	0.552	0.7±0.6	0.6±1.0	1.0±1.1	0.1±0.2	0.604	1.6±0.7	0.8±1.1	0.367
Hyaluronan and proteoglycan link protein 4*	HPLN4_ HUMAN	0.0±0.0	0.0±0.0	0.2±0.3	0.0±0.0	n/a	0.0±0.0	0.6±0.6	0.0±0.0	0.0±0.0	n/a	0.3±0.6	0.0±0.0	n/a
Insulin-like growth factor-binding protein 7	C7EDN1_PIG	2.0±1.2	4.3±3.8	22.3±2.8	11.1±9.9	**0.008**	2.1±2.3	1.5±1.7	21.0±7.4	8.8±0.8	**0.001**	2.7±1.7	6.4±5.0	0.329

Inter-alpha-trypsin inhibitor heavy chain H2	ITIH2_PIG	8.4±3.7	4.5±2.1	3.6±2.2	4.1±1.6	0.163	6.8±1.5	6.4±3.9	5.7±1.8	6.1±5.2	0.985	7.2±1.4	2.1±1.6	**0.011**
Lactadherin	MFGM_PIG	7.9±4.8	11.7±5.7	17.8±9.7	19.1±15.3	0.499	4.8±3.8	9.3±7.2	19.7±5.5	6.1±0.6	**0.022**	13.5±7.6	11.8±2.5	0.686
Laminin subunit alpha-4	F1RZM4_PIG	6.2±1.5	2.1±1.5	3.5±1.5	11.2±3.5	**0.004**	6.7±4.6	3.9±2.2	3.6±3.9	3.9±1.5	0.655	6.5±4.6	9.1±5.2	0.522
Laminin subunit beta-1	F1SAE9_PIG	2.8±1.3	1.4±1.2	6.2±4.7	9.4±1.0	**0.020**	1.6±1.9	1.4±1.0	4.6±2.7	2.0±1.2	0.188	3.6±2.6	7.6±1.7	0.060
Laminin subunit beta-2	F1SPT5_PIG	8.8±2.3	8.1±0.2	7.1±0.9	8.7±1.3	0.462	6.2±3.7	11.0±2.8	8.3±5.3	4.3±1.9	0.205	9.4±2.0	10.5±3.3	0.630
Laminin subunit gamma-1	F1S663_PIG	41.7±11.2	35.9±1.9	38.7±5.3	47.8±8.8	0.330	36.6±21.7	39.7±6.9	42.7±18.6	16.7±4.9	0.213	41.1±7.8	51.6±4.7	0.080
Latent-TGFß-binding protein 1	F1S405_PIG	0.7±0.7	0.4±0.1	0.3±0.2	0.2±0.2	0.526	0.3±0.1	0.5±0.5	0.6±0.5	0.0±0.0	0.285	0.5±0.5	0.2±0.3	0.272
Latent-TGFß-binding protein 2	F1S2T5_PIG	2.5±1.3	2.9±2.0	5.5±1.0	2.7±2.4	0.213	2.4±1.1	2.4±1.8	10.2±0.8	9.1±1.6	**0.000**	3.3±2.5	2.3±1.5	0.558
Latent-TGFß-binding protein 4	LTBP4_PIG	3.7±1.9	0.1±0.1	0.0±0.0	4.9±5.6	0.177	5.5±1.7	1.1±1.7	1.4±0.6	2.8±2.9	0.074	1.0±1.9	2.9±0.9	n/a
Leukocyte elastase inhibitor	ILEU_PIG	0.0±0.0	0.0±0.0	0.0±0.0	0.1±0.2	n/a	1.0±0.4	1.6±2.8	0.0±0.0	0.0±0.0	0.463	1.3±1.7	0.0±0.0	n/a
Lipoprotein lipase*	LIPL_PIG	1.8±0.4	1.2±2.0	0.0±0.0	0.0±0.0	0.150	1.4±0.6	6.1±2.7	3.3±2.1	0.0±0.0	**0.012**	1.4±1.0	0.0±0.0	n/a
Lumican	F1SQ09_PIG	288.9±36.6	204.3±53.9	312.6±49.2	431.5±212.7	0.188	257.0±73.7	277.8±152.9	282.2±61.7	405.1±59.0	0.286	201.5±83.1	274.7±84.1	0.310
Lysyl oxidase homolog 1	F1SIC9_PIG	5.7±5.2	0.7±0.6	3.9±1.2	7.8±3.3	0.110	6.2±7.8	2.0±1.7	6.6±4.9	11.3±1.1	0.195	2.3±2.5	8.9±5.1	0.140
Macrophage-capping protein	F1SVB0_PIG	0.0±0.0	0.0±0.0	0.1±0.1	0.6±1.0	n/a	0.1±0.1	0.0±0.0	0.2±0.2	0.4±0.2	0.060	0.0±0.0	0.1±0.1	n/a
Matrix Gla protein	MGP_PIG	1.2±0.4	1.7±0.1	2.5±1.1	1.3±0.8	0.149	1.3±0.7	1.3±0.7	2.8±0.3	1.4±0.5	**0.035**	1.1±0.6	1.3±0.7	0.726
Matrix-remodeling-associated protein 5	F1RZ07_PIG	0.3±0.4	6.3±5.4	6.5±9.2	7.4±9.7	0.631	0.1±0.2	3.9±1.9	7.3±9.9	11.5±5.5	0.175	5.8±7.9	2.3±3.1	0.467
Mimecan	I3L9T6_PIG	426.0±40.0	220.5±139.0	255.7±34.2	495.6±304.8	0.220	389.9±27.1	292.7±193.6	283.7±7.3	581.3±152.7	0.061	222.1±65.9	359.4±47.8	**0.024**
Myeloperoxidase	K7GRV6_PIG	1.1±1.1	0.3±0.5	0.0±0.0	0.7±1.2	0.479	2.6±2.9	4.4±7.5	0.0±0.0	0.0±0.0	0.494	5.0±5.4	0.0±0.0	n/a
Nidogen-1	NID1_PIG	1.5±0.8	2.2±2.2	4.3±1.7	6.1±2.5	0.070	2.0±0.7	3.8±2.2	5.3±2.6	8.1±2.7	**0.049**	1.3±0.3	2.2±0.6	0.095
Nidogen-2	F1SFF3_PIG	109.6±14.8	137.7±31.0	155.9±5.2	173.2±56.0	0.187	104.0±32.6	157.8±56.4	161.3±12.5	96.8±25.8	0.109	107.0±40.5	191.0±42.9	0.055
Papilin	F1S3J7_PIG	0.6±1.0	0.3±0.6	0.2±0.2	0.1±0.2	0.800	0.6±0.5	0.7±0.5	0.3±0.3	0.0±0.0	0.218	1.5±2.1	0.6±0.5	0.428
Pentraxin-related protein PTX3*	F1SJM0_PIG	0.9±0.8	1.2±1.1	0.0±0.0	0.1±0.1	0.138	0.8±0.3	0.5±0.9	1.4±1.1	0.0±0.0	0.234	1.6±0.5	0.0±0.0	n/a
Peptidyl-prolyl cis-trans isomerase A	PPIA_PIG	2.2±1.0	1.5±0.7	4.3±1.5	6.2±8.1	0.536	3.8±1.8	3.6±2.5	5.8±4.0	7.3±2.8	0.385	3.5±2.1	3.2±0.8	0.780
Periostin	F1RS37_PIG	2.5±2.3	22.6±19.5	100.3±69.3	148.3±199.7	0.361	0.5±0.5	6.8±7.0	86.6±62.7	287.5±33.2	**0.000**	18.4±18.6	24.1±13.7	0.660
Perlecan	PGBM_PIG	210.9±42.8	188.9±59.9	245.7±21.6	384.9±98.0	**0.019**	215.7±38.4	237.8±121.6	321.6±78.5	336.2±111.9	0.359	223.6±75.7	314.7±59.1	0.134
Peroxidasin homolog	I3LDA4_PIG	0.0±0.0	0.3±0.3	0.2±0.1	0.2±0.4	0.565	0.0±0.0	0.0±0.0	0.1±0.2	0.0±0.0	n/a	0.3±0.3	0.1±0.2	n/a
Pigment epithelium-derived factor	Q0PM28_PIG	0.4±0.5	0.5±0.9	2.2±0.9	0.9±1.2	0.134	0.3±0.5	0.2±0.3	3.3±2.7	1.9±1.3	0.101	0.8±1.1	0.7±0.5	0.876
Plasminogen	PLMN_PIG	57.8±54.2	79.7±55.9	10.7±5.6	2.1±1.8	0.114	34.6±16.9	146.3±54.8	11.2±6.5	2.6±1.8	**0.001**	28.7±24.0	0.4±0.6	0.099
Podocan	I3LEB7_PIG	0.8±0.4	0.1±0.2	1.1±0.8	2.8±1.6	**0.030**	0.6±0.7	0.5±0.3	0.9±1.1	1.0±0.8	0.888	0.9±0.8	3.7±1.3	**0.045**
Procollagen C-endopeptidase enchancer 1	I3LEE6_PIG	0.2±0.1	0.1±0.1	0.8±0.5	0.7±0.3	0.069	0.2±0.2	0.1±0.1	2.7±3.8	1.1±0.5	0.366	0.4±0.5	0.9±0.7	0.373
Prolargin	F1S6B4_PIG	269.7±21.2	200.2±42.2	300.6±54.5	608.6±187.3	**0.005**	263.7±49.7	255.3±109.7	341.3±134.5	995.5±337.7	**0.004**	203.8±44.9	319.0±81.4	0.117
Prolow-density lipoprotein receptor-related protein 1	K9IVL7_PIG	1.1±0.3	1.4±1.6	3.5±3.5	4.2±2.1	0.295	1.4±1.2	0.7±0.5	3.6±2.8	4.5±1.2	0.066	3.7±1.9	1.8±1.4	0.189

Properdin	K7GQR1_PIG	0.7±0.6	0.3±0.3	0.0±0.0	0.3±0.3	0.228	0.6±0.7	0.6±0.7	0.3±0.5	0.2±0.1	0.749	0.7±0.6	0.1±0.1	0.152
Prophenin and tritrpticin	PF11_PIG	63.9±15.1	16.9±10.5	2.1±1.0	8.0±13.4	**0.001**	94.1±47.6	186.5±155.5	9.8±2.0	1.1±1.6	0.074	116.0±100.2	0.3±0.5	n/a
Proteoglycan 4	I3L5Z3_PIG	0.5±0.2	0.0±0.0	0.0±0.0	0.0±0.0	n/a	0.0±0.1	0.1±0.2	0.0±0.0	0.0±0.0	0.554	0.0±0.0	0.0±0.0	n/a
RPE-spondin	RPESP_PIG	4.8±2.1	7.9±7.7	5.8±3.3	1.5±1.3	0.393	9.0±9.3	4.7±2.9	9.3±5.6	2.4±0.4	0.415	6.6±1.5	7.6±0.6	0.274
Secreted frizzled-related protein 1	I3LB66_PIG	0.0±0.0	0.0±0.0	0.4±0.6	0.9±0.9	0.183	0.0±0.0	0.0±0.0	0.2±0.3	0.7±0.0	**0.001**	0.0±0.0	0.8±0.4	n/a
Serine protease HTRA1	F1SEH4_PIG	7.0±1.7	10.8±4.9	46.7±13.0	45.6±41.4	0.100	5.5±2.7	6.5±3.8	37.4±17.4	37.2±21.0	**0.029**	5.9±3.4	24.5±17.8	0.208
Serotransferrin	TRFE_PIG	0.4±0.4	2.3±0.7	1.7±1.8	3.2±5.6	0.710	3.0±2.3	6.0±2.7	1.6±2.0	6.6±9.7	0.624	3.3±3.0	0.2±0.3	n/a
Serum amyloid P-component	SAMP_PIG	0.1±0.1	0.0±0.0	0.0±0.0	0.0±0.0	n/a	0.1±0.1	0.0±0.0	0.0±0.0	0.0±0.1	0.713	0.2±0.3	0.0±0.0	n/a
SPARC	SPRC_PIG	0.3±0.6	3.6±1.3	3.5±1.4	0.8±1.0	**0.010**	0.4±0.7	0.5±0.7	3.2±1.9	4.7±1.2	**0.008**	1.4±1.6	3.1±0.6	0.122
Spondin-1	SPON1_PIG	0.0±0.0	0.1±0.1	0.5±0.5	0.4±0.7	0.449	0.1±0.1	0.1±0.2	0.5±0.3	0.9±0.8	0.187	0.2±0.4	0.5±0.4	n/a
Sulfhydryl oxidase	F1S682_PIG	0.0±0.0	0.0±0.0	0.0±0.0	0.0±0.0	n/a	0.0±0.0	0.1±0.2	0.0±0.0	0.0±0.0	n/a	0.1±0.2	0.0±0.0	n/a
Superoxide dismutase [Cu-Zn]	Q007T6_PIG	1.1±0.4	0.2±0.2	1.6±0.6	1.3±0.7	**0.042**	1.8±1.5	0.2±0.2	1.3±0.3	2.1±0.6	0.098	0.9±1.0	3.2±1.9	0.156
Target of Nesh-SH3*	F1SL03_PIG	3.1±1.9	0.9±1.5	1.3±2.0	4.1±4.5	0.466	4.3±2.0	0.8±0.8	3.3±1.0	13.5±5.4	**0.004**	1.0±1.7	2.7±2.2	0.339
Tenascin	TENA_PIG	64.2±20.0	52.4±13.9	257.6±39.4	168.2±84.9	**0.003**	44.9±12.4	82.6±47.7	168.9±41.0	106.5±33.4	**0.017**	81.9±36.9	36.0±30.0	0.131
Tenascin XB*	A5A8W4_PIG	5.5±2.3	4.4±7.1	3.4±4.8	9.4±11.0	0.747	5.7±4.1	5.9±5.4	1.8±1.4	6.1±5.3	0.586	2.8±4.7	3.4±2.3	0.831
Tetranectin	F1SRC8_PIG	1.6±0.5	0.9±0.8	2.5±2.0	2.3±0.4	0.324	1.7±0.8	2.2±2.0	3.5±2.6	6.7±2.1	0.059	1.1±1.0	1.4±0.7	0.698
TGFß-1*	TGFB1_PIG	0.0±0.0	0.0±0.0	0.0±0.0	0.0±0.0	n/a	0.0±0.0	0.2±0.3	0.0±0.0	0.0±0.0	n/a	0.0±0.0	0.0±0.0	n/a
TGFß-3*	K7GSJ9_PIG	0.0±0.0	0.0±0.0	0.0±0.0	0.0±0.0	n/a	0.0±0.0	0.0±0.0	0.0±0.0	0.6±0.9	n/a	0.0±0.0	0.0±0.0	n/a
TGFß-induced protein ig-h3	BGH3_PIG	19.5±5.0	15.1±11.9	9.5±4.3	27.0±17.6	0.333	9.0±3.3	15.7±8.3	22.6±19.7	8.6±4.8	0.415	34.6±17.0	16.1±8.1	0.121
Thrombospondin-1	K7GPJ3_PIG	5.8±2.3	4.2±1.7	7.2±2.1	2.7±0.9	0.073	4.3±0.9	6.3±2.1	7.1±1.8	6.1±3.2	0.491	5.7±0.9	0.4±0.4	**0.000**
Tryptase	TRYT_PIG	0.0±0.0	0.0±0.0	0.0±0.0	3.8±6.6	n/a	0.0±0.0	0.0±0.1	0.0±0.0	0.4±0.7	0.475	0.0±0.0	0.0±0.0	n/a
Tubulointerstitial nephritis antigen-like	F1SVA2_PIG	83.0±10.1	56.6±25.4	53.2±6.7	65.1±9.5	0.142	71.7±13.9	67.8±36.6	69.5±11.8	43.5±5.7	0.364	58.3±3.7	67.8±14.1	0.362
Versican	F1REZ2_PIG	70.2±5.8	103.0±18.5	153.5±7.9	148.5±26.1	**0.001**	112.2±54.7	81.1±31.6	231.4±38.8	398.1±137.4	**0.004**	106.1±58.1	142.6±42.5	0.381
Vitamin D-binding protein	I3LN42_PIG	8.7±5.6	1.3±1.0	2.7±1.1	1.4±1.8	0.051	5.3±1.1	9.0±5.5	2.8±1.9	1.4±1.0	0.062	7.3±7.7	0.5±0.5	0.173
Vitronectin	VTNC_PIG	298.1±250.1	239.7±90.3	148.2±65.3	87.3±94.7	0.352	202.6±40.6	694.9±156.0	235.4±154.0	82.8±48.1	**0.001**	149.0±66.3	43.5±29.8	**0.043**
von Willebrand factor A domain-containing protein 1	F1RJE3_PIG	17.6±8.1	8.6±3.6	10.6±3.4	14.5±6.4	0.294	18.7±5.6	11.7±6.0	14.6±4.6	7.3±4.4	0.129	11.1±2.7	16.8±5.1	0.183
WD repeat-containing protein 1	K9IVR7_PIG	0.0±0.0	0.1±0.2	0.1±0.1	0.1±0.2	0.537	0.0±0.0	0.0±0.0	0.0±0.1	0.0±0.1	0.595	0.0±0.1	0.1±0.0	0.598

P values for changes in BMS and DES over time were identified for each stent type separately by one-way ANOVA (BMS: n=3 [BMS1/3/7/28], 1-way ANOVA; DES: n=3 [DES 1/3/7/28], 1-way ANOVA). ANOVA was not applied if a protein was detected at only a single time point. *P* values for POBA are based on unpaired Student's *t*-tests with unequal variance for changes between early (n=4 [day 1 + 3] and late (n=3 [day 14 + 28] stage. *T*-test was not performed if a protein was undetectable in the majority of samples from 1 of the 2 groups compared. 'n/a' denotes 'not applicable'. Proteins only identified in the media are marked with*. Results in bold indicate $P < 0.05$. Values are average (Av) total ion current (TIC) x 10^6 ± standard deviation (SD).

5.5 ECM remodelling in the neointima

To study neointimal ECM composition in response to different stent types, the neointima lesions of coronary arteries 28 days post-stent implantation were analysed separately by proteomics.

5.5.1 Method reproducibility

The neointima samples were run in duplicates to test reproducibility for the LC-MS/MS analysis. Indeed, the method showed good reproducibility for spectral counts and sequence coverage as well as the number of identified peptides, as illustrated in *Figure 20A and B*.

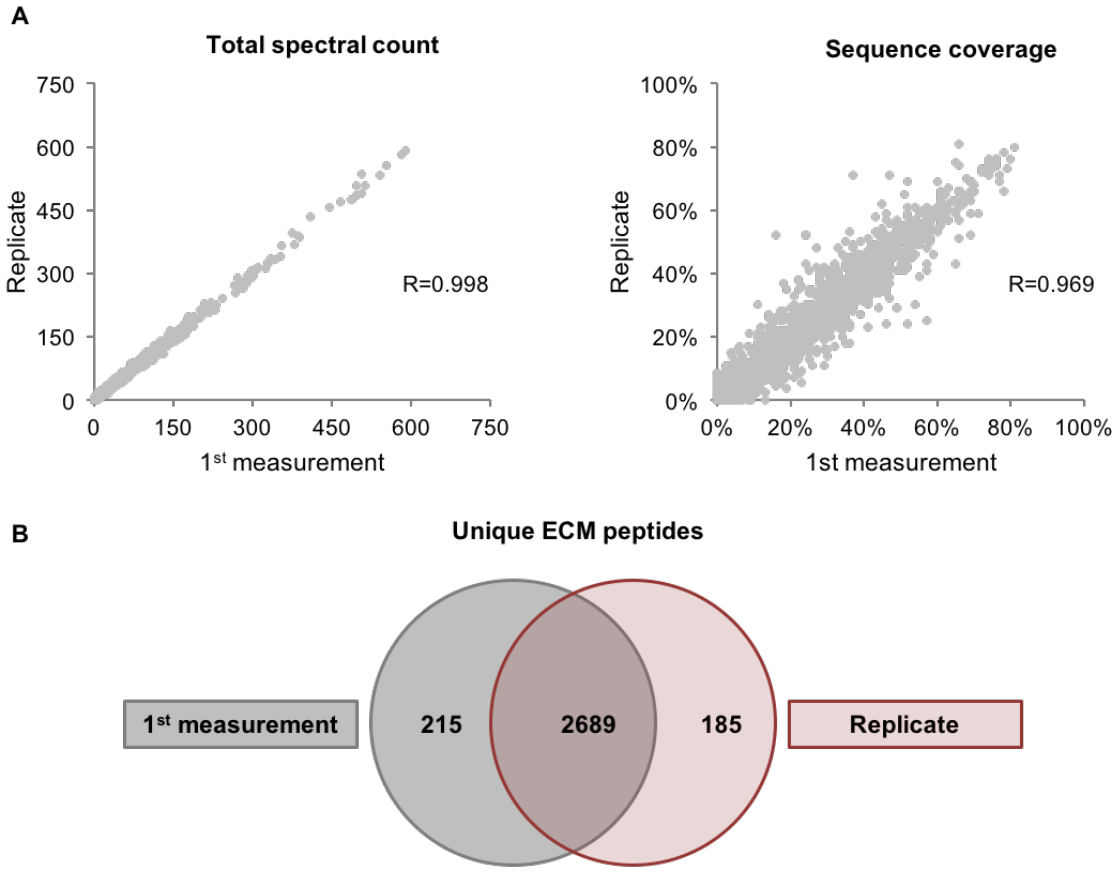

Figure 20. **Reproducibility of LC-MS/MS**. The neointima samples were run in duplicates by LC-MS/MS. (A) The total spectral counts (R=0.998) and the sequence coverage (R=0.969) for each ECM protein correlated well between technical replicates. n=140 proteins x 14 samples (Pearson correlation). The Venn diagram displays the unique peptides identified either in both or only in the 1st or 2nd analysis.

5.5.2 Neointima comparison between DES and BMS

The differentially expressed proteins between the neointimas of DES and BMS are shown in the heat map in *Figure 21A*. Compared to BMS, the neointima of arteries with DES implantation contained less structural ECM constituents like collagen type I, III, V as well

as regulatory ECM proteins such as biglycan, lumican, fibromodulin or periostin; in contrast, proteins involved in the regulation of calcification such as matrix Gla protein (MGP), secreted phosphoprotein 24 (SPP24) and bone morphogenetic protein 1 (BMP1) were increased in DES (*Figure 21B*). Immunohistochemistry localised MGP and SPP24 in human coronary arteries with atherosclerotic plaques with and without stent implantation (*Figure 21C*). Interestingly, proteomics also revealed the presence of chondroadherin in coronary arteries with DES (*Figure 21B*). This SLRP has not been previously reported in the vasculature.

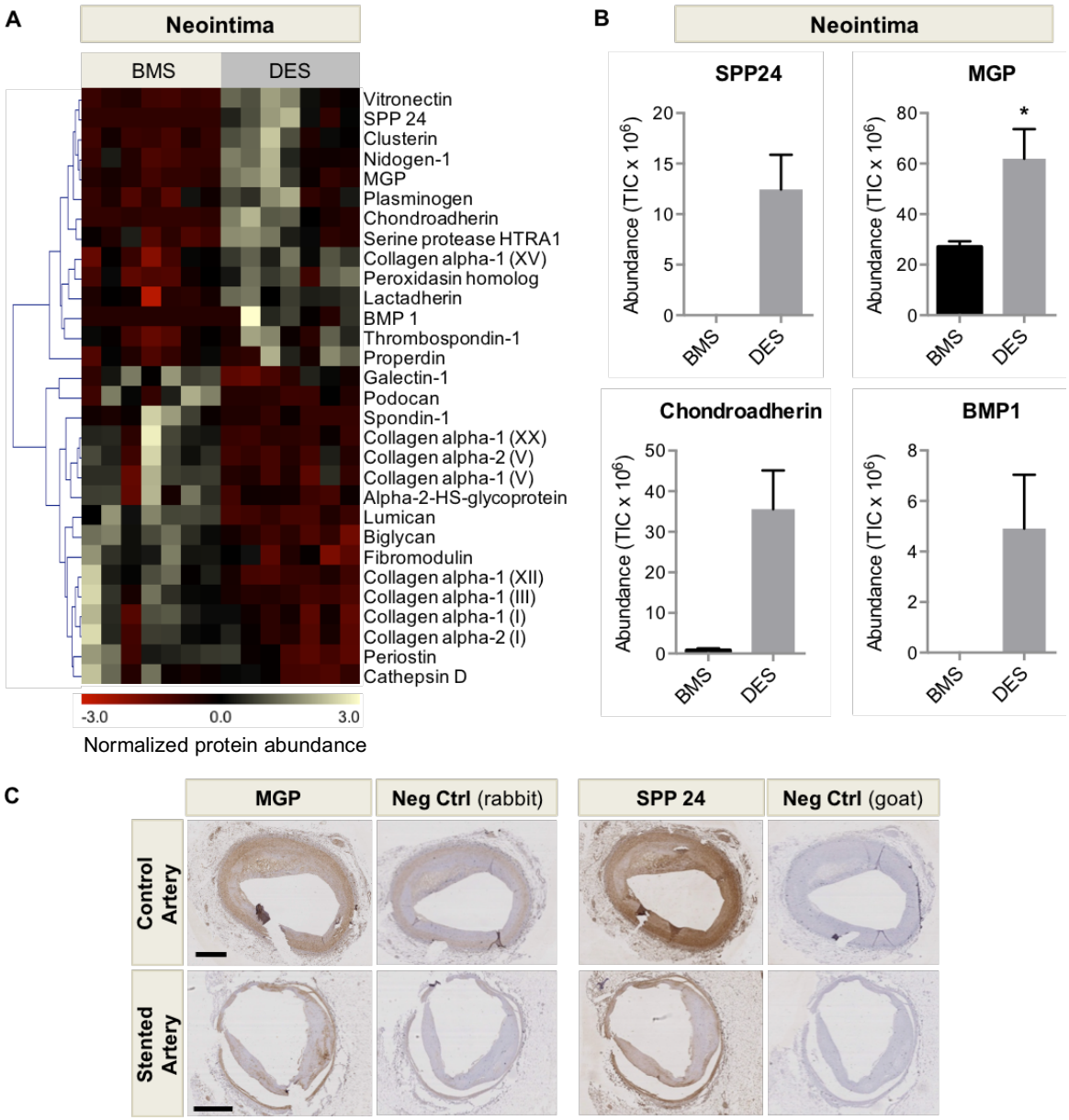

Figure 21. Comparison of neointimal BMS and DES. **(A)** Heat map of differentially expressed proteins. n=7 per group (*t*-test with unequal variance). Pearson correlation. **(B)** Proteins involved in the regulation of calcification (SPP24, MGP, BMP1) and chondroadherin were predominantly found in the DES group. **P*<0.05. TIC = total ion current. BMP 1, chondroadherin and SPP24 were not detected in the control group, thus a *t*-test was not performed. **(C)** MGP and SPP24 in human stented and control coronary arteries detected by immunohistochemistry. Scale bars=1 mm.

5.6 ECM remodelling in the media

5.6.1 Temporal changes in the media post-stenting

ECM remodelling in response to stent implantation was compared over a time course of 28 days. Coronary arteries subject to POBA served as controls. Distinct clusters of differentially expressed proteins over time were observed (*Figure 22A-C*). At an early stage, proteins regulating haemostasis (e.g. plasminogen, fibrinogen, antithrombin-III, thrombospondin-1) and inflammation (e.g. pentraxin-related protein PTX3, prophenin and tritrpticin precursor) were increased. Similarly, apolipoproteins found on VLDL particles, including apoC-III, apoE and apoR[259] showed an early rise, within the first few days upon intervention. They subsequently decreased with the increase of other ECM proteins. Proteins with a late response included large aggregating proteoglycans (aggrecan, versican) fibrillar collagens (e.g. type I, III and V), SLRPs (decorin, biglycan, fibromodulin, podocan, asporin) and matricellular proteins (e.g. periostin, tenascin, SPARC). Generally, fewer proteins significantly changed in POBA than in stented arteries and more pronounced changes were seen in DES compared to BMS. A comparison of POBA late versus BMS stented arteries at day 28 returned 5 differentially expressed proteins, while the comparison of POBA late with DES revealed significant changes in 29 proteins (*Figure 22D, Supplemental table 3*). Differences between DES and BMS became most obvious at day 28. While up to 7 days only few proteins were differentially expressed between DES and BMS, significant differences were seen in 11 proteins at day 28 (*Figure 22E, Supplemental table 4*). Thus, DES affects the composition of the ECM.

5.6.2 Media comparison between DES and BMS

At day 28 basement membrane proteins such as collagen alpha-2 IV (CO4A2), collagen alpha-1 XVIII (COIA1), laminin beta-1 (LAMB1), laminin beta-2 (LAMB2) and laminin gamma-1 (LAMC1) were uniformly downregulated in arteries with DES compared to BMS (*Figure 23A*). Since DES inhibit cell proliferation, this finding likely reflects the reduced cellularity in arteries with DES. In contrast, the large aggregating proteoglycan aggrecan (PGCA) was upregulated after stenting, particularly in DES (*Figure 23B*). Aggrecan is the major proteoglycan in the articular cartilage and interacts with hyaluronic acid to form large aggregates. Its rise mirrored the increase of versican, the major large aggregating proteoglycan in the vasculature (*Figure 23B*). Aggregates of aggrecan and versican with hyaluronic acid are stabilized by hyaluronan and the proteoglycan link protein 1 (HPLN1). HPLN1 was reduced in the media of DES compared to BMS (*Figure 23B*).

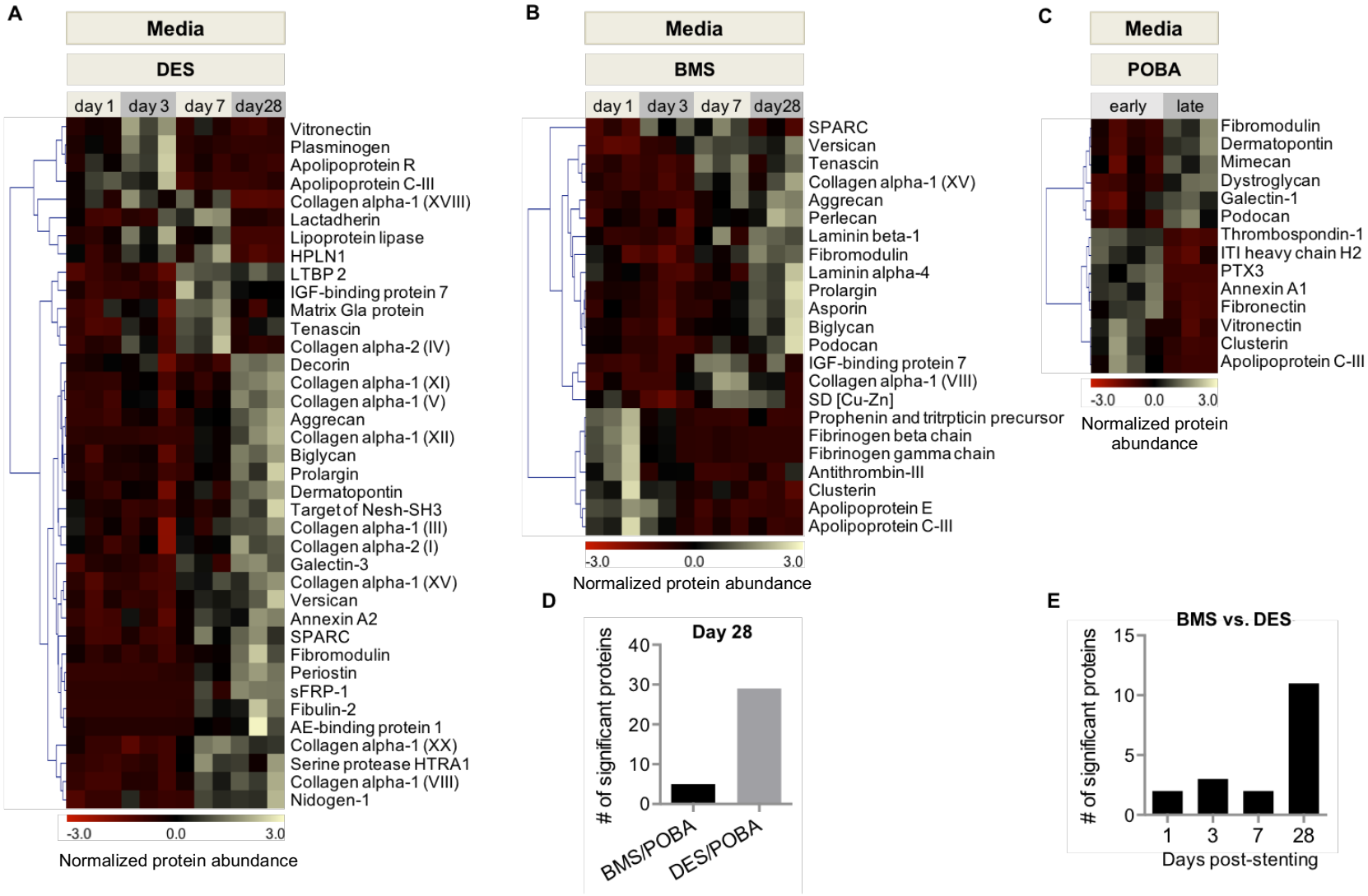

Figure 22. ECM remodelling in the media over time. (A-C) Heat maps of significantly differentially expressed ECM proteins over time in DES, BMS and the POBA group. BMS/DES: n=3 per time point. *P*<0.05 (1-way ANOVA). POBA: n=3-4 per group. *P*<0.05 (*t*-test with unequal variance). Pearson correlation. **(D)** Number of significant protein changes in POBA late compared to BMS/DES at day 28. **(E)** Number of differentially expressed proteins between DES vs. BMS over time. Abbreviations: ITI heavy chain H2, inter-alpha-trypsin inhibitor heavy chain H2; PTX3, pentraxin-related protein PTX3; sFRP-1, secreted frizzled-related protein 1; IGF, insulin-like growth factor; SD=superoxide dismutase; LTBP, latent-transforming growth factor beta-binding protein; AE, adipocyte enhancer.

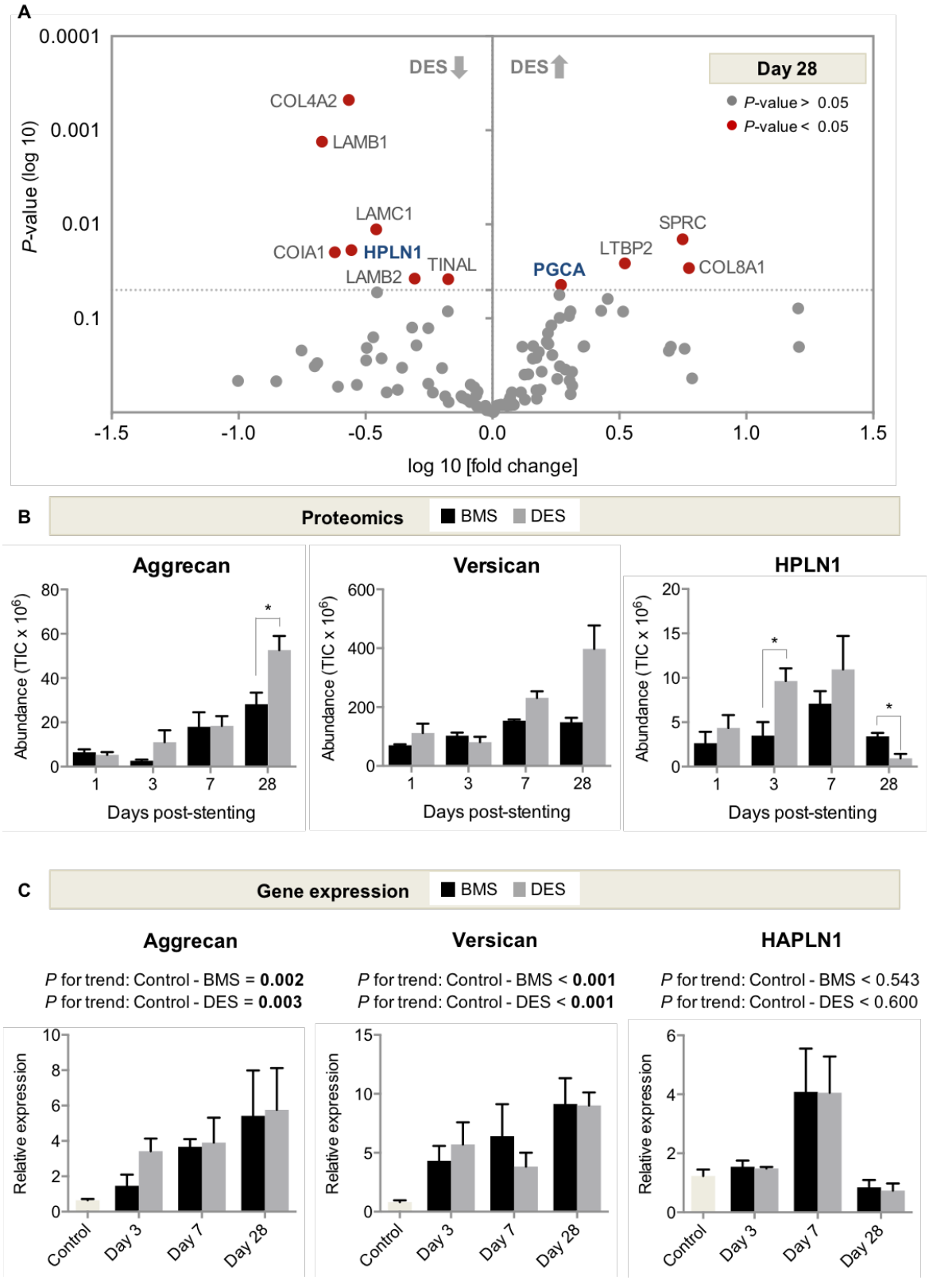

Figure 23. Comparison of BMS vs. DES in the media. Volcano plot of differentially expressed proteins between DES and BMS at day 28. n=3 per group (*t*-test with unequal variance). PGCA, aggrecan; HPLN1, hyaluronan and the proteoglycan link protein 1 **(B)** Time- and stent-dependent changes in aggrecan, versican and HPLN1 protein levels. n=3 per group. **P*<0.05 (*t*-test with unequal variance). TIC, total ion current. **(C)** Corresponding gene expression in stented (n=3 per time point, except DES day 3: n=2) and unstented control coronary arteries (n=6); Gene expression values were normalized to unstented control arteries. Linear regression analysis for *P*-value for trend.

5.7 Validation of proteomics findings

5.7.1 Stent-induced changes in aggrecan and its fragments

Due to its novelty in the vasculature and its significant time-dependent increase upon stenting, as well as its differential increase in DES over BMS at day 28, aggrecan was selected for further validation. For comparison, we used versican as it is structurally and functionally related to aggrecan, and which also showed a significant time-dependent increase upon stenting. Firstly, gene expression analysis was performed to validate the proteomics findings. However, samples of day 1 were excluded, due to the poor RNA yield in all DES day 1 samples, as also indicated by unreliable results for the measured housekeeping genes. It is likely that this was due to toxic drug effects as we have also observed decreased RNA levels and cell loss upon drug treatment of ECs in our in vitro studies (*Figure 26C*). Except for DES day 3 (n=2), again due to poor RNA yield, all 3 biological replicates were analysed for the other stented groups. A temporal increase of both, aggrecan and versican expression after stenting was confirmed at the transcript level (*Figure 23C*). However, there was no difference in aggrecan expression in DES compared to BMS at the transcript level. Consistent with the proteomics findings, there was no increase in HPLN1 at day 28 on gene expression level.

Besides gene expression, protein degradation determines the abundance of ECM proteins in the vessel wall. Degradation of aggrecan and versican in the vessel wall is regulated by members of the ADAMTS family, the so called aggrecanases. Thus, we used neoepitope antibodies that only recognize aggrecan and versican upon cleavage by ADAMTS proteases for western blot analysis in porcine GuHCl extracts (*Figure 24A*). For aggrecan, we probed for the signature cleavage at NITEGE^{373}-ARGTV in the interglobular domain at the N-terminus. Western blot analysis showed that the rise in aggrecan as seen by proteomics was accompanied by increased detectability of the NITEGE neoepitope over time, however more pronounced in DES than BMS (*Figure 24B).* Similarly, an increase was seen for the ADAMTS-generated DPEAAE fragments of versican. When the fragment levels were compared in BMS and DES, again both were found to be higher in DES compared to BMS at day 28 in a second cohort of media samples, consistent with the increased levels of aggrecan observed in DES by proteomics (*Figure 24C*).

Next, we evaluated the abundance of the proteoglycan fragments in BMS vs. DES in the different fractions and compared the intra- (SDS) and extracellular (NaCl and GuHCl) distribution of the fragments in BMS and DES. Aggrecan neoepitopes were not detectable in the NaCl and SDS extracts, while versican neoepitopes were detectable in all three extracts, indicating the lower abundance of aggrecan fragments. While the extracellular fractions (NaCl and GuHCl) showed an identical distribution pattern,

confirming the higher abundance of the versican fragments in DES compared to BMS stented arteries, in the intracellular fraction, no difference between BMS and DES was seen (*Figure 24D*). This finding may be indicative for differential extracellular degradation of the proteins in BMS and DES or differential internalization.

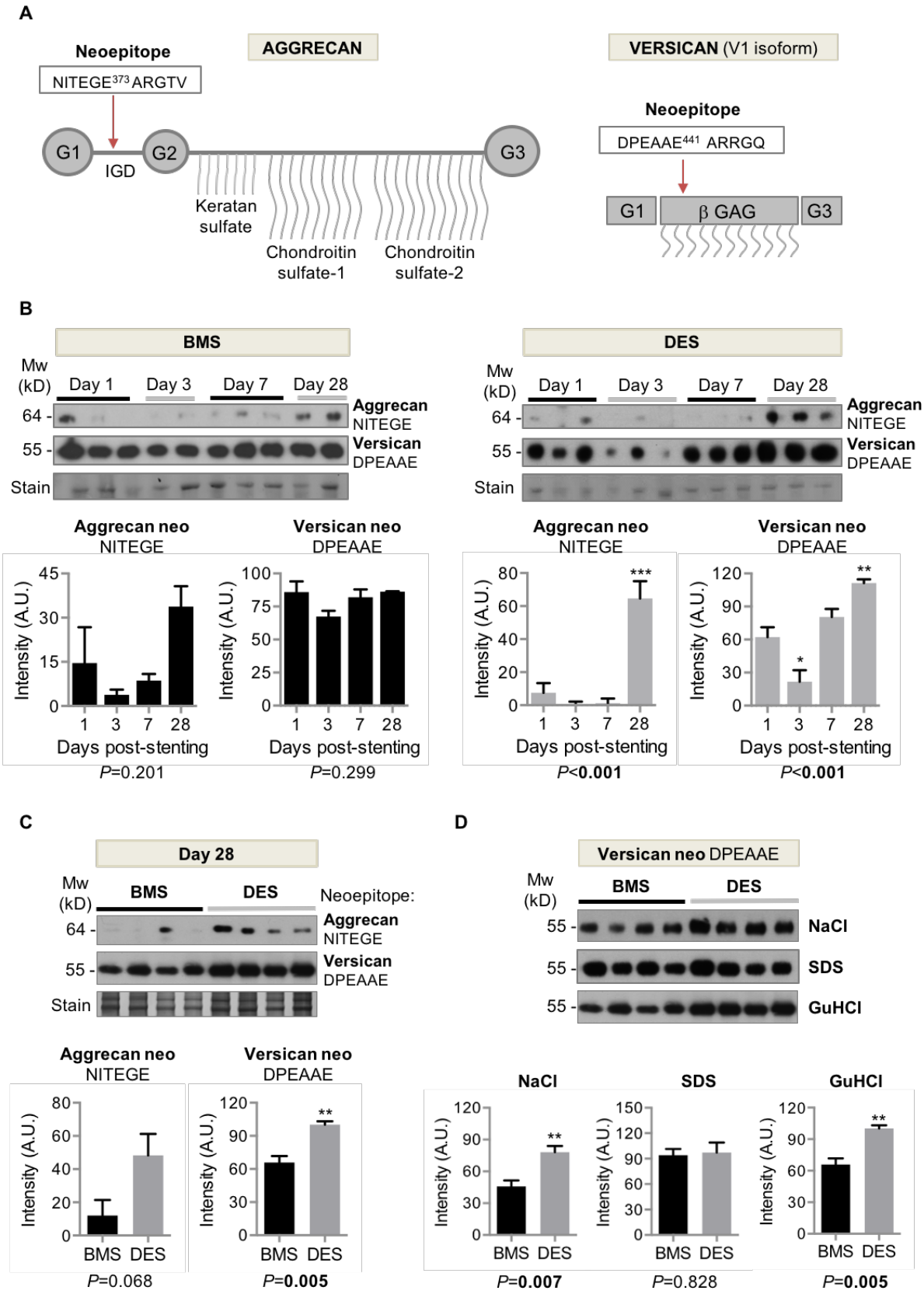

Figure 24. Aggrecan fragments in DES and BMS (A) The aggrecan neoepitope NITEGE and the versican neoepitope DPEAAE are generated by aggrecanase cleavage. Schematic illustration of the cleavage site by the red arrow. **(B)** Immunoblots for the aggrecan NITEGE and versican DPEAAE neoepitopes over time in BMS and DES stented arteries in GuHCl extracts. Ponceau stain below. Quantification by densitometry is shown below. n=3 per time point (except BMS day 3 and day 28: n=2). **P*<0.05, ***P*<0.01, ****P*<0.001 (1-way ANOVA [*P*<0.001] with Dunnett post hoc test to day 1) **(C)** Differences between BMS and DES at day 28 in the GuHCl extracts. Silver stain and densitometry below. n=4 per group (samples of a 2nd cohort of BMS/DES stented arteries at day 28). ***P*<0.01 (*t*-test with unequal variance). (**D**) Comparison of versican DPEAAE fragments between BMS and DES at day 28 in all three extracts (NaCl, SDS, GuHCl). Densitometry is shown below. n=4 per group (samples of a 2nd cohort of BMS/DES stented arteries at day 28). ***P*<0.01 (*t*-test with unequal variance).

5.7.2 Aggrecanase changes in stented arteries

Next, we assessed the expression levels of ADAMTS1 and ADAMTS4, the two predominant ADAMTS isoforms in men. Both, ADAMTS1 and ADAMTS4 were detectable in porcine coronary arteries, with significantly higher expression levels for ADAMTS1 in normal arteries (*Figure 25A)*. Upon stenting, there was a notable loss of ADAMTS1, followed by a rise in ADAMTS4 expression. To evaluate the EC content of the tissue the endothelial specific marker cadherin 5 was measured (*Figure 25B*), as stenting induces EC injury. The re-expression of cadherin 5, possibly indicating re-endothelialisation, coincided with the shift in ADAMTS4 expression.

Besides its expression levels, the extracellular activity of the ADAMTS enzymes is regulated by their endocytic clearance. Low density lipoprotein receptor-related protein 1 (LRP1) was shown to be involved in the endocytic clearance of ADAMTS-4 and ADAMTS-5.[260, 261] Thus, we investigated the abundance levels of LRP1 in BMS and DES stented arteries at day 28, to evaluate its impact on ADAMTS activity and consequently on aggrecan and versican turn-over. We probed for the 85 kDa light beta-chain containing the transmembrane domain in the neointima samples to evaluate the contribution of both SMCs and ECs to extracellular ADAMTS clearance. Significantly higher LRP1 protein levels were found in DES stented samples (*Figure 25C*), possibly indicating an increased LRP1 mediated ADAMTS clearance.

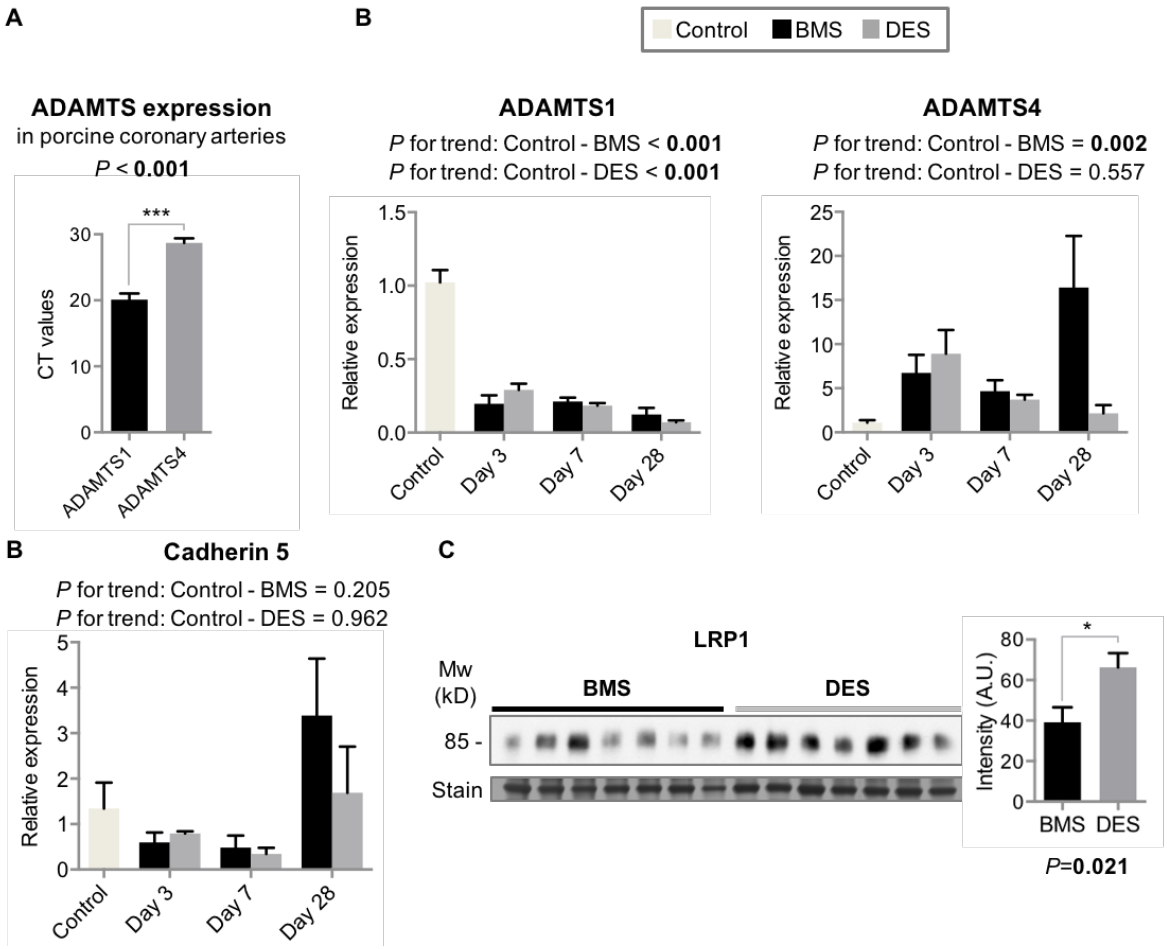

Figure 25. Aggrecanase changes in stented porcine coronary arteries. (**A**) Raw CT values of ADAMTS1 and ADAMTS4 in unstented control coronary arteries in pigs. n=6 per group. ***P<0.001 (t-test with unequal variance). (**B**) Relative gene expression levels for ADAMTS1, ADAMTS4 and cadherin 5 in porcine tissue upon stenting. n=3 per time point for BMS/DES; except DES day 3: n=2. n=6 for control coronary arteries. Gene expression values were normalized to unstented control arteries. Linear regression analysis for P-value for trend. (**C)** Comparison of LRP1 abundance between BMS and DES in the neointima at day 28. Silver stain below. Densitometry on the right. n=7 per group. *P<0.05 (t-test with unequal variance).

5.7.3 Aggrecanase expression in cultured ECs and SMCs

Since stenting induces endothelial injury and the changes in aggrecanases coincided with the EC marker, expression levels of ADAMTS1 and ADAMTS4 in human ECs from different vascular territories (umbilical vein ECs, saphenous vein ECs, aortic ECs and coronary ECs) were investigated. Human coronary artery ECs expressed high levels of ADAMTS1 (*Figure 26A*), indicating a more prominent role for ADAMTS-1 in coronary ECs compared to other vascular territories. Furthermore, we evaluated basal expression levels of the aggrecanases and their substrates, as well as HAPLN1 in cultured human coronary artery ECs and SMCs. Both, aggrecanases and aggrecan are expressed in HCASMCs, however HCAECs express only the aggrecanases (*Figure 26B*), but not aggrecan or HAPLN1. To investigate whether a direct drug effect could be responsible for the changes seen in the ADAMTS enzymes, we cultured HCASMCs and HCAECs in the presence of everolimus, the drug eluted from the stents used in our porcine model. Upon drug

treatment ECs showed a substantial decrease in RNA levels, indicating a limited tolerance to the drug. This was confirmed by significantly reduced cell count and viability of everolimus treated ECs as assessed by automated cell counting of total and dead cells (*Figure 26C*). Thus, all proteases were reduced in treated ECs (data not shown). However, in SMCs, which better tolerated the drug, an effect was only seen in ADAMTS4, while the expression levels for ADAMTS1 remained unchanged (*Figure 26D)*.

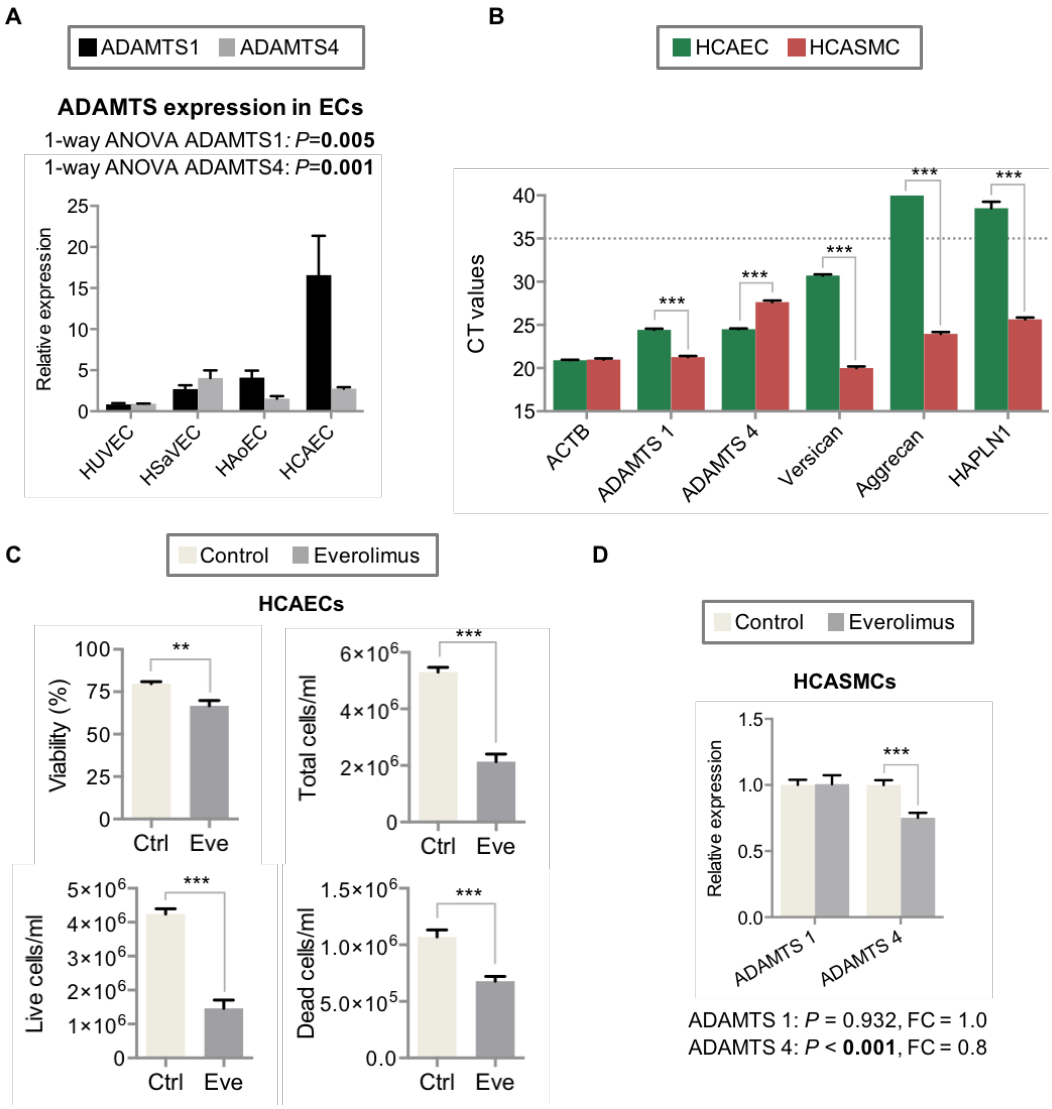

Figure 26. Validation of findings in cultured cells. (**A**) Gene expression of ADAMTS1 and 4 in arterial and venous ECs. n=4, 2 independent cell passages of 2 different cell lines, except HSaVEC: n=3 independent cell passages of 1 cell line. *P*-values were derived from 1-way ANOVA. HUVEC, human umbilical vein ECs; HSaVEC, human saphenous vein EC; HAoEC, human aortic ECs; HCAEC, human coronary artery ECs. (**B**) Raw CT values of ADAMTS1 and 4 as well as versican, aggrecan and HAPLN1 in ECs and SMCs of coronary arteries. n=triplicates of 3 independent cell passages. HCASMC (p7,9,11), HCAECs (p7,8,9). ***P<0.001 (*t*-test with unequal variance). (**C**) Viability and cell count of HCAECs treated with everolimus or DMSO (controls) as determined by Nucleo Counter® NC-3000™. n=6 per group. ** P<0.01, ***P<0.001 (*t*-test with unequal variance). (**D**) Relative gene expression levels of ADAMTS1 and ADAMTS4 in control and everolimus treated HCASMCs. n=triplicates of 3 independent cell passages. HCASMCs (p7, p9, p11) ***P<0.001 (*t*-test with unequal variance). Gene expression values were normalized to the control group in each passage.

5.8 Aggrecan in human vasculature

5.8.1 Aggrecan in human stented arteries

To confirm the presence of aggrecan and its fragments also in stented human coronary arteries immunostaining was used. Aggrecan and ADAMTS-generated aggrecan fragments were co-localized in the coronary arteries. Again, as for the validation of neointimal changes, coronary arteries with atherosclerotic plaques but without stents served as a reference control. Aggrecan and HPLN1 co-localized in the media of control arteries (*Figure 27A*). In stented coronary arteries, staining for the aggrecan NITEGE neoepitope was observed predominantly in the intimal and medial layer at the contacts of the stent struts with the artery as demonstrated by immunofluorescence *(Figure 27B*; all images in appropriate channels and corresponding IgG controls are shown in *Figure 28*).

5.8.2 Aggrecan in human aorta and vein

Since the major role of aggrecan in cartilage is to confer resistance to pressure, we assumed a similar function in the vasculature. Thus, to further investigate the role of aggrecan in the human vasculature we compared specimens of human thoracic aorta and human saphenous veins, as representatives of the high- and low-pressure system, respectively. Targeted proteomics analysis revealed that similar to versican, aggrecan was more abundant in the aorta than in veins (*Figure 29A*). The SLRP decorin served as a control. Likewise, by western blotting it was shown that the ADAMTS-generated aggrecan NITEGE neoepitope was more abundant in the aorta (*Figure 29B*). Aggrecan and aggrecan cleavage was found throughout the media of the human aorta as confirmed by immunofluorescence staining (*Figure 29C*).

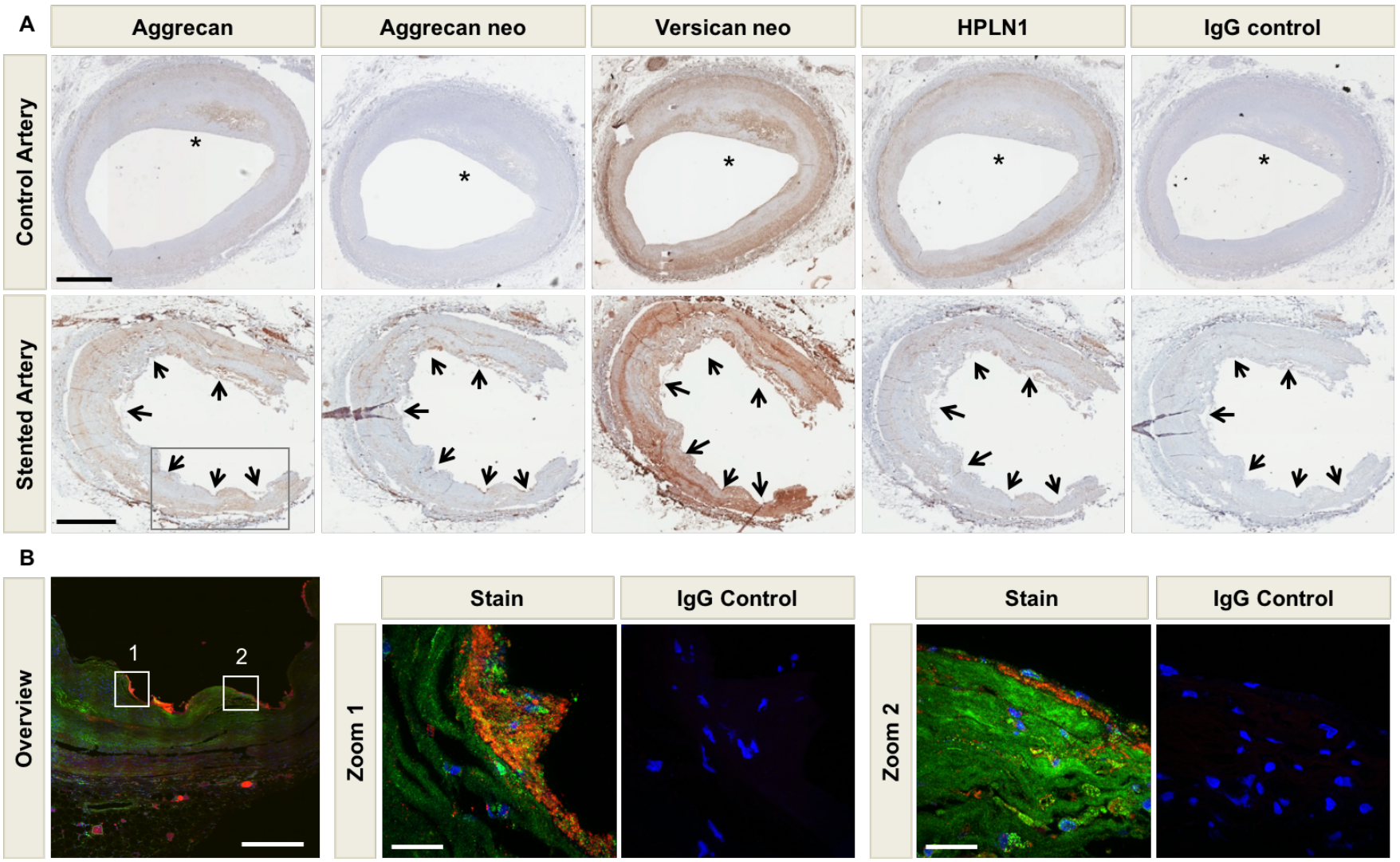

Figure 27. **Immunostaining on human coronary arteries. (A)** Localization of aggrecan, the aggrecan NITEGE and versican DPEAAE neoepitopes (neo), and HPLN1 in stented and control human coronary arteries with presence of atherosclerosis (*). Arrows mark the contacts of the stent struts with the coronary artery. Scale bars=1 mm**. (B)** Co-localization of aggrecan (Alexa 633, displayed in green) and aggrecan NITEGE neoepitope (Alexa 568, displayed in red) in human stented coronary arteries by immunofluorescence is displayed on a magnified section as marked in (A). Note the presence of aggrecan fragments at the contacts of the stent struts with the artery and in the subendothelial layer (zoomed-in areas). Overview image 20x, scale bar=500 µm; Zoomed-in areas 60x, scale bar=25 µm. Sections were provided by Dr. Steve White of University of Bristol. Fluorescence images were taken with Dr. Chris Molenaar of King's College London.

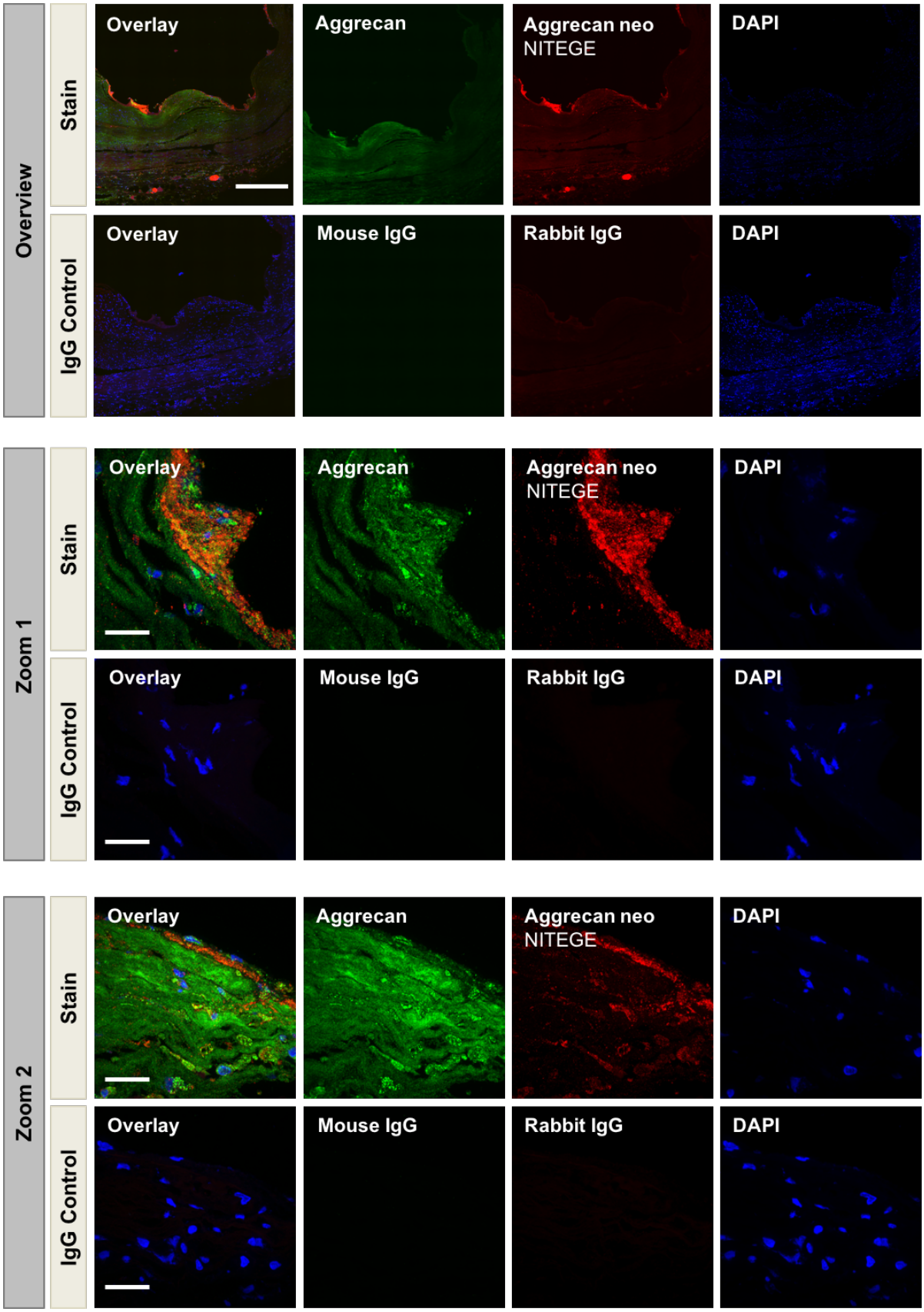

Figure 28. Aggrecan in human stented coronary artery. Detail images to figure 25B. Co-localization of aggrecan (Alexa 633, displayed in green) and aggrecan NITEGE neoepitope (Alexa 568, displayed in red) in human stented coronary artery visualized by immunofluorescence. Overview image 20x, scale bar=500 µm; Zoomed-in areas 60x, scale bar=25 µm.

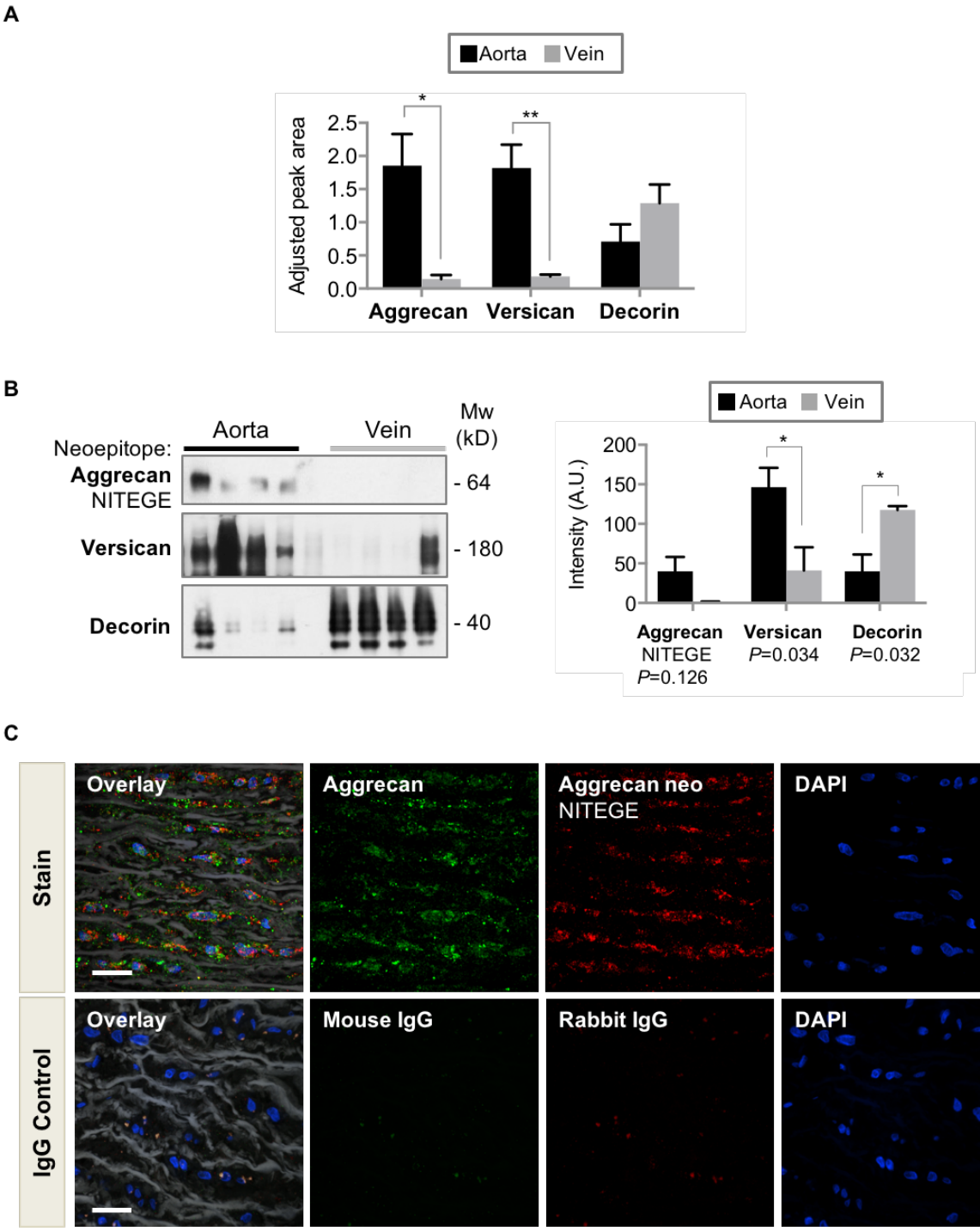

Figure 29. Aggrecan in human vessels. (A) Adjusted peak area for aggrecan, versican and decorin in the human thoracic aorta and saphenous veins as determined by targeted proteomics. n=7 per group. **P*<0.05, ***P*<0.01 (*t*-test with unequal variance). **(B)** Immunoblots for the aggrecan NITEGE neoepitope and versican in the human thoracic aorta and saphenous veins. The SLRP decorin served as a loading control. Quantification by densitometry is shown on the right. n=4 per group. **P*<0.05 (*t*-test with unequal variance). (**C**) Co-localization of aggrecan (Alexa 633, displayed in green) and aggrecan NITEGE neoepitope (Alexa 568, displayed in red) in human aorta visualized by immunofluorescence. Elastin fibres in white (autofluoresence with 488nm laser excitation captured in the green emission channel). Control sections stained with matching isotope IgGs. Magnification 60x, scale bars=20 µm.

5.9 Aggrecan in a mouse model of venous bypass graft

5.9.1 Role of mechanical forces in aggrecan expression

The higher abundance of aggrecan in stented coronary arteries and aorta compared to veins and its role in the cartilage to absorb pressure, let us hypothesize that mechanical stretch might induce aggrecan expression in the vasculature, similar to its role in the cartilage. In order to explore this potential mechanism, veins were grafted into carotid arteries of mice (*Figure 30A*). After grafting, mice were fed a diet of stable isotope labelled amino acids for 28 days to label all newly synthesized proteins (*Figure 30B*). Using targeted LC-MS/MS analysis, the incorporation of the stable isotope labelled amino acids was compared between ECM proteins in veins, vein grafts and arteries (*Figure 30C*). 60% of aggrecan peptides were found to be labelled in the murine aorta, demonstrating active synthesis of this proteoglycan in the arterial wall. In contrast, labelled aggrecan peptides were undetectable in veins, thus no aggrecan was produced in the normal vein. The incorporation ratio in vein grafts, however, was comparable with the aorta. Thus, aggrecan synthesis was inducible in veins by exposure to arterial blood pressure. Representative histological sections of mice fed a normal chow are shown in *Figure 30D*, where aggrecan was markedly elevated after grafting. The upregulation coincided with cleavage of the versican core as indicated by staining for the ADAMTS-specific DPEAAE neoepitope. Thus, besides its role in cartilage, aggrecan might be an important contributor to ECM remodelling in the vasculature, particularly in response to arterial blood pressure.

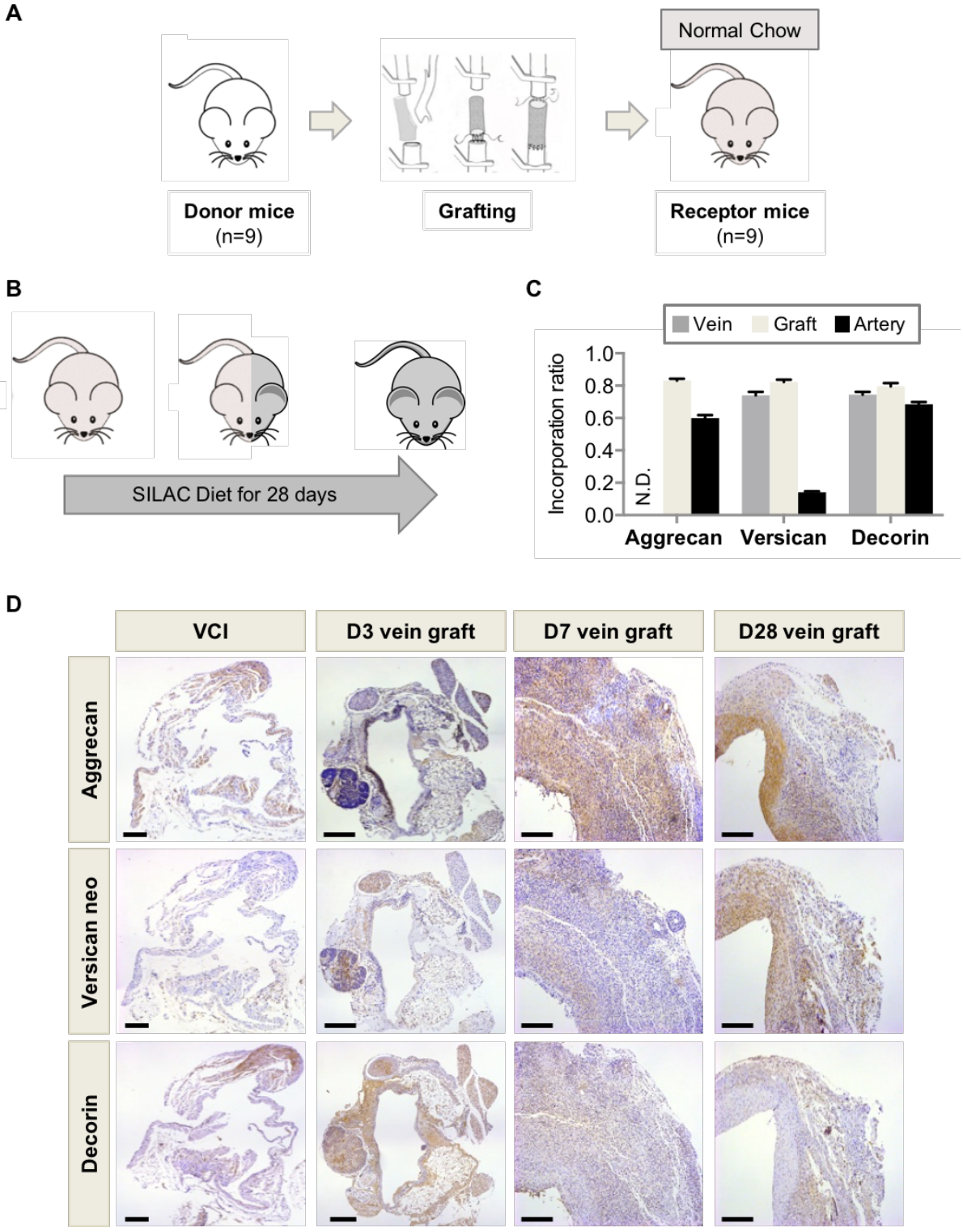

Figure 30. Aggrecan induction upon mechanical forces. (**A**) Isogenic *venae cavae* of donor mice were grafted to carotid arteries of receptor mice. (**B**) Upon grafting, mice were fed a diet with stable isotope labelled amino acids for 28 days with subsequent analysis of the vessels by targeted MS. (**C**) Incorporation ratios for aggrecan, versican and decorin in interposition grafts, vena cava inferior and aortas are plotted. n=8-9 per group. N.D.=not detectable. **(D)** Immunostaining for aggrecan, the versican DPEAAE neoepitope and decorin. Magnification 10x, scale bars=200 µm. Mice graft surgery was carried out by Dr. Ursula Mayr.

6 DISCUSSION

The vascular ECM plays a critical role in providing structural support to the vessel wall and influences cell behaviour and signalling. In ISR, a complication of stent implantation in coronary arteries, the ECM constitutes over 50% of the tissue.[155] However, to date, the composition of the ECM and the functional importance of ECM remodelling post coronary artery stenting are only poorly characterised at a molecular level. Our current knowledge of ECM changes after stent injury and during neointima formation is mainly based on histopathological analysis. To gain a more profound understanding of the ECM composition, we have applied proteomics analysis to stented porcine coronary arteries. This study is a significant advance over the published literature as it provides the first proteomics analysis of ECM remodelling in stented coronary arteries over time and a comparison of the effects of DES versus BMS on the vascular ECM. It revealed a previously unrecognized expression and cleavage of aggrecan during ECM remodelling upon stent implantation. Findings in the large animal model were validated in human specimen and followed-up in a small animal model. Diverging from the traditional ECM focus on collagens and MMPs, this study highlights the contribution of aggrecan and aggrecanases to vascular remodelling after stent implantation. Thus far, little is known about the role of aggrecan in the vasculature and stimuli that induce its expression.[262] We have demonstrated that aggrecan synthesis is higher in arteries than in veins and that it is inducible upon grafting a vein into arterial circulation, which might be related to high circulatory pressure. However, this needs to be confirmed with further experiments, such as comparing the aggrecan content in the aorta of a hypertensive animal model to a non-treated animal.

Our findings provide a blue-print of the healing process in the coronary vasculature, which may lay the foundations for a better understanding of complications, such as ISR including neoatherosclerosis and thrombosis and suggest potential new drug targets to alter ECM remodelling in the vasculature.

6.1 Porcine animal model of stent injury

Animal models are essential to investigate temporal changes post stent implantation. Pigs are ideal, since the stages of the healing process closely resemble human disease.[263] The time course, however, is notably different: stent healing in pigs occurs approximately six times faster than in humans.[264] In the porcine model, peak neointima growth is observed at 28 days after stent deployment corresponding to six months in human. Few changes occur beyond this time point, with the exception of slight neointima thinning later on.[264]

Obvious reasons for the more rapid healing process in pigs are the absence of atherosclerotic lesions. In human samples, it has been shown that stent struts with an underlying necrotic core heal slower than stents in close proximity to areas with adaptive intimal thickening containing many SMCs.[265] A slower healing response also applies to stents overlying calcified and densely fibrotic and hypocellular plaques. Notably, the presence of a lipid core of the underlying atherosclerotic lesions in human, likely influences drug retention and therefore further delaying healing and re-endothelialization.[60] The lack of a realistic atherosclerosis model is trying to be addressed by using pigs with metabolic syndrome or genetically modified models, particularly PCSK9 engineered minimpigs.[85] A further explanation for the rapid healing of stented pig coronary arteries is their young age. At the same time these are the shortcomings of our animal model: unlike patients, juvenile pigs are free of atherosclerosis. This might also be the reason for the rather unexpected OCT findings. In our study the neointima of DES showed almost entirely a homogenous pattern at day 28, while this pattern was seen at only about 60% of the BMS neointima. 39.8% of the neointima in BMS displayed a layered pattern at day 28. On the other hand, histopathological studies of atherosclerotic human arteries related a layered and heterogeneous OCT pattern rather to DES in-stent restenosis, while homogenous was typical for BMS.[50] A previous study correlating OCT patterns of neointima formation to histopathologic findings using a healthy pig model similar to our study, found that heterogeneous and layered patterns had significantly thicker neointima compared to homogenous patterns.[266] Further, peri-strut inflammation was less frequently found in the homogeneous pattern. Thus, for a more in-depth molecular characterization of the neointima formation upon stenting we have used proteomics.

6.2 miRNA changes in the stent injury model

Previous studies demonstrated a role for miRNAs in vascular disease.[77] To complement the protein measurements in the large animal model, we have measured the expression of few selected miRNAs known to be involved in the proliferative response upon stent injury. Indeed, pronounced changes were observed between control and stented arteries, especially for miR-21 and miR-221, which were significantly upregulated upon stenting in our model. Both miRNAs are highly expressed in SMCs as well as ECs, indicating their important role in vascular remodelling.[267] miR-21 and miR-221 are known to promote the synthetic phenotype of SMCs and induce their proliferation.[77, 81] miR-221 was found to play a critical role in vascular SMC proliferation and neointima formation after angioplasty in a rat model.[81] In contrast, antiproliferative effects have been reported on ECs via c-kit inhibition for miR-221.[268] Thus, the upregulation of both miRNAs upon stenting in our model is likely associated with proliferative vascular SMCs, whereas their increase may

be a cause or effect of the proliferation. In addition, our observation for miR-21 is in line with previous reports of a prominent miR-21 upregulation after stent injury.[257, 269] Wang et al. found that anti-miR-21 coated stents implanted in a humanized myointimal hyperplasia model in rats, were effective in decreasing ISR without interfering with re-endothelialisation.[269] Similarly, McDonald et al, demonstrated that an inhibition of miR-21 attenuated neointimal formation in mice post-stenting.[257]

Unlike miR-21 and miR-221, miRNAs, which inhibit SMC proliferation (miR-133a, miR-143, miR-145 and miR-195)[267] were initially down-regulated upon stenting, consistent with the proliferative state of SMCs upon vascular injury. Both, miR-143 and miR-145 maintain SMCs in a differentiated state, and it was shown that miR-145 overexpression inhibits neointimal growth[76].

6.3 Strengths and caveats of the proteomics approach

Proteomics provides a valuable tool to comprehensively characterize the ECM composition of cardiovascular tissues.[114, 253, 270] As proteins are the actual effector molecules carrying out cellular functions, proteomics is better suited than transcriptomics to analyse the ECM composition. The untargeted discovery-based proteomics approach, allowed an unbiased identification and relative quantification of ECM protein changes upon stenting.[271] In contrast, conventional methods such as immunohistochemistry or western blotting, require *a priori* knowledge on the proteins of interest and tend to focus only on single proteins at a time. In addition, they rely on the availability of good antibodies. Besides notorious limitations of antibodies such as epitope masking or non-specific binding, the abundance of the same protein can only be relatively quantified across different samples; however, the abundances of different proteins cannot be reliably compared, since the sensitivity and specificity of antibodies may differ. On the other hand, a caveat of data-dependent LC-MS/MS analysis is that low abundant proteins often escape detection in complex samples. Thus, to overcome this limitation, we have subfractionated the tissue and enriched for ECM proteins as previously described by our group.[170]

The initial hypothesis-generating proteomics approach allowed us to identify candidate proteins, in particular aggrecan, which we have further investigated using a targeted MS approach and other independent techniques. In addition to validating the proteomics findings, techniques such as immunostaining, complemented the proteomics data by providing insights into protein localization, and this spatial information helped to further elucidate the potential role of aggrecan in the vasculature.

6.4 The role of databases in proteomics data analysis

Improvements in MS instrumentation and database software have immensely contributed to the advances made in proteomics. However, the availability of complete and accurately annotated sequence databases for many species are equally important.[199] For humans, several databases exist, with different degrees of completeness, redundancy and annotations.[272] When peptide spectra are assigned to the database search, the potential peptide assignments are matched and thus limited to those sequences present in the database. For pigs, well-annotated and comprehensive protein databases are not yet available. Thus, we have generated a custom-made database that included as many known ECM proteins as possible to improve protein identification and quantification. For example, for perlecan, the database search with the combined human and porcine database returned only two thirds of the spectra that were identified using our custom-made database. With our expanded database, the coverage of the identified proteins as well as the accuracy of our protein expression analysis increased. Thus, the output of proteomics studies depends on the comprehensiveness of the available databases.

6.5 Identification of ECM proteins using discovery-based proteomics

Porcine coronary arteries were stented with BMS/DES or were subjected to POBA serving as control. The arteries were analysed 1, 3, 7, 14 and 28 days post-stenting by proteomics. At day 28, the evolved neointimal tissue on top of the stent struts was separated and subjected to a separate proteomics analysis.

6.5.1 ECM changes in the neointima

Our proteomics comparison of the neointima revealed the following findings:

- First, a more diverse composition of the neointima compared to the media of the same stented vessel at day 28 was observed. Further, basement membrane proteins were more abundant in the neointima than in the media. This observation is likely due to the higher cellularity in the neointima, since SMCs proliferate and migrate from the media towards the intima followed by ECM production.[60] BM proteins including fibronectin are responsible for cellular anchorage, thus their abundance is tightly linked to tissue cellularity.
- Secondly, a more organized and structured ECM assembly in the neointima forming over BMS compared to DES was seen. This was indicated by the increased abundance of fibrillar collagens and SLRPs, which contribute to collagen fibril formation and organization such as lumican, biglycan or fibromodulin in BMS stented arteries. Presumably, ECM organization indicating healing occurs at an earlier stage in arteries treated with BMS compared to DES.

- Thirdly, an upregulation of proteins associated with the regulation of calcification in neointimal lesions of arteries treated with DES became apparent.

Vascular calcification generally refers to the accumulation of calcium phosphate crystals in vascular medial and intimal layers. Vascular intimal calcification associated with atherosclerosis is the most common form of calcific vasculopathy and different from medial Mönckeberg calcification, which can occur independently from intimal calcification.[273] Intimal calcification is suggested to be similar to the process observed in bone formation.[144, 274] Upon triggers such as inflammatory cytokines and mineral imbalance as prominently seen in chronic kidney disease vascular SMCs undergo chondrocyte and osteoblast-like differentiation. An osteogenic signalling pathway for example involves the BMP2/4 induced activation of the transcription factor Runx2, which is involved in osteoblastic differentiation.[275] This transformation is characterized by the release of matrix vesicles, containing calcium and phosphate in form of hydroxyapatite crystals. Further, apoptotic SMCs releasing apoptotic bodies may serve to nucleate hydroxyapatites. Notably, vascular calcification is efficiently prevented by the calcification inhibitor MGP, either directly or by inhibiting BMP2 induced osteogenic differentiation.[144] The importance of MGP in calcification inhibition is stressed in studies showing that MGP deficient mice develop spontaneous vascular calcification.[275, 276]

In our study, we observed an upregulation of the calcification inhibitor MGP[277] and SPP24 in the neointima of DES treated arteries. Similarly, SPP24 is anti-osteogenic as its C-terminal fragment binds to and inhibits the activity of BMP2.[278] The upregulation of these proteins may be a protective response of the vasculature as demonstrated by the presence of MGP and SPP24 in human control arteries. However, it is unclear whether their predominant abundance in the neointima of DES is due to a compensatory mechanism to a potentially increased calcification tendency or a primary inhibition of calcification. As neoatherosclerosis with or without calcification, is more frequently and rapidly observed in DES than BMS, a higher calcification tendency in DES is plausible.[56] On the other hand, recently it was shown that mTOR signalling inhibition decreases phosphate-induced vascular calcification via the upregulation of the Klotho gene expression.[279] In the latter study the observed inhibition of calcification in aortas of chronic renal failure rats with mTOR inhibitors was independent of autophagy or apoptosis. *In vitro* calcification assays with everolimus treated cells might be a useful model to further elucidate the role mTOR inhibitors and consequently of DES in vascular calcification. In summary, the observed changes for these proteins in DES may also be due to the effects of the drug on phenotypic modulation of SMCs[280], as these genes are modulated in the

transition. This may also explain why they appear increased in normal vessels vs stented human vessels.

Finally, we observed chondroadherin in DES stented arteries. This SLRP is mainly expressed in cartilaginous tissue[281] and its fragmentation has been previously associated with disc degeneration,[282] but its expression in the vasculature at the protein level has - to our knowledge - never been reported. Yet, there is evidence for an association of chondroadherin with vascular pathology, since its transcription was found to be specifically induced in atherosclerotic plaques of femoral arteries in the Tampere Vascular Study.[283] It remains to be elucidated, if chondroadherin might provide a link to the increased incidence or accelerated course of *de novo* atherosclerosis within DES-stented vessels.[73]

6.5.2 Early changes upon vascular stent/balloon injury

The early response to injury was independent of the deployed stent type. Similar protein changes were also observed after POBA in the early phase. Thus, their up-regulation indicates primarily a response to vascular injury, including balloon dilatation, rather than stenting. We have identified three different functional classes among these "early" proteins:

- Proteins involved in haemostasis such as fibrinogen, plasminogen, antithrombin III and thrombospondin were increased. This is in line with findings in histopathological studies of platelet activation and thrombosis formation during the early stage of vascular healing.[284]
- Furthermore, inflammatory proteins associated with innate immunity such as PTX3[285] or prophenin and tritrpticin (C6)[286] were increased. Also Cathepsin G was only detected at day 1 of BMS stented arteries. Cathepsin G, for example, has also important effects in regulating chemotaxis.[287] An explanation for their upregulation is the recruitment of inflammatory cells to the site of vascular injury. Clinical studies reported a rise of inflammatory markers following PCI.[288] Lactadherin expression peaked around 7 days post-stent implantation in the DES group. Lactadherin plays an important role in the promotion of mucosal healing and contributes to phagocytic removal of apoptotic cells.[289, 290]
- Finally, various apolipoproteins, such as apolipoproteins E, C-III and R[259] and also lipoprotein lipase were retained in all groups. It is noteworthy that these are VLDL-associated apolipoproteins. Apolipoprotein R is pig-specific.[259] Their upregulation likely resulted from the disruption of the endothelial lining with subsequent exposure of the vascular ECM. This endothelial injury may have allowed VLDL-associated apolipoproteins to bind to vascular proteoglycans, such as versican

and biglycan, that are known to retain apolipoproteins in the vessel wall.[14] However, apolipoproteins also contribute to innate immune responses, as carriers of proinflammatory oxidation by-products.[291] Clearly, the lack of detection of other apolipoproteins does not exclude their contribution to the vascular injury response.

- Apart from insulin-like growth factor-binding protein 7, cytokines and growth factors were barely detected in our proteomics analysis of the GuHCl extracts. This is likely due to their very low abundance compared to other proteins, thus they may escape detection by LC-MS/MS without further enrichment steps.

6.5.3 ECM changes in the media

In the early phase upon stent insertion, most ECM proteins showed no significant change. ECM changes were observed predominantly after 28 days. Notably, in our study the pigs used for the time point day 28 were all female compared to the groups of the other time points, which had an equal distribution of the two sexes. In addition, the pigs of day 28 weighed on an average 9.6 kg less than their counterparts of other time points. In general, for this study both female and castrated male pigs were used, which is in line with other studies from major pathology labs deploying the porcine vascular injury model.[86, 292] Thus, from this aspect no major impacts of male sexual hormones should be expected on our findings. Moreover, the fact that all pigs were female at day 28 is not based on any selection bias, as the pigs were distributed randomly into the groups as they were available from the supplier regardless of their sex but with similar age. The similar age would presuppose a similar stage of growth in all pigs. However, it is a fact that the day 28 pigs were significantly smaller, for which we cannot provide an obvious explanation, as all animals were on the same diet. On a positive note, there were no significant weight or sex differences within the group, especially excluding an impact with regard to the BMS vs. DES comparison. Taken together, we cannot exclude any impact of the smaller animal size by the time of stent implantation on the vascular remodeling process. However, it appears more plausible, that the ECM changes predominantly observed at day 28 were due to the time it takes SMCs to lay down enough new ECM, rather than their size at stent implantation.

Significant increase at day 28 were seen in fibrillar collagens, such as type I, III and V, the structural ECM components, but also in matricellular proteins (periostin, tenascin, SPARC) and SLRPs (decorin, biglycan, fibromodulin, podocan, asporin).

- As highlighted in the introduction, SLRPs are important regulatory proteins, involved in a variety of cellular functions such as collagen fibril assembly, inflammation, cell proliferation, adhesion, migration as well as fibrosis.[108, 117] Decorin for example was found to negatively regulate fibrosis in cardiac tissue via

its inhibition of the TGF-β pathway.[293] Despite high sequence and structural homology between decorin and biglycan, they were found to have distinct kinetics during neointima formation after arterial stent injury.[294] Unlike biglycan, decorin did not occur in the neointima of control, non-atherosclerotic rabbit aortas, but appeared in the atherosclerotic aortas in the confined area of SMCs surrounding macrophages around stent struts.[294]

- Like the SLRPs, matricellular proteins have important regulatory functions. The term 'matricellular' refers to their ability to modulate cell-matrix interactions and cell functions.[116] SPARC, for example, facilitates collagen crosslinking and is therefore needed for proper healing after myocardial infarction.[295] It has been shown that the absence of SPARC in mice caused increased cardiac rupture and dysfunction after myocardial infarction. Similarly, the upregulation of SPARC found in our study might indicate its importance in proper vascular healing post stent injury.
- Interestingly, we have also found the lecticans aggrecan and versican increased at late stage. Aggrecan and its functionally related ECM protein, the link protein or hyaluronan and proteoglycan link protein 1 (HPLN1) were also among the differentially expressed proteins between BMS and DES at day 28. However, HPLN1, serves as the stabilizing link protein by binding to both lecticans and hyaluronan[296], and was found to be downregulated in the DES group unlike aggrecan.

To conclude the results of the identified ECM proteins, proteomics uncovered a coordinated ECM remodelling in response to vascular injury, including proteins such as aggrecan, which have not been described in the vasculature in connection with stent injury to date. Generally, more proteins showed a significant change in the DES compared to BMS group, with the differences being more pronounced at later stages. In DES, a uniform down-regulation of basement membrane proteins, indicative of a reduced cellularity, was accompanied by an increase in aggrecan.

6.6 Aggrecan: more than just a cartilage protein

6.6.1 Aggrecan structure and function

Aggrecan is above all known for its role as the major proteoglycan in cartilage. It is characterized by its ability to bind hyaluronan, a large carbohydrate polymer, to form even larger aggregates, stabilized by the link protein (*Figure 31A*).[109] The aggrecan gene, ACAN, in human is found on chromosome 15q26.1 and is composed of 19 exons. Exons 1 and 9 are non-coding and exons 2-18 code for the core protein with around 2450 amino

acids, with a calculated molecular mass of approximately 250 kDa. Aggrecan is a multimodular protein consisting of three globular domains, two located at the N-terminus (G1 and G2) and one at the C-terminus (G3).[297, 298] Thus, it is reminiscent of a barbell like shape with globular domains at either end (*Figure 31B).* The G1 domain has the same structural motif as link proteins and functionally anchors aggrecan to hyaluronan and link protein, forming a stable ternary complex in the ECM. The G2 domain is unique to aggrecan among the lecticans and is homologous to the tandem repeats of G1. However, no interaction with hyaluronan, link protein or other ECM proteins were described for this domain. It has been suggested that the G2 domain is involved in regulating protein processing through the secretory pathway in order to produce a mature functional molecule.[299] Its C-terminal G3 domain consists of different structural motifs: two epidermal growth factor (EGF)-like repeats, a C-type lectin domain (CLD) and a complement regulatory protein (CRP, also known as sushi) repeat.[297] The G3 domain links the aggrecan aggregates to other ECM proteins such as tenascins, fibulins or fibrillin-1. An interglobular domain (IGD) of approximately 150 amino acids separates G1 from G2. The central and largest part of aggrecan lies between its G2 and G3 domains and carries numerous GAGs, namely keratan sulfate (around 30) and chondroitin sulfate (around 100) chains, which give the protein its enormous amount of fixed negative charges. In fact, its glycosylation increases its molecular weight from around 250 kDa for its core protein to around 2.5 MD.[297] These highly negatively charged GAGs attract counter-ions and draw water into the tissue providing the basis for the viscoelastic properties of cartilage. However, the numerous GAG side chains of aggrecan are not only important for cartilage resilience. It has also been shown that aggrecan is an important component of the perineuronal net, a matrix substructure in the central nervous system, involved in regulating brain synaptic plasticity and in glial scar formation after brain injury.[109, 297] In addition, aggrecan in perineuronal nets was shown to exert neuroprotective actions by reducing oxidative stress through scavenging redox-active cations.[300]

6.6.2 Aggrecan cleavage

Aggrecan is known to be extensively degraded in tissue and aggrecan aggregates constantly undergo turnover in cartilage.[301] Aggrecan degradation and its consequent loss from the cartilage for example, is one of the earliest events that occurs in association with osteoarthritis.[302, 303] Especially cleavage of aggrecan in its interglobular domain between G1 and G2 is known to be of central importance for the pathology, as this releases the C-terminal GAG carrying region of aggrecan from the cartilage, which is responsible for its water-entrapping function. Aggrecan was shown to be cleaved by multiple proteolytic enzymes, including MMP3 (also at its IGD generating a fragment terminating in DIPEN[341])

and the ADAMTS enzymes.[304] In fact, previously, there has been an active debate over the relative importance of the different enzymes responsible for cartilage aggrecan degradation.[305] However, it is now well established that ADAMTS - the aggrecanases - are the primary enzymes responsible for aggrecan cleavage in cartilage.[306] Although aggrecanases cleave aggrecan at multiple sites[307] (even more efficiently within its C-terminus) (*Figure 31B*), the aggrecanase cleavage at the NITEGE[373] and ARGSV[374] bond is the most relevant for pathology, as the loss of the GAG-rich region compromises its function.

While ADAMTS-5 (aggrecanase-2) was found to be the major aggrecanase in mouse cartilage[308], in human ADAMTS-4 (aggrecanase-1) and ADAMTS-5 are suggested to be equally important in aggrecan cleavage in osteoarthritis.[309] With only a single thrombospondin motif ADAMTS-4 is the shortest member of the ADAMTS family, while ADAMTS-5 is ranked second with two thrombospondin motifs (*Figure 7*). Moreover, it has been suggested that ADAMTS-4 expression is inducible, while ADAMTS-5 is constitutively expressed in human – for example, ADAMTS-4 was induced following stimulation with TGF-β, however ADAMTS-5 was not and neither by IL-1 nor TNF-α.[310] Thus, expression of these aggrecanases seem to be differentially regulated. Also, ADAMTS-1 was shown to cleave aggrecan[311], though this aggrecanase, is not as prominent in aggrecan turnover in cartilage.[312]

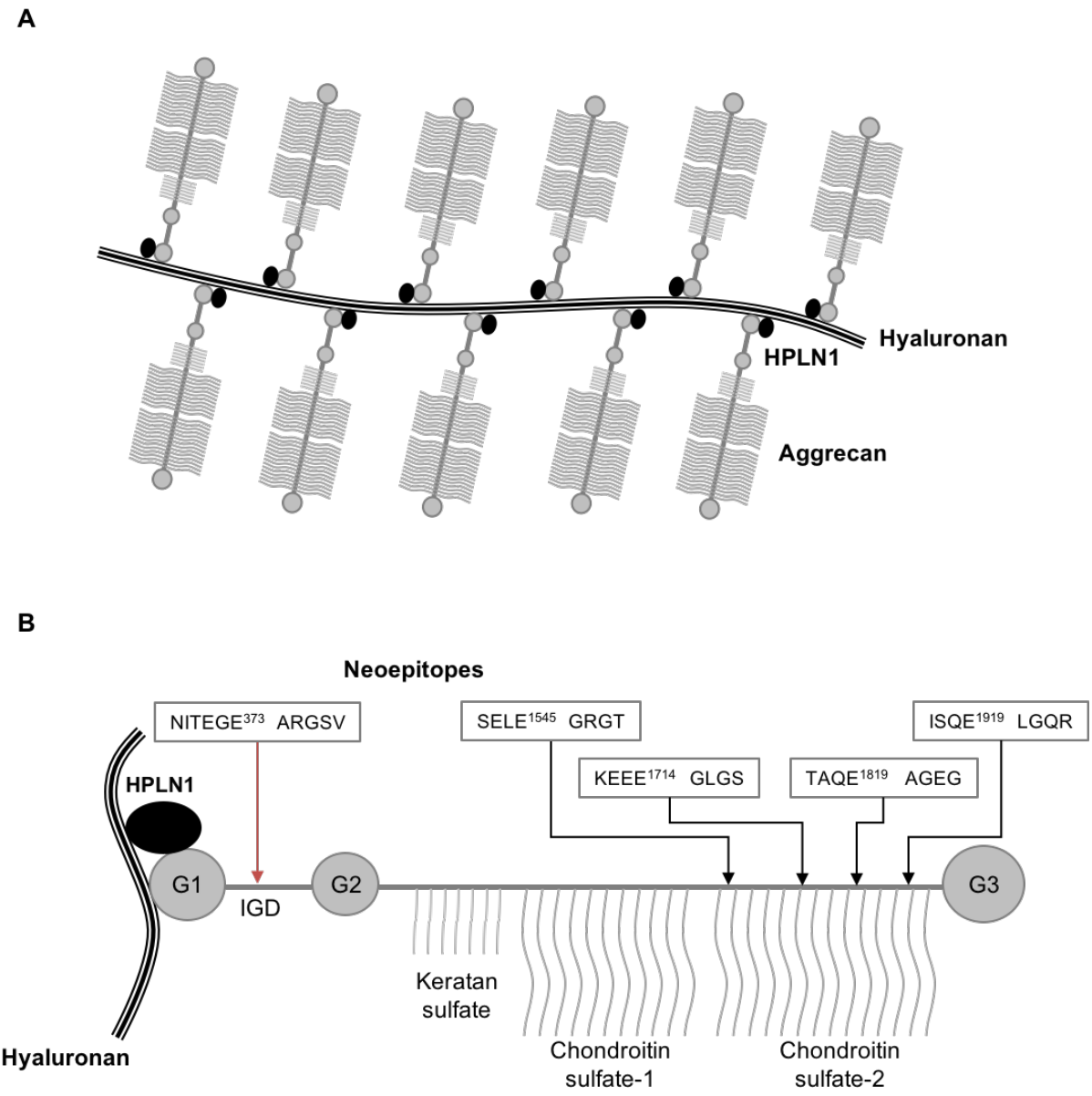

Figure 31. Schematic structure of aggrecan and its cleavage sites (**A**) Illustration of large aggrecan aggregates with hyaluronan. HPLN1 (black dots) stabilizes the binding. (**B**) Domain structure of aggrecan core protein with attached GAG side chains is shown. G2 domain is unique to aggrecan among the lecticans. Aggrecanase cleavage sites and neoepitopes in the aggrecan core protein are shown for their human sequence. The critical cleavage site within the IGD is marked with red arrow (the NITEGE^{373} ARGSV).

6.7 Aggrecan in the vasculature

Aggrecan turnover is altered in disease such as osteoarthritis and is well-studied herein[303, 313], but its expression and function in the vasculature has only recently begun to be appreciated. Proteoglycans with their GAG side chains are known to present growth factors and cytokines to the surrounding tissue for cell differentiation.[104] Also their multiple interactions with other ECM components modulate a wide range of cellular responses,

including inflammation.[314] Fibulin-2 for example, is a high-affinity ligand for the C-type lectin motif in the G3 domain of aggrecan, which links aggrecan aggregates to the ECM.[315] Fibulin-2 was also found to be increased upon DES stenting in our study. These functions of proteoglycans might contribute to vascular healing after stenting.

On the other hand, it has also been suggested that lipoprotein binding to negatively charged GAG side chains might contribute to atherosclerosis.[316, 317] While this has been repeatedly shown for versican in several studies[14, 262], as it is a major structural component of the vessel wall, there is also evidence for aggrecan contributing to atherogenesis. Aggrecan expression was demonstrated in advanced lesions of atherosclerotic aortas of ApoE/LDLr deficient mice by immunohistochemistry, further supporting that cartilage-associated ECM proteins may be involved in the pathogenesis of atherosclerosis.[318] Similarly, we have observed staining for aggrecan in the atherosclerotic lesion of the human control coronary artery (*Figure 27A*, *indicates plaque location). Furthermore, a previous proteomics analysis discovered aggrecan in vascular intimal hyperplasia.[319] Finally, aggrecan deposition was reported in leptomeningeal arteries of hereditary brain haemorrhage with amyloidosis.[320]

Our proteomics study provides evidence for an upregulation of aggrecan after stenting. This unexpected finding in the porcine stent model was substantiated by findings in mice upon grafting veins from a low- to a high-pressure environment. Similarly, aggrecan was more abundant in the high-pressure environment of the human aorta, than in veins. Also, aggrecan and its fragments were co-localized in the media of the human thoracic aorta. These findings may suggest, that due to its water-attracting property that confers resistance to compression, aggrecan may be part of an adaptive response of the vasculature to absorb increased mechanical forces – similar to its function in cartilage. Though increased mechanical stretch seems to be a plausible mechanism for the induction of aggrecan upon grafting a vein into a high-pressure environment, other factors also remain eligible to have induced aggrecan synthesis in our model. For example, surgical or ischemic injury may be partly responsible for triggering inflammation in the graft model and the consequent release of cytokines and growth factors initiating SMC proliferation and aggrecan synthesis. To confirm that mechanical force induces aggrecan synthesis, an animal model of hypertension would be a useful tool. Finally, the exact mechanisms and the stimuli leading to aggrecan synthesis remain to be further elucidated.

6.8 Aggrecanases in the vasculature

Besides aggrecan, we have detected the aggrecan NITEGE neoepitope in porcine coronary arteries upon stenting as well as in stented human arteries and the aorta. This

aggrecan neoepitope is generated upon proteolytic cleavage by aggrecanases. Importantly, neoepitope antibodies fail to recognize the same sequence in the undigested protein, thus their detection provides a signature for enzyme activity.[127] However, the detectability is equally dependent on substrate availability, thus more substrates result in increased fragment detection. We have probed for the critical site at NITEGE[373] within the IGD, due to the functional importance of this cleavage site. Indeed, as observed in proteomics and in gene expression analysis, aggrecan increases upon stenting. However, at the protein level the increase is more pronounced in DES. Similarly, the aggrecan neoepitopes become detectable by day 28 in DES, suggesting increased aggrecan build-up. Likewise, the deglycosylated versican DPEAAE fragment of the V1 isoform showed an increase upon stent injury corresponding to the versican induction. However, unlike aggrecan, the versican fragment is already detectable at baseline. This is consistent with the much higher abundance of versican compared to aggrecan, especially in normal arteries. As expected, at day 28 the fragments in DES stented arteries were increased compared to BMS. This observed difference at day 28 was in line with the proteomics findings and suggested that differential degradation/turn-over of aggrecan in BMS and DES might explain the difference between protein abundance and gene expression. Aggrecan and versican mRNA levels at day 28 were similar in both groups. Aggrecan and versican protein levels, however, were higher in DES, both in the proteomics analysis and the western blots using neoepitope antibodies to visualise the smaller fragments that are readily separated on a gel.

Thus, we compared the expression levels of the aggrecanases ADAMTS-1 and ADAMTS-4. The involvement of ADAMTS-4 in vascular pathology has been highlighted in the introduction. Very recently Kumar *et al*. reported that loss of ADAMTS-4 reduced atherosclerosis in a high fat diet-induced atherosclerosis mouse model.[321] Notably, this was associated with reduced aggrecan cleavage and decreased macrophage infiltration. Though ADAMTS-1 is not considered as important in the cartilage field, we investigated ADAMTS-1 in our study, as important roles were attributed to ADAMTS-1 in the vasculature, in particular in atherogenesis[129, 152] and plaque instability[153]. Further, ADAMTS-1 is known to be involved in versican proteolysis in the human aorta[322] and in angiogenesis.[323] However, the reports on the role of ADAMTS-1 in angiogenesis are contradictive: ADAMTS-1 was reported to be a potent inhibitor of angiogenesis as it inhibits EC proliferation by sequestering VEGF.[324] It directly binds VEGF and consequently interferes with the binding of VEGF to its receptor. On the other hand, also a proangiogenic role for ADAMTS-1 has been implicated, as it was shown that VEGF-A can induce ADAMTS-1 expression to cleave versican at its DPEAAE site, which facilitates mother vessel formation.[325] These reports highlight the fine balance required for the

regulation of angiogenesis. Moreover, a very recent study highlighted a role for ADAMTS-1 as a major mediator of vascular homeostasis, as the decrease of the protease induced thoracic aortic aneurysms in mice.[326] This effect was found to be induced by an increase in NO due to activation of the inducible nitric oxide synthase (NOS2) by ADAMTS-1 deficiency, suggesting a previously underexplored ADAMTS1-NOS2 axis. The authors proposed that NOS2 activation was mediated by Akt and NF-κB, which again where activated by increased syndecan 4 levels[327], which is a substrate of ADAMTS-1. Thus, the accumulation of ADAMTS-1 targets, including aggrecan, upon ADAMTS-1 loss, might contribute to vascular pathology. Notably, as mTOR is an upstream target of this axis, its inhibition by drugs also reverts the NOS2 induction.

Indeed, in pig coronary arteries, like in human SMCs, we have found ADAMTS1 to be highly expressed. Upon stenting, ADAMTS1 was markedly reduced.

6.8.1 Shift in vascular aggrecanase activity

The two aggrecanases ADAMTS-1 and ADAMTS-4 showed a notable shift in expression in stented arteries, which likely coincided with impaired/delayed re-endothelialisation in DES and faster SMC recovery in BMS. Previous studies have shown that the initial regenerated endothelium in stented regions is incompetent in regard to its functionality (i.e. reduced expression of eNOS and antithrombotic molecules) but also to its barrier function (i.e. poorly formed cell-to-cell junctions)[328], particularly in DES.[329] In rabbit iliac arteries transmission electron microscopy has shown poorly formed cell contacts upon DES deployment. Furthermore, the expression of the antithrombotic cofactor thrombomodulin was absent or reduced in ECs of DES compared to BMS. In particular, several clinical studies demonstrated that regenerated endothelium in DES is more affected by dysfunctionality than in BMS, by assessing the endothelium-dependent vasodilation: vasoconstriction was observed in response to acetylcholine or exercise at six months after DES implantation, while the same stimuli induced the expected vasodilation in BMS stented arteries.[330, 331] Despite the high-resolution images of OCT, recognition of EC structure of the coronary arterial endothelium remains difficult. As observed in our study, at day 14, the neointimal volume was higher in BMS compared to DES, whereas no difference was seen at day 28. However, it is the EC function rather than the coverage which is crucial, but cannot be optimally assessed by OCT.

In our study, ADATMS-1 expression was high in coronary arteries, but was markedly reduced upon stent implantation. We observed high levels of ADAMTS1 expression especially in coronary artery ECs (compared to ECs of other vascular territories), suggesting that the loss of competent coronary artery ECs may contribute to the decrease of ADAMTS-1 upon stenting. Similarly, ECs treated with everolimus showed

a loss of both enzymes. However, this effect is not limited to ADAMTS enzymes, as other proteases including MMPs showed a significant decrease upon everolimus treatment (data not shown) and is likely explained by general inhibition of protein synthesis or even toxic drug effects as demonstrated by the cell counting and viability assay. Instead, ADAMTS4 expression was increased, in particular in BMS, which could be due to their faster re-endothelialisation and/or uninhibited SMC proliferation, as SMCs are also an important source of ADAMTS-4. There is further support for the contribution of ECs to ADAMTS4 expression as it coincided with the re-expression of the endothelial specific marker cadherin 5. Our *in vivo* finding was complemented by *in vitro* data showing that everolimus treated SMCs had a significant reduction of ADAMTS4, while ADAMTS1 expression was unaffected. Thus, a drug effect might contribute to the repression of ADAMTS-4 in DES. However, also macrophages have been shown as an important source of the pro-inflammatory cytokine inducible aggrecanase ADAMTS-4.[154] Thus, all three cell types could be involved in the more pronounced increase of ADAMTS-4 in BMS.

Both, aggrecanases and aggrecan are expressed in human coronary artery SMCs, but human coronary artery ECs express only the aggrecanases. This finding suggests that ECs influence aggrecanase activity and aggrecan levels without producing aggrecan. Further, we have seen that in stented human arteries staining for aggrecan neoepitopes was particularly pronounced at the contact points of the stent struts (Figure 27A, arrow marks), suggesting again either increased aggrecan production and/or increased aggrecanase activity at sites of mechanical injury. Besides ECs, both SMCs and macrophages are likely contributors to this injury response. Taken together, these findings suggest that a loss of functional arterial ECs upon stenting might contribute to reduced aggrecanase expression and activity in the vessel wall. Moreover, delayed/impaired re-endothelialisation and reduced aggrecanase secretion i.e. by DES, would facilitate the accumulation of large aggregating proteoglycans in the vessel wall. Notably, both the detectability of versican and aggrecan neoepitopes in the western blots predominantly correlated with substrate availability rather than ADAMTS expression.

6.8.2 Regulation of aggrecanase activity

Our findings of altered aggrecanase levels suggest their import contribution to the build-up of large aggregating proteoglycans upon stenting. Especially, as enzymes are responsible for potent effects even in small amounts, due to their catalytic activity speeding up biochemical reactions. However, our current picture is incomplete and may not reflect the actual aggrecanase activity, as enzyme levels and activity are regulated on various levels: on mRNA as well as protein levels.

Besides aggrecanase synthesis, (*Figure32, 1*), which we have investigated in this study by measuring mRNA levels, ADAMTS secretion and activation (*Figure32, 2)* determines enzyme activity. Aggrecanases are synthesized as inactive zymogens and the cleavage of the propeptide is required for enzymatic activity. This control mechanism allows the ADAMTS enzymes to exert their activity at precise locations. Proprotein convertases (PC) such as furin, paired basic amino acid cleaving enzyme 4 (PACE4), PC5/6 or PC7 were shown to activate aggrecanases.[332] Activation can either take place at the trans-Golgi network by membrane-bound PCs, as shown for ADAMTS-1[333] and ADAMTS-4[334] or extracellularly by constitutively secreted PCs, as demonstrated for ADAMTS-5 processing[335]. However, ADAMTS-4 activation also occurs extracellularly by PACE4. PACE4 is thought to be vital for aggrecanase activation in cartilage, and its expression was found to be increased in osteoarthritis.[336] Also, the authors demonstrated an inhibition of the aggrecanase activity by reducing PACE4 expression with siRNA. These studies highlight the important contribution of PCs to aggrecanase activity. Thus, to gain a better understanding of enzyme activity, mRNA expression in tissue can only be an indication and further studies are required determining the levels of PCs or their regulation.

Moreover, aggrecanase activity is regulated by inhibitors (*Figure32, 3).* As mentioned in the introduction the small protein TIMP-3 is a potent endogenous inhibitor of the aggrecanases, which inhibits ADATMS-1[311] as well as very potently ADAMTS-4 and ADAMTS-5[337]. Due to its aggrecanase inhibition, it is not surprising that TIMP-3 is suggested to play a chondroprotective role.[338, 339] Evidence for this role was further supported by the finding that *Timp3*-knockout mice showed increased aggrecanase and collagenase activity and developed early cartilage degradation as seen in osteoarthritis.[340] However, effects of TIMP-3 were also postulated for vascular remodelling and hypertension[341], as well as for atherosclerosis[342]. However, it is unclear whether these TIMP-3 effects on the vasculature are also mediated by aggrecanase inhibition, as TIMP-3 is known to inhibit multiple enzymes, including members of the MMP family, which play a critical role in atherosclerosis and plaque stability.[136]

Finally, extracellular levels and activity of aggrecanases are regulated by endocytosis (*Figure 32, 4*). Recently, the large integral protein LRP1 was shown to be responsible for ADAMTS-5[261], as well as ADAMTS-4 clearance[260] in cartilage (‘protease sink’) and loss of LRP1 has been associated with osteoarthritis. These studies demonstrated that siRNA-mediated knockdown of LRP1 in chondrocytes markedly reduced the cellular uptake of aggrecanases. LRP1 is an endocytic transmembrane receptor consisting of an extracellular 515 kDa heavy or alpha chain and the 85 kDa light or beta chain containing the transmembrane and cytoplasmic domain. It is involved in the

internalization of multiple other ligands including lipoproteins and proteinases. Notably, LRP1 was reported to modulate atherogenesis, as deletion of macrophage LRP1 was associated with increased atherosclerosis and increased MMP9 levels.[343]

In our study, we have found the light chain of LRP1 in the neointima samples of the porcine arteries, indicating that LRP1-induced endocytosis of aggrecanases might also contribute to reduced aggrecanase levels in DES as LRP1 was more abundant in DES compared to BMS samples. A consequent increased uptake of proteases in DES would contribute to the build-up of aggrecan and versican in DES stented arteries. But again, the increase in aggrecan neoepitopes as observed in DES, might be the consequence of increased substrate levels. On the other hand, it was also shown that the aggrecanase inhibitor TIMP-3 is endocytosed by LRP1.[344] However, aggrecanase and TIMP-3 internalization are not dependent of each other.[261] Even though TIMP-3 endocytosis would suggest an increase of aggrecanase activity, the authors have shown in addition that the LRP1 – TIMP3 complex can also shed from the cell surface, whereby TIMP-3 remains its inhibitory function. Moreover, in LRP1 null mice increased proteolytic activity was observed in the aorta alongside increased fragmentation of ECM proteins.[345] Thus, LRP1 rather inhibits protease activity. Also, two very recent studies have targeted LRP1 mediated TIMP-3 internalization to increase extracellular TIMP-3 activity for a chondroprotective effect. The approach of the first study was to 'trap' TIMP-3 extracellularly by generating a soluble minireceptor (a distinct binding cluster of LRP1) blocking its internalization.[346] The other study mutated TIMP-3 in a way, which reduced binding to LRP1 but remained an unaltered inhibitory activity.[347]

In summary, aggrecanase activity is determined at multiple levels, which need to be taken into consideration collectively to describe the net effect of aggrecanase activity.

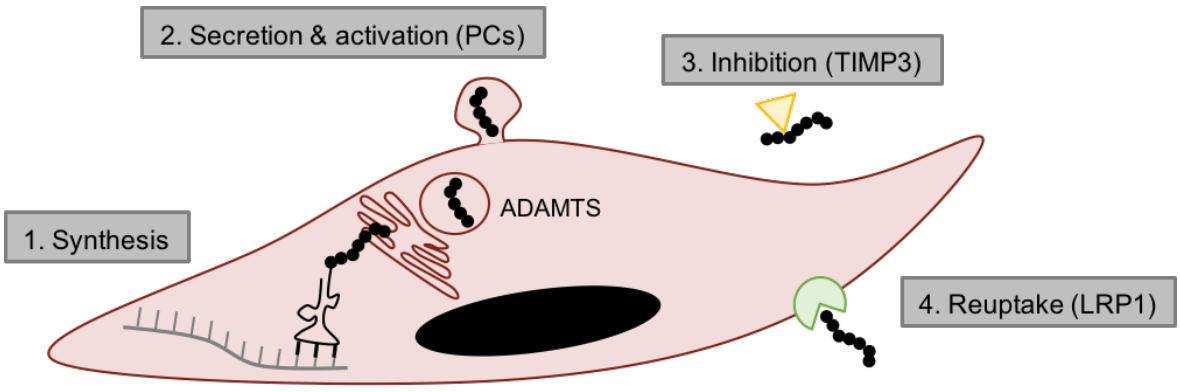

Figure 32. Regulation of aggrecanase activity. ADAMTS activity is determined at multiple levels. Besides the mRNA level (1), posttranslational regulation on protein level by enzyme secretion and activation (2) by proprotein convertases (PC) such as furin determine activity levels. Furthermore, the inhibition (3) of aggrecanases by TIMP3 and the LRP1 mediated internalization (4) of ADAMTS are crucial to consider for aggrecanase activity.

6.8.3 Differential aggrecan turnover in DES and BMS

Stenting and vascular mechanical stretch induce a vascular remodelling with increased large aggregating proteoglycans in BMS as well as DES stented arteries. However, in DES stented arteries aggrecan and versican accumulation was more pronounced than in BMS. This could, at least in part, be explained by the loss of aggrecanases in DES. Loss of aggrecanase activity is associated with the impaired and delayed re-endothelialisation with incompetent EC function as well as a direct drug effect on SMCs (*Summary figure 33*). The increased aggrecan and versican neoepitopes in DES compared to BMS at day 28 are consistent with the build-up of the substrate and not necessarily indicative of higher enzymatic activity. Even at lower enzymatic activity, more substrate may result in more neoepitope staining. This would be supported by our finding that the aggrecanase shift seen for ADAMTS-4 in BMS did not result in more detectable neoepitopes in BMS. In addition, as explained above in detail the aggrecanase activity is regulated at multiple levels, which we have not taken into account at the current state of the study. Thus, it is not unlikely that drug induced expression differences in proprotein convertases or TIMP-3 activity levels, might contribute to different enzyme activity in BMS and DES - similar to what we have observed for LRP1 abundance in BMS and DES neointima. Moreover, it is possible that there is increased internalization of the fragments by vascular cells in BMS stented arteries. Even though we were not able to show aggrecan fragments in the SDS extracts, the intracellular fraction, presumably due to its low concentrations, versican fragments were detected in all three fractions. The two extracellular fractions (NaCl and GuHCl) showed an increase for the fragments in DES compared to BMS, while no difference was detected intracellularly. This might be a result of differential extracellular degradation, by equal intracellular synthesis. However, it is also possible that the intracellular difference was compensated due to increased internalization of the fragments in BMS stented arteries. There is further support for this theory in the literature. It has been shown, that aggrecan NITEGE fragments as well as the link protein bound to hyaluronan are internalized by cells via a mechanism that requires CD44.[348] In fact, this study showed that CD44 mediated endocytosis represents a major mechanism for the clearance of G1 domains after aggrecanolysis. Moreover, a further study demonstrated that aggrecan degradation was required to allow for hyaluronan internalization via CD44.[301] This implicates that hyaluronan endocytosis is regulated mainly by extracellular processing of hyaluronan-bound proteoglycans. The processing requirement for internalization would explain, why less fragments are found in BMS, despite higher aggrecanases and consequent fragmentation. Finally, a further mechanism might be involved: HPLN1 is critical for locking aggrecan (and versican) onto hyaluronic acid. Aggrecan diffuses from the cartilage in mice that lack HPLN1.[349] Thus, the relative

reduction of HPLN1 in DES as observed in the proteomics analysis might release the NITEGE fragment from hyaluronan and contribute to its increased detection and at the same time prevent its internalization with hyaluronan. However, the reason for HPLN1 decrease in DES at day 28 is currently unclear.

Taken together, the detectability of neoepitopes is influenced by enzymatic activity, substrate availability and the intracellular uptake of the proteolytic fragments, i.e. via CD44. Whether the increased accumulation of aggrecan in DES can explain the clinically observed increased neoatherosclerosis findings in DES[56] due to increased lipoprotein binding remains to be elucidated in further research.

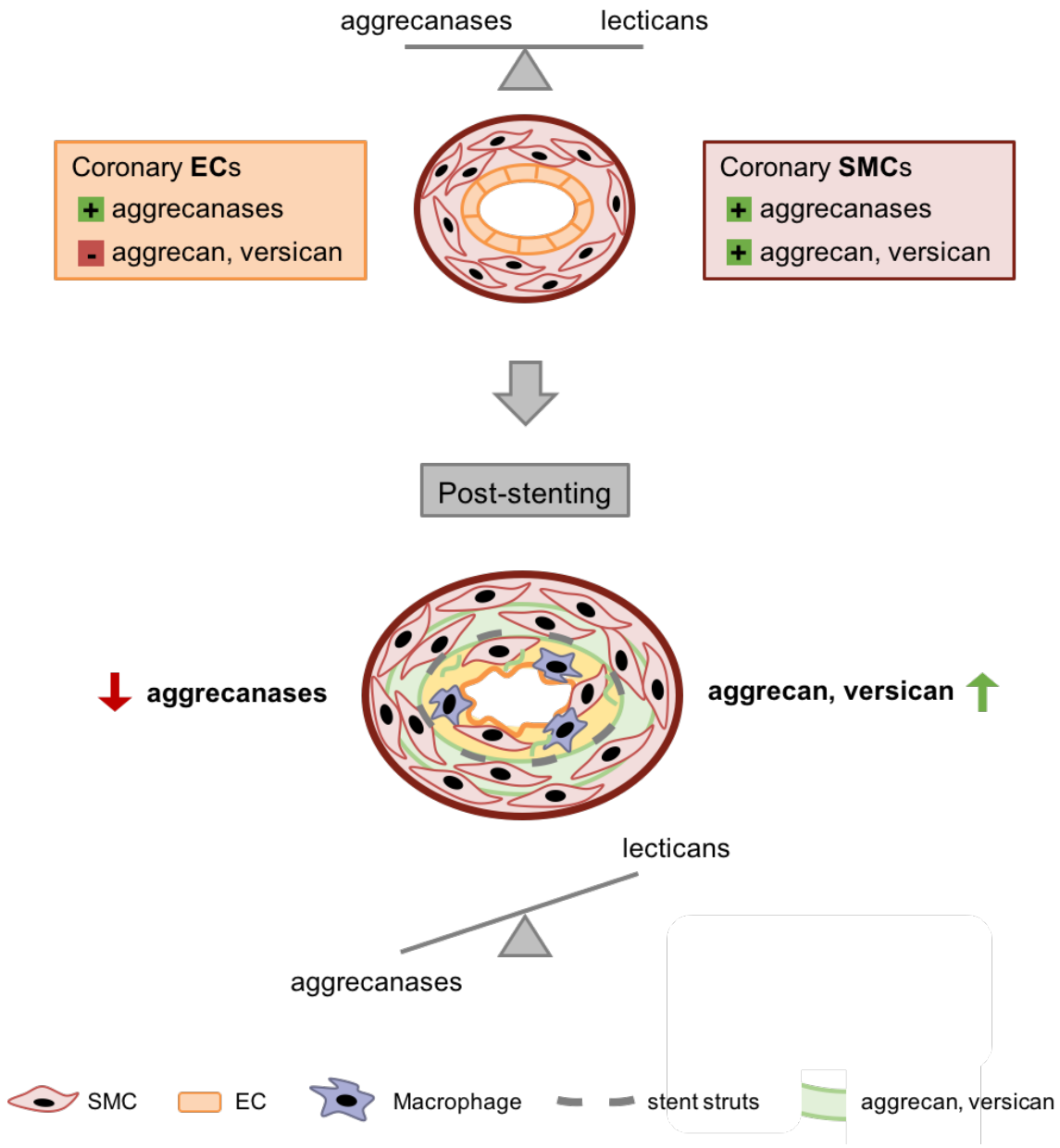

Figure 33. Induction of large aggregating proteoglycans upon stenting. Our results showed a loss of ADAMTS expression upon stenting and a corresponding increase of the large aggregating proteoglycans both in BMS and DES stented arteries. However, in DES stented arteries aggrecan and versican accumulation was more pronounced than in BMS. The latter showed an increase of ADAMTS-4, which was absent in DES. In cultured HCASMCs, everolimus inhibited expression of ADAMTS-4. Moreover, impaired re-endothelialization in DES likely contributes to loss of aggrecanases. Thus, reduced aggrecanase activity, could contribute to the build-up of aggrecan and versican in DES.

6.9 Strengths and limitations

A particular strength of our study is the combination of proteomics with a clinically relevant large animal model of human disease. The majority of studies in cardiovascular research are conducted in mice despite the notorious limitations regarding their translational potential of models in rodents.[350] Due to higher similarity to human, pigs are better suited to explore basic pathophysiological mechanisms granting a higher translational potential. However, unlike in human, our pigs were young and free of atherosclerosis. Another main limitation of using pigs is that they are expensive, hence the relatively smaller sample size. Despite the smaller sample size, significant differences were observed for proteoglycans and basement membrane proteins in stented arteries. Moreover, the study was not limited to a single time point, but samples were collected at multiple time points to obtain an accurate description of ECM remodelling over time. A caveat of working with porcine tissue is the limited availability of antibodies, limiting the possibilities for validation studies. Thus, proteomics was key for a comprehensive protein analysis without constraints imposed by antibodies.

7 FUTURE WORK

One objective of our future research is to delineate the mechanisms responsible for the observed ECM protein changes, i.e. the regulation of aggrecan, aggrecanases and HAPLN1 during vascular remodelling. Especially the significance of the cartilage protein aggrecan in arteries is of interest; its presence in arteries is a relatively new discovery. It remains to be elucidated, whether aggrecan exerts a protective and beneficial role in the vasculature or contributes to the pathogenesis of atherosclerosis. However, it is more likely to be involved in both as these are not mutually exclusive. Notably, prominent staining of aggrecan is observed in the media of the human aorta. Aggrecan is barely detectable in the normal coronary artery, but clearly visible in atherosclerosis and upon stenting. We will evaluate aggrecan levels in other vascular territories and relate its expression to haemodynamic stress. Another objective will be to elucidate the changes seen in calcification regulatory proteins and whether these findings might provide a mechanistic link to the increased incidence or accelerated course of neoatherosclerosis in DES-stented vessels.

Significance of aggrecan in the vasculature

Based on our findings of aggrecan changes in stented arteries and high-pressure exposed vein grafts we postulate that aggrecan absorbs increased mechanical forces in the vasculature due to its water-attracting properties. Thus, aggrecan expression could be important for arterial stiffness and we will pursue the validation of this hypothesis by measuring the levels of aggrecan and fragments in aortic tissue of patients with different degrees of arterial stiffness as assessed by pulse wave velocity (PWV). As PWV is a strong predictor of cardiovascular events and all-cause mortality[351], the latest European guidelines for managing arterial hypertension recommend arterial stiffness measurement for the evaluation of target organ damage.[352] PWV will be measured in consented patients prior to coronary artery bypass grafting (CABG) surgery. The small aortic tissue, which is routinely excised during the CABG procedure to establish the anastomosis between the aorta and the bypass vein will be used for targeted proteomics analysis. Similarly, serum samples will be collected from the patients to correlate the tissue proteomics changes with their concentrations in systemic circulation as potential biomarkers.

Role of aggrecan in stented arteries

Even though we have demonstrated that aggrecan is an essential component of arteries and provided evidence for its induction upon stenting, it remains unclear whether the

observed changes in aggrecan between BMS and DES could be linked to pathologies such as ISR and neoatherosclerosis. Therefore, it is of interest to investigate the biological function of aggrecan degradation in neointimal lesions of BMS and DES stented arteries in larger patient cohorts. Maybe akin to its prominent role in osteoarthritis, aggrecan degradation contributes to inflammation in arteries exposed to abnormal mechanical stress.

In order to investigate the intracellular effects in BMS and DES treated arteries the SDS extracts of the pig coronary arteries, the second step of our three-step protein extraction method, will be analysed. SDS induces decellularization releasing the intracellular proteins. A focus will be especially on LRP1, since this protein is involved in the endocytic clearance of ADAMTS-4 and -5.

In our neointima comparison of BMS vs. DES stented arteries at day 28, we have seen an upregulation of proteins involved in the regulation of calcification for DES. We want to investigate whether direct drug effects may interfere with calcification regulatory proteins as downstream targets. For this reason, we will perform calcification assays. Cresolphthalein assays will be performed in HCASMC treated with everolimus or DMSO as a control and calcification levels for both conditions will be compared. Moreover, we will look for effects of everolimus on apoptosis, since apoptosis is known to induce calcification.

Effects of miRNAs for differential expression of ECM proteins

Previous studies have shown that miRNAs are critically involved in neointimal hyperplasia in proliferative vascular diseases.[76, 77] Also in our study we saw pronounced changes for anti-fibrotic miRNAs between unstented controls and stented arteries. Thus, we aim to expand our miRNA studies to investigate miRNA regulation of target ECM proteins, similar to our previous publications.[353, 354] Different miRNA prediction algorithms will be employed to identify miRNA binding sites responsive to the ECM proteins of interest. Promising candidates will then be measured in our porcine samples. We will then go on to explore whether there is interdependency between the miRNAs that change and the ECM proteins that show differential expression. However, this will become a separate line of investigation that is beyond the scope of the present thesis.

8 CONCLUSION

We have provided the first proteomics characterization of ECM remodelling in response to vascular stenting in a large animal model. The remodelling response was different between BMS and DES as well as POBA. The most pronounced changes occurred in DES stented arteries. Our findings imply that the effects of DES go beyond inhibition of SMC proliferation, but have a wider impact on vascular remodelling by altering the composition of the ECM. The antiproliferative effect of DES was evident by a reduction in basement membrane proteins. Moreover, the decreased cellularity was accompanied by increased production of large proteoglycans like aggrecan and versican and attenuated aggrecanase expression. These *in vivo* observations were supported by our *in vitro* findings that HCAECs express high levels of ADAMTS-1 and that everolimus suppresses ADAMTS-4, but not ADAMTS-1 in HCASMCs.

The importance of aggrecan as an integral component of the arterial wall was demonstrated by its evidence in the arterial over the venous vessel as well as its induction upon grafting veins into a high-pressure environment. Our novel observation that aggrecan is induced and aggrecanases are altered during ECM remodelling after stent implantation may open novel therapeutic avenues to improve vascular healing and prevent ISR.

9 SUPPLEMENTAL TABLES

Supplemental table 1. Porcine ECM database entries

	Human		Porcine		
Protein name	**UniProt ID**	**Length**	**UniProt ID**	**Length**	**Genebank ID**
A disintegrin and metalloproteinase with thrombospondin motifs 1	ATS1_HUMAN	967	Q2N1I7_PIG	947	
A disintegrin and metalloproteinase with thrombospondin motifs 15	ATS15_HUMAN	950	F1S6D2_PIG	956	
A disintegrin and metalloproteinase with thrombospondin motifs 20	ATS20_HUMAN	1910	H9BR48_PIG	1915	
A disintegrin and metalloproteinase with thrombospondin motifs 3	ATS3_HUMAN	1205	F1RUN5_PIG	338	XM_003129104.4
A disintegrin and metalloproteinase with thrombospondin motifs 4	ATS4_HUMAN	837	F1S1A7_PIG	836	
A disintegrin and metalloproteinase with thrombospondin motifs 5	ATS5_HUMAN	930	F1SHP0_PIG	923	
A disintegrin and metalloproteinase with thrombospondin motifs 8	ATS8_HUMAN	889	F1S6D3_PIG	1020	
A disintegrin and metalloproteinase with thrombospondin motifs 8	ATS8_HUMAN	889	F1S6D3_PIG	1020	
A disintegrin and metalloproteinase with thrombospondin motifs 9	ATS9_HUMAN	1935	F1SFS3_PIG	1936	
Adipocyte enhancer-binding protein 1	AEBP1_HUMAN	1158	F1SSF7_PIG	1140	
Aggrecan	PGCA_HUMAN	2415	F1SKR0_PIG	2,284	
Agrin	AGRIN_HUMAN	2067	I3LGD9_PIG	2039	
Alpha-1-antitrypsin	A1AT_HUMAN	418	A1AT_PIG	421	
Alpha-2-HS-glycoprotein	FETUA_HUMAN	367	FETUA_PIG	362	
Ameloblastin	AMBN_HUMAN	447	AMBN_PIG	421	
Anionic trypsin-2	TRY2_HUMAN	247	C6L245_PIG	247	
Annexin A1	ANXA1_HUMAN	346	ANXA1_PIG	346	
Annexin A2	ANXA2_HUMAN	339	ANXA2_PIG	339	
Antileukoproteinase	SLPI_HUMAN	132	SLPI_PIG	129	
Antithrombin-III	ANT3_HUMAN	464	Q7M364_PIG	431	
Apolipoprotein A-I	APOA1_HUMAN	267	APOA1_PIG	265	
Apolipoprotein A-I–binding protein	AIBP_PIG	288	NNRE_PIG	288	

Apolipoprotein A-IV	APOA4_HUMAN	396	APOA4_PIG	382
Apolipoprotein B-100	APOB_HUMAN	4563	Q29021_PIG	2629
Apolipoprotein C-III	APOC3_HUMAN	99	APOC3_PIG	96
Apolipoprotein D	APOD_HUMAN	189	F1SQX9_PIG	190
Apolipoprotein E	APOE_HUMAN	317	APOE_PIG	317
Apolipoprotein H	APOH_HUMAN	345	I3LGN5_PIG	268
Apolipoprotein L4	APOL4_HUMAN	351	F1SPT9_PIG	336
Apolipoprotein M	APOM_HUMAN	188	APOM_PIG	188
Apolipoprotein O	APOO_HUMAN	198	K7GPW3_PIG	198
Apolipoprotein O-like	APOOL_HUMAN	268	K7GNC6_PIG	268
Apolipoprotein R	n/a	n/a	APOR_PIG	202
Asporin	ASPN_HUMAN	380	F1SUE4_PIG	370
Biglycan	PGS1_HUMAN	368	K7GP55_PIG	369
Bone morphogenetic protein 1	BMP1_HUMAN	986	F1RMB2_PIG	1009
Cadherin-13	CAD13_HUMAN	713	A8D737_PIG	713
Carboxypeptidase A1	CBPA1_HUMAN	419	CBPA1_PIG	419
Carboxypeptidase-like protein X2	CPXM2_HUMAN	756	F1SEC6_PIG	761
Cartilage intermediate layer protein 1	CILP1_HUMAN	1184	F1SJL4_PIG	1189
Cartilage intermediate layer protein 2	CILP2_HUMAN	1156	F1S6Q3_PIG	1157
Cartilage oligomeric matrix protein	COMP_HUMAN	757	F1S902_PIG	756
Cathepsin D	CATD_HUMAN	412	Q4U1U3_PIG	410
Cathepsin F	CATF_HUMAN	484	F1RU48_PIG	460
Cathepsin G	CATG_HUMAN	255	F1SGS1_PIG	255
Cathepsin Z	CATZ_HUMAN	303	A5GFX7_PIG	304
Chitinase-3-like protein 1	CH3L1_HUMAN	383	CH3L1_PIG	383
Chondroadherin-like protein	CHADL_HUMAN	762	F1SRC2_PIG	757
Chymase	CMA1_HUMAN	247	I3LDA9_PIG	255
Clusterin	CLUS_HUMAN	449	CLUS_PIG	446
Coagulation factor VIII	FA8_HUMAN	2,351	FA8_PIG	2133

Coatomer subunit alpha	COPA_HUMAN	1224	F1RJX8_PIG	1224	
Collagen alpha-1 (I)	CO1A1_HUMAN	1464	n/a	n/a	XM_005668928.1
Collagen alpha-1 (II)	CO2A1_HUMAN	1487	I3LSV6_PIG	1365	
Collagen alpha-1 (III)	CO3A1_HUMAN	1466	F1RYI8_PIG	1466	
Collagen alpha-1 (IV)	CO4A1_HUMAN	1669	M3V819_PIG	1669	
Collagen alpha-1 (V)	CO5A1_HUMAN	1838	F1S021_PIG	1826	
Collagen alpha-1 (VI)	CO6A1_HUMAN	1028	I3LS72_PIG	435	XM_005659047.1
Collagen alpha-1 (VII)	CO7A1_HUMAN	2944	F1SKM1_PIG	2939	
Collagen alpha-1 (VIII)	CO8A1_HUMAN	744	F1SKX7_PIG	745	
Collagen alpha-1 (XI)	COBA1_HUMAN	1806	F1S571_PIG	1607	
Collagen alpha-1 (XII)	COCA1_HUMAN	3063	F1RQI0_PIG	960	XM_005659436.1
Collagen alpha-1 (XIII)	CODA1_HUMAN	717	F1SUE9_PIG	635	
Collagen alpha-1 (XIV)	COEA1_HUMAN	1796	F1S285_PIG	1790	
Collagen alpha-1 (XIX)	COJA1_HUMAN	1142	F1RTT4_PIG	1142	
Collagen alpha-1 (XV)	COFA1_HUMAN	1388	F1SSE7_PIG	192	XM_005660284.1
Collagen alpha-1 (XVI)	COGA1_HUMAN	1604	F1SV99_PIG	1594	
Collagen alpha-1 (XVII)	COHA1_HUMAN	1497	F1S5P1_PIG	1081	
Collagen alpha-1 (XVIII)	COIA1_HUMAN	1754	n/a	n/a	XR_299377.1
Collagen alpha-1 (XX)	COKA1_HUMAN	1284	F1S285_PIG	1790	XM_005662881.1
Collagen alpha-1 (XXII)	COMA1_HUMAN	1626	n/a	n/a	XM_005674527.1
Collagen alpha-1 (XXVII)	CO27A1_HUMAN	1714	n/a	n/a	XM_005660374.1
Collagen alpha-1 (XXVIII)	COSA1_HUMAN	1125	F1SF83_PIG	1034	
Collagen alpha-2 (I)	CO1A2_HUMAN	1366	F1SFA7_PIG	1366	
Collagen alpha-2 (IV)	CO4A2_HUMAN	1712	F1RLL9_PIG	1654	
Collagen alpha-2 (IX)	CO9A2_HUMAN	689	I3L8B2_PIG	688	
Collagen alpha-2 (V)	CO5A2_HUMAN	1499	Q59IP2_PIG	1499	
Collagen alpha-2 (VI)	CO6A2_HUMAN	1019	I3LQ84_PIG	989	
Collagen alpha-2 (VIII)	CO8A2_HUMAN	703	F1SV48_PIG	705	
Collagen alpha-2 (XI)	COBA2_HUMAN	1736	A5D9K7_PIG	1651	

Collagen alpha-3 (IV)	CO4A3_HUMAN	1670	F1SNP0_PIG	807	XM_005658969.1
Collagen alpha-3 (V)	CO5A3_HUMAN	1745	Q59IP1_PIG	1748	
Collagen alpha-3 (VI)	CO6A3_HUMAN	3177	I3LUR7_PIG	3170	
Collagen alpha-4 (IV)	CO4A4_HUMAN	1690	F1SNP1_PIG	1711	
Collagen alpha-4 (VI)	n/a	n/a	n/a	n/a	XM_005669267.1
Collagen alpha-5 (VI)	CO6A5_HUMAN	2615	F1RS99_PIG	2599	
Collagen alpha-6 (VI)	CO6A6_HUMAN	2263	F1RS99_PIG	2599	XM_005669265.1
Complement C1q tumor necrosis factor-related protein 9	C1QT9_HUMAN	333	F1RTM0_PIG	333	
Complement C3	CO3_HUMAN	1663	CO3_PIG	1661	
Complement component C8 beta chain	CO8B_HUMAN	591	A0SEH2_PIG	611	
Complement component C9	CO9_HUMAN	559	A0SEG9_PIG	543	
Connective tissue growth factor	CTGF_PIG	349	CTGF_PIG	349	
Cysteine-rich protein 2	CRIP2_HUMAN	208	K7ZMG1_PIG	198	
Decorin	PGS2_HUMAN	359	PGS2_PIG	360	
Dehydrogenase/reductase SDR family member 7C	DRS7C_HUMAN	312	F1SS86_PIG	311	
Dermatopontin	DERM_HUMAN	201	DERM_PIG	183	
Disintegrin and metalloproteinase domain-containing protein 11	ADA11_HUMAN	769	F1RQZ7_PIG	770	
Disintegrin and metalloproteinase domain-containing protein 28	ADA28_HUMAN	775	F1RM87_PIG	777	
Dystroglycan	DAG1_HUMAN	895	I3LD20_PIG	877	
EMILIN-1	EMIL1_HUMAN	1016	F1SDQ5_PIG	1018	
EMILIN-2	EMIL2_HUMAN	1053	F1SBC8_PIG	967	
EMILIN-3	EMIL3_HUMAN	766	F1SDV5_PIG	765	
Endonuclease domain-containing 1 protein	ENDD1_HUMAN	500	F1STI9_PIG	500	
Endoplasmic reticulum aminopeptidase 1	ERAP1_HUMAN	941	K9J6I5_PIG	942	
Estradiol 17-beta-dehydrogenase 11	DHB11_HUMAN	300	F1S3H8_PIG	312	
Extracellular matrix protein FRAS1	FRAS1_HUMAN	4008	F1RYS0_PIG	3985	
Extracellular superoxide dismutase	SODE_HUMAN	240	Q007T6_PIG	244	
Fibrillin-1	FBN1_HUMAN	2871	FBN1_PIG	2871	
Fibrillin-2	FBN2_HUMAN	2912	F1RKK1_PIG	2432	

Fibrinogen beta chain	FIBB_HUMAN	491	F1RX37_PIG	495	
Fibrinogen gamma chain	FIBG_HUMAN	453	F1RX35_PIG	438	
Fibroblast growth factor 1	FGF1_HUMAN	155	FGF1_PIG	152	
Fibroblast growth factor 11	FGF11_HUMAN	225	I3L7I1_PIG	225	
Fibroblast growth factor 23	FGF23_HUMAN	251	F1SKZ1_PIG	244	
Fibromodulin	FMOD_HUMAN	376	F1S6B5_PIG	379	
Fibronectin	FINC_HUMAN	2386	F1SS24_PIG	2478	
Fibronectin type III domain-containing protein 1	FNDC1_HUMAN	1894	F1SB59_PIG	1885	
Fibulin-1	FBLN1_HUMAN	703	F1SM61_PIG	709	
Fibulin-2	FBLN2_HUMAN	1184	n/a	n/a	AK346749.1
Fibulin-3	FBLN3_HUMAN	493	F8SIP2_PIG	490	
Fibulin-4	FBLN4_HUMAN	443	F1RU22_PIG	443	
Fibulin-5	FBLN5_HUMAN	448	F1SD87_PIG	448	
Filamin-A	FLNA_HUMAN	2647	Q2YHQ3_PIG	167	XM_003134702.2
FRAS1-related extracellular matrix protein 2	FREM2_HUMAN	3169	F1RS31_PIG	3167	
FRAS1-related extracellular matrix protein 3	FREM3_HUMAN	2139	n/a	n/a	XM_005656529.1
Galectin-1	LEG1_HUMAN	135	LEG1_PIG	135	
Galectin-3	LEG3_HUMAN	250	A3EX84_PIG	260	
Galectin-3-bining protein	LG3BP_HUMAN	585	M3V7X9_PIG	552	
Galectin-8	LEG8_HUMAN	317	F1RGZ0_PIG	317	
Galectin-9	LEG9_HUMAN	355	F1RJ33_PIG	355	
Gelsolin	GELS_HUMAN	782	GELS_PIG	772	
Glypican-1	GPC1_HUMAN	558	F1SIQ5_PIG	552	
Glypican-2	GPC2_HUMAN	579	F1RNM8_PIG	578	
Glypican-3	GPC3_HUMAN	580	F1RTE0_PIG	501	
Glypican-4	GPC4_HUMAN	556	F1RTE1_PIG	503	
Glypican-6	GPC6_HUMAN	555	A3KDL8_PIG	171	XM_001925471.5
Granzyme A	GRAA_HUMAN	262	E3VSK1_PIG	259	
Group 10 secretory phospholipase A2	PA2GX_HUMAN	165	F1SUN7_PIG	157	

Growth/differentiation factor 7	GDF7_HUMAN	450	I3LB35_PIG	449	
Hemicentin-1	HMCN1_HUMAN	5635	n/a	n/a	XM_005653746.1
Hemicentin-2	HMCN2_HUMAN	5059	F1S0Y1_PIG	4061	
Hyaluronan and proteoglycan link protein 1	HPLN1_HUMAN	354	HPLN1_PIG	354	
Insulin-degrading enzyme	IDE_HUMAN	1019	F1SC98_PIG	990	
Insulin-like growth factor 1 receptor	IGF1R_HUMAN	1367	IGF1R_PIG	304	
Insulin-like growth factor I	IGF1_HUMAN	195	IGF1_PIG	153	
Insulin-like growth factor-binding protein 7	IBP7_HUMAN	282	C7EDN1_PIG	282	
Inter-alpha-trypsin inhibitor heavy chain H1	ITIH1_HUMAN	911	ITIH1_PIG	902	
Inter-alpha-trypsin inhibitor heavy chain H2	ITIH2_HUMAN	946	ITIH2_PIG	935	
Intercellular adhesion molecule 1	ICAM1_HUMAN	532	F1S3J9_PIG	537	
Kallistatin	KAIN_HUMAN	427	n/a	n/a	XM_003356792.2
Kininogen-1	KNG1_HUMAN	644	F1SFI4_PIG	385	AK233327.1
Lactadherin	MFGM_HUMAN	387	MFGM_PIG	409	
Laminin subunit alpha-1	LAMA1_HUMAN	3075	I3LCP3_PIG	517	XM_005658563.1
Laminin subunit alpha-2	LAMA2_HUMAN	3122	F1S2Z4_PIG	925	XM_005659200.1
Laminin subunit alpha-3	LAMA3_HUMAN	3333	F1SBB3_PIG	1724	XM_003482045.2
Laminin subunit alpha-4	LAMA4_HUMAN	1823	F1RZM4_PIG	1471	
Laminin subunit beta-1	LAMB1_HUMAN	1786	F1SAE9_PIG	1799	
Laminin subunit beta-2	LAMB2_HUMAN	1798	F1SPT5_PIG	1642	
Laminin subunit beta-3	LAMB3_HUMAN	1172	I3LI99_PIG	959	
Laminin subunit gamma-1	LAMC1_HUMAN	1609	F1S663_PIG	1606	
Laminin subunit gamma-3	LAMC3_HUMAN	1575	F1S0X0_PIG	1583	
Latent-TGFβ-binding protein 1	LTBP1_HUMAN	1721	F1S405_PIG	1343	
Latent-TGFβ-binding protein 2	LTBP2_HUMAN	1821	F1S2T5_PIG	1821	
Latent-TGFβ-binding protein 3	LTBP3_HUMAN	1303	F1RRJ9_PIG	1244	
Latent-TGFβ-binding protein 4	LTBP4_HUMAN	1624	n/a	n/a	XM_005674643.1
Leukocyte elastase inhibitor	ILEU_HUMAN	379	ILEU_PIG	378	
Lipoprotein lipase	LIPL_HUMAN	475	LIPL_PIG	478	

Low-density lipoprotein receptor-related protein 2	LRP2_HUMAN	4655	K9IVL7_PIG	4544	
Low-density lipoprotein receptor-related protein 6	LRP6_HUMAN	1613	F1SQ65_PIG	1470	
Lumican	LUM_HUMAN	338	F1SQ09_PIG	341	
Lysyl oxidase homolog 1	LOXL1_HUMAN	574	F1SIC9_PIG	591	
Macrophage-capping protein	CAPG_HUMAN	348	F1SVB0_PIG	349	
Mast/stem cell growth factor receptor	KIT_HUMAN	976	KIT_PIG	972	
Matrilin-2	MATN2_HUMAN	956	F1S0M0_PIG	303	AK234298.1
Matrilin-4	MATN4_HUMAN	622	F1SDQ7_PIG	627	
Matrix Gla protein	MGP_HUMAN	103	MGP_PIG	103	
Matrix metalloproteinase-2	MMP2_HUMAN	660	Q95JA4_PIG	661	
Matrix remodeling-associated protein 5	MXRA5_HUMAN	2828	F1RZ07_PIG	2830	
Melanotransferrin	TRFM_HUMAN	738	F1SQX4_PIG	736	
Metalloproteinase inhibitor 1	TIMP1_HUMAN	207	TIMP1_PIG	207	
Metalloproteinase inhibitor 3	TIMP3_HUMAN	211	F1SPS4_PIG	172	
Microfibril-associated glycoprotein 4	MFAP4_HUMAN	255	F1S0X3_PIG	461	
Microfibrillar-associated protein 1	MFAP1_HUMAN	439	n/a	n/a	AK397307.1
Mimecan	MIME_HUMAN	298	I3L9T6_PIG	216	
Myeloperoxidase	PERM_HUMAN	745	K7GRV6_PIG	743	
Neural cell adhesion molecule 1	NCAM1_HUMAN	858	K7GMV4_PIG	839	
Neural cell adhesion molecule L1-like protein	CHL1_HUMAN	1208	F1SFM3_PIG	1210	
Nidogen-1	NID1_HUMAN	1247	I3LJT1_PIG	381	XM_005658402.1
Nidogen-2	NID2_HUMAN	1375	F1SFF3_PIG	1385	
Osteoclast-stimulating factor 1	OSTF1_HUMAN	214	OSTF1_PIG	214	
Osteopontin	OSTP_PIG	314	OSTP_PIG	303	
Papilin	PPN_HUMAN	1278	F1S3J7_PIG	1301	
Pentraxin-related protein PTX3	PTX3_HUMAN	381	F1SJM0_PIG	382	
Peptidyl-prolyl cis-trans isomerase A	PPIA_HUMAN	165	PPIA_PIG	164	
Periostin	POSTN_HUMAN	836	F1RS37_PIG	836	
Perlecan	PGBM_HUMAN	4391	F1SU03_PIG	1848	XM_005656042.1

Peroxidasin homolog	PXDN_HUMAN	1479	I3LDA4_PIG	1479	
Pigment epithelium-derived factor	PEDF_HUMAN	418	Q0PM28_PIG	413	
Pikachurin	EGFLA_HUMAN	1,017	I3LEG7_PIG	1020	
Plasma glutamate carboxypeptidase	PGCP_HUMAN	472	F1S0L6_PIG	283	AK392015.1
Plasminogen	PLMN_HUMAN	810	PLMN_PIG	809	
Podocan	PODN_HUMAN	613	I3LEB7_PIG	642	
Proactivator polypeptide	SAP_HUMAN	524	F1SU97_PIG	524	
Procollagen C-endopeptidase enhancer 1	PCOC1_HUMAN	449	I3LEE6_PIG	470	
Prolargin	PRELP_HUMAN	382	F1S6B4_PIG	375	
Properdin	PROP_HUMAN	469	K7GQR1_PIG	463	
Prophenin and tritrpticin	n/a	n/a	PF11_PIG	212	
Protein ELFN1	ELFN1_HUMAN	828	I3LFQ3_PIG	806	
Proteoglycan 4	PRG4_HUMAN	1404	I3L5Z3_PIG	1383	
Reticulon-3	RTN3_HUMAN	1032	F1RPY3_PIG	236	XM_005660769.1
Retinol-binding protein 3	RET3_HUMAN	1247	F1SEL7_PIG	1282	
RPE-spondin	RPESP_HUMAN	264	F1RWI4_PIG	193	XM_003125598.4
Sclerostin	SOST_HUMAN	213	F1S1H5_PIG	212	
SCO-spondin	SSPO_HUMAN	5147	n/a	n/a	XM_005658106.1
Secreted frizzled-related protein 1	SFRP1_HUMAN	314	I3LB66_PIG	315	
Secreted frizzled-related protein 3	SFRP3_HUMAN	325	F1RYL4_PIG	325	
Secreted phosphoprotein 24	SPP24_HUMAN	211	SPP24_PIG	204	
Serine protease HTRA1	HTRA1_HUMAN	480	F1SEH4_PIG	524	
Serotransferrin	TRFE_HUMAN	698	TRFE_PIG	696	
Serum amyloid P-component	SAMP_HUMAN	223	SAMP_PIG	224	
SPARC	SPRC_HUMAN	303	SPRC_PIG	300	
Spondin-1	SPON1_HUMAN	807	F1S981_PIG	281	XM_003122966.4
Target of Nesh-SH3	TARSH_HUMAN	1075	F1SL03_PIG	952	
Tenascin	TENA_HUMAN	2201	TENA_PIG	1746	
Tenascin-X	TENX_HUMAN	4289	A5A8W4_PIG	4317	

Tetranectin	TETN_HUMAN	202	F1SRC8_PIG	202	
TGFβ receptor type 1	TGFR1_HUMAN	503	Q19ML9_PIG	503	
TGFβ receptor type 3	TGBR3_HUMAN	851	TGBR3_PIG	848	
TGFβ-1	TGFB1_HUMAN	390	TGFB1_PIG	390	
TGFβ-2	TGFB2_HUMAN	414	F1S9L0_PIG	436	
TGFβ-3	TGFB3_HUMAN	412	K7GSJ9_PIG	456	
TGFβ-induced protein ig-h3	BGH3_HUMAN	683	BGH3_PIG	683	
Thrombospondin type-1 domain-containing protein 7A	THS7A_HUMAN	1657	I3L9B1_PIG	1593	
Thrombospondin-1	TSP1_HUMAN	1170	K7GPJ3_PIG	1085	
Thrombospondin-4	TSP4_HUMAN	961	F1RF28_PIG	944	
Transferrin receptor protein 1	TFR1_HUMAN	760	TFR1_PIG	768	
Tryptase-1	TRYB1_HUMAN	275	TRYT_PIG	275	
Tubulointerstitial nephritis antigen-like	TINAL_HUMAN	467	F1SVA2_PIG	467	
Uncharacterized aarF domain-containing protein kinase 1	ADCK1_HUMAN	530	K9J4Q5_PIG	523	
Usherin	USH2A_HUMAN	5202	n/a	n/a	XM_003130490.4
Versican	CSPG2_HUMAN	3396	F1REZ2_PIG	3382	
Vitamin D-binding protein	VTDB_HUMAN	474	I3LN42_PIG	476	
Vitronectin	VTNC_HUMAN	478	VTNC_PIG	459	
von Willebrand factor A domain-containing protein 1	VWA1_HUMAN	445	F1RJE3_PIG	413	
von Willebrand factor A domain-containing protein 8	VWA8_HUMAN	1905	I3LI96_PIG	419	XM_005668452.1
WD repeat-containing protein 1	WDR1_HUMAN	606	K9IVR7_PIG	606	

Extracellular proteins for which the porcine sequences were included in the protein database for proteomics search. The UniProt IDs for the human and their porcine counterparts are shown. For protein sequences, which were deduced from public nucleotide databases the used Genebank ID is given. The length indicates the number of amino acids for each entry in UniProt. n/a denotes not applicable. The porcine ECM database with the amino acid sequences of the porcine proteins are attached to the thesis in an electronic form.

Supplemental table 2. Extracellular proteins identified by proteomics analysis in the neointima of stented porcine coronary arteries.

Identified Proteins	UniProt ID	MW (kDa)	BMS	DES	*P*	FC DES/BMS
			Total ion current x 10^6 Av±SD			
Adipocyte enhancer-binding protein 1	F1SSF7_PIG	128	165.6±93.4	142.4±32.5	0.554	0.9
Aggrecan	F1SKR0_PIG	238	41.2±69.5	70.8±34.1	0.338	1.7
Agrin	I3LGD9_PIG	216	116.6±65.1	128.5±40.2	0.688	1.1
Alpha-1-antitrypsin*	A1AT_PIG	47	33.6±30.2	11.8±8.0	0.109	0.4
Alpha-2-HS-glycoprotein	FETUA_PIG	38	472.0±223.6	263.1±75.3	**0.050**	0.6
Annexin A1	ANXA1_PIG	39	231.1±142.4	129.4±45.3	0.113	0.6
Annexin A2	ANXA2_PIG	39	571.0±247.8	430.9±65.4	0.192	0.8
Antithrombin-III	Q7M364_PIG	49	92.2±38.7	71.2±18.1	0.228	0.8
Apolipoprotein A-I	APOA1_PIG	30	619.6±234.8	549.4±270.4	0.614	0.9
Apolipoprotein A-IV	APOA4_PIG	43	7.6±4.0	10.9±8.3	0.362	1.4
Apolipoprotein B*	Q29021_PIG	300	27.7±33.0	11.8±15.5	0.278	0.4
Apolipoprotein C-III	APOC3_PIG	11	16.2±9.2	18.8±11.9	0.658	1.2
Apolipoprotein E	APOE_PIG	37	76.6±73.2	63.8±70.2	0.745	0.8
Apolipoprotein H	I3LGN5_PIG	29	141.2±84.9	128.0±131.6	0.827	0.9
Apolipoprotein R	APOR_PIG	23	27.0±17.6	40.8±22.6	0.228	1.5
Asporin	F1SUE4_PIG	42	137.6±70.1	80.2±33.0	0.083	0.6
Biglycan	K7GP55_PIG	41	1767.1±214.9	1130.6±169.0	**0.000**	0.6
Bone morphogenic protein 1*	F1RMB2_PIG	114	0.0±0.0	4.9±5.6	n/a	n/a
Carboxypeptidase-like protein X2	F1SEC6_PIG	86	24.9±26.1	15.8±5.3	0.397	0.6
Cathepsin D	Q4U1U3_PIG	44	79.6±46.1	34.5±24.3	**0.047**	0.4
Cathepsin G	F1SGS1_PIG	29	0.4±1.0	0.0±0.0	n/a	0.0
Cathepsin Z*	A5GFX7_PIG	34	2.9±5.6	0.0±0.0	n/a	0.0
Chitinase-3-like protein 1	CH3L1_PIG	43	31.8±39.8	2.6±4.6	n/a	0.1
Chondroadherin*	CHAD_HUMAN	40	0.8±1.3	35.6±25.3	n/a	46.5
Clusterin	CLUS_PIG	52	149.6±28.5	301.7±99.0	**0.006**	2.0
Coatomer subunit alpha*	F1RJX8_PIG	138	16.3±14.7	14.6±7.2	0.796	0.9
Collagen alpha-1 (I)	CO1A1_PIG	100	2798.6±873.9	1842.9±504.6	**0.032**	0.7
Collagen alpha-1 (III)	F1RYI8_PIG	139	698.6±329.3	224.0±93.9	**0.008**	0.3
Collagen alpha-1 (IV)	M3V819_PIG	160	49.1±20.8	47.8±10.7	0.887	1.0
Collagen alpha-1 (V)	F1S021_PIG	182	205.5±64.2	137.6±35.9	**0.036**	0.7
Collagen alpha-1 (VI)	CO6A1_PIG	43	36.4±27.4	19.2±7.1	0.155	0.5
Collagen alpha-1 (VIII)	F1SKX7_PIG	73	14.1±5.2	19.8±5.7	0.075	1.4
Collagen alpha-1 (XI)	F1S571_PIG	159	19.4±20.4	10.9±12.2	0.369	0.6
Collagen alpha-1 (XII)	COCA1_PIG	229	484.1±151.0	218.6±50.9	**0.003**	0.5
Collagen alpha-1 (XV)	COFA1_PIG	27	68.8±36.2	137.6±20.6	**0.002**	2.0
Collagen alpha-1 (XVIII)	COIA1_PIG	62	216.1±61.8	248.4±36.7	0.263	1.1
Collagen alpha-1 (XX)	COKA1_PIG	192	1190.7±613.9	440.1±145.6	**0.017**	0.4
Collagen alpha-2 (I)	F1SFA7_PIG	129	1305.6±466.3	845.6±261.8	**0.048**	0.6
Collagen alpha-2 (IV)	F1RLL9_PIG	161	89.9±26.6	82.8±13.2	0.542	0.9
Collagen alpha-2 (V)	Q59IP2_PIG	145	134.8±55.5	66.7±26.4	**0.018**	0.5
Collagen alpha-2 (VI)	I3LQ84_PIG	106	124.7±110.6	57.2±29.7	0.163	0.5
Collagen alpha-3 (V)	Q59IP1_PIG	172	2.1±5.5	0.0±0.0	n/a	0.0
Collagen alpha-3 (VI)	I3LUR7_PIG	342	371.3±357.3	92.9±63.2	0.086	0.3
Collagen alpha-6 (VI)	CO6A6_PIG	250	8.1±12.9	0.0±0.0	n/a	0.0
Complement C3	CO3_PIG	187	805.6±730.5	687.7±404.2	0.717	0.9
Complement component C8B*	A0SEH2_PIG	69	23.1±18.9	27.3±18.4	0.682	1.2
Complement component C9	A0SEG9_PIG	62	2.4±1.5	6.9±6.4	0.115	2.9
Connective tissue growth factor	CTGF_PIG	38	1.2±3.1	6.3±7.4	n/a	5.4
Decorin	PGS2_PIG	40	185.4±59.1	104.5±81.3	0.057	0.6
Dermatopontin	DERM_PIG	22	55.8±23.6	38.1±14.2	0.121	0.7
Dystroglycan	I3LD20_PIG	95	3.3±4.4	1.7±2.5	n/a	0.5
EMILIN-1	F1SDQ5_PIG	107	64.1±34.1	62.4±12.4	0.905	1.0
EMILIN-2*	F1SBC8_PIG	106	0.5±1.2	0.0±0.0	n/a	0.0
Fibrillin-1	FBN1_PIG	313	23.8±28.1	10.4±10.8	0.274	0.4

Fibrinogen beta chain	F1RX37_PIG	56	5135.7±4558.0	4487.1±2656.8	0.752	0.9
Fibrinogen gamma chain	F1RX35_PIG	50	4287.0±3582.2	3875.7±2485.5	0.808	0.9
Fibromodulin	F1S6B5_PIG	44	549.7±94.2	350.4±115.8	**0.004**	0.6
Fibronectin	F1SS24_PIG	272	10317.1±3240.8	11617.1±2173.3	0.398	1.1
Fibronectin type III domain-containing protein 1	F1SB59_PIG	204	26.8±41.2	11.7±9.9	n/a	0.4
Fibulin-1	F1SM61_PIG	78	120.4±47.0	149.3±43.4	0.255	1.2
Fibulin-2	FBLN2_PIG	54	20.9±22.8	16.5±14.2	0.670	0.8
Fibulin-3	F8SIP2_PIG	54	190.2±94.1	155.0±53.8	0.412	0.8
Fibulin-4*	F1RU22_PIG	49	36.2±11.8	38.3±7.7	0.694	1.1
Fibulin-5	F1SD87_PIG	50	300.0±137.6	351.1±84.6	0.422	1.2
Filamin-C*	F1SMN5_PIG	290	310.9±151.2	387.0±102.9	0.295	1.2
Galectin-1	LEG1_PIG	15	353.4±61.5	265.0±52.4	**0.014**	0.7
Galectin-3	A3EX84_PIG	27	87.2±91.7	29.8±14.2	0.151	0.3
Galectin-3-binding protein	M3V7X9_PIG	61	14.3±11.8	52.4±42.3	0.056	3.7
Galectin-9*	F1RJ33_PIG	40	1.3±1.7	0.3±0.6	n/a	0.3
Gelatinase A*	Q95JA4_PIG	74	6.6±8.5	0.5±0.9	n/a	0.1
Gelsolin	GELS_PIG	85	1242.1±295.1	1123.4±194.5	0.394	0.9
Hemicentin-1*	HMCN1_PIG	180	1.3±2.2	0.7±1.8	n/a	0.5
Hyaluronan and proteoglycan link protein 1	HPLN1_PIG	40	7.7±10.8	16.2±15.4	0.257	2.1
Insulin-like growth factor-binding protein 7	C7EDN1_PIG	29	395.2±201.4	468.1±122.0	0.432	1.2
Inter-alpha-trypsin inhibitor heavy chain H1*	ITIH1_PIG	100	145.1±77.4	143.1±46.0	0.955	1.0
Inter-alpha-trypsin inhibitor heavy chain H2	ITIH2_PIG	105	95.1±63.8	63.5±16.7	0.247	0.7
Intercellular adhesion molecule 1*	F1S3J9_PIG	58	0.8±2.2	0.0±0.0	n/a	0.0
Kininogen-1*	KNG1_PIG	48	20.6±15.8	14.8±11.8	0.450	0.7
Lactadherin	MFGM_PIG	46	253.9±104.7	407.3±57.5	**0.008**	1.6
Laminin subunit alpha-4	F1RZM4_PIG	164	75.8±28.8	74.4±31.8	0.933	1.0
Laminin subunit beta-1	F1SAE9_PIG	199	246.4±69.2	265.6±65.1	0.604	1.1
Laminin subunit beta-2	F1SPT5_PIG	179	39.4±46.5	39.7±31.1	0.987	1.0
Laminin subunit gamma-1	F1S663_PIG	177	406.9±140.2	440.3±100.8	0.619	1.1
Latent TGFβ-binding protein 1	F1S405_PIG	148	28.3±9.3	19.5±6.9	0.068	0.7
Latent TGFβ-binding protein 2	F1S2T5_PIG	196	174.6±79.5	198.0±58.4	0.544	1.1
Latent TGFβ-binding protein 4	LTBP4_PIG	112	38.5±26.7	35.6±14.9	0.811	0.9
Leukocyte elastase inhibitor	ILEU_PIG	43	27.5±31.0	7.0±5.3	0.134	0.3
Lumican	F1SQ09_PIG	39	490.7±128.7	145.1±44.0	**0.000**	0.3
Lysyl oxidase homolog 1	F1SIC9_PIG	65	68.5±29.0	63.0±19.0	0.687	0.9
Macrophage capping protein	F1SVB0_PIG	39	109.4±87.6	62.1±38.0	0.226	0.6
Matrilin-4*	F1SDQ7_PIG	69	0.5±1.2	0.7±1.9	n/a	1.5
Matrix Gla protein	MGP_PIG	12	27.1±5.8	61.9±31.1	**0.025**	2.3
Matrix-remodeling-associated protein 5	F1RZ07_PIG	308	47.9±48.7	13.7±8.9	0.114	0.3
Metalloproteinase inhibitor 1*	TIMP1_PIG	23	0.4±0.9	0.0±0.0	n/a	0.0
Mimecan	I3L9T6_PIG	25	108.2±29.8	96.8±26.8	0.467	0.9
Myeloperoxidase	K7GRV6_PIG	84	4.5±8.1	0.0±0.0	n/a	0.0
Nidogen-1	NID1_PIG	50	29.1±17.4	76.6±35.8	**0.012**	2.6
Nidogen-2	F1SFF3_PIG	152	948.4±283.4	713.1±127.3	0.079	0.8
Osteoclast-stimulating factor 1*	OSTF1_PIG	24	13.8±11.9	6.3±5.4	0.166	0.5
Papilin	F1S3J7_PIG	141	0.1±0.2	0.7±1.8	n/a	9.3
Peptidyl-prolyl cis-trans isomerase A	PPIA_PIG	18	732.6±221.5	646.6±224.5	0.484	0.9
Periostin	F1RS37_PIG	93	2380.0±652.6	1489.0±573.9	**0.019**	0.6
Perlecan	PGBM_PIG	365	3168.6±652.1	3467.1±535.4	0.368	1.1
Peroxidasin homolog	I3LDA4_PIG	164	13.3±8.3	31.7±10.6	**0.004**	2.4
Pigment epithelium-derived factor	Q0PM28_PIG	46	264.7±46.4	314.9±70.6	0.146	1.2
Plasma glutamate carboxypeptidase*	PGCP_PIG	52	2.3±3.2	1.3±1.7	n/a	0.6
Plasminogen	PLMN_PIG	91	272.3±106.8	514.1±199.6	**0.019**	1.9
Podocan	I3LEB7_PIG	72	60.1±38.7	23.4±10.0	**0.047**	0.4
Procollagen C-endopeptidase enhancer 1	I3LEE6_PIG	50	40.2±10.6	41.9±11.6	0.778	1.0

Prolargin	F1S6B4_PIG	43	451.1±102.9	351.1±138.2	0.153	0.8
Prolow-density lipoprotein receptor-related protein 1	K9IVL7_PIG	505	30.4±26.2	20.5±7.4	0.372	0.7
Properdin	K7GQR1_PIG	51	57.9±29.3	117.1±61.8	**0.049**	2.0
Prophenin and tritrpticin	PF11_PIG	24	230.0±297.6	7.5±8.9	0.095	0.0
Proteoglycan 4	I3L5Z3_PIG	149	0.9±1.5	0.0±0.0	n/a	0.0
Reticulon-3*	RTN3_PIG	105	0.0±0.0	0.6±1.5	n/a	n/a
RPE-spondin	RPESP_PIG	32	1.1±3.0	1.9±3.3	n/a	1.6
Secreted frizzled-related protein 1	I3LB66_PIG	35	12.1±6.0	9.2±6.4	0.400	0.8
Secreted frizzled-related protein 3*	F1RYL4_PIG	36	3.3±3.6	2.5±1.1	0.591	0.8
Secreted phosphoprotein 24*	SPP24_PIG	23	0.0±0.0	12.4±9.1	n/a	n/a
Serine protease HTRA1	F1SEH4_PIG	56	138.2±102.9	348.3±183.4	**0.026**	2.5
Serotransferrin	TRFE_PIG	77	3167.4±2227.2	1765.1±729.6	0.156	0.6
Serum amyloid P-component	SAMP_PIG	26	3.2±6.3	14.2±14.9	n/a	4.4
SPARC	SPRC_PIG	34	128.6±37.6	154.1±75.8	0.448	1.2
Spondin-1	SPON1_PIG	66	5.7±4.8	0.7±1.0	**0.033**	0.1
Sulfhydryl oxidase	F1S682_PIG	81	19.2±11.1	11.8±6.2	0.154	0.6
Superoxide dismutase [Cu-Zn]	Q007T6_PIG	26	236.2±133.9	155.7±49.9	0.176	0.7
T-cadherin*	A8D737_PIG	78	22.0±12.0	13.9±6.9	0.153	0.6
Tenascin	TENA_PIG	191	861.4±309.9	1192.9±318.3	0.072	1.4
Tetranectin	F1SRC8_PIG	22	156.6±34.1	171.5±75.3	0.644	1.1
TGFβ-induced protein ig-h3	BGH3_PIG	74	64.8±20.5	55.1±13.0	0.317	0.9
Thrombospondin-1	K7GPJ3_PIG	120	344.4±124.1	565.3±195.2	**0.030**	1.6
Thrombospondin-4*	F1RF28_PIG	104	8.9±7.9	33.3±26.4	0.051	3.7
Translationally-controlled tumor protein*	TCTP_PIG	20	50.9±23.5	49.1±19.5	0.874	1.0
Tryptase	TRYT_PIG	30	0.1±0.3	0.0±0.0	n/a	0.0
Tubulointerstitial nephritis antigen-like	F1SVA2_PIG	52	98.8±33.3	128.6±24.4	0.083	1.3
Versican	F1REZ2_PIG	369	1073.4±242.9	797.6±234.6	0.052	0.7
Vitamin D-binding protein	I3LN42_PIG	53	143.0±62.4	106.4±38.1	0.215	0.7
Vitronectin	VTNC_PIG	53	419.9±72.3	1038.1±338.7	**0.003**	2.5
von Willebrand factor A domain-containing protein 1	F1RJE3_PIG	44	8.3±6.4	10.0±7.6	0.660	1.2
WD repeat-containing protein 1	K9IVR7_PIG	66	288.7±36.1	297.6±112.3	0.848	1.0

P values for differential expression between neointimal DES and BMS are based on unpaired Student's *t*-tests with unequal variance (n=7 [BMS] and n=7 [DES]). *T*-test was not performed if a protein was undetectable in the majority of samples from 1 of the 2 groups compared. n/a denotes not applicable, FC denotes fold change. Proteins only identified in the neointima are marked with*. Results in bold indicate $P < 0.05$. Values are average (Av) total ion current (TIC) x 10^6 ± standard deviation (SD).

Supplemental table 3. Significant extracellular protein changes between BMS/DES day 28 vs. POBA late

Identified Proteins	UniProt ID	MW (kDa)	BMS/POBA *P*	BMS/POBA FC	DES/POBA *P*	DES/POBA FC
RPE-spondin	RPESP_PIG	32	**0.006**	0.2	**<0.001**	0.3
Laminin subunit gamma-1	F1S663_PIG	177	0.562	0.9	**<0.001**	0.3
Galectin-3	A3EX84_PIG	27	0.395	23.4	**0.002**	6.8
Collagen alpha-1 (XI)	F1S571_PIG	159	0.272	1.8	**0.002**	3.4
Periostin	F1RS37_PIG	93	0.394	6.1	**0.002**	11.9
Biglycan	K7GP55_PIG	41	0.167	1.5	**0.004**	2.0
Collagen alpha-1 (V)	F1S021_PIG	182	0.267	1.8	**0.006**	2.6
Latent-TGFß-binding protein 2	F1S2T5_PIG	196	0.833	1.2	**0.006**	3.9
Collagen alpha-1 (XVIII)	COIA1_PIG	62	**0.027**	0.6	**0.007**	0.2
Collagen alpha-1 (I)	CO1A1_PIG	100	0.584	1.3	**0.007**	1.9
Apolipoprotein H	I3LGN5_PIG	29	0.463	1.5	**0.008**	3.1
Dermatopontin	DERM_PIG	22	0.328	1.7	**0.008**	2.0
Collagen alpha-2 (I)	F1SFA7_PIG	129	0.639	1.2	**0.010**	2.0
Laminin subunit beta-1	F1SAE9_PIG	199	0.197	1.2	**0.013**	0.3
Fibronectin	F1SS24_PIG	272	0.243	1.6	**0.014**	2.9
Aggrecan	F1SKR0_PIG	238	0.250	1.6	**0.017**	3.0
Collagen alpha-1 (II)	I3LSV6_PIG	130	0.961	1.0	**0.018**	1.7
Annexin A1	ANXA1_PIG	39	0.364	4.0	**0.022**	7.4
Collagen alpha-2 (XI)	A5D9K7_PIG	162	0.436	1.5	**0.024**	2.1
Collagen alpha-1 (XII)	COCA1_PIG	229	0.284	13.7	**0.026**	15.7
Collagen alpha-1 (VIII)	F1SKX7_PIG	73	0.301	2.6	**0.028**	15.3
Tetranectin	F1SRC8_PIG	22	0.118	1.7	**0.036**	4.9
Gelsolin	GELS_PIG	85	0.267	0.7	**0.036**	0.6
Agrin	I3LGD9_PIG	216	0.693	0.9	**0.040**	0.6
Nidogen-2	F1SFF3_PIG	152	0.687	0.9	**0.042**	0.5
Galectin-1	LEG1_PIG	15	0.080	0.7	**0.042**	0.6
Dystroglycan	I3LD20_PIG	95	**0.046**	0.3	**0.043**	0.4
Podocan	I3LEB7_PIG	72	0.502	0.8	**0.049**	0.3
Lactadherin	MFGM_PIG	46	0.498	1.6	**0.050**	0.5
Thrombospondin-1	K7GPJ3_PIG	120	**0.031**	6.5	0.090	14.8
SPARC	SPRC_PIG	34	**0.033**	0.3	0.144	1.5

P values and FC for changes between BMS/DES day 28 and POBA late are shown. *P* values are based on unpaired Student's *t*-tests with unequal variance (n=3 [BMS day 28]/ n=3 [DES day 28], n=3 [POBA late]). *T*-test was not performed if a protein was undetectable in the majority of samples from 1 of the 2 groups compared. Results in bold indicate $P < 0.05$.

Supplemental table 4. Differentially expressed proteins between DES and BMS over time

Identified Proteins	UniProt ID	MW (kDa)	Day1		Day3		Day7		Day28	
			P	FC	*P*	FC	*P*	FC	*P*	FC
Collagen alpha-2 (IV)	F1RLL9_PIG	161	0.362	0.6	0.338	0.6	0.707	1.2	**<0.001**	0.3
Laminin subunit beta-1	F1SAE9_PIG	199	0.432	0.6	0.975	1.0	0.639	0.7	**0.001**	0.2
Laminin subunit gamma-1	F1S663_PIG	177	0.741	0.9	0.440	1.1	0.753	1.1	**0.011**	0.3
SPARC	SPRC_PIG	34	n/a	1.3	**0.036**	0.1	0.802	0.9	**0.014**	5.6
Hyaluronan and proteoglycan link protein 1	HPLN1_PIG	40	0.427	1.7	**0.043**	2.8	0.419	1.5	**0.019**	0.3
Collagen alpha-1 (XVIII)	COIA1_PIG	62	0.540	0.8	0.921	1.0	0.788	1.1	**0.020**	0.2
Latent-TGFß-binding protein 2	F1S2T5_PIG	196	0.952	1.0	0.753	0.8	**0.003**	1.9	**0.026**	3.3
Collagen alpha-1 (VIII)	F1SKX7_PIG	73	n/a	0.6	n/a	2.0	0.645	1.2	**0.029**	5.9
Laminin subunit beta-2	F1SPT5_PIG	179	0.364	0.7	0.201	1.4	0.728	1.2	**0.038**	0.5
Tubulointerstitial nephritis antigen-like	F1SVA2_PIG	52	0.326	0.9	0.686	1.2	0.125	1.3	**0.038**	0.7
Aggrecan	F1SKR0_PIG	238	0.523	0.8	0.263	4.1	0.971	1.0	**0.044**	1.9
TGFß-induced protein ig-h3	BGH3_PIG	74	**0.045**	0.5	0.950	1.0	0.368	2.4	0.206	0.3
Prophenin and tritrpticin	PF11_PIG	24	0.388	1.5	0.199	11.1	**0.010**	4.6	0.467	0.1
Collagen alpha-1 (XII)	COCA1_PIG	229	**0.045**	0.8	0.849	1.1	0.810	0.8	0.846	1.1
Vitronectin	VTNC_PIG	53	0.578	0.7	**0.019**	2.9	0.440	1.6	0.947	0.9

P values between DES and BMS at each time point are based on unpaired *t*-tests with unequal variance (n=3 [BMS day 1/3/7/28], n=3 [DES 1/3/7/28]). *T*-test was not performed if a protein was undetectable in the majority of samples from 1 of the 2 groups compared. Only proteins with at least one significant result at any time point are shown. FC denotes fold change (DES/BMS). Results in bold indicate $P < 0.05$.

10 ATTACHMENT

The porcine ECM database is attached to the thesis in electronic form.

Porcine ECM database

1. Protein sequences retrieved from UniProt……...2
2. Protein sequences deduced from public nucleotide databases……74

11 REFERENCES

1. Mortality GBD and Causes of Death C. Global, regional, and national age-sex specific all-cause and cause-specific mortality for 240 causes of death, 1990-2013: a systematic analysis for the Global Burden of Disease Study 2013. *Lancet*. 2015;385:117-71.
2. Townsend N, Wilson L, Bhatnagar P, Wickramasinghe K, Rayner M and Nichols M. Cardiovascular disease in Europe: epidemiological update 2016. *Eur Heart J*. 2016.
3. Libby P. Inflammation in atherosclerosis. *Arterioscler Thromb Vasc Biol*. 2012;32:2045-51.
4. Yusuf S, Hawken S, Ounpuu S, Dans T, Avezum A, Lanas F, McQueen M, Budaj A, Pais P, Varigos J, Lisheng L and Investigators IS. Effect of potentially modifiable risk factors associated with myocardial infarction in 52 countries (the INTERHEART study): case-control study. *Lancet*. 2004;364:937-52.
5. Libby P and Theroux P. Pathophysiology of coronary artery disease. *Circulation*. 2005;111:3481-8.
6. Everett BM, Smith RJ and Hiatt WR. Reducing LDL with PCSK9 Inhibitors--The Clinical Benefit of Lipid Drugs. *N Engl J Med*. 2015;373:1588-91.
7. Stoekenbroek RM, Kastelein JJ and Huijgen R. PCSK9 inhibition: the way forward in the treatment of dyslipidemia. *BMC Med*. 2015;13:258.
8. Libby P and Hansson GK. Inflammation and immunity in diseases of the arterial tree: players and layers. *Circ Res*. 2015;116:307-11.
9. Brown AJ, Teng Z, Evans PC, Gillard JH, Samady H and Bennett MR. Role of biomechanical forces in the natural history of coronary atherosclerosis. *Nat Rev Cardiol*. 2016;13:210-20.
10. Hahn C and Schwartz MA. Mechanotransduction in vascular physiology and atherogenesis. *Nat Rev Mol Cell Biol*. 2009;10:53-62.
11. Yahagi K, Kolodgie FD, Otsuka F, Finn AV, Davis HR, Joner M and Virmani R. Pathophysiology of native coronary, vein graft, and in-stent atherosclerosis. *Nat Rev Cardiol*. 2016;13:79-98.
12. Tabas I, Garcia-Cardena G and Owens GK. Recent insights into the cellular biology of atherosclerosis. *J Cell Biol*. 2015;209:13-22.
13. Nakashima Y, Fujii H, Sumiyoshi S, Wight TN and Sueishi K. Early human atherosclerosis: accumulation of lipid and proteoglycans in intimal thickenings followed by macrophage infiltration. *Arterioscler Thromb Vasc Biol*. 2007;27:1159-65.
14. Skalen K, Gustafsson M, Rydberg EK, Hulten LM, Wiklund O, Innerarity TL and Boren J. Subendothelial retention of atherogenic lipoproteins in early atherosclerosis. *Nature*. 2002;417:750-4.
15. Bennett MR, Sinha S and Owens GK. Vascular Smooth Muscle Cells in Atherosclerosis. *Circ Res*. 2016;118:692-702.
16. Shankman LS, Gomez D, Cherepanova OA, Salmon M, Alencar GF, Haskins RM, Swiatlowska P, Newman AA, Greene ES, Straub AC, Isakson B, Randolph GJ and Owens GK. KLF4-dependent phenotypic modulation of smooth muscle cells has a key role in atherosclerotic plaque pathogenesis. *Nat Med*. 2015;21:628-37.
17. Mann J and Davies MJ. Mechanisms of progression in native coronary artery disease: role of healed plaque disruption. *Heart*. 1999;82:265-8.
18. Kubo T, Maehara A, Mintz GS, Doi H, Tsujita K, Choi SY, Katoh O, Nasu K, Koenig A, Pieper M, Rogers JH, Wijns W, Bose D, Margolis MP, Moses JW, Stone GW and Leon MB. The dynamic nature of coronary artery lesion morphology assessed by serial virtual histology intravascular ultrasound tissue characterization. *J Am Coll Cardiol*. 2010;55:1590-7.
19. Langley SR, Willeit K, Didangelos A, Matic LP, Skroblin P, Barallobre-Barreiro J, Lengquist M, Rungger G, Kapustin A, Kedenko L, Molenaar C, Lu R, Barwari T, Suna G,

Yin X, Iglseder B, Paulweber B, Willeit P, Shalhoub J, Pasterkamp G, Davies AH, Monaco C, Hedin U, Shanahan CM, Willeit J, Kiechl S and Mayr M. Extracellular matrix proteomics identifies molecular signature of symptomatic carotid plaques. *J Clin Invest*. 2017.
20. Gruntzig AR, Senning A and Siegenthaler WE. Nonoperative dilatation of coronary-artery stenosis: percutaneous transluminal coronary angioplasty. *N Engl J Med*. 1979;301:61-8.
21. Farooq V, Gogas BD and Serruys PW. Restenosis: delineating the numerous causes of drug-eluting stent restenosis. *Circ Cardiovasc Interv*. 2011;4:195-205.
22. Lafont A, Durand E, Samuel JL, Besse B, Addad F, Levy BI, Desnos M, Guerot C and Boulanger CM. Endothelial dysfunction and collagen accumulation: two independent factors for restenosis and constrictive remodeling after experimental angioplasty. *Circulation*. 1999;100:1109-15.
23. Sangiorgi G, Taylor AJ, Farb A, Carter AJ, Edwards WD, Holmes DR, Schwartz RS and Virmani R. Histopathology of postpercutaneous transluminal coronary angioplasty remodeling in human coronary arteries. *Am Heart J*. 1999;138:681-7.
24. Sigwart U, Puel J, Mirkovitch V, Joffre F and Kappenberger L. Intravascular stents to prevent occlusion and restenosis after transluminal angioplasty. *N Engl J Med*. 1987;316:701-6.
25. Fischman DL, Leon MB, Baim DS, Schatz RA, Savage MP, Penn I, Detre K, Veltri L, Ricci D, Nobuyoshi M and et al. A randomized comparison of coronary-stent placement and balloon angioplasty in the treatment of coronary artery disease. Stent Restenosis Study Investigators. *N Engl J Med*. 1994;331:496-501.
26. Serruys PW, de Jaegere P, Kiemeneij F, Macaya C, Rutsch W, Heyndrickx G, Emanuelsson H, Marco J, Legrand V, Materne P and et al. A comparison of balloon-expandable-stent implantation with balloon angioplasty in patients with coronary artery disease. Benestent Study Group. *N Engl J Med*. 1994;331:489-95.
27. Holmes DR, Jr., Savage M, LaBlanche JM, Grip L, Serruys PW, Fitzgerald P, Fischman D, Goldberg S, Brinker JA, Zeiher AM, Shapiro LM, Willerson J, Davis BR, Ferguson JJ, Popma J, King SB, 3rd, Lincoff AM, Tcheng JE, Chan R, Granett JR and Poland M. Results of Prevention of REStenosis with Tranilast and its Outcomes (PRESTO) trial. *Circulation*. 2002;106:1243-50.
28. Serruys PW, Kutryk MJ and Ong AT. Coronary-artery stents. *N Engl J Med*. 2006;354:483-95.
29. Hoffmann R, Mintz GS, Dussaillant GR, Popma JJ, Pichard AD, Satler LF, Kent KM, Griffin J and Leon MB. Patterns and mechanisms of in-stent restenosis. A serial intravascular ultrasound study. *Circulation*. 1996;94:1247-54.
30. Inoue T, Croce K, Morooka T, Sakuma M, Node K and Simon DI. Vascular inflammation and repair: implications for re-endothelialization, restenosis, and stent thrombosis. *JACC Cardiovasc Interv*. 2011;4:1057-66.
31. Morice MC, Serruys PW, Sousa JE, Fajadet J, Ban Hayashi E, Perin M, Colombo A, Schuler G, Barragan P, Guagliumi G, Molnar F, Falotico R and Lesions RSGRSwtS-CBVB-ESitToPwdNNCA. A randomized comparison of a sirolimus-eluting stent with a standard stent for coronary revascularization. *N Engl J Med*. 2002;346:1773-80.
32. Moses JW, Leon MB, Popma JJ, Fitzgerald PJ, Holmes DR, O'Shaughnessy C, Caputo RP, Kereiakes DJ, Williams DO, Teirstein PS, Jaeger JL, Kuntz RE and Investigators S. Sirolimus-eluting stents versus standard stents in patients with stenosis in a native coronary artery. *N Engl J Med*. 2003;349:1315-23.
33. Stone GW, Ellis SG, Cox DA, Hermiller J, O'Shaughnessy C, Mann JT, Turco M, Caputo R, Bergin P, Greenberg J, Popma JJ, Russell ME and Investigators T-I. A polymer-based, paclitaxel-eluting stent in patients with coronary artery disease. *N Engl J Med*. 2004;350:221-31.
34. Stettler C, Wandel S, Allemann S, Kastrati A, Morice MC, Schomig A, Pfisterer ME, Stone GW, Leon MB, de Lezo JS, Goy JJ, Park SJ, Sabate M, Suttorp MJ, Kelbaek H, Spaulding C, Menichelli M, Vermeersch P, Dirksen MT, Cervinka P, Petronio AS, Nordmann AJ, Diem P, Meier B, Zwahlen M, Reichenbach S, Trelle S, Windecker S and

Juni P. Outcomes associated with drug-eluting and bare-metal stents: a collaborative network meta-analysis. *Lancet*. 2007;370:937-48.
35. Stone GW, Moses JW, Ellis SG, Schofer J, Dawkins KD, Morice MC, Colombo A, Schampaert E, Grube E, Kirtane AJ, Cutlip DE, Fahy M, Pocock SJ, Mehran R and Leon MB. Safety and efficacy of sirolimus- and paclitaxel-eluting coronary stents. *N Engl J Med*. 2007;356:998-1008.
36. Alfonso F and Fernandez C. Second-generation drug-eluting stents. Moving the field forward. *J Am Coll Cardiol*. 2011;58:26-9.
37. Raber L, Magro M, Stefanini GG, Kalesan B, van Domburg RT, Onuma Y, Wenaweser P, Daemen J, Meier B, Juni P, Serruys PW and Windecker S. Very late coronary stent thrombosis of a newer-generation everolimus-eluting stent compared with early-generation drug-eluting stents: a prospective cohort study. *Circulation*. 2012;125:1110-21.
38. Erbel R, Di Mario C, Bartunek J, Bonnier J, de Bruyne B, Eberli FR, Erne P, Haude M, Heublein B, Horrigan M, Ilsley C, Bose D, Koolen J, Luscher TF, Weissman N, Waksman R and Investigators P-A. Temporary scaffolding of coronary arteries with bioabsorbable magnesium stents: a prospective, non-randomised multicentre trial. *Lancet*. 2007;369:1869-75.
39. Pilgrim T, Heg D, Roffi M, Tuller D, Muller O, Vuilliomenet A, Cook S, Weilenmann D, Kaiser C, Jamshidi P, Fahrni T, Moschovitis A, Noble S, Eberli FR, Wenaweser P, Juni P and Windecker S. Ultrathin strut biodegradable polymer sirolimus-eluting stent versus durable polymer everolimus-eluting stent for percutaneous coronary revascularisation (BIOSCIENCE): a randomised, single-blind, non-inferiority trial. *Lancet*. 2014;384:2111-22.
40. Serruys PW, Onuma Y, Dudek D, Smits PC, Koolen J, Chevalier B, de Bruyne B, Thuesen L, McClean D, van Geuns RJ, Windecker S, Whitbourn R, Meredith I, Dorange C, Veldhof S, Hebert KM, Sudhir K, Garcia-Garcia HM and Ormiston JA. Evaluation of the second generation of a bioresorbable everolimus-eluting vascular scaffold for the treatment of de novo coronary artery stenosis: 12-month clinical and imaging outcomes. *J Am Coll Cardiol*. 2011;58:1578-88.
41. Kraak RP, Grundeken MJ, Koch KT, de Winter RJ and Wykrzykowska JJ. Bioresorbable scaffolds for the treatment of coronary artery disease: current status and future perspective. *Expert Rev Med Devices*. 2014;11:467-80.
42. Cassese S, Byrne RA, Ndrepepa G, Kufner S, Wiebe J, Repp J, Schunkert H, Fusaro M, Kimura T and Kastrati A. Everolimus-eluting bioresorbable vascular scaffolds versus everolimus-eluting metallic stents: a meta-analysis of randomised controlled trials. *Lancet*. 2016;387:537-44.
43. Finn AV and Virmani R. The clinical challenge of disappearing stents. *Lancet*. 2016;387:510-2.
44. Pepine CJ, Hirshfeld JW, Macdonald RG, Henderson MA, Bass TA, Goldberg S, Savage MP, Vetrovec G, Cowley M, Taussig AS and et al. A controlled trial of corticosteroids to prevent restenosis after coronary angioplasty. M-HEART Group. *Circulation*. 1990;81:1753-61.
45. Tesfamariam B. Drug release kinetics from stent device-based delivery systems. *J Cardiovasc Pharmacol*. 2008;51:118-25.
46. Sanchez OD, Yahagi K, Koppara T, Virmani R and Joner M. The everolimus-eluting Xience stent in small vessel disease: bench, clinical, and pathology view. *Med Devices (Auckl)*. 2015;8:37-45.
47. Abbott. The XIENCE V® and XIENCE nano® Everolimus Eluting Coronary Stent Systems. Instructions for Use. 2015.
48. Costa MA and Simon DI. Molecular basis of restenosis and drug-eluting stents. *Circulation*. 2005;111:2257-73.
49. Ma XM and Blenis J. Molecular mechanisms of mTOR-mediated translational control. *Nat Rev Mol Cell Biol*. 2009;10:307-18.

50. Byrne RA, Joner M, Alfonso F and Kastrati A. Treatment of In-Stent Restenosis. In: D. L. Bhatt, ed. *Cardiovascular intervention : a companion to Braunwald's heart disease*; 2016: 1 online resource.
51. Alfonso F, Byrne RA, Rivero F and Kastrati A. Current treatment of in-stent restenosis. *J Am Coll Cardiol*. 2014;63:2659-73.
52. Cassese S, Byrne RA, Tada T, Pinieck S, Joner M, Ibrahim T, King LA, Fusaro M, Laugwitz KL and Kastrati A. Incidence and predictors of restenosis after coronary stenting in 10 004 patients with surveillance angiography. *Heart*. 2014;100:153-9.
53. Byrne RA, Joner M and Kastrati A. Stent thrombosis and restenosis: what have we learned and where are we going? The Andreas Gruntzig Lecture ESC 2014. *Eur Heart J*. 2015;36:3320-31.
54. Tada T, Byrne RA, Simunovic I, King LA, Cassese S, Joner M, Fusaro M, Schneider S, Schulz S, Ibrahim T, Ott I, Massberg S, Laugwitz KL and Kastrati A. Risk of stent thrombosis among bare-metal stents, first-generation drug-eluting stents, and second-generation drug-eluting stents: results from a registry of 18,334 patients. *JACC Cardiovasc Interv*. 2013;6:1267-74.
55. Nakano M, Otsuka F, Yahagi K, Sakakura K, Kutys R, Ladich ER, Finn AV, Kolodgie FD and Virmani R. Human autopsy study of drug-eluting stents restenosis: histomorphological predictors and neointimal characteristics. *Eur Heart J*. 2013;34:3304-13.
56. Nakazawa G, Otsuka F, Nakano M, Vorpahl M, Yazdani SK, Ladich E, Kolodgie FD, Finn AV and Virmani R. The pathology of neoatherosclerosis in human coronary implants bare-metal and drug-eluting stents. *J Am Coll Cardiol*. 2011;57:1314-22.
57. Mitra AK and Agrawal DK. In stent restenosis: bane of the stent era. *J Clin Pathol*. 2006;59:232-9.
58. Otsuka F, Finn AV, Yazdani SK, Nakano M, Kolodgie FD and Virmani R. The importance of the endothelium in atherothrombosis and coronary stenting. *Nat Rev Cardiol*. 2012;9:439-53.
59. Gimbrone MA, Jr. and Garcia-Cardena G. Endothelial Cell Dysfunction and the Pathobiology of Atherosclerosis. *Circ Res*. 2016;118:620-36.
60. Chaabane C, Otsuka F, Virmani R and Bochaton-Piallat ML. Biological responses in stented arteries. *Cardiovasc Res*. 2013;99:353-63.
61. Wenaweser P, Daemen J, Zwahlen M, van Domburg R, Juni P, Vaina S, Hellige G, Tsuchida K, Morger C, Boersma E, Kukreja N, Meier B, Serruys PW and Windecker S. Incidence and correlates of drug-eluting stent thrombosis in routine clinical practice. 4-year results from a large 2-institutional cohort study. *J Am Coll Cardiol*. 2008;52:1134-40.
62. Mauri L, Kereiakes DJ, Yeh RW, Driscoll-Shempp P, Cutlip DE, Steg PG, Normand SL, Braunwald E, Wiviott SD, Cohen DJ, Holmes DR, Jr., Krucoff MW, Hermiller J, Dauerman HL, Simon DI, Kandzari DE, Garratt KN, Lee DP, Pow TK, Ver Lee P, Rinaldi MJ, Massaro JM and Investigators DS. Twelve or 30 months of dual antiplatelet therapy after drug-eluting stents. *N Engl J Med*. 2014;371:2155-66.
63. Iakovou I, Schmidt T, Bonizzoni E, Ge L, Sangiorgi GM, Stankovic G, Airoldi F, Chieffo A, Montorfano M, Carlino M, Michev I, Corvaja N, Briguori C, Gerckens U, Grube E and Colombo A. Incidence, predictors, and outcome of thrombosis after successful implantation of drug-eluting stents. *JAMA*. 2005;293:2126-30.
64. Joner M, Finn AV, Farb A, Mont EK, Kolodgie FD, Ladich E, Kutys R, Skorija K, Gold HK and Virmani R. Pathology of drug-eluting stents in humans: delayed healing and late thrombotic risk. *J Am Coll Cardiol*. 2006;48:193-202.
65. Nakazawa G, Finn AV, Joner M, Ladich E, Kutys R, Mont EK, Gold HK, Burke AP, Kolodgie FD and Virmani R. Delayed arterial healing and increased late stent thrombosis at culprit sites after drug-eluting stent placement for acute myocardial infarction patients: an autopsy study. *Circulation*. 2008;118:1138-45.
66. Koskinas KC, Chatzizisis YS, Antoniadis AP and Giannoglou GD. Role of endothelial shear stress in stent restenosis and thrombosis: pathophysiologic mechanisms and implications for clinical translation. *J Am Coll Cardiol*. 2012;59:1337-49.

67. Deuse T, Hua X, Wang D, Maegdefessel L, Heeren J, Scheja L, Bolanos JP, Rakovic A, Spin JM, Stubbendorff M, Ikeno F, Langer F, Zeller T, Schulte-Uentrop L, Stoehr A, Itagaki R, Haddad F, Eschenhagen T, Blankenberg S, Kiefmann R, Reichenspurner H, Velden J, Klein C, Yeung A, Robbins RC, Tsao PS and Schrepfer S. Dichloroacetate prevents restenosis in preclinical animal models of vessel injury. *Nature*. 2014;509:641-4.
68. Holy EW, Jakob P, Eickner T, Camici GG, Beer JH, Akhmedov A, Sternberg K, Schmitz KP, Luscher TF and Tanner FC. PI3K/p110alpha inhibition selectively interferes with arterial thrombosis and neointima formation, but not re-endothelialization: potential implications for drug-eluting stent design. *Eur Heart J*. 2014;35:808-20.
69. Otsuka F, Byrne RA, Yahagi K, Mori H, Ladich E, Fowler DR, Kutys R, Xhepa E, Kastrati A, Virmani R and Joner M. Neoatherosclerosis: overview of histopathologic findings and implications for intravascular imaging assessment. *Eur Heart J*. 2015;36:2147-59.
70. Park SJ, Kang SJ, Virmani R, Nakano M and Ueda Y. In-stent neoatherosclerosis: a final common pathway of late stent failure. *J Am Coll Cardiol*. 2012;59:2051-7.
71. Kang SJ, Mintz GS, Akasaka T, Park DW, Lee JY, Kim WJ, Lee SW, Kim YH, Whan Lee C, Park SW and Park SJ. Optical coherence tomographic analysis of in-stent neoatherosclerosis after drug-eluting stent implantation. *Circulation*. 2011;123:2954-63.
72. Kang SJ, Mintz GS, Park DW, Lee SW, Kim YH, Lee CW, Han KH, Kim JJ, Park SW and Park SJ. Tissue characterization of in-stent neointima using intravascular ultrasound radiofrequency data analysis. *Am J Cardiol*. 2010;106:1561-5.
73. Romero ME, Yahagi K, Kolodgie FD and Virmani R. Neoatherosclerosis From a Pathologist's Point of View. *Arterioscler Thromb Vasc Biol*. 2015;35:e43-9.
74. Taniwaki M, Windecker S, Zaugg S, Stefanini GG, Baumgartner S, Zanchin T, Wenaweser P, Meier B, Juni P and Raber L. The association between in-stent neoatherosclerosis and native coronary artery disease progression: a long-term angiographic and optical coherence tomography cohort study. *Eur Heart J*. 2015;36:2167-76.
75. Otsuka F, Vorpahl M, Nakano M, Foerst J, Newell JB, Sakakura K, Kutys R, Ladich E, Finn AV, Kolodgie FD and Virmani R. Pathology of second-generation everolimus-eluting stents versus first-generation sirolimus- and paclitaxel-eluting stents in humans. *Circulation*. 2014;129:211-23.
76. Cheng Y, Liu X, Yang J, Lin Y, Xu DZ, Lu Q, Deitch EA, Huo Y, Delphin ES and Zhang C. MicroRNA-145, a novel smooth muscle cell phenotypic marker and modulator, controls vascular neointimal lesion formation. *Circ Res*. 2009;105:158-66.
77. Ji R, Cheng Y, Yue J, Yang J, Liu X, Chen H, Dean DB and Zhang C. MicroRNA expression signature and antisense-mediated depletion reveal an essential role of MicroRNA in vascular neointimal lesion formation. *Circ Res*. 2007;100:1579-88.
78. Sunderland N, Skroblin P, Barwari T, Huntley RP, Lu R, Joshi A, Lovering RC and Mayr M. MicroRNA Biomarkers and Platelet Reactivity: The Clot Thickens. *Circ Res*. 2017;120:418-435.
79. Denli AM, Tops BB, Plasterk RH, Ketting RF and Hannon GJ. Processing of primary microRNAs by the Microprocessor complex. *Nature*. 2004;432:231-5.
80. Maegdefessel L, Rayner KJ and Leeper NJ. MicroRNA regulation of vascular smooth muscle function and phenotype: early career committee contribution. *Arterioscler Thromb Vasc Biol*. 2015;35:2-6.
81. Liu X, Cheng Y, Zhang S, Lin Y, Yang J and Zhang C. A necessary role of miR-221 and miR-222 in vascular smooth muscle cell proliferation and neointimal hyperplasia. *Circ Res*. 2009;104:476-87.
82. Cordes KR, Sheehy NT, White MP, Berry EC, Morton SU, Muth AN, Lee TH, Miano JM, Ivey KN and Srivastava D. miR-145 and miR-143 regulate smooth muscle cell fate and plasticity. *Nature*. 2009;460:705-10.

83. Harris TA, Yamakuchi M, Ferlito M, Mendell JT and Lowenstein CJ. MicroRNA-126 regulates endothelial expression of vascular cell adhesion molecule 1. *Proc Natl Acad Sci U S A*. 2008;105:1516-21.
84. Leistner DM, Boeckel JN, Reis SM, Thome CE, De Rosa R, Keller T, Palapies L, Fichtlscherer S, Dimmeler S and Zeiher AM. Transcoronary gradients of vascular miRNAs and coronary atherosclerotic plaque characteristics. *Eur Heart J*. 2016;37:1738-49.
85. Iqbal J, Chamberlain J, Francis SE and Gunn J. Role of Animal Models in Coronary Stenting. *Ann Biomed Eng*. 2016;44:453-65.
86. Schwartz RS, Murphy JG, Edwards WD, Camrud AR, Vliestra RE and Holmes DR. Restenosis after balloon angioplasty. A practical proliferative model in porcine coronary arteries. *Circulation*. 1990;82:2190-200.
87. Abtahian F and Jang I-K. Optical Coherence Tomography. In: D. L. Bhatt, ed. *Cardiovascular intervention : a companion to Braunwald's heart disease*; 2016.
88. Sinclair H, Bourantas C, Bagnall A, Mintz GS and Kunadian V. OCT for the identification of vulnerable plaque in acute coronary syndrome. *JACC Cardiovasc Imaging*. 2015;8:198-209.
89. Yabushita H, Bouma BE, Houser SL, Aretz HT, Jang IK, Schlendorf KH, Kauffman CR, Shishkov M, Kang DH, Halpern EF and Tearney GJ. Characterization of human atherosclerosis by optical coherence tomography. *Circulation*. 2002;106:1640-5.
90. Gonzalo N, Serruys PW, Okamura T, van Beusekom HM, Garcia-Garcia HM, van Soest G, van der Giessen W and Regar E. Optical coherence tomography patterns of stent restenosis. *Am Heart J*. 2009;158:284-93.
91. Tada T, Kadota K, Hosogi S, Miyake K, Ohya M, Amano H, Izawa Y, Kanazawa T, Kubo S, Ichinohe T, Hyoudou Y, Hayakawa Y, Sabbah MM, Otsuru S, Hasegawa D, Habara S, Tanaka H, Fuku Y, Katoh H, Goto T and Mitsudo K. Association between tissue characteristics assessed with optical coherence tomography and mid-term results after percutaneous coronary intervention for in-stent restenosis lesions: a comparison between balloon angioplasty, paclitaxel-coated balloon dilatation, and drug-eluting stent implantation. *Eur Heart J Cardiovasc Imaging*. 2015;16:1101-11.
92. Bonnans C, Chou J and Werb Z. Remodelling the extracellular matrix in development and disease. *Nat Rev Mol Cell Biol*. 2014;15:786-801.
93. Wagenseil JE and Mecham RP. Vascular extracellular matrix and arterial mechanics. *Physiol Rev*. 2009;89:957-89.
94. Hynes RO. The extracellular matrix: not just pretty fibrils. *Science*. 2009;326:1216-9.
95. Fitzsimmons CM and Shanahan CM. Vascular Extracellular Matrix. *Pan Vascular Medicine Integrated Clinical Management*. 2002:XV, 1941p. 1800 illus.
96. Engel J and Chiquet M. An Overview of Extracellular Matrix Structure and Function. In: R. P. Mecham, ed. *The Extracellular Matrix: an Overview*; 2011.
97. Barallobre-Barreiro J, Gupta SK, Zoccarato A, Kitazume-Taneike R, Fava M, Yin X, Werner T, Hirt MN, Zampetaki A, Viviano A, Chong M, Bern M, Kourliouros A, Domenech N, Willeit P, Shah AM, Jahangiri M, Schaefer L, Fischer JW, Iozzo RV, Viner R, Thum T, Heineke J, Kichler A, Otsu K and Mayr M. Glycoproteomics Reveals Decorin Peptides With Anti-Myostatin Activity in Human Atrial Fibrillation. *Circulation*. 2016.
98. O'Reilly MS, Boehm T, Shing Y, Fukai N, Vasios G, Lane WS, Flynn E, Birkhead JR, Olsen BR and Folkman J. Endostatin: an endogenous inhibitor of angiogenesis and tumor growth. *Cell*. 1997;88:277-85.
99. Yurchenco PD. Basement membranes: cell scaffoldings and signaling platforms. *Cold Spring Harb Perspect Biol*. 2011;3.
100. Yousif LF, Di Russo J and Sorokin L. Laminin isoforms in endothelial and perivascular basement membranes. *Cell Adh Migr*. 2013;7:101-10.
101. Kalluri R. Basement membranes: structure, assembly and role in tumour angiogenesis. *Nat Rev Cancer*. 2003;3:422-33.

102. Alberts B, Bray D, Hopkin K, Johnson A, Lewis J, Raff M, Roberts K and Walter P. Cell Junctions, Cell Adhesion, and the Extracellular Matrix. In: B. Alberts, J. Wilson and T. Hunt, eds. *Molecular biology of the cell.* 5th ed. Abingdon: Garland Science; 2008.
103. Mongiat M, Sweeney SM, San Antonio JD, Fu J and Iozzo RV. Endorepellin, a novel inhibitor of angiogenesis derived from the C terminus of perlecan. *J Biol Chem*. 2003;278:4238-49.
104. Rienks M, Papageorgiou AP, Frangogiannis NG and Heymans S. Myocardial extracellular matrix: an ever-changing and diverse entity. *Circ Res*. 2014;114:872-88.
105. Humphrey JD, Dufresne ER and Schwartz MA. Mechanotransduction and extracellular matrix homeostasis. *Nat Rev Mol Cell Biol*. 2014;15:802-12.
106. Jacob MP. Extracellular matrix remodeling and matrix metalloproteinases in the vascular wall during aging and in pathological conditions. *Biomed Pharmacother*. 2003;57:195-202.
107. Mouw JK, Ou G and Weaver VM. Extracellular matrix assembly: a multiscale deconstruction. *Nat Rev Mol Cell Biol*. 2014;15:771-85.
108. Chen S and Birk DE. The regulatory roles of small leucine-rich proteoglycans in extracellular matrix assembly. *FEBS J*. 2013;280:2120-37.
109. Morawski M, Bruckner G, Arendt T and Matthews RT. Aggrecan: Beyond cartilage and into the brain. *Int J Biochem Cell Biol*. 2012;44:690-3.
110. Lynch M, Barallobre-Barreiro J, Jahangiri M and Mayr M. Vascular proteomics in metabolic and cardiovascular diseases. *J Intern Med*. 2016.
111. Wight TN and Merrilees MJ. Proteoglycans in atherosclerosis and restenosis: key roles for versican. *Circ Res*. 2004;94:1158-67.
112. Wight TN. Versican: a versatile extracellular matrix proteoglycan in cell biology. *Curr Opin Cell Biol*. 2002;14:617-23.
113. Wight TN, Lara S, Riessen R, Le Baron R and Isner J. Selective deposits of versican in the extracellular matrix of restenotic lesions from human peripheral arteries. *Am J Pathol*. 1997;151:963-73.
114. Didangelos A, Yin X, Mandal K, Saje A, Smith A, Xu Q, Jahangiri M and Mayr M. Extracellular matrix composition and remodeling in human abdominal aortic aneurysms: a proteomics approach. *Mol Cell Proteomics*. 2011;10:M111 008128.
115. Theocharis AD, Tsolakis I, Hjerpe A and Karamanos NK. Human abdominal aortic aneurysm is characterized by decreased versican concentration and specific downregulation of versican isoform V(0). *Atherosclerosis*. 2001;154:367-76.
116. Karsdal MA, Nielsen MJ, Sand JM, Henriksen K, Genovese F, Bay-Jensen AC, Smith V, Adamkewicz JI, Christiansen C and Leeming DJ. Extracellular matrix remodeling: the common denominator in connective tissue diseases. Possibilities for evaluation and current understanding of the matrix as more than a passive architecture, but a key player in tissue failure. *Assay Drug Dev Technol*. 2013;11:70-92.
117. Merline R, Schaefer RM and Schaefer L. The matricellular functions of small leucine-rich proteoglycans (SLRPs). *J Cell Commun Signal*. 2009;3:323-35.
118. Vial C, Gutierrez J, Santander C, Cabrera D and Brandan E. Decorin interacts with connective tissue growth factor (CTGF)/CCN2 by LRR12 inhibiting its biological activity. *J Biol Chem*. 2011;286:24242-52.
119. Morgan MR, Humphries MJ and Bass MD. Synergistic control of cell adhesion by integrins and syndecans. *Nat Rev Mol Cell Biol*. 2007;8:957-69.
120. Cox D, Brennan M and Moran N. Integrins as therapeutic targets: lessons and opportunities. *Nat Rev Drug Discov*. 2010;9:804-20.
121. Ross TD, Coon BG, Yun S, Baeyens N, Tanaka K, Ouyang M and Schwartz MA. Integrins in mechanotransduction. *Curr Opin Cell Biol*. 2013;25:613-8.
122. Finney AC, Stokes KY, Pattillo CB and Orr AW. Integrin signaling in atherosclerosis. *Cell Mol Life Sci*. 2017.
123. Ley K, Rivera-Nieves J, Sandborn WJ and Shattil S. Integrin-based therapeutics: biological basis, clinical use and new drugs. *Nat Rev Drug Discov*. 2016;15:173-83.

124. Katsaros KM, Kastl SP, Zorn G, Maurer G, Wojta J, Huber K, Christ G and Speidl WS. Increased restenosis rate after implantation of drug-eluting stents in patients with elevated serum activity of matrix metalloproteinase-2 and -9. *JACC Cardiovasc Interv*. 2010;3:90-7.
125. Murphy G. The ADAMs: signalling scissors in the tumour microenvironment. *Nat Rev Cancer*. 2008;8:929-41.
126. White JM. ADAMs: modulators of cell-cell and cell-matrix interactions. *Curr Opin Cell Biol*. 2003;15:598-606.
127. Stanton H, Melrose J, Little CB and Fosang AJ. Proteoglycan degradation by the ADAMTS family of proteinases. *Biochim Biophys Acta*. 2011;1812:1616-29.
128. Majerus EM, Zheng X, Tuley EA and Sadler JE. Cleavage of the ADAMTS13 propeptide is not required for protease activity. *J Biol Chem*. 2003;278:46643-8.
129. Salter RC, Ashlin TG, Kwan AP and Ramji DP. ADAMTS proteases: key roles in atherosclerosis? *J Mol Med (Berl)*. 2010;88:1203-11.
130. Visse R and Nagase H. Matrix metalloproteinases and tissue inhibitors of metalloproteinases: structure, function, and biochemistry. *Circ Res*. 2003;92:827-39.
131. Galis ZS, Sukhova GK, Lark MW and Libby P. Increased expression of matrix metalloproteinases and matrix degrading activity in vulnerable regions of human atherosclerotic plaques. *J Clin Invest*. 1994;94:2493-503.
132. Dollery CM, McEwan JR and Henney AM. Matrix metalloproteinases and cardiovascular disease. *Circ Res*. 1995;77:863-8.
133. Tamarina NA, McMillan WD, Shively VP and Pearce WH. Expression of matrix metalloproteinases and their inhibitors in aneurysms and normal aorta. *Surgery*. 1997;122:264-71; discussion 271-2.
134. Badier-Commander C, Verbeuren T, Lebard C, Michel JB and Jacob MP. Increased TIMP/MMP ratio in varicose veins: a possible explanation for extracellular matrix accumulation. *J Pathol*. 2000;192:105-12.
135. Goldin A, Beckman JA, Schmidt AM and Creager MA. Advanced glycation end products: sparking the development of diabetic vascular injury. *Circulation*. 2006;114:597-605.
136. Galis ZS and Khatri JJ. Matrix metalloproteinases in vascular remodeling and atherogenesis: the good, the bad, and the ugly. *Circ Res*. 2002;90:251-62.
137. Galis ZS, Muszynski M, Sukhova GK, Simon-Morrissey E, Unemori EN, Lark MW, Amento E and Libby P. Cytokine-stimulated human vascular smooth muscle cells synthesize a complement of enzymes required for extracellular matrix digestion. *Circ Res*. 1994;75:181-9.
138. Yanagi H, Sasaguri Y, Sugama K, Morimatsu M and Nagase H. Production of tissue collagenase (matrix metalloproteinase 1) by human aortic smooth muscle cells in response to platelet-derived growth factor. *Atherosclerosis*. 1991;91:207-16.
139. Jiang D, Liang J and Noble PW. Hyaluronan in tissue injury and repair. *Annu Rev Cell Dev Biol*. 2007;23:435-61.
140. Arroyo AG and Iruela-Arispe ML. Extracellular matrix, inflammation, and the angiogenic response. *Cardiovasc Res*. 2010;86:226-35.
141. Rzucidlo EM, Martin KA and Powell RJ. Regulation of vascular smooth muscle cell differentiation. *J Vasc Surg*. 2007;45 Suppl A:A25-32.
142. Owens GK, Kumar MS and Wamhoff BR. Molecular regulation of vascular smooth muscle cell differentiation in development and disease. *Physiol Rev*. 2004;84:767-801.
143. Gomez D and Owens GK. Smooth muscle cell phenotypic switching in atherosclerosis. *Cardiovasc Res*. 2012;95:156-64.
144. Demer LL and Tintut Y. Vascular calcification: pathobiology of a multifaceted disease. *Circulation*. 2008;117:2938-48.
145. Allahverdian S, Chehroudi AC, McManus BM, Abraham T and Francis GA. Contribution of intimal smooth muscle cells to cholesterol accumulation and macrophage-like cells in human atherosclerosis. *Circulation*. 2014;129:1551-9.

146. Feil S, Fehrenbacher B, Lukowski R, Essmann F, Schulze-Osthoff K, Schaller M and Feil R. Transdifferentiation of vascular smooth muscle cells to macrophage-like cells during atherogenesis. *Circ Res*. 2014;115:662-7.
147. Wang M, Zhao D, Spinetti G, Zhang J, Jiang LQ, Pintus G, Monticone R and Lakatta EG. Matrix metalloproteinase 2 activation of transforming growth factor-beta1 (TGF-beta1) and TGF-beta1-type II receptor signaling within the aged arterial wall. *Arterioscler Thromb Vasc Biol*. 2006;26:1503-9.
148. Merrilees MJ, Beaumont BW, Braun KR, Thomas AC, Kang I, Hinek A, Passi A and Wight TN. Neointima formed by arterial smooth muscle cells expressing versican variant V3 is resistant to lipid and macrophage accumulation. *Arterioscler Thromb Vasc Biol*. 2011;31:1309-16.
149. Newby AC. Metalloproteinase expression in monocytes and macrophages and its relationship to atherosclerotic plaque instability. *Arterioscler Thromb Vasc Biol*. 2008;28:2108-14.
150. Ponticos M and Smith BD. Extracellular matrix synthesis in vascular disease: hypertension, and atherosclerosis. *J Biomed Res*. 2014;28:25-39.
151. Brown DL, Hibbs MS, Kearney M, Loushin C and Isner JM. Identification of 92-kD gelatinase in human coronary atherosclerotic lesions. Association of active enzyme synthesis with unstable angina. *Circulation*. 1995;91:2125-31.
152. Jonsson-Rylander AC, Nilsson T, Fritsche-Danielson R, Hammarstrom A, Behrendt M, Andersson JO, Lindgren K, Andersson AK, Wallbrandt P, Rosengren B, Brodin P, Thelin A, Westin A, Hurt-Camejo E and Lee-Sogaard CH. Role of ADAMTS-1 in atherosclerosis: remodeling of carotid artery, immunohistochemistry, and proteolysis of versican. *Arterioscler Thromb Vasc Biol*. 2005;25:180-5.
153. Lee CW, Hwang I, Park CS, Lee H, Park DW, Kang SJ, Lee SH, Kim YH, Park SW and Park SJ. Comparison of ADAMTS-1, -4 and -5 expression in culprit plaques between acute myocardial infarction and stable angina. *J Clin Pathol*. 2011;64:399-404.
154. Wagsater D, Bjork H, Zhu C, Bjorkegren J, Valen G, Hamsten A and Eriksson P. ADAMTS-4 and -8 are inflammatory regulated enzymes expressed in macrophage-rich areas of human atherosclerotic plaques. *Atherosclerosis*. 2008;196:514-22.
155. Farb A, Kolodgie FD, Hwang JY, Burke AP, Tefera K, Weber DK, Wight TN and Virmani R. Extracellular matrix changes in stented human coronary arteries. *Circulation*. 2004;110:940-7.
156. Matsuura R, Isaka N, Imanaka-Yoshida K, Yoshida T, Sakakura T and Nakano T. Deposition of PG-M/versican is a major cause of human coronary restenosis after percutaneous transluminal coronary angioplasty. *J Pathol*. 1996;180:311-6.
157. Chung IM, Gold HK, Schwartz SM, Ikari Y, Reidy MA and Wight TN. Enhanced extracellular matrix accumulation in restenosis of coronary arteries after stent deployment. *J Am Coll Cardiol*. 2002;40:2072-81.
158. Nikol S, Isner JM, Pickering JG, Kearney M, Leclerc G and Weir L. Expression of transforming growth factor-beta 1 is increased in human vascular restenosis lesions. *J Clin Invest*. 1992;90:1582-92.
159. Backes A, Seay U, Sedding DG, Tillmanns HH and Braun-Dullaeus RC. Inhibition of matrix deposition: a new strategy for prevention of restenosis after balloon angioplasty. *J Cardiovasc Pharmacol*. 2010;55:213-8.
160. Karimi-Shah BA and Chowdhury BA. Forced vital capacity in idiopathic pulmonary fibrosis--FDA review of pirfenidone and nintedanib. *N Engl J Med*. 2015;372:1189-91.
161. King TE, Jr., Bradford WZ, Castro-Bernardini S, Fagan EA, Glaspole I, Glassberg MK, Gorina E, Hopkins PM, Kardatzke D, Lancaster L, Lederer DJ, Nathan SD, Pereira CA, Sahn SA, Sussman R, Swigris JJ, Noble PW and Group AS. A phase 3 trial of pirfenidone in patients with idiopathic pulmonary fibrosis. *N Engl J Med*. 2014;370:2083-92.
162. Lander ES, Linton LM, Birren B, Nusbaum C, Zody MC, Baldwin J, Devon K, Dewar K, Doyle M, FitzHugh W, Funke R, Gage D, Harris K, Heaford A, Howland J, Kann L, Lehoczky J, LeVine R, McEwan P, McKernan K, Meldrim J, Mesirov JP, Miranda C,

Morris W, Naylor J, Raymond C, Rosetti M, Santos R, Sheridan A, Sougnez C, Stange-Thomann Y, Stojanovic N, Subramanian A, Wyman D, Rogers J, Sulston J, Ainscough R, Beck S, Bentley D, Burton J, Clee C, Carter N, Coulson A, Deadman R, Deloukas P, Dunham A, Dunham I, Durbin R, French L, Grafham D, Gregory S, Hubbard T, Humphray S, Hunt A, Jones M, Lloyd C, McMurray A, Matthews L, Mercer S, Milne S, Mullikin JC, Mungall A, Plumb R, Ross M, Shownkeen R, Sims S, Waterston RH, Wilson RK, Hillier LW, McPherson JD, Marra MA, Mardis ER, Fulton LA, Chinwalla AT, Pepin KH, Gish WR, Chissoe SL, Wendl MC, Delehaunty KD, Miner TL, Delehaunty A, Kramer JB, Cook LL, Fulton RS, Johnson DL, Minx PJ, Clifton SW, Hawkins T, Branscomb E, Predki P, Richardson P, Wenning S, Slezak T, Doggett N, Cheng JF, Olsen A, Lucas S, Elkin C, Uberbacher E, Frazier M, Gibbs RA, Muzny DM, Scherer SE, Bouck JB, Sodergren EJ, Worley KC, Rives CM, Gorrell JH, Metzker ML, Naylor SL, Kucherlapati RS, Nelson DL, Weinstock GM, Sakaki Y, Fujiyama A, Hattori M, Yada T, Toyoda A, Itoh T, Kawagoe C, Watanabe H, Totoki Y, Taylor T, Weissenbach J, Heilig R, Saurin W, Artiguenave F, Brottier P, Bruls T, Pelletier E, Robert C, Wincker P, Smith DR, Doucette-Stamm L, Rubenfield M, Weinstock K, Lee HM, Dubois J, Rosenthal A, Platzer M, Nyakatura G, Taudien S, Rump A, Yang H, Yu J, Wang J, Huang G, Gu J, Hood L, Rowen L, Madan A, Qin S, Davis RW, Federspiel NA, Abola AP, Proctor MJ, Myers RM, Schmutz J, Dickson M, Grimwood J, Cox DR, Olson MV, Kaul R, Raymond C, Shimizu N, Kawasaki K, Minoshima S, Evans GA, Athanasiou M, Schultz R, Roe BA, Chen F, Pan H, Ramser J, Lehrach H, Reinhardt R, McCombie WR, de la Bastide M, Dedhia N, Blocker H, Hornischer K, Nordsiek G, Agarwala R, Aravind L, Bailey JA, Bateman A, Batzoglou S, Birney E, Bork P, Brown DG, Burge CB, Cerutti L, Chen HC, Church D, Clamp M, Copley RR, Doerks T, Eddy SR, Eichler EE, Furey TS, Galagan J, Gilbert JG, Harmon C, Hayashizaki Y, Haussler D, Hermjakob H, Hokamp K, Jang W, Johnson LS, Jones TA, Kasif S, Kaspryzk A, Kennedy S, Kent WJ, Kitts P, Koonin EV, Korf I, Kulp D, Lancet D, Lowe TM, McLysaght A, Mikkelsen T, Moran JV, Mulder N, Pollara VJ, Ponting CP, Schuler G, Schultz J, Slater G, Smit AF, Stupka E, Szustakowki J, Thierry-Mieg D, Thierry-Mieg J, Wagner L, Wallis J, Wheeler R, Williams A, Wolf YI, Wolfe KH, Yang SP, Yeh RF, Collins F, Guyer MS, Peterson J, Felsenfeld A, Wetterstrand KA, Patrinos A, Morgan MJ, de Jong P, Catanese JJ, Osoegawa K, Shizuya H, Choi S, Chen YJ, Szustakowki J and International Human Genome Sequencing C. Initial sequencing and analysis of the human genome. *Nature*. 2001;409:860-921.

163. Lottspeich F. Introduction to proteomics. *Methods Mol Biol*. 2009;564:3-10.

164. Lindsey ML, Mayr M, Gomes AV, Delles C, Arrell DK, Murphy AM, Lange RA, Costello CE, Jin YF, Laskowitz DT, Sam F, Terzic A, Van Eyk J, Srinivas PR, American Heart Association Council on Functional G, Translational Biology CoCDitYCoCCCoC, Stroke Nursing CoH and Stroke C. Transformative Impact of Proteomics on Cardiovascular Health and Disease: A Scientific Statement From the American Heart Association. *Circulation*. 2015;132:852-72.

165. Wilkins MR, Pasquali C, Appel RD, Ou K, Golaz O, Sanchez JC, Yan JX, Gooley AA, Hughes G, Humphery-Smith I, Williams KL and Hochstrasser DF. From proteins to proteomes: large scale protein identification by two-dimensional electrophoresis and amino acid analysis. *Biotechnology (N Y)*. 1996;14:61-5.

166. Wilkins MR, Sanchez JC, Gooley AA, Appel RD, Humphery-Smith I, Hochstrasser DF and Williams KL. Progress with proteome projects: why all proteins expressed by a genome should be identified and how to do it. *Biotechnol Genet Eng Rev*. 1996;13:19-50.

167. Tyers M and Mann M. From genomics to proteomics. *Nature*. 2003;422:193-7.

168. Pechlaner R, Tsimikas S, Yin X, Willeit P, Baig F, Santer P, Oberhollenzer F, Egger G, Witztum JL, Alexander VJ, Willeit J, Kiechl S and Mayr M. Very-Low-Density Lipoprotein-Associated Apolipoproteins Predict Cardiovascular Events and Are Lowered by Inhibition of APOC-III. *J Am Coll Cardiol*. 2017;69:789-800.

169. Anderson NL and Anderson NG. The human plasma proteome: history, character, and diagnostic prospects. *Molecular & cellular proteomics : MCP*. 2002;1:845-67.

170. Didangelos A, Yin X, Mandal K, Baumert M, Jahangiri M and Mayr M. Proteomics characterization of extracellular space components in the human aorta. *Mol Cell Proteomics*. 2010;9:2048-62.
171. Fu Q, Bovenkamp DE and Van Eyk JE. A rapid, economical, and reproducible method for human serum delipidation and albumin and IgG removal for proteomic analysis. *Methods Mol Biol*. 2007;357:365-71.
172. Cuello F, Shankar-Hari M, Mayr U, Yin X, Marshall M, Suna G, Willeit P, Langley SR, Jayawardhana T, Zeller T, Terblanche M, Shah AM and Mayr M. Redox-state of pentraxin 3 as a novel biomarker for resolution of inflammation and survival in sepsis. *Molecular & cellular proteomics : MCP*. 2014.
173. Walther TC and Mann M. Mass spectrometry-based proteomics in cell biology. *J Cell Biol*. 2010;190:491-500.
174. Cravatt BF, Simon GM and Yates JR, 3rd. The biological impact of mass-spectrometry-based proteomics. *Nature*. 2007;450:991-1000.
175. Dunham WH, Mullin M and Gingras AC. Affinity-purification coupled to mass spectrometry: basic principles and strategies. *Proteomics*. 2012;12:1576-90.
176. Mellacheruvu D, Wright Z, Couzens AL, Lambert JP, St-Denis NA, Li T, Miteva YV, Hauri S, Sardiu ME, Low TY, Halim VA, Bagshaw RD, Hubner NC, Al-Hakim A, Bouchard A, Faubert D, Fermin D, Dunham WH, Goudreault M, Lin ZY, Badillo BG, Pawson T, Durocher D, Coulombe B, Aebersold R, Superti-Furga G, Colinge J, Heck AJ, Choi H, Gstaiger M, Mohammed S, Cristea IM, Bennett KL, Washburn MP, Raught B, Ewing RM, Gingras AC and Nesvizhskii AI. The CRAPome: a contaminant repository for affinity purification-mass spectrometry data. *Nat Methods*. 2013;10:730-6.
177. Barallobre-Barreiro J, Didangelos A, Yin X, Domenech N and Mayr M. A sequential extraction methodology for cardiac extracellular matrix prior to proteomics analysis. *Methods Mol Biol*. 2013;1005:215-23.
178. Didangelos A, Yin X and Mayr M. Method for protein subfractionation of cardiovascular tissues before DIGE analysis. *Methods Mol Biol*. 2012;854:287-97.
179. Matt P, Fu Z, Fu Q and Van Eyk JE. Biomarker discovery: proteome fractionation and separation in biological samples. *Physiol Genomics*. 2008;33:12-7.
180. Yates JR, 3rd, Gilchrist A, Howell KE and Bergeron JJ. Proteomics of organelles and large cellular structures. *Nat Rev Mol Cell Biol*. 2005;6:702-14.
181. Thakur SS, Geiger T, Chatterjee B, Bandilla P, Frohlich F, Cox J and Mann M. Deep and highly sensitive proteome coverage by LC-MS/MS without prefractionation. *Mol Cell Proteomics*. 2011;10:M110 003699.
182. Nilsson T, Mann M, Aebersold R, Yates JR, 3rd, Bairoch A and Bergeron JJ. Mass spectrometry in high-throughput proteomics: ready for the big time. *Nat Methods*. 2010;7:681-5.
183. Arrell DK, Neverova I and Van Eyk JE. Cardiovascular proteomics: evolution and potential. *Circ Res*. 2001;88:763-73.
184. Martens L and Apweiler R. Algorithms and databases. *Methods Mol Biol*. 2009;564:245-59.
185. Wittmann-Liebold B, Graack HR and Pohl T. Two-dimensional gel electrophoresis as tool for proteomics studies in combination with protein identification by mass spectrometry. *Proteomics*. 2006;6:4688-703.
186. Klose J. Protein mapping by combined isoelectric focusing and electrophoresis of mouse tissues. A novel approach to testing for induced point mutations in mammals. *Humangenetik*. 1975;26:231-43.
187. O'Farrell PH. High resolution two-dimensional electrophoresis of proteins. *J Biol Chem*. 1975;250:4007-21.
188. Gorg A, Weiss W and Dunn MJ. Current two-dimensional electrophoresis technology for proteomics. *Proteomics*. 2004;4:3665-85.
189. Kriegel K, Seefeldt I, Hoffmann F, Schultz C, Wenk C, Regitz-Zagrosek V, Oswald H and Fleck E. An alternative approach to deal with geometric uncertainties in computer analysis of two-dimensional electrophoresis gels. *Electrophoresis*. 2000;21:2637-40.

190. Unlu M, Morgan ME and Minden JS. Difference gel electrophoresis: a single gel method for detecting changes in protein extracts. *Electrophoresis*. 1997;18:2071-7.
191. Viswanathan S, Unlu M and Minden JS. Two-dimensional difference gel electrophoresis. *Nat Protoc*. 2006;1:1351-8.
192. Fenn JB, Mann M, Meng CK, Wong SF and Whitehouse CM. Electrospray ionization for mass spectrometry of large biomolecules. *Science*. 1989;246:64-71.
193. Karas M and Hillenkamp F. Laser desorption ionization of proteins with molecular masses exceeding 10,000 daltons. *Anal Chem*. 1988;60:2299-301.
194. Aebersold R and Mann M. Mass spectrometry-based proteomics. *Nature*. 2003;422:198-207.
195. Tang N, Tornatore P and Weinberger SR. Current developments in SELDI affinity technology. *Mass Spectrom Rev*. 2004;23:34-44.
196. Gillet LC, Leitner A and Aebersold R. Mass Spectrometry Applied to Bottom-Up Proteomics: Entering the High-Throughput Era for Hypothesis Testing. *Annu Rev Anal Chem (Palo Alto Calif)*. 2016;9:449-72.
197. Domon B and Aebersold R. Options and considerations when selecting a quantitative proteomics strategy. *Nat Biotechnol*. 2010;28:710-21.
198. Kellie JF, Tran JC, Lee JE, Ahlf DR, Thomas HM, Ntai I, Catherman AD, Durbin KR, Zamdborg L, Vellaichamy A, Thomas PM and Kelleher NL. The emerging process of Top Down mass spectrometry for protein analysis: biomarkers, protein-therapeutics, and achieving high throughput. *Mol Biosyst*. 2010;6:1532-9.
199. Nesvizhskii AI and Aebersold R. Interpretation of shotgun proteomic data: the protein inference problem. *Mol Cell Proteomics*. 2005;4:1419-40.
200. Perkins DN, Pappin DJ, Creasy DM and Cottrell JS. Probability-based protein identification by searching sequence databases using mass spectrometry data. *Electrophoresis*. 1999;20:3551-67.
201. Siepen JA, Keevil EJ, Knight D and Hubbard SJ. Prediction of missed cleavage sites in tryptic peptides aids protein identification in proteomics. *J Proteome Res*. 2007;6:399-408.
202. Wells JM and McLuckey SA. Collision-induced dissociation (CID) of peptides and proteins. *Methods Enzymol*. 2005;402:148-85.
203. Steen H and Mann M. The ABC's (and XYZ's) of peptide sequencing. *Nat Rev Mol Cell Biol*. 2004;5:699-711.
204. Medzihradszky KF and Chalkley RJ. Lessons in de novo peptide sequencing by tandem mass spectrometry. *Mass Spectrom Rev*. 2015;34:43-63.
205. Nesvizhskii AI. Protein identification by tandem mass spectrometry and sequence database searching. *Methods Mol Biol*. 2007;367:87-119.
206. Sadygov RG, Cociorva D and Yates JR, 3rd. Large-scale database searching using tandem mass spectra: looking up the answer in the back of the book. *Nat Methods*. 2004;1:195-202.
207. Eng JK, McCormack AL and Yates JR. An approach to correlate tandem mass spectral data of peptides with amino acid sequences in a protein database. *J Am Soc Mass Spectrom*. 1994;5:976-89.
208. Duncan DT, Craig R and Link AJ. Parallel tandem: a program for parallel processing of tandem mass spectra using PVM or MPI and X!Tandem. *J Proteome Res*. 2005;4:1842-7.
209. Ma B, Zhang K, Hendrie C, Liang C, Li M, Doherty-Kirby A and Lajoie G. PEAKS: powerful software for peptide de novo sequencing by tandem mass spectrometry. *Rapid Commun Mass Spectrom*. 2003;17:2337-42.
210. Bassols A, Costa C, Eckersall PD, Osada J, Sabria J and Tibau J. The pig as an animal model for human pathologies: A proteomics perspective. *Proteomics Clin Appl*. 2014;8:715-31.
211. Everett J and Kerr D. Changing from porcine to human insulin. *Drugs*. 1994;47:286-96.

212. Hather G, Higdon R, Bauman A, von Haller PD and Kolker E. Estimating false discovery rates for peptide and protein identification using randomized databases. *Proteomics*. 2010;10:2369-76.
213. Mirza SP. Quantitative mass spectrometry-based approaches in cardiovascular research. *Circ Cardiovasc Genet*. 2012;5:477.
214. Old WM, Meyer-Arendt K, Aveline-Wolf L, Pierce KG, Mendoza A, Sevinsky JR, Resing KA and Ahn NG. Comparison of label-free methods for quantifying human proteins by shotgun proteomics. *Mol Cell Proteomics*. 2005;4:1487-502.
215. Bantscheff M, Schirle M, Sweetman G, Rick J and Kuster B. Quantitative mass spectrometry in proteomics: a critical review. *Anal Bioanal Chem*. 2007;389:1017-31.
216. Ong SE, Blagoev B, Kratchmarova I, Kristensen DB, Steen H, Pandey A and Mann M. Stable isotope labeling by amino acids in cell culture, SILAC, as a simple and accurate approach to expression proteomics. *Mol Cell Proteomics*. 2002;1:376-86.
217. Kruger M, Moser M, Ussar S, Thievessen I, Luber CA, Forner F, Schmidt S, Zanivan S, Fassler R and Mann M. SILAC mouse for quantitative proteomics uncovers kindlin-3 as an essential factor for red blood cell function. *Cell*. 2008;134:353-64.
218. Doherty MK, Whitehead C, McCormack H, Gaskell SJ and Beynon RJ. Proteome dynamics in complex organisms: using stable isotopes to monitor individual protein turnover rates. *Proteomics*. 2005;5:522-33.
219. Mann M. Functional and quantitative proteomics using SILAC. *Nat Rev Mol Cell Biol*. 2006;7:952-8.
220. Thompson A, Schafer J, Kuhn K, Kienle S, Schwarz J, Schmidt G, Neumann T, Johnstone R, Mohammed AK and Hamon C. Tandem mass tags: a novel quantification strategy for comparative analysis of complex protein mixtures by MS/MS. *Anal Chem*. 2003;75:1895-904.
221. Ross PL, Huang YN, Marchese JN, Williamson B, Parker K, Hattan S, Khainovski N, Pillai S, Dey S, Daniels S, Purkayastha S, Juhasz P, Martin S, Bartlet-Jones M, He F, Jacobson A and Pappin DJ. Multiplexed protein quantitation in Saccharomyces cerevisiae using amine-reactive isobaric tagging reagents. *Mol Cell Proteomics*. 2004;3:1154-69.
222. Gygi SP, Rist B, Gerber SA, Turecek F, Gelb MH and Aebersold R. Quantitative analysis of complex protein mixtures using isotope-coded affinity tags. *Nat Biotechnol*. 1999;17:994-9.
223. Langley SR, Dwyer J, Drozdov I, Yin X and Mayr M. Proteomics: from single molecules to biological pathways. *Cardiovasc Res*. 2013;97:612-22.
224. Stewart, II, Thomson T and Figeys D. 18O labeling: a tool for proteomics. *Rapid Commun Mass Spectrom*. 2001;15:2456-65.
225. Mirza SP, Greene AS and Olivier M. 18O labeling over a coffee break: a rapid strategy for quantitative proteomics. *J Proteome Res*. 2008;7:3042-8.
226. Storms HF, van der Heijden R, Tjaden UR and van der Greef J. Considerations for proteolytic labeling-optimization of 18O incorporation and prohibition of back-exchange. *Rapid Commun Mass Spectrom*. 2006;20:3491-7.
227. Hicks WA, Halligan BD, Slyper RY, Twigger SN, Greene AS and Olivier M. Simultaneous quantification and identification using 18O labeling with an ion trap mass spectrometer and the analysis software application "ZoomQuant". *J Am Soc Mass Spectrom*. 2005;16:916-25.
228. Kuster B and Mann M. 18O-labeling of N-glycosylation sites to improve the identification of gel-separated glycoproteins using peptide mass mapping and database searching. *Anal Chem*. 1999;71:1431-40.
229. Picotti P, Bodenmiller B and Aebersold R. Proteomics meets the scientific method. *Nat Methods*. 2013;10:24-7.
230. Method of the Year 2012. *Nat Methods*. 2013;10:1.
231. Picotti P and Aebersold R. Selected reaction monitoring-based proteomics: workflows, potential, pitfalls and future directions. *Nat Methods*. 2012;9:555-66.

232. Picotti P, Rinner O, Stallmach R, Dautel F, Farrah T, Domon B, Wenschuh H and Aebersold R. High-throughput generation of selected reaction-monitoring assays for proteins and proteomes. *Nat Methods*. 2010;7:43-6.
233. Lange V, Picotti P, Domon B and Aebersold R. Selected reaction monitoring for quantitative proteomics: a tutorial. *Mol Syst Biol*. 2008;4:222.
234. Escher C, Reiter L, MacLean B, Ossola R, Herzog F, Chilton J, MacCoss MJ and Rinner O. Using iRT, a normalized retention time for more targeted measurement of peptides. *Proteomics*. 2012;12:1111-21.
235. Kusebauch U, Campbell DS, Deutsch EW, Chu CS, Spicer DA, Brusniak MY, Slagel J, Sun Z, Stevens J, Grimes B, Shteynberg D, Hoopmann MR, Blattmann P, Ratushny AV, Rinner O, Picotti P, Carapito C, Huang CY, Kapousouz M, Lam H, Tran T, Demir E, Aitchison JD, Sander C, Hood L, Aebersold R and Moritz RL. Human SRMAtlas: A Resource of Targeted Assays to Quantify the Complete Human Proteome. *Cell*. 2016;166:766-78.
236. Kennedy JJ, Abbatiello SE, Kim K, Yan P, Whiteaker JR, Lin C, Kim JS, Zhang Y, Wang X, Ivey RG, Zhao L, Min H, Lee Y, Yu MH, Yang EG, Lee C, Wang P, Rodriguez H, Kim Y, Carr SA and Paulovich AG. Demonstrating the feasibility of large-scale development of standardized assays to quantify human proteins. *Nat Methods*. 2014;11:149-55.
237. Peterson AC, Russell JD, Bailey DJ, Westphall MS and Coon JJ. Parallel reaction monitoring for high resolution and high mass accuracy quantitative, targeted proteomics. *Mol Cell Proteomics*. 2012;11:1475-88.
238. Kiseleva OI, Romashova YA, Moskaleva NE, Petushkova NA, Teryaeva NB, Belyaev AY and Lisitsa AV. Plasma preparation to measure FDA-approved protein markers by selected reaction monitoring. *Clin Transl Med*. 2015;4:32.
239. Gillette MA and Carr SA. Quantitative analysis of peptides and proteins in biomedicine by targeted mass spectrometry. *Nat Methods*. 2013;10:28-34.
240. Sajic T, Liu Y and Aebersold R. Using data-independent, high-resolution mass spectrometry in protein biomarker research: perspectives and clinical applications. *Proteomics Clin Appl*. 2015;9:307-21.
241. Bern M, Finney G, Hoopmann MR, Merrihew G, Toth MJ and MacCoss MJ. Deconvolution of mixture spectra from ion-trap data-independent-acquisition tandem mass spectrometry. *Anal Chem*. 2010;82:833-41.
242. Panchaud A, Jung S, Shaffer SA, Aitchison JD and Goodlett DR. Faster, quantitative, and accurate precursor acquisition independent from ion count. *Anal Chem*. 2011;83:2250-7.
243. Panchaud A, Scherl A, Shaffer SA, von Haller PD, Kulasekara HD, Miller SI and Goodlett DR. Precursor acquisition independent from ion count: how to dive deeper into the proteomics ocean. *Anal Chem*. 2009;81:6481-8.
244. Purvine S, Eppel JT, Yi EC and Goodlett DR. Shotgun collision-induced dissociation of peptides using a time of flight mass analyzer. *Proteomics*. 2003;3:847-50.
245. Venable JD, Dong MQ, Wohlschlegel J, Dillin A and Yates JR. Automated approach for quantitative analysis of complex peptide mixtures from tandem mass spectra. *Nat Methods*. 2004;1:39-45.
246. Gillet LC, Navarro P, Tate S, Rost H, Selevsek N, Reiter L, Bonner R and Aebersold R. Targeted data extraction of the MS/MS spectra generated by data-independent acquisition: a new concept for consistent and accurate proteome analysis. *Mol Cell Proteomics*. 2012;11:O111 016717.
247. Schmidlin T, Garrigues L, Lane CS, Mulder TC, van Doorn S, Post H, de Graaf EL, Lemeer S, Heck AJ and Altelaar AF. Assessment of SRM, MRM(3) , and DIA for the targeted analysis of phosphorylation dynamics in non-small cell lung cancer. *Proteomics*. 2016;16:2193-205.
248. Schubert OT, Gillet LC, Collins BC, Navarro P, Rosenberger G, Wolski WE, Lam H, Amodei D, Mallick P, MacLean B and Aebersold R. Building high-quality assay libraries for targeted analysis of SWATH MS data. *Nat Protoc*. 2015;10:426-41.

249. Guo T, Kouvonen P, Koh CC, Gillet LC, Wolski WE, Rost HL, Rosenberger G, Collins BC, Blum LC, Gillessen S, Joerger M, Jochum W and Aebersold R. Rapid mass spectrometric conversion of tissue biopsy samples into permanent quantitative digital proteome maps. *Nat Med*. 2015;21:407-13.
250. Zou Y, Dietrich H, Hu Y, Metzler B, Wick G and Xu Q. Mouse model of venous bypass graft arteriosclerosis. *Am J Pathol*. 1998;153:1301-10.
251. Keller A, Nesvizhskii AI, Kolker E and Aebersold R. Empirical statistical model to estimate the accuracy of peptide identifications made by MS/MS and database search. *Analytical chemistry*. 2002;74:5383-92.
252. Nesvizhskii AI, Keller A, Kolker E and Aebersold R. A statistical model for identifying proteins by tandem mass spectrometry. *Analytical chemistry*. 2003;75:4646-58.
253. Barallobre-Barreiro J, Didangelos A, Schoendube FA, Drozdov I, Yin X, Fernandez-Caggiano M, Willeit P, Puntmann VO, Aldama-Lopez G, Shah AM, Domenech N and Mayr M. Proteomics analysis of cardiac extracellular matrix remodeling in a porcine model of ischemia/reperfusion injury. *Circulation*. 2012;125:789-802.
254. Cuello F, Shankar-Hari M, Mayr U, Yin X, Marshall M, Suna G, Willeit P, Langley SR, Jayawardhana T, Zeller T, Terblanche M, Shah AM and Mayr M. Redox state of pentraxin 3 as a novel biomarker for resolution of inflammation and survival in sepsis. *Mol Cell Proteomics*. 2014;13:2545-57.
255. Alberts B, Bray D, Hopkin K, Johnson A, Lewis J, Raff M, Roberts K and Walter P. Manipulating Proteins, DNA, and RNA. In: B. Alberts, J. Wilson and T. Hunt, eds. *Molecular Biology of the Cell*; 2008.
256. Livak KJ and Schmittgen TD. Analysis of relative gene expression data using real-time quantitative PCR and the 2(-Delta Delta C(T)) Method. *Methods*. 2001;25:402-8.
257. McDonald RA, Halliday CA, Miller AM, Diver LA, Dakin RS, Montgomery J, McBride MW, Kennedy S, McClure JD, Robertson KE, Douglas G, Channon KM, Oldroyd KG and Baker AH. Reducing In-Stent Restenosis: Therapeutic Manipulation of miRNA in Vascular Remodeling and Inflammation. *J Am Coll Cardiol*. 2015;65:2314-27.
258. McDonald RA, White KM, Wu J, Cooley BC, Robertson KE, Halliday CA, McClure JD, Francis S, Lu R, Kennedy S, George SJ, Wan S, van Rooij E and Baker AH. miRNA-21 is dysregulated in response to vein grafting in multiple models and genetic ablation in mice attenuates neointima formation. *Eur Heart J*. 2013;34:1636-43.
259. Cooper ST and Attie AD. Pig apolipoprotein R: a new member of the short consensus repeat family of proteins. *Biochemistry*. 1992;31:12328-36.
260. Yamamoto K, Owen K, Parker AE, Scilabra SD, Dudhia J, Strickland DK, Troeberg L and Nagase H. Low density lipoprotein receptor-related protein 1 (LRP1)-mediated endocytic clearance of a disintegrin and metalloproteinase with thrombospondin motifs-4 (ADAMTS-4): functional differences of non-catalytic domains of ADAMTS-4 and ADAMTS-5 in LRP1 binding. *J Biol Chem*. 2014;289:6462-74.
261. Yamamoto K, Troeberg L, Scilabra SD, Pelosi M, Murphy CL, Strickland DK and Nagase H. LRP-1-mediated endocytosis regulates extracellular activity of ADAMTS-5 in articular cartilage. *FASEB J*. 2013;27:511-21.
262. Didangelos A, Mayr U, Monaco C and Mayr M. Novel role of ADAMTS-5 protein in proteoglycan turnover and lipoprotein retention in atherosclerosis. *J Biol Chem*. 2012;287:19341-5.
263. Virmani R, Kolodgie FD, Farb A and Lafont A. Drug eluting stents: are human and animal studies comparable? *Heart*. 2003;89:133-8.
264. Schwartz RS, Chronos NA and Virmani R. Preclinical restenosis models and drug-eluting stents: still important, still much to learn. *J Am Coll Cardiol*. 2004;44:1373-85.
265. Farb A, Sangiorgi G, Carter AJ, Walley VM, Edwards WD, Schwartz RS and Virmani R. Pathology of acute and chronic coronary stenting in humans. *Circulation*. 1999;99:44-52.
266. Kim JS, Afari ME, Ha J, Tellez A, Milewski K, Conditt G, Cheng Y, Hua Yi G, Kaluza GL and Granada JF. Neointimal patterns obtained by optical coherence

tomography correlate with specific histological components and neointimal proliferation in a swine model of restenosis. *Eur Heart J Cardiovasc Imaging*. 2014;15:292-8.
267. Gareri C, De Rosa S and Indolfi C. MicroRNAs for Restenosis and Thrombosis After Vascular Injury. *Circ Res*. 2016;118:1170-84.
268. Liu X, Cheng Y, Yang J, Xu L and Zhang C. Cell-specific effects of miR-221/222 in vessels: molecular mechanism and therapeutic application. *J Mol Cell Cardiol*. 2012;52:245-55.
269. Wang D, Deuse T, Stubbendorff M, Chernogubova E, Erben RG, Eken SM, Jin H, Li Y, Busch A, Heeger CH, Behnisch B, Reichenspurner H, Robbins RC, Spin JM, Tsao PS, Schrepfer S and Maegdefessel L. Local MicroRNA Modulation Using a Novel Anti-miR-21-Eluting Stent Effectively Prevents Experimental In-Stent Restenosis. *Arterioscler Thromb Vasc Biol*. 2015;35:1945-53.
270. Barallobre-Barreiro J, Oklu R, Lynch M, Fava M, Baig F, Yin X, Barwari T, Potier DN, Albadawi H, Jahangiri M, Porter KE, Watkins MT, Misra S, Stoughton J and Mayr M. Extracellular matrix remodelling in response to venous hypertension: proteomics of human varicose veins. *Cardiovasc Res*. 2016;110:419-30.
271. Aebersold R and Mann M. Mass-spectrometric exploration of proteome structure and function. *Nature*. 2016;537:347-55.
272. Apweiler R, Bairoch A and Wu CH. Protein sequence databases. *Current opinion in chemical biology*. 2004;8:76-80.
273. Otsuka F, Sakakura K, Yahagi K, Joner M and Virmani R. Has our understanding of calcification in human coronary atherosclerosis progressed? *Arterioscler Thromb Vasc Biol*. 2014;34:724-36.
274. Shanahan CM, Crouthamel MH, Kapustin A and Giachelli CM. Arterial calcification in chronic kidney disease: key roles for calcium and phosphate. *Circ Res*. 2011;109:697-711.
275. Speer MY, Yang HY, Brabb T, Leaf E, Look A, Lin WL, Frutkin A, Dichek D and Giachelli CM. Smooth muscle cells give rise to osteochondrogenic precursors and chondrocytes in calcifying arteries. *Circ Res*. 2009;104:733-41.
276. Luo G, Ducy P, McKee MD, Pinero GJ, Loyer E, Behringer RR and Karsenty G. Spontaneous calcification of arteries and cartilage in mice lacking matrix GLA protein. *Nature*. 1997;386:78-81.
277. Schurgers LJ, Cranenburg EC and Vermeer C. Matrix Gla-protein: the calcification inhibitor in need of vitamin K. *Thromb Haemost*. 2008;100:593-603.
278. Tian H, Li CS, Zhao KW, Wang JC, Duarte ME, David CL, Phan K, Atti E, Brochmann EJ and Murray SS. A carboxy terminal BMP/TGF-beta binding site in secreted phosphoprotein 24 kD independently affects BMP-2 activity. *J Cell Biochem*. 2015;116:667-76.
279. Zhao Y, Zhao MM, Cai Y, Zheng MF, Sun WL, Zhang SY, Kong W, Gu J, Wang X and Xu MJ. Mammalian target of rapamycin signaling inhibition ameliorates vascular calcification via Klotho upregulation. *Kidney Int*. 2015;88:711-21.
280. Xie Y, Jin Y, Merenick BL, Ding M, Fetalvero KM, Wagner RJ, Mai A, Gleim S, Tucker DF, Birnbaum MJ, Ballif BA, Luciano AK, Sessa WC, Rzucidlo EM, Powell RJ, Hou L, Zhao H, Hwa J, Yu J and Martin KA. Phosphorylation of GATA-6 is required for vascular smooth muscle cell differentiation after mTORC1 inhibition. *Sci Signal*. 2015;8:ra44.
281. Haglund L, Tillgren V, Onnerfjord P and Heinegard D. The C-terminal peptide of chondroadherin modulates cellular activity by selectively binding to heparan sulfate chains. *J Biol Chem*. 2013;288:995-1008.
282. Akhatib B, Onnerfjord P, Gawri R, Ouellet J, Jarzem P, Heinegard D, Mort J, Roughley P and Haglund L. Chondroadherin fragmentation mediated by the protease HTRA1 distinguishes human intervertebral disc degeneration from normal aging. *J Biol Chem*. 2013;288:19280-7.
283. Levula M, Oksala N, Airla N, Zeitlin R, Salenius JP, Jarvinen O, Venermo M, Partio T, Saarinen J, Somppi T, Suominen V, Virkkunen J, Hautalahti J, Laaksonen R, Kahonen

M, Mennander A, Kytomaki L, Soini JT, Parkkinen J, Pelto-Huikko M and Lehtimaki T. Genes involved in systemic and arterial bed dependent atherosclerosis--Tampere Vascular study. *PLoS One*. 2012;7:e33787.
284. Grewe PH, Deneke T, Machraoui A, Barmeyer J and Muller KM. Acute and chronic tissue response to coronary stent implantation: pathologic findings in human specimen. *J Am Coll Cardiol*. 2000;35:157-63.
285. Fornai F, Carrizzo A, Forte M, Ambrosio M, Damato A, Ferrucci M, Biagioni F, Busceti C, Puca AA and Vecchione C. The inflammatory protein Pentraxin 3 in cardiovascular disease. *Immun Ageing*. 2016;13:25.
286. Arias M, Hoffarth ER, Ishida H, Aramini JM and Vogel HJ. Recombinant expression, antimicrobial activity and mechanism of action of tritrpticin analogs containing fluoro-tryptophan residues. *Biochim Biophys Acta*. 2016;1858:1012-23.
287. Burster T, Macmillan H, Hou T, Boehm BO and Mellins ED. Cathepsin G: roles in antigen presentation and beyond. *Mol Immunol*. 2010;47:658-65.
288. Liuzzo G, Buffon A, Biasucci LM, Gallimore JR, Caligiuri G, Vitelli A, Altamura S, Ciliberto G, Rebuzzi AG, Crea F, Pepys MB and Maseri A. Enhanced inflammatory response to coronary angioplasty in patients with severe unstable angina. *Circulation*. 1998;98:2370-6.
289. Ait-Oufella H, Kinugawa K, Zoll J, Simon T, Boddaert J, Heeneman S, Blanc-Brude O, Barateau V, Potteaux S, Merval R, Esposito B, Teissier E, Daemen MJ, Leseche G, Boulanger C, Tedgui A and Mallat Z. Lactadherin deficiency leads to apoptotic cell accumulation and accelerated atherosclerosis in mice. *Circulation*. 2007;115:2168-77.
290. Raymond A, Ensslin MA and Shur BD. SED1/MFG-E8: a bi-motif protein that orchestrates diverse cellular interactions. *J Cell Biochem*. 2009;106:957-66.
291. Tsimikas S, Lau HK, Han KR, Shortal B, Miller ER, Segev A, Curtiss LK, Witztum JL and Strauss BH. Percutaneous coronary intervention results in acute increases in oxidized phospholipids and lipoprotein(a): short-term and long-term immunologic responses to oxidized low-density lipoprotein. *Circulation*. 2004;109:3164-70.
292. Farooq V, Serruys PW, Heo JH, Gogas BD, Onuma Y, Perkins LE, Diletti R, Radu MD, Raber L, Bourantas CV, Zhang Y, van Remortel E, Pawar R, Rapoza RJ, Powers JC, van Beusekom HM, Garcia-Garcia HM and Virmani R. Intracoronary optical coherence tomography and histology of overlapping everolimus-eluting bioresorbable vascular scaffolds in a porcine coronary artery model: the potential implications for clinical practice. *JACC Cardiovasc Interv*. 2013;6:523-32.
293. Jahanyar J, Joyce DL, Southard RE, Loebe M, Noon GP, Koerner MM, Torre-Amione G and Youker KA. Decorin-mediated transforming growth factor-beta inhibition ameliorates adverse cardiac remodeling. *J Heart Lung Transplant*. 2007;26:34-40.
294. Yamakawa T, Bai HZ, Masuda J, Sawa Y, Shirakura R, Ogata J and Matsuda H. Differential expression of proteoglycans biglycan and decorin during neointima formation after stent implantation in normal and atherosclerotic rabbit aortas. *Atherosclerosis*. 2000;152:287-97.
295. Schellings MW, Vanhoutte D, Swinnen M, Cleutjens JP, Debets J, van Leeuwen RE, d'Hooge J, Van de Werf F, Carmeliet P, Pinto YM, Sage EH and Heymans S. Absence of SPARC results in increased cardiac rupture and dysfunction after acute myocardial infarction. *J Exp Med*. 2009;206:113-23.
296. Neame PJ and Barry FP. The link proteins. *EXS*. 1994;70:53-72.
297. Aspberg A. The different roles of aggrecan interaction domains. *J Histochem Cytochem*. 2012;60:987-96.
298. Kiani C, Chen L, Wu YJ, Yee AJ and Yang BB. Structure and function of aggrecan. *Cell Res*. 2002;12:19-32.
299. Kiani C, Lee V, Cao L, Chen L, Wu Y, Zhang Y, Adams ME and Yang BB. Roles of aggrecan domains in biosynthesis, modification by glycosaminoglycans and product secretion. *Biochem J*. 2001;354:199-207.

300. Suttkus A, Rohn S, Weigel S, Glockner P, Arendt T and Morawski M. Aggrecan, link protein and tenascin-R are essential components of the perineuronal net to protect neurons against iron-induced oxidative stress. *Cell Death Dis*. 2014;5:e1119.
301. Danielson BT, Knudson CB and Knudson W. Extracellular processing of the cartilage proteoglycan aggregate and its effect on CD44-mediated internalization of hyaluronan. *J Biol Chem*. 2015;290:9555-70.
302. Arner EC. Aggrecanase-mediated cartilage degradation. *Curr Opin Pharmacol*. 2002;2:322-9.
303. Huang K and Wu LD. Aggrecanase and aggrecan degradation in osteoarthritis: a review. *J Int Med Res*. 2008;36:1149-60.
304. Lark MW, Bayne EK, Flanagan J, Harper CF, Hoerrner LA, Hutchinson NI, Singer, II, Donatelli SA, Weidner JR, Williams HR, Mumford RA and Lohmander LS. Aggrecan degradation in human cartilage. Evidence for both matrix metalloproteinase and aggrecanase activity in normal, osteoarthritic, and rheumatoid joints. *J Clin Invest*. 1997;100:93-106.
305. Sandy JD. A contentious issue finds some clarity: on the independent and complementary roles of aggrecanase activity and MMP activity in human joint aggrecanolysis. *Osteoarthritis Cartilage*. 2006;14:95-100.
306. Little CB, Flannery CR, Hughes CE, Mort JS, Roughley PJ, Dent C and Caterson B. Aggrecanase versus matrix metalloproteinases in the catabolism of the interglobular domain of aggrecan in vitro. *Biochem J*. 1999;344 Pt 1:61-8.
307. Tortorella MD, Pratta M, Liu RQ, Austin J, Ross OH, Abbaszade I, Burn T and Arner E. Sites of aggrecan cleavage by recombinant human aggrecanase-1 (ADAMTS-4). *J Biol Chem*. 2000;275:18566-73.
308. Stanton H, Rogerson FM, East CJ, Golub SB, Lawlor KE, Meeker CT, Little CB, Last K, Farmer PJ, Campbell IK, Fourie AM and Fosang AJ. ADAMTS5 is the major aggrecanase in mouse cartilage in vivo and in vitro. *Nature*. 2005;434:648-52.
309. Song RH, Tortorella MD, Malfait AM, Alston JT, Yang Z, Arner EC and Griggs DW. Aggrecan degradation in human articular cartilage explants is mediated by both ADAMTS-4 and ADAMTS-5. *Arthritis Rheum*. 2007;56:575-85.
310. Yamanishi Y, Boyle DL, Clark M, Maki RA, Tortorella MD, Arner EC and Firestein GS. Expression and regulation of aggrecanase in arthritis: the role of TGF-beta. *J Immunol*. 2002;168:1405-12.
311. Rodriguez-Manzaneque JC, Westling J, Thai SN, Luque A, Knauper V, Murphy G, Sandy JD and Iruela-Arispe ML. ADAMTS1 cleaves aggrecan at multiple sites and is differentially inhibited by metalloproteinase inhibitors. *Biochem Biophys Res Commun*. 2002;293:501-8.
312. Little CB, Mittaz L, Belluoccio D, Rogerson FM, Campbell IK, Meeker CT, Bateman JF, Pritchard MA and Fosang AJ. ADAMTS-1-knockout mice do not exhibit abnormalities in aggrecan turnover in vitro or in vivo. *Arthritis Rheum*. 2005;52:1461-72.
313. Heinegard D and Saxne T. The role of the cartilage matrix in osteoarthritis. *Nat Rev Rheumatol*. 2011;7:50-6.
314. Wu YJ, La Pierre DP, Wu J, Yee AJ and Yang BB. The interaction of versican with its binding partners. *Cell Res*. 2005;15:483-94.
315. Olin AI, Morgelin M, Sasaki T, Timpl R, Heinegard D and Aspberg A. The proteoglycans aggrecan and Versican form networks with fibulin-2 through their lectin domain binding. *J Biol Chem*. 2001;276:1253-61.
316. Tabas I, Williams KJ and Boren J. Subendothelial lipoprotein retention as the initiating process in atherosclerosis: update and therapeutic implications. *Circulation*. 2007;116:1832-44.
317. Williams KJ. Arterial wall chondroitin sulfate proteoglycans: diverse molecules with distinct roles in lipoprotein retention and atherogenesis. *Curr Opin Lipidol*. 2001;12:477-87.

318. Strom A, Ahlqvist E, Franzen A, Heinegard D and Hultgardh-Nilsson A. Extracellular matrix components in atherosclerotic arteries of Apo E/LDL receptor deficient mice: an immunohistochemical study. *Histol Histopathol*. 2004;19:337-47.
319. Talusan P, Bedri S, Yang S, Kattapuram T, Silva N, Roughley PJ and Stone JR. Analysis of intimal proteoglycans in atherosclerosis-prone and atherosclerosis-resistant human arteries by mass spectrometry. *Mol Cell Proteomics*. 2005;4:1350-7.
320. Snorradottir AO, Isaksson HJ, Kaeser SA, Skodras AA, Olafsson E, Palsdottir A and Bragason BT. Deposition of collagen IV and aggrecan in leptomeningeal arteries of hereditary brain haemorrhage with amyloidosis. *Brain Res*. 2013;1535:106-14.
321. Kumar S, Chen M, Li Y, Wong FH, Thiam CW, Hossain MZ, Poh KK, Hirohata S, Ogawa H, Angeli V and Ge R. Loss of ADAMTS4 reduces high fat diet-induced atherosclerosis and enhances plaque stability in ApoE(-/-) mice. *Sci Rep*. 2016;6:31130.
322. Sandy JD, Westling J, Kenagy RD, Iruela-Arispe ML, Verscharen C, Rodriguez-Mazaneque JC, Zimmermann DR, Lemire JM, Fischer JW, Wight TN and Clowes AW. Versican V1 proteolysis in human aorta in vivo occurs at the Glu441-Ala442 bond, a site that is cleaved by recombinant ADAMTS-1 and ADAMTS-4. *J Biol Chem*. 2001;276:13372-8.
323. Vazquez F, Hastings G, Ortega MA, Lane TF, Oikemus S, Lombardo M and Iruela-Arispe ML. METH-1, a human ortholog of ADAMTS-1, and METH-2 are members of a new family of proteins with angio-inhibitory activity. *J Biol Chem*. 1999;274:23349-57.
324. Luque A, Carpizo DR and Iruela-Arispe ML. ADAMTS1/METH1 inhibits endothelial cell proliferation by direct binding and sequestration of VEGF165. *J Biol Chem*. 2003;278:23656-65.
325. Fu Y, Nagy JA, Brown LF, Shih SC, Johnson PY, Chan CK, Dvorak HF and Wight TN. Proteolytic cleavage of versican and involvement of ADAMTS-1 in VEGF-A/VPF-induced pathological angiogenesis. *J Histochem Cytochem*. 2011;59:463-73.
326. Oller J, Mendez-Barbero N, Ruiz EJ, Villahoz S, Renard M, Canelas LI, Briones AM, Alberca R, Lozano-Vidal N, Hurle MA, Milewicz D, Evangelista A, Salaices M, Nistal JF, Jimenez-Borreguero LJ, De Backer J, Campanero MR and Redondo JM. Nitric oxide mediates aortic disease in mice deficient in the metalloprotease Adamts1 and in a mouse model of Marfan syndrome. *Nat Med*. 2017;23:200-212.
327. Partovian C, Ju R, Zhuang ZW, Martin KA and Simons M. Syndecan-4 regulates subcellular localization of mTOR Complex2 and Akt activation in a PKCalpha-dependent manner in endothelial cells. *Mol Cell*. 2008;32:140-9.
328. van Beusekom HM, Whelan DM, Hofma SH, Krabbendam SC, van Hinsbergh VW, Verdouw PD and van der Giessen WJ. Long-term endothelial dysfunction is more pronounced after stenting than after balloon angioplasty in porcine coronary arteries. *J Am Coll Cardiol*. 1998;32:1109-17.
329. Joner M, Nakazawa G, Finn AV, Quee SC, Coleman L, Acampado E, Wilson PS, Skorija K, Cheng Q, Xu X, Gold HK, Kolodgie FD and Virmani R. Endothelial cell recovery between comparator polymer-based drug-eluting stents. *J Am Coll Cardiol*. 2008;52:333-42.
330. Hofma SH, van der Giessen WJ, van Dalen BM, Lemos PA, McFadden EP, Sianos G, Ligthart JM, van Essen D, de Feyter PJ and Serruys PW. Indication of long-term endothelial dysfunction after sirolimus-eluting stent implantation. *Eur Heart J*. 2006;27:166-70.
331. Togni M, Windecker S, Cocchia R, Wenaweser P, Cook S, Billinger M, Meier B and Hess OM. Sirolimus-eluting stents associated with paradoxic coronary vasoconstriction. *J Am Coll Cardiol*. 2005;46:231-6.
332. Tortorella MD, Arner EC, Hills R, Gormley J, Fok K, Pegg L, Munie G and Malfait AM. ADAMTS-4 (aggrecanase-1): N-terminal activation mechanisms. *Arch Biochem Biophys*. 2005;444:34-44.
333. Longpre JM and Leduc R. Identification of prodomain determinants involved in ADAMTS-1 biosynthesis. *J Biol Chem*. 2004;279:33237-45.

334. Wang P, Tortorella M, England K, Malfait AM, Thomas G, Arner EC and Pei D. Proprotein convertase furin interacts with and cleaves pro-ADAMTS4 (Aggrecanase-1) in the trans-Golgi network. *J Biol Chem*. 2004;279:15434-40.
335. Longpre JM, McCulloch DR, Koo BH, Alexander JP, Apte SS and Leduc R. Characterization of proADAMTS5 processing by proprotein convertases. *Int J Biochem Cell Biol*. 2009;41:1116-26.
336. Malfait AM, Arner EC, Song RH, Alston JT, Markosyan S, Staten N, Yang Z, Griggs DW and Tortorella MD. Proprotein convertase activation of aggrecanases in cartilage in situ. *Arch Biochem Biophys*. 2008;478:43-51.
337. Kashiwagi M, Tortorella M, Nagase H and Brew K. TIMP-3 is a potent inhibitor of aggrecanase 1 (ADAM-TS4) and aggrecanase 2 (ADAM-TS5). *J Biol Chem*. 2001;276:12501-4.
338. Gendron C, Kashiwagi M, Hughes C, Caterson B and Nagase H. TIMP-3 inhibits aggrecanase-mediated glycosaminoglycan release from cartilage explants stimulated by catabolic factors. *FEBS Lett*. 2003;555:431-6.
339. Morris KJ, Cs-Szabo G and Cole AA. Characterization of TIMP-3 in human articular talar cartilage. *Connect Tissue Res*. 2010;51:478-90.
340. Sahebjam S, Khokha R and Mort JS. Increased collagen and aggrecan degradation with age in the joints of Timp3(-/-) mice. *Arthritis Rheum*. 2007;56:905-9.
341. Basu R, Lee J, Morton JS, Takawale A, Fan D, Kandalam V, Wang X, Davidge ST and Kassiri Z. TIMP3 is the primary TIMP to regulate agonist-induced vascular remodelling and hypertension. *Cardiovasc Res*. 2013;98:360-71.
342. Casagrande V, Menghini R, Menini S, Marino A, Marchetti V, Cavalera M, Fabrizi M, Hribal ML, Pugliese G, Gentileschi P, Schillaci O, Porzio O, Lauro D, Sbraccia P, Lauro R and Federici M. Overexpression of tissue inhibitor of metalloproteinase 3 in macrophages reduces atherosclerosis in low-density lipoprotein receptor knockout mice. *Arterioscler Thromb Vasc Biol*. 2012;32:74-81.
343. Overton CD, Yancey PG, Major AS, Linton MF and Fazio S. Deletion of macrophage LDL receptor-related protein increases atherogenesis in the mouse. *Circ Res*. 2007;100:670-7.
344. Scilabra SD, Troeberg L, Yamamoto K, Emonard H, Thogersen I, Enghild JJ, Strickland DK and Nagase H. Differential regulation of extracellular tissue inhibitor of metalloproteinases-3 levels by cell membrane-bound and shed low density lipoprotein receptor-related protein 1. *J Biol Chem*. 2013;288:332-42.
345. Muratoglu SC, Belgrave S, Hampton B, Migliorini M, Coksaygan T, Chen L, Mikhailenko I and Strickland DK. LRP1 protects the vasculature by regulating levels of connective tissue growth factor and HtrA1. *Arterioscler Thromb Vasc Biol*. 2013;33:2137-46.
346. Scilabra SD, Yamamoto K, Pigoni M, Sakamoto K, Muller SA, Papadopoulou A, Lichtenthaler SF, Troeberg L, Nagase H and Kadomatsu K. Dissecting the interaction between tissue inhibitor of metalloproteinases-3 (TIMP-3) and low density lipoprotein receptor-related protein-1 (LRP-1): Development of a "TRAP" to increase levels of TIMP-3 in the tissue. *Matrix Biol*. 2016.
347. Doherty CM, Visse R, Dinakarpandian D, Strickland DK, Nagase H and Troeberg L. Engineered Tissue Inhibitor of Metalloproteinases-3 Variants Resistant to Endocytosis Have Prolonged Chondroprotective Activity. *J Biol Chem*. 2016;291:22160-22172.
348. Ariyoshi W, Knudson CB, Luo N, Fosang AJ and Knudson W. Internalization of aggrecan G1 domain neoepitope ITEGE in chondrocytes requires CD44. *J Biol Chem*. 2010;285:36216-24.
349. Czipri M, Otto JM, Cs-Szabo G, Kamath RV, Vermes C, Firneisz G, Kolman KJ, Watanabe H, Li Y, Roughley PJ, Yamada Y, Olsen BR and Glant TT. Genetic rescue of chondrodysplasia and the perinatal lethal effect of cartilage link protein deficiency. *J Biol Chem*. 2003;278:39214-23.
350. Seok J, Warren HS, Cuenca AG, Mindrinos MN, Baker HV, Xu W, Richards DR, McDonald-Smith GP, Gao H, Hennessy L, Finnerty CC, Lopez CM, Honari S, Moore EE,

Minei JP, Cuschieri J, Bankey PE, Johnson JL, Sperry J, Nathens AB, Billiar TR, West MA, Jeschke MG, Klein MB, Gamelli RL, Gibran NS, Brownstein BH, Miller-Graziano C, Calvano SE, Mason PH, Cobb JP, Rahme LG, Lowry SF, Maier RV, Moldawer LL, Herndon DN, Davis RW, Xiao W, Tompkins RG, Inflammation and Host Response to Injury LSCRP. Genomic responses in mouse models poorly mimic human inflammatory diseases. *Proc Natl Acad Sci U S A*. 2013;110:3507-12.

351. Vlachopoulos C, Aznaouridis K and Stefanadis C. Prediction of cardiovascular events and all-cause mortality with arterial stiffness: a systematic review and meta-analysis. *J Am Coll Cardiol*. 2010;55:1318-27.

352. Mancia G, Fagard R, Narkiewicz K, Redon J, Zanchetti A, Bohm M, Christiaens T, Cifkova R, De Backer G, Dominiczak A, Galderisi M, Grobbee DE, Jaarsma T, Kirchhof P, Kjeldsen SE, Laurent S, Manolis AJ, Nilsson PM, Ruilope LM, Schmieder RE, Sirnes PA, Sleight P, Viigimaa M, Waeber B, Zannad F, Redon J, Dominiczak A, Narkiewicz K, Nilsson PM, Burnier M, Viigimaa M, Ambrosioni E, Caufield M, Coca A, Olsen MH, Schmieder RE, Tsioufis C, van de Borne P, Zamorano JL, Achenbach S, Baumgartner H, Bax JJ, Bueno H, Dean V, Deaton C, Erol C, Fagard R, Ferrari R, Hasdai D, Hoes AW, Kirchhof P, Knuuti J, Kolh P, Lancellotti P, Linhart A, Nihoyannopoulos P, Piepoli MF, Ponikowski P, Sirnes PA, Tamargo JL, Tendera M, Torbicki A, Wijns W, Windecker S, Clement DL, Coca A, Gillebert TC, Tendera M, Rosei EA, Ambrosioni E, Anker SD, Bauersachs J, Hitij JB, Caulfield M, De Buyzere M, De Geest S, Derumeaux GA, Erdine S, Farsang C, Funck-Brentano C, Gerc V, Germano G, Gielen S, Haller H, Hoes AW, Jordan J, Kahan T, Komajda M, Lovic D, Mahrholdt H, Olsen MH, Ostergren J, Parati G, Perk J, Polonia J, Popescu BA, Reiner Z, Ryden L, Sirenko Y, Stanton A, Struijker-Boudier H, Tsioufis C, van de Borne P, Vlachopoulos C, Volpe M and Wood DA. 2013 ESH/ESC guidelines for the management of arterial hypertension: the Task Force for the Management of Arterial Hypertension of the European Society of Hypertension (ESH) and of the European Society of Cardiology (ESC). *Eur Heart J*. 2013;34:2159-219.

353. Abonnenc M, Nabeebaccus AA, Mayr U, Barallobre-Barreiro J, Dong X, Cuello F, Sur S, Drozdov I, Langley SR, Lu R, Stathopoulou K, Didangelos A, Yin X, Zimmermann WH, Shah AM, Zampetaki A and Mayr M. Extracellular matrix secretion by cardiac fibroblasts: role of microRNA-29b and microRNA-30c. *Circ Res*. 2013;113:1138-47.

354. Zampetaki A, Attia R, Mayr U, Gomes RS, Phinikaridou A, Yin X, Langley SR, Willeit P, Lu R, Fanshawe B, Fava M, Barallobre-Barreiro J, Molenaar C, So PW, Abbas A, Jahangiri M, Waltham M, Botnar R, Smith A and Mayr M. Role of miR-195 in aortic aneurysmal disease. *Circ Res*. 2014;115:857-66.

12 CURRICULUM VITAE

Education

10/2013-	PhD student, Cardiovascular Division, King's College London, UK
06/2013	Successfully passed the Swiss Board Examination in General Internal Medicine to attain the title as specialist in Internal Medicine
08/2009-04/2010	Diploma thesis in Glycoimmunology at Max Planck Institute of Colloids and Interfaces; Department of Biomolecular Systems, Berlin, Germany.
10/2004-10/2010	MD, Medical study at Innsbruck and Vienna Medical University, Austria and at Charité Universitätsmedizin Berlin, Germany (ERASMUS)

Previous employment

07/2011-09/2013	Registrar in the Department of Internal Medicine in Cantonal hospital Baden, Switzerland; including rotations in the Emergency Department, Intermediate care and Intensive care.
01-06/2011	Registrar in the Department of Internal Medicine in the University Hospital Zurich, Switzerland; Outpatient clinic for pulmonary hypertension
2007-2009	Instructor for Medical Physiology at the Medical University Innsbruck

Selected trainings

02/2016	Diploma in Mountain Medicine of the Swiss Society of Mountain Medicine, Switzerland
08/2014	Good Clinical Practice and the Medicines for Human Use (Clinical Trials) Regulations at King's Health Partners Clinical Trials Office, UK
06/2014	Cardiovascular Magnetic Resonance (SCMR level I course) at the Department of Cardiovascular Imaging, St Thomas' Hospital, UK
01/2013	Advanced Cardiac Life Support (ACLS) Course of the American Heart Association (AHA)
11/2012	Fundamental Critical Care Support (FCCS) Course of the Society of Critical Care Medicine

06/2011	Basic Course of Ultrasound Abdomen of the Swiss Society of Ultrasound in Medicine (SGUM)
01/2011	Pulmonary Arterial Hypertension (PAH) University Course at Hôpital Antoine Béclère, South Paris University, Clamart, France

Presentations at congresses within this PhD

09/2016+09/2014	Poster presentation at the British Atherosclerosis Society Autumn meeting 2014 and 2016, Cambridge, UK
07/2016	Poster presentation at the Frontiers in CardioVascular Biology 2016 of the European Society of Cardiology (ESC), Florence, Italy
05/2016	Oral presentation at the BHF Symposium 2016, London, UK
11/2015	Poster presentation at the AHA Scientific Sessions in Orlando, USA
06/2015	Poster presentation at the Basic Science Summer School of the ESC in Sophia Antipolis, France
04/2015	Poster presentation at the BHF Symposium 2015, London, UK
09/2014	Poster presentation at the BHF and JCI Symposium 2014: Recent Advances in Heart Failure, London, UK
07/2014	Poster presentation at the Stratified Medicine Symposium, London, UK
06/2014	Poster presentation at the Cardiac Regeneration and Vascular Biology meeting in San Servolo, Italy

Awards and prizes

11/2015	Functional Genomics and Translational Biology (FGTB) International Travel Grant to the AHA Scientific Sessions, Orlando (FL), USA
11/2015	Conference Fund Grant of the Postgraduate School, King's College London, UK
06/2015	Poster award (3rd prize) at the Basic Science Summer School of the ESC, Sophia Antipolis, France
07/2014	Best poster award at the Stratified Medicine Symposium, London, UK

Teaching

10/2013 – 07/2016	Proteomics workshops for master students at King's College London, UK
05 - 07/2015	Weekly bedside teaching of third year medical students at King's College Hospital London, UK

10/2014 - 10/2015 Objective Structured Clinical Examinations (OSCE) of medical students at King's College London, UK

03/2007 - 05/2009 Medical Physiology for second year medical students at Innsbruck Medical University, Austria

Publications

In revision

1. **Suna G**, Wojakowski W, Lynch M, Barallobre-Barreiro J, Yin X, Mayr U, Baig F, Lu R, Kwan S, Molenaar C, White SJ, Roleder T, Milewski KP, Gasior P, Buszman PP, Buszman P, Jahangiri M, Hill J, Mayr M.
   Extracellular Matrix Proteomics Reveals Aggrecan and Aggrecanases as Novel Contributors to Vascular Remodelling in Stented Coronary Arteries. In revision (*Circulation*).

Published

1. Langley SR, Willeit K, Didangelos A, Matic LP, Skroblin P, Barallobre-Barreiro J, Lengquist M, Rungger G, Kapustin A, Kedenko L, Molenaar C, Lu R, Barwari T, Suna G, Yin X, Iglseder B, Paulweber B, Willeit P, Shalhoub J, Pasterkamp G, Davies AH, Monaco C, Hedin U, Shanahan CM, Willeit J, Kiechl S, Mayr M. Extracellular matrix proteomics identifies molecular signature of symptomatic carotid plaques. *J Clin Invest*. 2017.
2. Puntmann V, Carr-White G, Jabbour A, Yu CY, Gebker R, Kelle S, Hinojar R, Doltra A, Varma N, Child N, Rogers T, **Suna G**, Arroyo Ucar E, Goodman B, Khan S, Dabir D, Herrmann E, Zeiher AM, Nagel E.
   International T1 Multicentre CMR Outcome Study. T1-Mapping and Outcome in Nonischemic Cardiomyopathy: All-Cause Mortality and Heart Failure. *JACC Cardiovasc imaging*. 2016; *9* : 40-50.
3. Cuello F, Shankar-Hari M, Mayr U, Yin X, Marshall M, **Suna G**, Willeit P, Langley SR, Jayawardhana T, Zeller T, Terblanche M, Shah AM, Mayr M.
   Redox-state of pentraxin 3 as a novel biomarker for resolution of inflammation and survival in sepsis. *Mol Cell Proteomics*. 2014; *13* : 2545-2557
4. **Suna G**, Mayr M.
   Tracing the proteomic fingerprint of the diabetic aorta? *Circ Cardiovasc Genet*. 2014; *7* : 100-101.
5. **Suna G**, Somaini U.
   Chronic thromboembolic pulmonary hypertension (CTEPH). *Praxis*. 2011;100:1141-1151.